Design and Fabrication of a New Ultrasonic Device and Its Application for Drug Delivery

Zhang Hong Ye

School of Mechanical and Aerospace Engineering

A thesis submitted to the Nanyang Technological University
in fulfillment of the requirement for the degree of
Doctor of Philosophy

2005

ABSTRACT

Recently, ultrasound enhanced transdermal drug delivery technology (sonophoresis) has received increasing attention. Sonophoresis devices developed with various types of transducers have been patented, such as the horn-type and disk-type devices. However, the major drawbacks in drug delivery are the large physical size and weight of the conventional ultrasound transducer devices which render them to be impractical and the high electrical power requirement which is associated with mechanical fracture and fatigue, heat generation and depolarization to drive the device.

On the other hand, ultrasound provides a good method for an externally controlled system, in which release rate of encapsulated drug can be changed by applying external ultrasound energy. Much of the work has been conducted using sonicators, water-bath sonicators or commercially available transducers. The operating ultrasound frequency is in the range of 20 kHz to 1.6 MHz and the sound intensities vary between 2.5 to 200 W/cm^2. In general, the stronger the ultrasound is, the greater the possibility that the polymer membrane may be damaged by cavitations. Thus, the recovery of the permeability of the sonicated polymer membrane is crucial for its membrane-controlled release application. Also, acoustic waves of high intensity are capable of rupturing blood vessels or cells as a result of the formation and oscillation of cavities when using ultrasound to trigger the implanted polymeric devices. It is precisely these cavitation bubbles that are responsible for hemolysis and hemorrhage. Therefore, it is necessary to study the effect of ultrasound irradiation on the permeability of the polymer membrane at relatively low ultrasound frequency and intensity with regards to the bio-safety issues.

In this research, two new prototype devices, namely 'A' and 'B', were developed based on flat flextensional ultrasound transducers. Device 'A' that has a single flat flextensional transducer was designed to verify the feasibility of such a transducer for the drug delivery applications. Device 'B' which has dual flat flextensional transducers (named Transducer '1' and Transducer '2') was developed based on the acoustic interference principle in order to generate more acoustic power with lower input electrical power. The physical characteristics especially the first resonance frequency and its corresponding output acoustic intensity were studied based on the requirement of the ultrasound enhanced drug delivery. The drug delivery performances of both the devices were investigated. All the drug delivery experiments were conducted with silicone rubber membrane at low ultrasound frequency and low intensity.

The maximum spatial peak-temporal-peak intensity produced by a single flat flextensional transducer in device 'A' is found to be comparable to that achieved using a commercial sonicator. When dual transducers in device 'B' were operated simultaneously at low input electrical power (of 80 V), the output acoustic intensity has almost the same value as that generated by a single transducer in the same device operated at high electrical power (of 160 V). It is found that device ' B 'has the capability to reduce the applied voltage by twofold.

For the device 'A', the enhanced permeability of ' silicone rubber membrane was 2.81±0.73-fold higher when exposed to low intensity (41.13 mW/cm^2) and low ultrasound frequency (17.47 kHz) as compared with that of the unexposed membrane. The cumulative amount of the drug diffused through the sonicated silicone membrane is about

3.9% to 34.1% higher than that through the non-irradiated membrane. It is clearly shown that the permeability of the sonicated silicone membrane recovered partially.

For the device 'B', at high input electrical power (of 160 V), the enhanced transport rate is up to 2.11-fold and 2.52-fold achieved by Transducer '1' and Transducer '2' respectively. However, when both transducers in device 'B' were operated simultaneously at low input electrical power (of 80 V), the transport rate increased up to 2.77-fold. Once again, it demonstrated that dual transducers have the capability to generate more acoustic intensity to efficiently enhance the permeability of the silicone rubber membrane and to simultaneously reduce the required electrical power twofold for each transducer in device 'B'. It also manifested that the prototype device 'B' with dual flat flextensional transducers has the potential to be used as a low power consumption drug delivery device. In conclusion, all the experimental results and features of the prototype devices 'A' and 'B' show that they are practical ultrasonic devices to be used for the ultrasound enhanced drug delivery.

ACKNOWLEDGEMENT

I would like to express my sincere appreciation and deepest gratitude to my supervisor Associate Professor Yeo Swee Hock for his invaluable and constructive suggestions throughout the period of this research. Without his well-organized and systematic guidance, this research would not be so successful. I am most obliged to him for giving me the freedom to set the research objectives and scopes.

Many thanks go to my group colleagues, Mr. Chua Loh You, Mr. Meenakshi Sundaram Murali and Mr. Tan Chin Boon, for their helpful discussion and support.

Sincere thanks are due to Associate Professor Subbu S.Venkatraman for his helpful discussion on the drug delivery technologies and lending me the useful books. Special thanks are due to Associate Professor Thomas Gong Hai Qing for his care and giving me a chance to present my research in the MicroMedicine research seminar. I also would like to express my sincere thanks to Assistant Professor Hu Jun Hui for his helpful discussion on the piezoelectric devices and lending me the piezoelectric materials.

I would also like to thank all the fellow members in PEN Center especially Dr. Deng Yuan Zi, and Dr. Xie Dong Zhu for their friendly cooperation, and all my friends in Metrology Lab. In addition, I owe great debts of gratitude to Nanyang Technological University and the Government of Singapore for providing the necessary funding and opportunity to undertake this research.

Words are inadequate to express my gratitude to my parents, my mother-in-law, my father-in-law and my wife Liu Wei, for their patience, love and immense support throughout my study.

TABLE OF CONTENTS

LIST OF ABBREVIATIONS

ABBREVIATIONS	DESCRIPTION
2D	Two-dimensional
3D	Three-dimensional
AC	Alternating current
APS	Advanced point selection
CCD	Charge coupled device
CPE	Chemical permeation enhancer
DC	Direct current
DMS	Data manage system
FEA	Finite element analysis
FEM	Finite element method
IR	Inferred
NAVMI	The nondimentionalized added virtual mass incremental
PVDF	Polyvinylidene fluoride
PZT	Lead zirconate titanate
SC	Stratum corneum
SEM	Scanning electron microscope

LIST OF SYMBOLS

SYMBOLS	DESCRIPTION
a	The radius of the vibration plate
A	Amplitude of the acoustic wave
c	Acoustic velocity in water
c_0	Equilibrium acoustic velocity
C_A	Molar concentration of component A
$[c^E]$	Stiffness matrix evaluated at constant electric field
d	The distance between acoustic source and center line
d_m	The vibration zone diameter
$[d]$	Piezoelectric matrix relating strain and electric field
$[d]^t$	Transposed piezoelectric matrix relating strain and electric field
d_{31}	Piezoelectric transverse coefficient
$d33$	Piezoelectric longitudinal coefficient
$\{D\}$	Electric displacement vector (three components x, y, z)
D_A	Molecular diffusivityof component A
$e31$	Piezoelectric stress coefficient
$[e]$	Piezoelectric matrix relating stress and electric field
$[e]^t$	Transposed piezoelectric matrix relating stress and electric field
E	Young's modulus
E_D	Eddy diffusivity
$\{E\}$	Electric field vector (three components x, y, z)

f_1	First resonance frequency
f_a	The resonance frequency in air
f_w	The resonance frequency in water
I	Acoustic intensity
I_{sum}	The sum of acoustic intensity radiated from two monopoles
$I(\mathrm{r})_{sum}$	The complex quantity of the sum of acoustic intensity radiated from two monopoles
$I(r_1)$	Acoustic intensity of acoustic source 1
$I(r_2)$	Acoustic intensity of acoustic source 2
I_{sptp}	The output spatial peak-temporal-peak intensity
k	Wave number
K_f^2	Intensity response factor
m	The number of radial nodal lines
M	The sensitivity of the hydrophone
n	The number of nodal circles
N_A	The diffusional flux across the membrane
p	Acoustic pressure
$p(r,t)_{sum}$	The sum of the acoustic pressure in the acoustic and geometric far field
$\bar{p}(r,t)_{sum}$	The complex numbers of $p(r,t)_{sum}$
Q	The ratio of Q_2 /Q,
Q_1	The amplitude of the source strength of the point monopole 1
Q_2	The amplitude of the source strength of the point monopole 2
Q_m	Mechanical quality factor
$\mathrm{Q}(t)$	The source strength of the point monopole

$Q(t)_1$	The source strength of the point monopole 1
$Q(t)_2$	The source strength of the point monopole 2
r	The distance from the center point of the two acoustic sources to the observation point
r_1	The distance from acoustic source 1 to the observation point
r_2	The distance from acoustic source 2 to the observation point
R_{coeff}	The ultrasound reflection coefficient
s_{11}^E	Elastic compliance
$[s^E]$	Compliance matrix evaluated at constant electric field
$\{S\}$	Strain vector (six components x, y, z, yz, xz, xy)
S	The distance between two piezoelectric rings
t	The thickness of the vibration plate
t_m	The thickness of the metal vibration plate
t_p	The thickness of the piezoelectric ring
t_{piezo}	The thickness of the piezoelectric material
$\{T\}$	Stress vector (six components x, y, z, yz, xz, xy)
u	Liquid velocity
u_1	First order approximation to steady solution of u
u_2	The streaming velocity
$u(r,t)_{sum}$	The sum of the particle velocity in the acoustic and geometric far field
$\tilde{u}(r,t)_{sum}$	The complex number of $u(r,t)_{sum}$
$\tilde{u}(r,t)^*_{sum}$	The complex conjugate of $\tilde{u}(r,t)_{sum}$
v_+	The compressional peak voltage amplitude
v_-	The rarefactional peak voltage amplitude

$\lvert v_- \rvert$	Absolute value of the rarefactional peak voltage amplitude
V_{TP}	The larger value of v_+ and $\lvert v_- \rvert$
z_0	The characteristic acoustic impedance
Z_1	The characteristic acoustic impedance of ultrasound transducer
Z_2	The characteristic acoustic impedance of the air
Z	The coordination number
α	Attenuation coefficient
ε_0	The dielectric permittivity of free space
ε_{11}^s	Clamped permittivity
$[\varepsilon^S]$	Dielectric matrix evaluated at constant strain
$[\varepsilon^T]$	Dielectric matrix evaluated at constant stress
$\phi(r,t)$	General velocity potential
$\phi(r_1,t)_1$	The velocity potential of acoustic source 1
$\phi(r_2,t)_2$	The velocity potential of acoustic source 2
$\phi(r,t)_{sum}$	The sum of the individual velocity potential
φ	The total phase angle between two point monopoles
μ	The shear viscosity coefficient
μ'	The bulk viscosity coefficient
θ	The angle between r and d
ρ_0	Equilibrium density
ρ_p	The density of the vibration plate
ρ_w	The density of water
σ	Poisson's ratio

ω	Angular frequency

LIST OF FIGURES

LIST OF TABLES

CHAPTER ONE
INTRODUCTION

1.1 Background

Transdermal drug delivery technology has gone mainstream. Doctors around the world are calling transdermal drug delivery "the delivery system of the future" [1]. Studies have shown that when the drugs are administered orally, only 5% of them could be introduced to the places where the drugs are needed, most of them are damaged by the liver, stomach and digestive system (Figure 1.1). In contrast, 95% of administered drugs could be absorbed and utilized by human body using transdermal drug delivery method, which offers several advantages over traditional delivery methods including injection and oral delivery. Compared with oral delivery, transdermal drug delivery avoids gastrointestinal drug metabolism, reduces first-pass effects and provides sustained release of drugs for up to seven days [2].

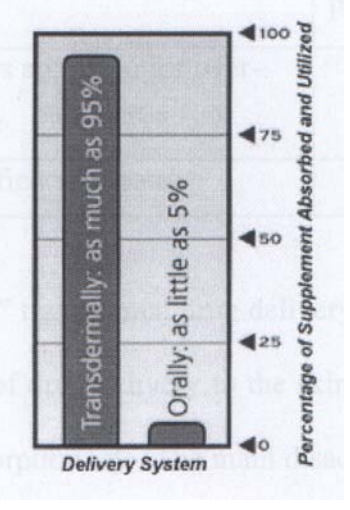

Figure 1.1 Drug absorption and utilization of transdermal delivery versus oral delivery [1].

Although transdermal drug delivery technology is the ideal method, the impermeability of the skin adds enormous barriers to this technology. Basically, there are two types of transdermal delivery systems: passive and active. The passive delivery systems date back to World War II, when munitions workers experienced less angina attacks while working with nitroglycerin. Table 1.1 lists the important milestones of passive transdermal drug delivery systems [3].

Table 1.1. Important milestones of the passive transdermal drug delivery systems [3].

Time	Products	Distributors
1981	First transdermal patch. Transderm-Scop for scopolamine	Developed by Alza Corp., Marketed by Ciba-Geigy
1982	Nitro-Dur, Nitro_disc	Key, Searle
1985	Catapress-TTS for clonidine	Boehringer Ingelheim, using Alza's technology
1986-1994	Estraderm for estradiol Nicotine patches Duragestic for fentanyl Tesoderm for testosterone Deponit, Nitrocine	Ciba Various companies Janssen Alza Corp. Wyeth-Ayerst, Schwartz Pharma
1995	Nicotine patches approved for over-the-counter sale	---
2001	FDA approves first skin patch	---

Most of the "patch type" transdermal drug delivery systems consist of two dosing systems, one controls the rate of drug delivery to the skin via a membrane and the other uses the skin to control the absorption rate. The main disadvantages are that few drugs are able to diffuse through the skin, and only relatively potent drugs can be utilized as a transdermal drug delivery system with a low precision controlled-release rate. Although a

transdermal patch is simple and portable, the passive variety finds difficulty in breaking the skin barrier. Thus, it is necessary to employ enhancement technologies to controllably, reversibly, and safely reduce the resistance of the skin [4]. Several methods exist for transdermal drug delivery. These include chemical enhancers, iontophoresis, electroporation and ultrasound [5-8].

Ultrasound enhanced transdermal drug delivery (also called sonophoresis) has received increased attention in the last decade. Recent studies have shown that ultrasound enhanced transdermal drug delivery offers promising potential for non-invasive drug administration [9-11]. The precise mechanism of ultrasound enhanced transdermal drug delivery by which the acoustic waves help to enhance permeability through the skin is not fully understood. It is hypothesized that the acoustic waves cause microcavitation in the drug medium and the skin itself, and this action helps the drug molecules to diffuse into and through the skin. It is further hypothesized that the ordered lipid bilayers of the skin maybe temporarily disrupted by the acoustic waves induced cavitation thus permitting molecules to pass [12- 13]. With sonophoresis, significant enhanced transportation of model drugs such as insulin has been verified by using commercial sonicators [9]. Developments of sonophoresis devices, with varying types of transducers, have been patented. Some of the patents and medical prototypes of the conventional sonophoresis systems are listed in chronological order in Table 1.2.

Table 1.2. US patents and prototype products of active sonophoresis delivery systems.

Year	Patent number	Title or prototype name	Company
1988 [14]	US 4,787,888	Disposable piezoelectric polymer bandage for percutaneous delivery of drugs and methods for such pertaneous delivery (A)	University of Connecticut
1993 [15]	US 5,230,334	Method and apparatus for generating localized heperthermia	Summit Technology Inc.
1995 [16]	US 5,421,816	Ultrasonic transdermal drug delivery system	Endodermic Medical Technologies Company
1997 [17]	US 5,618,275	Ultrasonic method and apparatus for cosmetic and dermatological applications	Sonex International Corperation
1999 [18]	US 5,895,263	Transdermal transport using ultrasound standing eaves	Abbott Laboratories
2000 [19]	US 6,024,717	Apparatus and method for sonically enhanced drug delivery	Vibrx, Inc.
2001 [20]	US 6,234,990 B1	Ultrasound enhancement of transdermal transport	Sontra Medical, Inc.
2003 [21]	---	U-Strip™	Encapsulation Systems Inc.
2004 [22]	---	SonoPrep® Skin Permeation Device	Sontra Medical, Inc.

1.2 Statement of the Problems

The conventional sonophoresis devices are divided into two groups. Some sonophoresis devices are constructed of a converter and a horn section. The converter is made up of a stack of piezoelectric disk designed to vibrate in the axial direction. This so-

called 'horn type' of sonophoresis device, although potentially quite efficient at producing permeation enhancement, is normally around 200 mm in length and weighs as much as one kilogram. In addition, in most of the drug delivery application a transducer has to operate around its fundamental resonance frequency in order to provide sufficient acoustic power. However, its size is inversely proportional to the working frequency. Thus the major drawback in drug delivery is the large size and weight of the conventional ultrasound transducer devices. These bulky devices would not be desirable as they are unsuitable for portable or wearable drug delivery devices. Other sonophoresis devices do not have a converter and a horn section. They consist of one or a small number of piezoelectric disk layers, which vibrate in the axial mode. Although these 'disk type' devices are relatively small and lightweight, they are generally not operated at the fundamental resonance frequency and this gives rise to very low efficiency. Since the size is small as compared with the wavelength in water around the resonance, the transfer of radiated acoustic power from surface of the transducer to the water is inefficient. This poor radiation characteristic often implies the need for high electrical power to excite the device, which is associated with mechanical fracture and fatigue, heat generation and depolarization [23]. The conventional sonophoresis devices' use of high electrical power gives rise to yet another problem associated with electrical safety.

But ultrasound provides a good method for externally controlled system, in which the release rate of the encapsulated drug can be changed by application of the ultrasound energy externally. Previous research work [7] [24-26] has studied in-vitro and in-vivo, both biodegradable and non-degradable polymers at ultrasound frequency of 20 kHz to 1.6 MHz and sound intensities of 2.5 to 200 W/cm^2. It was shown that both the degradation and the drug release rate of polymer were enhanced. It was assumed that

cavitation is the major reason for the enhancement, which may cause enhanced polymerization or depolymerization reactions by temporarily dispersing aggregates or permanently breaking chemical bonds in polymer chain [27-28]. In general, the stronger the ultrasound is, the greater the possibility that the polymer membrane may be damaged by cavitation. However, the recovery of the permeability of the sonicated polymer membrane is crucial for its membrane-controlled release application. Moreover, acoustic waves of high intensity are capable of rupturing blood vessels or cells as a result of the formation and oscillation of cavities when using ultrasound to trigger the implanted polymeric devices. It was clearly indicated that these cavitation bubbles were responsible for hemolysis [29-31] and hemorrhage [32]. In consideration of the bio-safety issues of the ultrasound regulated responsive drug delivery system, it is necessary to study the effect of ultrasound irradiation on the permeability of the polymer membrane at relatively lower ultrasound frequencies and intensities.

1.3 Objectives

The main objective of this research is to develop a new ultrasound medical device for drug delivery applications. It should have the capability to overcome or reduce the limitations (as detailed on page 55) of conventional sonophoresis devices. This research work is divided into two stages: 1) design and fabrication, and 2) investigation of the physical and drug delivery characteristics of the device. Therefore, the objectives corresponding to each stage are listed as follow:

1. To develop an ultrasonic drug delivery device with important considerations given to structural simplicity and lightweight issue. Under these requirements, prototype device ‘A’ with a single flat flextensional transducer was designed and fabricated.

It is the first effort to use a flat flextensional transducer with piezoelectric ring for ultrasound enhanced drug delivery application.

2. To develop an ultrasonic drug delivery device that could generate a high acoustic power with a low input electrical power requirement. Based on the acoustic interference principle, prototype device 'B' with dual flat flextensional transducers was designed and fabricated.
3. To study the effects of material properties and dimensional changes on the performance of the flat flextensional transducer using finite element analysis (FEA) based on the fluid-structure interactions.
4. To investigate the physical characteristics of the devices 'A' and 'B'. According to the previous research [33], the enhancement exhibited a strong dependence on the ultrasound intensity and the frequency. Therefore, in this experimental study, these parameters were examed.
5. To conduct experimental work to investigate the potential of device 'A' used as an external ultrasound source to trigger the responsive polymer drug delivery system at a low ultrasound frequency and intensity.
6. To explore the capability of the device 'B' with dual transducers to increase the output acoustic intensity and simultaneously reduce the required electrical power during the drug delivery experiments. It is the first effort to use dual flat flextensional transducers for ultrasound enhanced drug delivery applications.

1.4 The structure of the thesis

Chapter 1 outlines the background and objectives of this research work. The background knowledge and conventional sonophoresis devices developed for ultrasound enhanced drug delivery are described and reviewed in Chapter 2. This includes a

disposable piezoelectric polymer bandage type device, a transdermal device with stimuli components, a transdermal drug delivery device with a circulating system or a transfer promoting system, a multiple frequency transdermal drug delivery device, a sonophoresis device with controlled-release and recovery function, a transdermal device with a focused ultrasound beam, a sonophoresis device with a magnetic floating mass transducer, and a commercial prototype device namely SonoPrep® Skin Permeation Device. Background knowledge about FEA, ultrasound technologies, controlled-release, transdermal drug delivery technologies and ultrasound enhanced transdermal drug delivery technologies are reviewed. The major limitations of conventional sonophoresis devices based on the literature review are also presented in Chapter 2.

The typical structure of the flat flextensional transducer and its advantages over traditional disc type transducer for underwater application are described. A new ultrasonic device that could generate higher acoustic power with low power requirement is put forward base on the acoustic interference principle. The mechanism of the acoustic principle based on the structure of the new ultrasonic device is discussed in detail.

In Chapter 4, finite element method (FEM) was used to study the effects of material properties and dimensional changes on the performance of the flat flextensional transducer. The parametric study includes admittance, first resonance frequency, center displacement of the vibration plate and output acoustic pressure. The simulation results are compared with the experimental results. The FEA results in Chapter 4 provide a general rule to choose different types and dimensions of the materials for the flat flextensional transducer. The final structural dimensions of devices 'A' and 'B' were

obtained from the FEA results. The detailed fabrication procedure was described in the last portion of Chapter 4.

The physical characteristics of devices 'A' and 'B' were investigated and presented in Chapter 5. Two major parameters of the ultrasound enhanced drug delivery were studied which included the first resonance frequency and the output acoustic intensity of the devices 'A' and 'B'.

In Chapter 6, experiments were performed to investigate the drug delivery characteristics of the devices 'A' and 'B'. All the drug delivery experiments were conducted with the silicone rubber at relatively low acoustic power and low ultrasound frequency (17.46 kHz and 26.83 kHz). Some of the parameters such as acoustic intensity, ultrasound irradiation time and the reversibility of the silicone rubber were also examined and discussed in Chapter 6. Finally in Chapter 7, a summary of the research is presented along with conclusions and recommendations for further study.

CHAPTER TWO
LITERATURE REVIEW

In this chapter, review of essential background and techniques is given to establish some basic understanding. These include review of:

1) Finite element analysis
2) Ultrasound technology
3) Drug delivery
4) Transdermal drug delivery
5) Ultrasound enhanced transdermal drug delivery

A review of existing sonophoresis devices and their features for drug delivery are discussed. These include:

1) Disposable piezoelectric polymer bandage type device
2) Active transdermal system with stimuli components
3) Transdermal drug delivery device with circular systems
4) Transdermal drug delivery device with transfer promoting system
5) Transdermal drug delivery device using motile frequencies
6) Sonophoresis device with controlled-release and recovery function
7) Sonophoresis device with focused ultrasound beam
8) Sonophoresis system with feedback phase-tracking loop
9) Standing wave type sonophoresis device
10) Sonophoresis device with floating mass transducers
11) Horn type sonophoresis device.

2.1 Finite Element Analysis

With the advent of faster and more affordable computers, FEA is becoming an increasingly powerful engineering tool. Its ability to solve exceedingly large mathematical problems makes it ideal for analyzing structures that are too complex for manual calculation. Several commercial packages are available which allow the engineer to model many different cases including stress strain behavior, thermal transformation and electrical effects [34].

Broadly speaking, the objective of FEA is to approximate the values of the unknown of a differential equation with sufficient accuracy. In order to accomplish this, an analysis is typically performed using the following steps. First, a FEA model representative of the problem is created with defined quantities such as material properties, loading conditions and boundary conditions. Second, the model is divided into small regions called elements. Elements contain nodes in which values of unknown quantities are calculated.

Once elements, loads and boundary conditions have been established, governing equations describing the mass, momentum or energy are developed for each element [35]. There are usually differential or integral equations. From these, a set of approximation functions incorporating the material properties using simple and solvable expressions are derived. The precision and accuracy of the final solution is dependent on how fine the elements are. Smaller elements are more accurate but this increases solution time exponentially [36].

There are several advantages of using FEA in conjunction with typical experimental work. The computer models are capable of plotting a number of solution outputs such as displacement, acoustic pressure, stress or strain in contour graphs, making it much easier to visualize what is happening. This can lead to greater understanding of the mechanics of the problem. It is much simpler and less expensive to generate several computer models than to build several prototype parts, which makes modeling economically attractive. Small changes can usually be made much more easily on a virtual model than on a prototype [34].

Several commercial packages such as PZFLEX™, ATILA™ and ANSYS™ offer electromechanical modeling capabilities. These packages allow the coupling of electrical and mechanical boundary conditions, simulating piezoelectric materials [37]. With these capabilities, researchers have been able to model many different aspects of transducer design. Multi-layer transducers, composites, class IV and class V flextensional transducers have all been studied using the same basic modeling elements and procedures [38-46].

2.2 Ultrasound Technologies

The term ultrasound has acquired a wide rang of meanings, involving the field of physics, industrial technology, information and measurement technology, medicine, and biology [47]. It is a branch of acoustics that uses the acoustic bandwidth frequencies above the audible limit. The upper frequency limit is being constantly increased and, at present it shifts towards the region of hyper sound. The full spectrum is shown in Figure 2.1, where typical ranges for the phenomena of interests are indicated. The major reason for studying ultrasound is because it has many applications, which cover chemistry,

physics, engineering, biology, food industry, medicine, oceanography, seismology, and so on. All these applications are almost based on two unique features of ultrasound waves [47]:

1. Ultrasonic waves travel slowly, about 100,000 times slower than electromagnetic waves. This provides a way to display information in time, and create variable delay.
2. Ultrasonic waves can easily penetrate opaque materials, which could provide a highly desirable way to probe and image the interior structure of opaque objects.

All these ultrasonic applications are rigidly classified as being of either low or high intensity. At low intensity, ultrasound is used to investigate the properties of samples of materials or as a method of control. In most cases, it is important that the material of propagation does not suffer any permanent change in its structure and chemical properties. Many low intensity applications are made at very high frequencies, typically in the MHz range, and the acoustic powers involved may range from a few microwatts to several tens of milliwatts. At high intensities, ultrasound is generally used for changing the properties of the material through which it is passed. High intensity applications are almost always at low frequencies, just above the audible limit, and the acoustic power used may extend from a few milli watts to kilowatts.

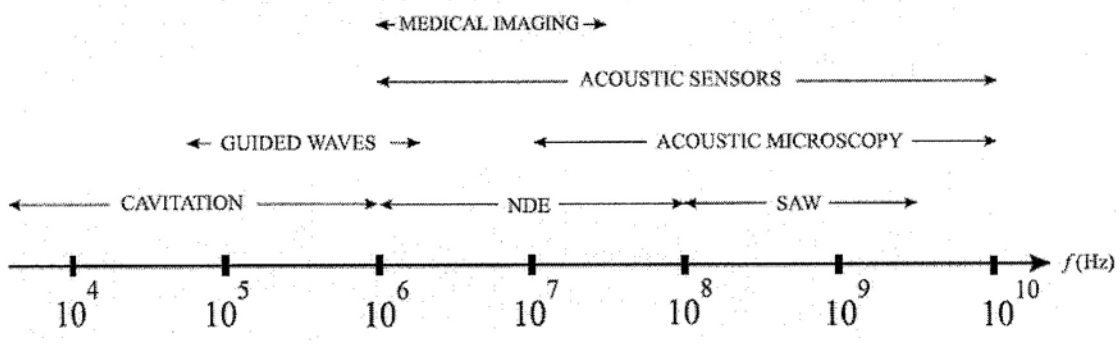

Figure 2.1. Common frequency ranges for various ultrasonic processes [47].

2.2.1 Ultrasound Generation

An ultrasonic transducer is an instrument designed to generate the disturbance from which the ultrasonic energy radiates. Therefore, any device capable of generating ultrasound is an ultrasonic transducer with wider ranging applications. The device may be a whistle, a piezoelectric plate, a magnetostrictive stack driving a piston, a diaphragm driven electromagnetically, a siren, a laser beam, or any of various mechanical devices such as rotating eccentrics [48].

2.2.1 .1 Piezoelectric Method

There are a number of ways to generate ultrasound, but the most common is by means of a piezoelectric transducer. Many books and articles have been written on the principle of piezoelectricity and piezoelectric effects in various materials. According to the definition by Mason [49], piezoelectricity is pressure electricity (in Greek, piezo equates to pressure); a pressure applied along certain crystallographic axis produces electrical charge on preferred crystallographic surfaces. So piezoelectricity or the piezoelectric effect is a phenomenon that certain crystals change their physical dimensions when subjected to an electric field and vice versa. The crystal consists of numerous dipoles that are in the normal state. The individual dipoles have a random orientation with no net surface charge. An electric field applied across the crystal will realign the dipoles due to repulsive or attractive electric forces resulting in compression or expansion of the crystal, depending on the direction of the electric field (Figure 2.2 [50]).For transmission of a short ultrasonic pulse, a voltage pulse of very short duration is applied, causing the crystal to initially contract and then vibrate for a short time at its resonance frequency. When the echoes are received, the longitudinal ultrasound waves

will compress and expand the crystal. The deformation realigns the dipoles, creating net charge on the surface (see Figure 2.2).

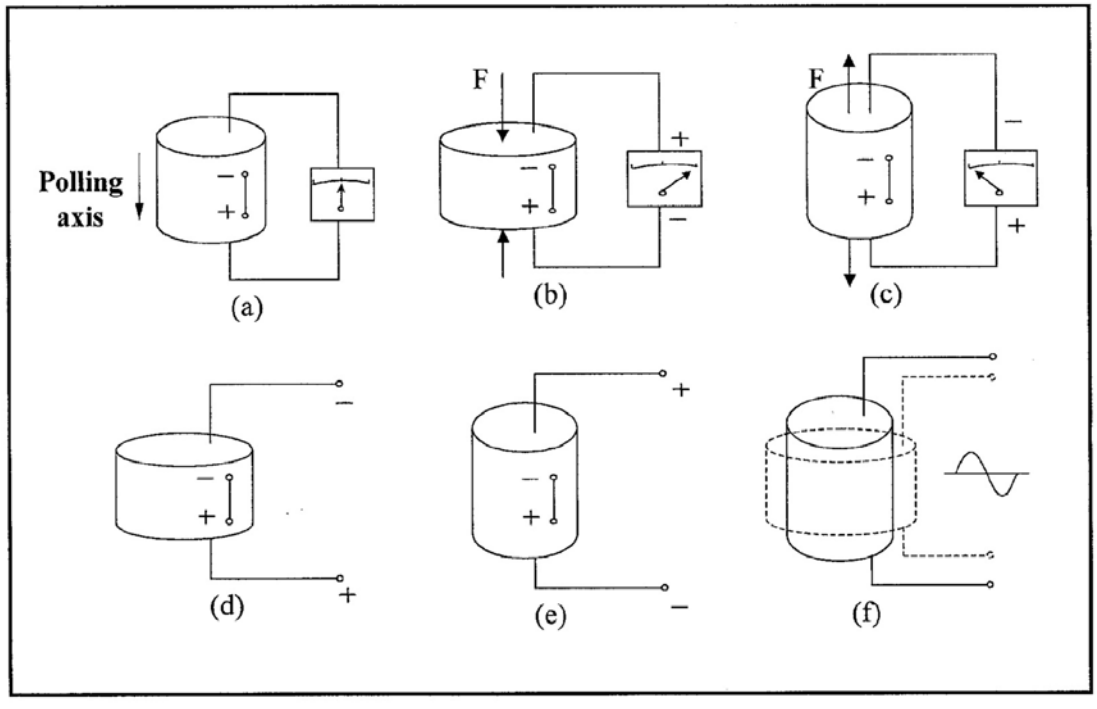

Figure 2.2. The piezoelectric effect in a cylinder of PZT material [50].

Ikeda [51] gave another definition of piezoelectricity that is a linear interaction between an electrical and a mechanical system. Actually, the interaction process does not only exist between electrical and mechanical systems, but also between electrical and thermal systems (called pyroelectricity) amongst them. Figure 2.3 lists all the linear interactions between any of two systems. It is clearly shown that many coupling coefficients and constitutive relations are among the interaction network (Figure 2.3). It is believed that good understanding of piezoelectricity is of benefit to all other linear interactions.

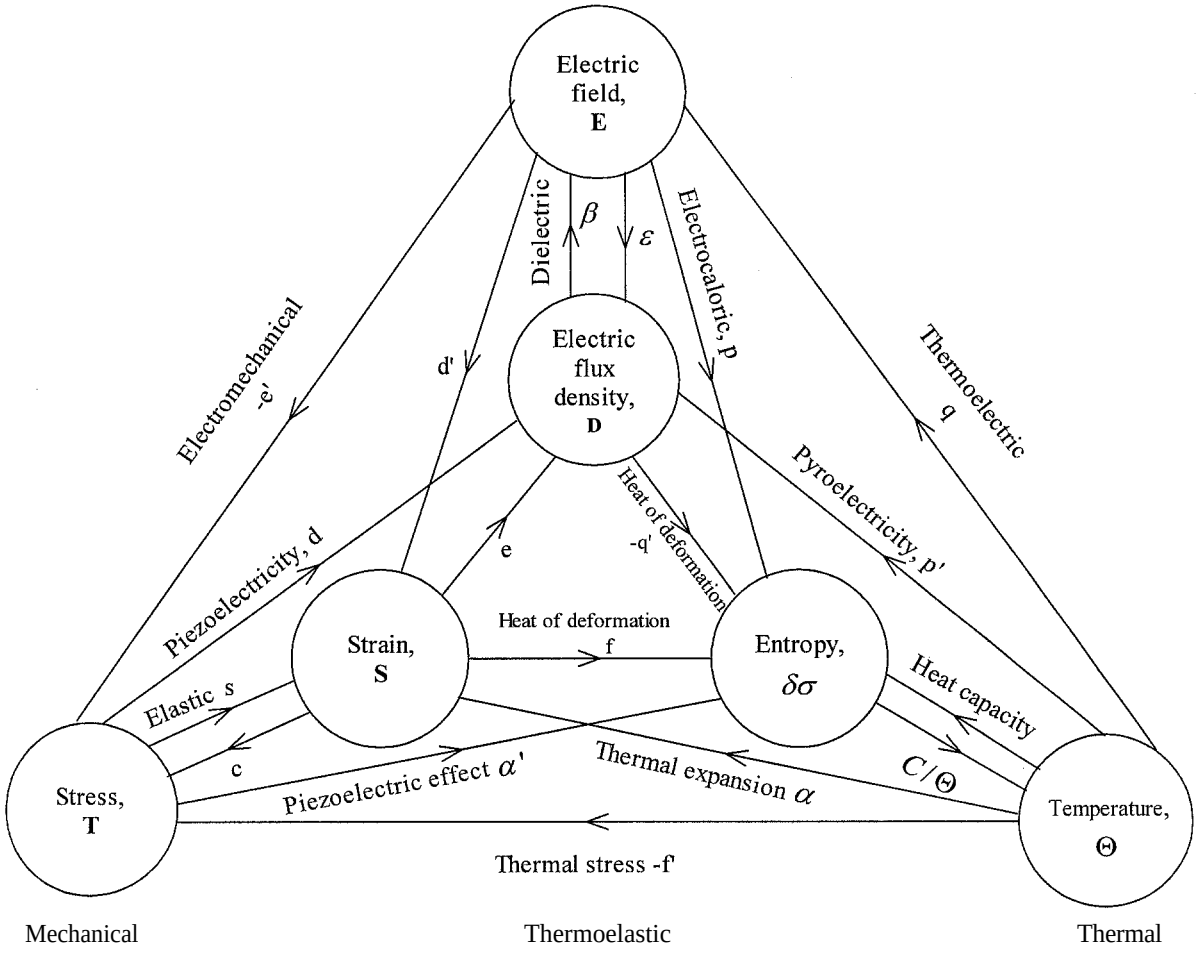

Figure 2.3. Interaction processes between the electrical, mechanical, and thermal systems [51].

2.2.1.2 Magnetostrictive Method

Magnetostriction is a property of ferromagnetic materials to undergo a change of their physical dimensions when subjected to a magnetic field. Due to the magnetostrictive effect, the magnetostrictive materials could convert magnetic energy into mechanical energy and vice versa, which are used for the building of both actuation and sensing devices.

It is simpler to polarize using a permanent magnet whose flux is contained within the core of the transducer as shown in Figure 2.4 [52]. In order to avoid the destructive

eddy currents, shims are used instead of solid blocks. A stack of thin shim stock (usually nickel) is brazed together and surrounded by a magnetic coil; alternating the polarity of the current passed through the coil alternates the polarity of the magnetic field which converts electrical energy to mechanical energy and vice versa.

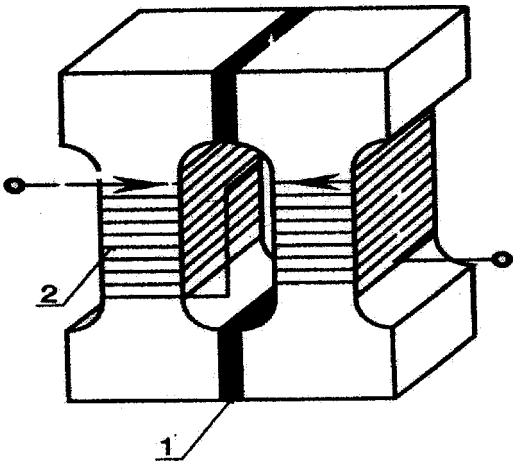

1- Permanent magnet; 2- Exitatory winding.

Figure 2.4. A magnetostrictive transducer with a polarization produced by a permanent magnet [52].

Magnetostrictive transducers are generally less efficient than their piezoelectric counterparts. This is due to the fact that the magnetostrictive transducer requires a dual energy conversion from electrical to magnetic and then from magnetic to mechanical. Because of inherent mechanical constraints on the physical size of the hardware as well as electrical and magnetic complications, high power magnetostrictive transducers seldom operate at frequencies substantially above 20 kHz. Current applications for magnetostrictive devices include ultrasonic cleaners, high force linear motors, positioners for adaptive optics, active vibration or noise control systems, medical, sonophoretic drug delivery, industrial ultrasonics, pumps, underwater sonar, surgical tools and chemical and material processing.

2.3 Drug Delivery Technologies

Drug delivery technology means introducing a drug into the body. It is almost as important as the drug itself. Drug delivery is used mostly with small molecules, such as individual peptides. Cutting-edge technologies meet the real challenge: how to package and deliver proteins and other large complex molecules so that delivery will be accurate, modulated, and effective. The development of a new drug involves more than the synthesis of a substance that has a particular effect on the body. The developer must also consider how to transport the drug to an appropriate part of the body and, once there, makes it available for use. It is necessary that the drug concentration in the blood be maintained at a level that provides maximum therapeutic benefits. Therefore, in this section, controlled release technologies and some of the main categories of drug administration routes are briefly reviewed.

2.3.1 Controlled-release

The technology by which a drug is delivered has a significant effect on its therapeutic efficacy. Some drugs have an optimum range for them to get the maximum therapeutic benefit, which is called the therapeutic window [53]. If the drug concentration is above or below this window, it can be toxic or produce no therapeutic effect (Figure 2.5). Conventional drug delivery systems, such as, oral delivery and injection initially make the drug concentration sharply increase to a peak above the therapeutic window (above the toxic level), and followed by rapid drug concentration decrease below the therapeutic level, therefore, the time spent in the optimum concentration range may be short and more drug administration times are needed. A sleeping pill is a good example for explaining the importance of drug concentration. If the drug concentration is below

the therapeutic level, enhancement of sleepless release is not notable. If the drug concentration is above the toxic level, potentially fatal drug addiction is encountered.

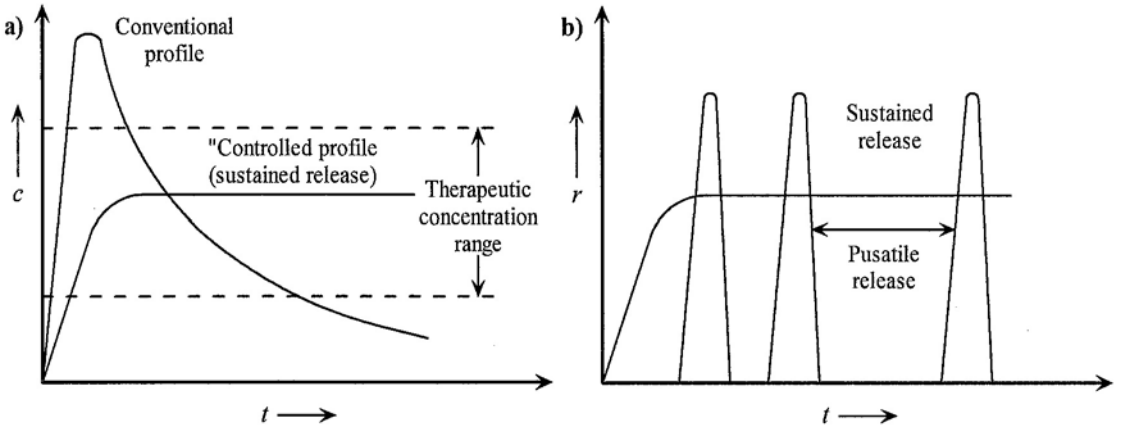

Figure 2.5. a) Exemplary concentration c versus time t profiles for conventional and controlled-release drug delivery devices. The controlled release profile here is characteristic of sustained release. b) Exemplary release rate $\boldsymbol{r}$ versus time t profiles demonstrating the difference between sustained release and pulsatile release [53].

Only in recent years have the controlled release systems been made feasible. Formerly, although drug delivery systems could target the drug into the right cells and tissues, precise control of drug release rate and prolonged dosage existed only as a dream. This is attributed by the application of polymer engineering. In a short time, the se controlled-release systems have made great impact on cardiology, immunology and gene-therapy. Controlled-release drug delivery combines well-characterized, reproducible form design with clinical pharmacology, particularly in steady state pharmacology that defines the required input or the desired drug delivery profile. This design typically includes additional characterization of the drug's permeation through the appropriate biological membrane and any first pass metabolic effects prior to entry of the drug into systemic circulation [54]. Potential advantages of these improved drug delivery include:

1. Continuous maintenance drug level in a therapeutically desirable range.

2. Reduction of the harmful side effects due to the drug targeting to the particular cells or tissues.
3. Improvement of the patient's compliance of the drugs.
4. Decrease of the drug dosage.
5. Release of the drug to the right site of the human body when necessary.

This field is potentially very rich in commercial applications and is expanding rapidly. Technologies have already been described in many scientific literatures, mostly in human medicines, dosage forms, and cosmetic formulations. In recent years there has been growth in financial investment in the area of controlled release, particularly in the pharmaceutical industries [54].

2.3. 1. 1 Sustained Release

The field of controlled-release initially focused on achieving a sustained (or continuous) release of drugs over a long period of time with minimal influence by outside factors. Much of this work uses polymers that release the drug at a nearly constant rate due to diffusion out of the polymer or by degradation of the polymer over time. Existing controlled-release systems are in several forms, such as, oral tablets, polymer implants and polymer microspheres or nanospheres. There are two commercially available polymer devices for constant drug release. One is a biodegradable wafer named Gliadel® [55] that is the first commercially available brain cancer treatment to delivery chemothererapy directly to the tumor site. The other is ReGel® [56]which is a patented drug delivery system developed to deliver active agents systematically or locally for one to six weeks. It is excellent for a wide range of active drugs.

Transdermal delivery is another method for the sustained release of drug. Several delivery systems were designed specifically for transdermal delivery, for example, transdermal patch and transdermal reservoir systems with adhesive layer by which the delivery system is stuck on the surface of skin. Drugs will diffuse through the skin continuously into the body. However, there is a time lag between the drug application and establishing the constant drug concentration in the bloodstream. Only a limited number of drugs can be diffused into the skin without any enhancer and external stimuli. Detailed discussion will be presented in section 2.4.

2.3.1.2 Pulsatile Release

The examples presented in the preceding section are designed to release drugs at constant rate. In some cases, sustained release is not the optimal method of drug delivery. Instead, delivering the drugs as pulse functions is a preferred method and this is the so-called pulsatile release. This delivery method works better in certain cases because it closely mimics the way in which the human body naturally produces some compounds. Insulin is a well-known example of a compound secreted by the body in a pulsatile manner [53].

Many previous works on the method of achieving the pulsatile release are focused on developing polymers that respond to external stimuli, such as, changing pH, changing of an electric field, an magnetic field, or exposure to an ultrasound signal [57-58].

Transdermal delivery, a typical delivery method for sustained release, also can be modified to produce pulsatile release in the presence of a low voltage (iontophoresis) high voltage pulses (electroporation) and ultrasound signals (sonophoresis).

2.4 Transdermal Drug Delivery Technologies

Transdermal delivery may be defined as the delivery of drugs through intact skin to reach the systemic circulation in sufficient quantity to administer a therapeutic dose [59]. During last two decades, transdermal drug delivery has received increasing attention in the face of growing awareness that drugs administered by conventional methods are frequently ineffective and excessively toxic. On the contrary, transdermal drug delivery offers many advantages over conventional drug delivery methods namely.

1. Avoids the passage of drugs through the stomach and intestine
2. Decreases the gastrointestinal side effects
3. Reduces hepatic first pass metabolism
4. Extends duration of drug activity
5. Improves the bio-availability
6. Decreases the dose to be administrated
7. Increases the patient compliance

Although transdermal delivery is the ideal method as compared with other conventional methods, the outmost layer of the skin provides a major challenge for this technology. Figure 2.6 shows the cross-sectional view of the skin structure [60]. There are two major layers: epidermis layer (about 0.06-0.8 mm) and dermis layer (typically 3-5 mm) [59]. The enormous barrier properties are attributed to the stratum corneum the outmost layer of the skin. The passive transdermal delivery occurs mostly through the lipid bilayers of the stratum corneum as indicated by a dotted line in Figure 2.7 [61]. It is called the intercellular route. The ordered structure of the intercellular lipid bilayers confers a low permeability to the skin. So effective enhancing methods are needed to achieve aqueous pathways across the stratum corenum as shown in the continuous line, which is called the

transcelluar route. Many approaches are available and divided into two groups: invasive methods and non-invasive methods.

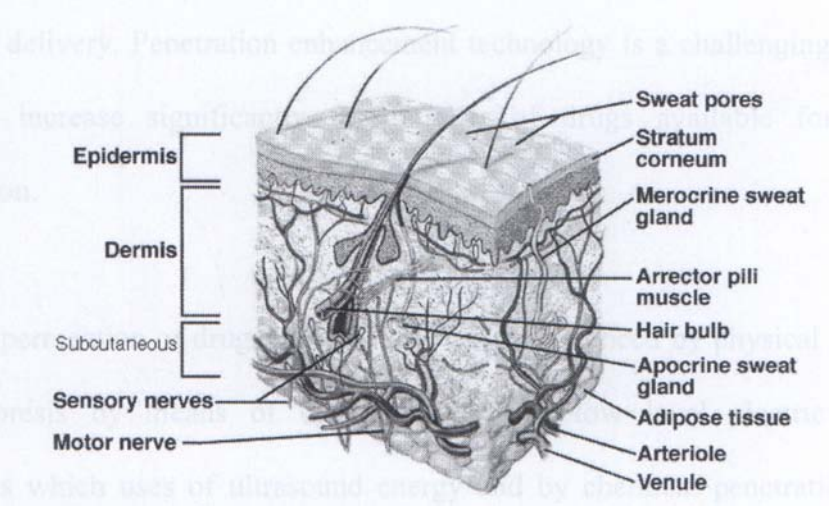

Figure 2.6. Cross-sectional view of human skin structure [60]

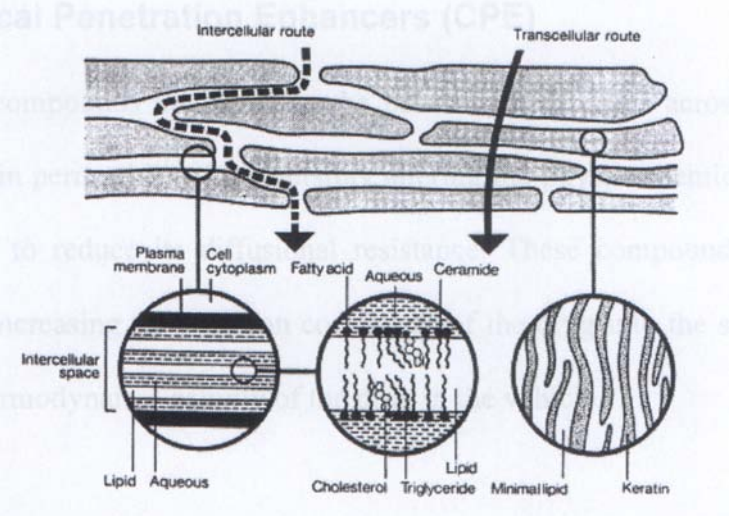

Figure 2.7. Possible micro routes of drug penetration through human skin intercellular and transcellular [61].

2.4.1 Enhanced Transdermal Drug Delivery

Transdermal drug delivery is the administration of therapeutic agents through intact skin for a systemic effect. Currently there are about eight drugs marketed as transdermal patches. Since skin is an excellent barrier for drug transport, only potent

drugs with appropriate physicochemical properties (low molecular weight, adequate solubility in aqueous and non-aqueous solvents, etc.) are suitable candidates for transdermal delivery. Penetration enhancement technology is a challenging development that would increase significantly the number of drugs available for transdermal administration.

The permeation of drugs through skin can be enhanced by physical methods such as iontophoresis by means of the application of low level electric current and sonophoresis which uses of ultrasound energy and by chemical penetration enhancers, which will be discussed in the following sections.

2.4.1.1 Chemical Penetration Enhancers (CPE)

CPE are compounds that enhance the permeation of drugs across the skin. The CPE increases skin permeability by reversibly altering the physicochemical nature of the stratum corneum to reduce its diffusional resistance. These compounds increase skin permeability by increasing the partition coefficient of the drug into the skin and also by increasing the thermodynamic activity of the drug in the vehicle.

CPE in general, promote drug diffusion by disturbing the structure of the stratum corneum and/or deeper layers. The specific mechanism can fall into one of the three categories [62]:

1. Disruption of the highly ordered structure of intercellular lipid channels.
2. Interaction with corneocyte intracellular protein components.
3. Enhanced partitioning of the drug in the presence or absence of the enhancer compound.

2.4.1.2 Iontophoresis

Iontophoresis is one strategy devised to facilitate transdermal drug delivery. Iontophoresis can be described as a process that transfers the ionic species including charged molecules by the application of electric current [63]. The route of entry is through the pores, the sweat glands, and the hair follicles. Additionally, in the present of the electric current, the electric resistance of the skin will decrease, allowing further water-soluble drugs passive diffusion through the skin. The skin will act as a drug reservoir extending the release into deeper layers of the skin after the iontophoresis device is removed (Figure 2.8).

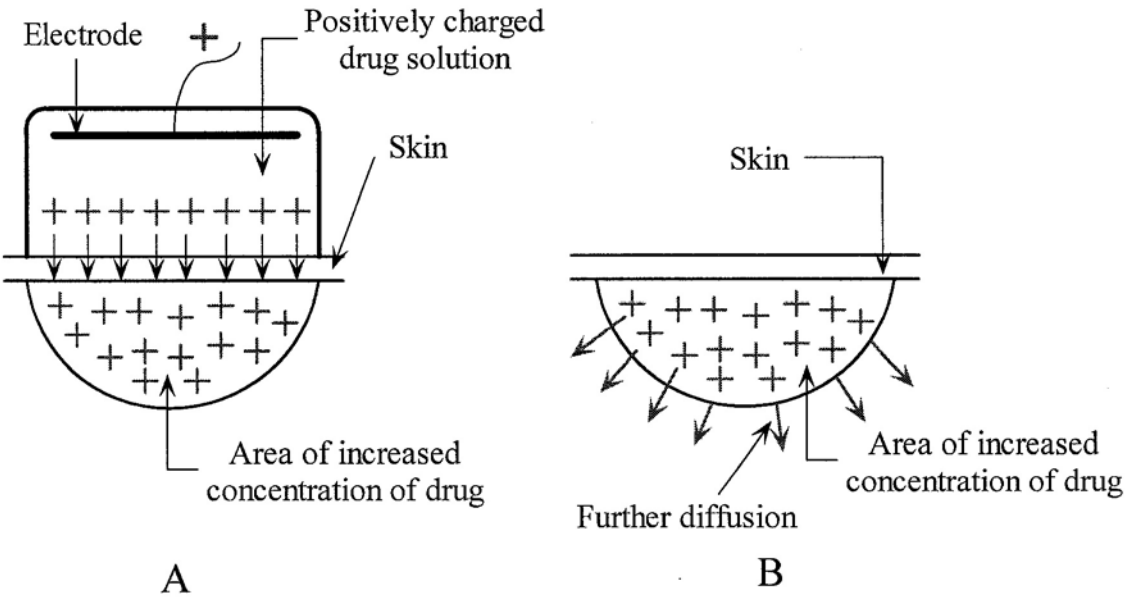

Figure 2.8. **A.** Schematic drawing of the basic theory of iontophoresis. **B.** The skin will act as a drug reservoir extending the release into deeper layers of the skin after the iontophoresis device is removed.

An iontophoresis device consists of (1) the power source, a low voltage direct current generator; (2) lead wires consisting of a positive lead and negative lead and (3) electrode, with an attached drug reservoir and a ground electrode (Figure 2.9) [64]. The

basic principle is that electricity can move different ions. When a direct current activates the electrode, cations move toward the negative electrode and anions move toward the positive electrode. The electrical current will drive the ions through the skin. The quantity of ions that are made to cross the skin barrier is directly proportional to the current density, application time and molecular weight.

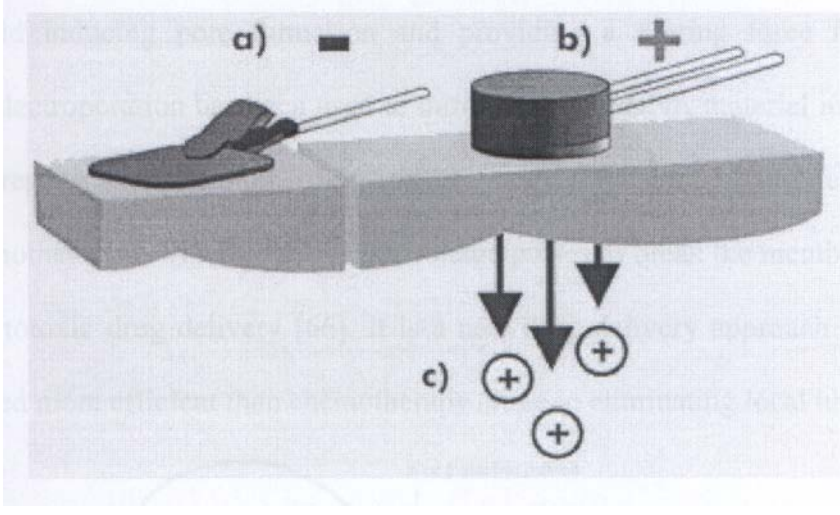

Figure 2.9. Electrode system applied to the skin surface. a). Negative electrode. b). Positive electrode with drug reservoir containing positively charged ions. c). Positive ions are forced through the stratum corneum by applying positive current [64].

The major advantage of iontophoresis is the control that provides over the drug input kinetics and the ability to customize drug input rates that can be optimized for a given patient. Although iontophoresis is an attractive technology for drug delivery, only low molecular weight (<8000 daltons) and water-soluble drugs can be delivered with low efficiency.

2.4.1.3 Electroporation

Electroporation also called electropermeabilization is the transitory structural perturbation of lipid bilayer membranes due to the application of high voltage pulses [7].

This phenomenon occurs in different kinds of lipid membranes. Hence, electroporation has been used for different applications. Electrical exposure typically involves electric field pulses that generate transmembrane potentials of approximately 1 V and last for 10 μs to 10 ms [7]. Reversible electrical break down and high molecular transport are observed, resulting from structural rearrangements of the cell membrane. It is hypothesized that the rearrangements consist of temporary aqueous pathways, with the electric field inducing pore formation and providing a driving force for molecular transport. Electroporation has been used to introduce some DNA material in to cells [65]. One interesting application of tissue electroporation (Figure 2.10) is electrochemotheraphy, which applies high voltage pulses to break the membrane of tumor cells for cytotoxic drug delivery [66]. It is a new drug delivery approach that has been demonstrated more efficient than chemotherapy alone in eliminating local tumors [67].

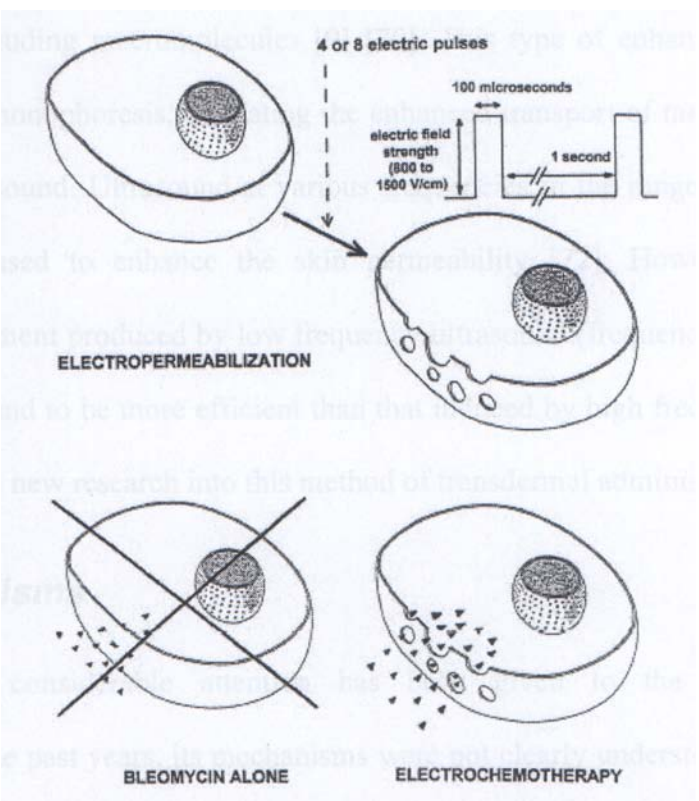

Figure 2.10. Mechanisms of electrochemotherapy. Cell electropermeabilization and use of cytotoxic nonpermeant drugs [66].

A major issue in the clinical application of transdermal drug delivery by electroporation is its effect on the skin and underlying tissues. A sensation or pain during electroporation has been reported, due to the current applied on the skin that causes a direct excitation of underlying nerves and muscles [68-69]. When the pulse rate, duration or voltage increases it tends to enhance levels of sensation. Indeed, during the high voltage pulses application to the skin, the immediate effect shown is the marks of the electrodes that will disappear after a few minutes. Current research evidence in electrochemotherapy shows that the patients did not require special pain control as the bearable pain dissipated immediately after application of the electric pulses.

2.5 Ultrasound Enhanced Transdermal Drug Delivery

Application of ultrasound has been shown to enhance transdermal transport of various drugs including macromolecules [9] [70]. This type of enhancement is termed sonophoresis or phonophoresis, indicating the enhanced transport of molecules under the influence of ultrasound. Ultrasound at various frequencies in the range of 20 kHz to 10 MHz has been used to enhance the skin permeability [72]. However, transdermal transport enhancement produced by low frequency ultrasound (frequency is less than 100 kHz) has been found to be more efficient than that induced by high frequency ultrasound [8] [9]. This led to new research into this method of transdermal administration.

2.5.1 *Mechanisms*

Although considerable attention has been given to the investigation of sonophoresis in the past years, its mechanisms were not clearly understood, reflecting the fact that several phenomena may occur in the skin upon ultrasound exposure. These include:

1. Cavitation

2. Thermal effects
3. Convector transport
4. Mechanical effects

Currently, significant attention has been devoted to understand the mechanisms of low frequency sonophoresis. Accordingly, if one can identify the dominant phenomena responsible for sonophoresis, a better selection of ultrasound and surrounding conditions can make this technology much more effective.

2.5.1 .1Cavitation

A sound field in a liquid may generate small bubbles whose motions bring about drastic effects such as chemical reactions, erosion, emission of light, and radiation of sound. These observable effects are characteristic of a physical phenomenon called acoustic cavitation [73], which occurs in water, organic solvents, biological fluids, molten metals as well as other fluids.

There are two types of cavitation stable or transient that have been involved in low frequency sonophoresis. Stable cavitation usually involves small amplitude oscillations about an equilibrium radius. Stable cavitation of a medium containing dissolved or entrained gas occurs when a bubble oscillates for a number of cycles without collapsing. Transient cavitation, on the other hand, involves much more variations in the bubble's size over a few acoustic cycles and this rapid growth usually terminates in the collapse of varying degree of violence. Transient cavitation occurs during the compression phase, in media that experience a tension stress during a portion of the rarefaction phase of the acoustic disturbance [74].

Cavitation may cause damage of biological materials in several ways. For transient cavitation, when it collapses, the maximum pressure generated would be about 10^{10} bar and the maximum temperature would be about 4×10^{4} times of the ambient temperature. The high-pressure shock waves that emanates from the location of the bubble have the capability to cause mechanical damage of the surrounding material. While, the violent stable cavitation could cause steady flow of the fluid medium surrounding the bubble named microstreaming [75]. If the microstreaming velocity is large enough, shear stress could be sufficient to damage the cell.

In low frequency sonophoresis, using acoustic spectroscopy, stable and transient cavitation has been quantified [76-77]. It is found that the strong role of low frequency sonophoresis is caused by transient cavitation. The dependence of transient cavitation on ultrasound intensity was found to be similar to that of conductivity enhancement [76-77]. According to Mitragotri and Kost [78], transient cavitation may have three mechanisms to enhance the skin permeability as shown in Figure 2.1 1. In Figure 2.1 1 (A), a spherical bubble produces shock waves that could potentially disrupt the stratum corneum when it collapses. However, the amplitude of the shock waves drops rapidly with distance. Figure 2.11 (B) shows that microjet may cause the change of the lipid bilayer of the stratum corneum without penetration. Figure 2.11 (C) shows that microjet induced by bubble collapsing near the surface of the stratum corneum that may physically penetrate the skin and change the structure. Specifically, there exists a threshold energy for stable and transient cavitation. The behavior of cavitation threshold values is summarized as follows [74].

1. Cavitation activity increases with increasing acoustic intensity.
2. Cavitation threshold increases with increasing frequency.

3. Cavitation threshold increases with increasing ambient pressure.
4. Cavitation threshold decreases with increasing gas content in liquid.
5. Cavitation threshold decreases with increasing liquid temperature.
6. Cavitation threshold increases with increasing liquid viscosity.

Currently, the effect of spherical collapses as well as microjets on the skin permeability enhancement has been studied. It is concluded that both types of cavitation events might be responsible for the low frequency sonophoresis [78].

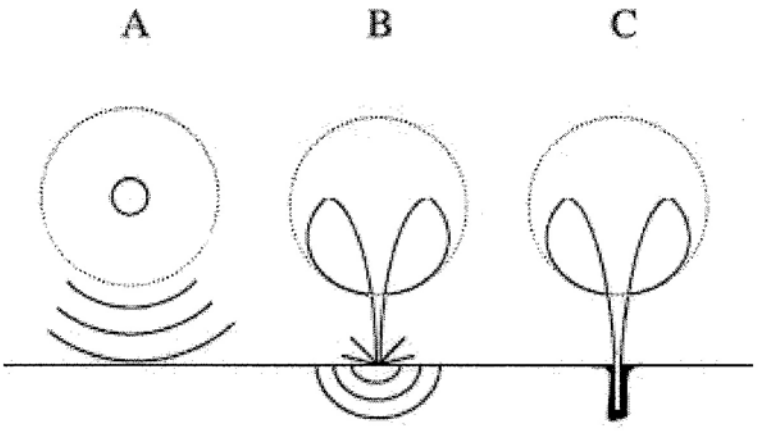

Figure 2.11. Three possible modes through which inertial cavitation may enhance SC permeability. (A) Spherical collapse near the SC surface emits shock waves, which can potentially disrupt the SC lipid bilayers. (B) Impact of an acoustic microjet on the SC surface. The microjet possessing a radius about one tenth of the maximum bubble diameter impacts the SC surface without penetrating into it. The impact pressure of the microjet may enhance SC permeability by disrupting SC lipid bilayers. (C) Microjets may physically penetrate into the SC and enhance the SC permeability [78].

2.5.1.2 Thermal Effect

The acoustic parameters of biological tissues are described by velocity and attenuation coefficients. The energy of the ultrasonic beam is attenuated by its passing through the tissues. There are two main mechanisms by which the acoustic energy is lost, absorption and dissipation. In the different regions of tissue, the acoustic impedance is

different, which reflect the acoustic beam to varying extents and scatter energy out of the primary beam to surrounding material. Some of this energy will be absorbed and lead to temperature increase locally. It is known that in soft tissues the attenuation coefficient is approximately proportional to the frequency, high frequency acoustic beams are more attenuated than the lower frequency acoustic beams [74].

Ultrasound induced heat is expected to enhance the transdermal delivery of various drugs by increasing skin permeability, body fluid circulation, blood vessel wall permeability, and drug solubility. Generally, it is known that heat could increase the kinetic energy of the drug molecules and the proteins, lipids in the cell membrane. During low frequency sonophoresis, the local temperature increase will dilate penetration pathways in the skin, increase kinetic energy and the movement of particles in the treated area, and facilitate drug absorption.

However, the experimental results show that a temperature increase of 10 °C causes about 2-fold increase in the estradiol skin permeability. Because the typical skin temperature increase in the sonophoresis experiments is less than 7 °C, it can be concluded that thermal effects are not a significant phenomenon that could cause the 13-fold increase in estradiol skin permeability. Thus, the thermal effect cannot play an important role in sonophoresis [12].

2.5.1.3 Convective Effect

Fluid velocities are generated in porous medium exposed to ultrasound due to interference of the incident and reflected ultrasound waves in the diffusion cell and oscillations of the cavitation bubbles. Fluid velocities generated in this way may affect transdermal transport by inducing convective transport of the drugs across the skin,

especially through hair follicles and sweat ducts. Experimental findings suggest that convective transport does not play an important role in the observed transdermal enhancement [12].

2.5.1.4 Mechanical Effect

Ultrasound is a longitudinal pressure wave inducing sinusoidal pressure variations in the skin, which induce sinusoidal density variation. At the lower frequency, the density variations can grow into a gas or vapor bubble and produce the cavitation. At higher frequency (> 1MHz), the density variations occur so rapidly that a small gaseous nucleus cannot grow and cavitational effects cease. But other effects due to density variations such as generation of stresses because of density changes that ultimately lead to fatigue of the medium may continue to occur. These stresses can easily disrupt the structure of lipid bilayers, which result in an increase in the bilayer permeability. However, non-significant mechanical effects do not play an important role in higher frequency sonophoresis. Thus cavitation induced lipid bilayer disordering is found to be the most important cause for ultrasonic enhancement of transdermal transport [12].

2.5.2 *Bio-effect*

Ultrasound enhanced drug delivery is to deliver the drugs to the diseased tissue with ultrasonic irradiation. However, the interaction between an ultrasound wave and the tissue can be attended with deleterious biological effects, especially at high wave intensities and lower frequencies. The most deleterious non-thermal bioeffects are produced by acoustic cavitation. Pressure waves of high intensity are capable of rupturing blood vessels and tissues as a result of the formation and oscillation of cavities. It is found that these cavitation bubbles are responsible for hemolysis [79-81], hemorrhage [82], and DNA fragmentation [83]. Cavitation generation is a threshold process and significantly

depends on the presence of nuclei in the liquid. The more the quantity of nuclei in the liquid, the smaller the wave amplitude needed for cavitation generation. Like any natural liquid, blood has cavitation nucleation agents, and therefore sufficiently high-amplitude ultrasound pulses can cavitate it.

Previous research [84] has reported the data identifying cavitation thresholds for tissue. Encapsulated microbubbles, especially of very small size, can be considered as additional cavitation nuclei. The administration of microbubbles in blood should therefore decrease its cavitation thresholds and enhance the risk of biological damage [85-86]. Actually, hemolysis and hemorrhage generated by ultrasonically activated contrast agents was detected at moderate pressure amplitudes both in vitro [87-88] and in vivo [80-81].

2.5.3 Combined methods

While all these above-mentioned enhancers have been individually shown to enhance transdermal drug delivery, their combinations have been demonstrated to be more effective compared to each of them alone. Over the last ten to twenty years several papers have been published to support this. Specifically, the following combinations have been used for transdermal drug delivery (Figure 2.12 [89])

1. Chemicals + iontophoresis [90-91]
2. Chemicals + electroporation [92]
3. Chemicals + ultrasound [5] [93-94]
4. Iontophoresis + ultrasound [95]
5. Electroporation + ultrasound [96]
6. Electroporation + iontophoresis [97-98]

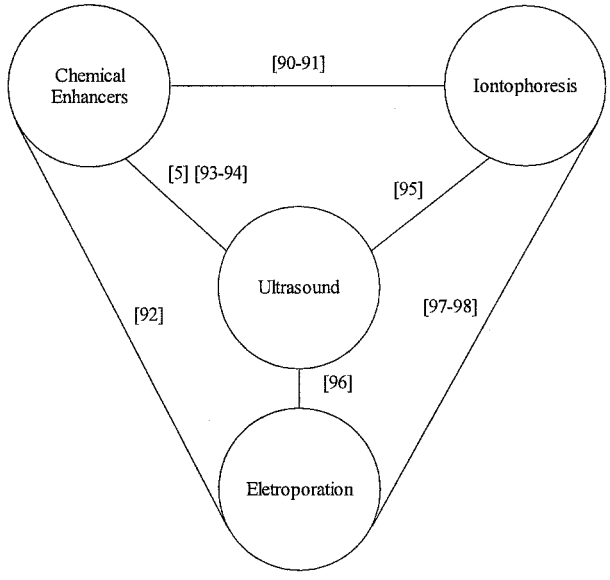

Figure 2.12. Various combinations of enhancers that have been studied. The four circles indicate the major enhancements that are used for transdermal transport, the lines indicate the various combinations that have been reported.

In addition to increasing transdermal transport, a combination of enhancers should reduce the severity of the enhancers required to achieve the desirable drug flux [89]. The enhancement induced by above-mentioned enhancers depends on their strength, the higher the strength, the higher the transdermal transport rate. But, high enhancement strength is always fraught with safety problems. By combining two more enhancers together, maybe this can reduce the strength of each enhancer. Table 2.1 and Figure 2.13 [89] show the features of each combination and the possible mechanisms for the combined enhancers.

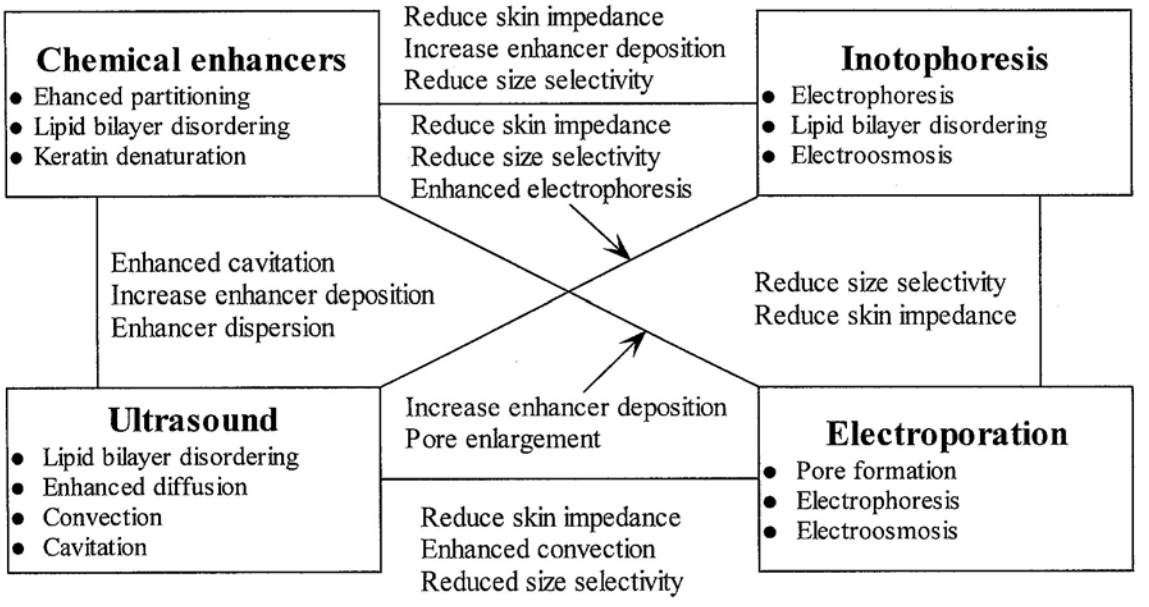

Figure 2.13. Possible mechanisms of various enhancers and their combinations [89].

Various enhancers including chemicals, electric fields, and ultrasound have been used to enhance transdermal drug transport . As an individual enhancer, the chemical one maybe faster than other individual enhancers, such as electric field and ultrasound. However, the chemical enhancer will cause potential safety problems with prolonged use because the chemical enhancer is also delivered into the human body at the same time with drug transportation and produces chemical concentration accumulation under the skin.

In addition to chemical enhancer, ultrasonic enhancer (sonophoresis) and electric field (iontophoresis) can also be used to enhance the delivery of drugs through the skin. Sonophoresis offers several advantages over iontophoresis. First, iontophoresis requires ionization of the substances to enhance delivery while sonophoresis does not. Second, ultrasonic wave produced during sonophoresis can penetrate much deeper into the tissue than iontophoresis does. Third, the drugs can reach their desired dosage level in the bloodstream faster than using iontophoresis to enhance delivery. Thus, sonophoresis

method for transdermal drug delivery is the best way among these methods. Although their combinations are significantly more effective compared to each of them alone, potential problems will be produced with the higher effectiveness. Table 2.1 has already elucidated the limitations of the various combinations. The common limitations are complex device and safety problems. So, what we should aim for is to use a single enhancer to enhance transdermal transport with a multifunction and user-friendly device.

Table 2.1 Features of various combinations.

	Advantages	Disadvantages
Iontophoresis + chemicals	Higher effectiveness than each of them alone and ease of application	1. Chemicals will be delivered deep into the skin and cause safety problems. 2. Complicated device.
Ultrasound + chemicals	Higher effectiveness and reduction of the required voltage/current to achieve the desired flux with ultrasound apllication alone	Relatively complex device compared to each of them alone.
Ultrasound + electroporation	Higher effectiveness and reduction of the required voltage/current to achieve the desired flux with ultrasound apllication alone	1. Relatively complex device compared to each of them alone. 2. Both of them are bilayer disrupting agents, thus cause their combination unnatural.
Iontophoresis + electroporation	Because of the difference between the mechanisms of action of both enhancer, the combination is natural	Relatively complex device compared to each of them alone.
Electroporation + chemicals	Higher effectiveness and the device requirements are not significantly different than those for electroporation alone	1. Chemicals will be delivered deep into the skin and cause safety problems. 2. Complicated device.
Ultrasound + iontophoresis	Higher effectiveness and reduction of the required voltage/current to achieve the desired flux with ultrasound apllication alone	1. Relatively complex device compared to each of them alone. 2. Both of them are bilayer disrupting agents, thus cause their combination unnatural.

2.6 Review of Existing Sonopohresis Devices

Research in the last two decades has dramatically increased the understanding of ultrasound and its effects on skin and transport of pharmaceutical agents. Many types of sonophoresis devices have been invented and patented. In this section, some typical

conventional sonophoresis devices are reviewed according to their different working principles and functions.

2.6.1 Disposable Piezoelectric Polymer Bandage Type

There are many types of polymeric materials, such as Polyvinylidene fluoride (PVDF), which exhibit piezoelectric effects and have the characteristic of being flexible rather than brittle, and in quantity are much less expensive than conventional piezoceramics [14]. A bandage type sonophoresis device that has the coupling between thickness and longitudinal mode in such piezoelectric polymers was invented by Fox [14]. Figure 2.14 (a) shows the detail structure of this type of device. The bandage member includes an annular element of the piezoelectric polymer operating in the thickness-longitudinal mode, and the central layers of piezoelectric polymers operating as bimorphs. The drug is stored in the annular body and central layers. The adhesive layer sticks the bandage member on the skin surface.

The basic concept of the operation is illustrated in Figure 2.14 (b). The annular polymer element pulls back and stretches the surface of the skin while the bimorph elements, operating at the same time, drive the drug into the enlarged pores. This action creates a number of conditions favorable to the enhanced passage of medicament through the skin surface [14]. Maybe it is possible to use external mechanical force to open and close the pores on the skin surface, but it only changes the outskirt dimension of the pores whose shape will be changed as shown in Figure 2.14 (b). Furthermore, the density and average dimension of pores are different from person to person, maybe it is difficult to use this device to maintain constant drug concentration in the bloodstream with various medical applications.

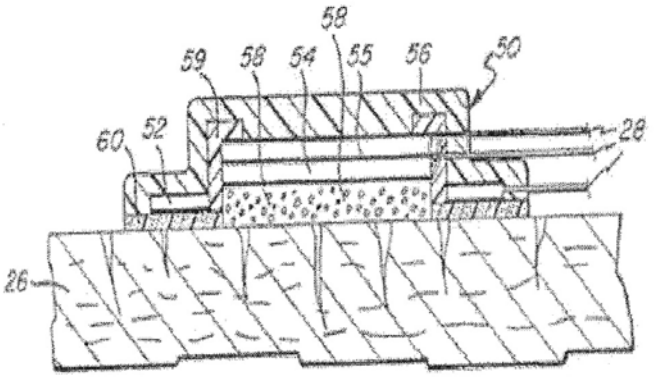

26- Skin
28- Electric wires
50- Bandage member
52- Annular polymer element
54- Bimorph elements
55- Biomorph elements
56- Cover element
58- Medicament composition
59- Annular body
60- Adhesive layer

(a)

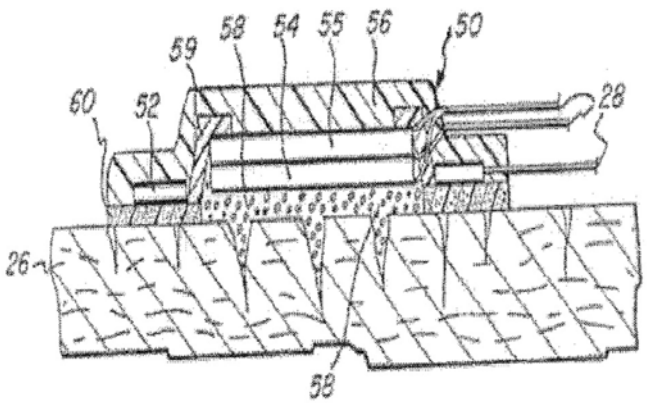

26- Skin
28- Electric wires
50- Bandage member
52- Annular polymer element
54- Biomorph elements
55- Biomorph elements
56- Cover element
58- Medicament composition
59- Annular body
60- Adhesive layer

(b)

Figure 2.14. (a). A schematic illustration view of a bandage type sonophoresis device and the pores and follicles of the skin. (b). A similar view of (a) after stretching of the underlying skin by the ultrasonic vibration [14].

2.6.2 *Active transdermal system with stimuli components*

In 1995, Lipkovker [16] invented a new and improved transdermal drug delivery system using ultrasonic wave to stimulate the nervous system of the skin. Accordingly, there are various paths that exist for drugs to move from the surface of the skin into the cell. One path is through the hair follicles and sweat glands to the capillary loops. Another path to the capillary loops is through the extracellular fluid that surrounds body cells. The third path is through inter and intracellular channels of cells. The primary path

for transdermally administrated drugs is through the follicles and glands, the next most significant path is the extracellular way [16]. Using ultrasonic pulses to excite or stimulate the nervous system of the skin, the stimulation causes both the dermal-epidermal junction membrane and the capillary endothelial joints to open so that the drugs can be moved through the skin.

The active transducer drug delivery system has a cone-shape structure that is made by two types of ultrasonic transducers: stimuli transducer and pumping transducers. The stimuli transducer is on the top of the cone, which has a flat, circular shape. The wall of the cone is defined by a number of transducer segments each of which forms a pumping transducer. Figure 2.15 [16] shows the cone-shaped ultrasonic assembly and its development. The resonance frequency of flat stimuli transducer is less than that of pumping transducers.

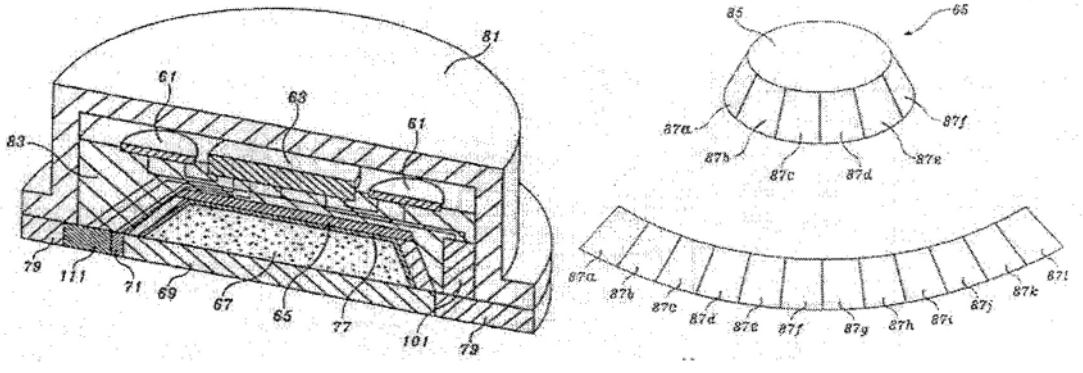

61- Power supply
63- Electronic control
65- Transducer assembly
67- Drug reservoir
69- Membrane
71- Temperature sensor
77- Drug impermeable laminate
79- Adhesive layer
81- Hat-shaped housing
83- Encapsulation material
85- Circular stimuli transducer
87a- 87i- Pump transducer segments

Figure 2.15. A cross-sectional, pictorial view of the ultrasonic transducer drug delivery system [16].

The control electronics apply ultrasonic stimuli pulses to the skin by energizing the stimuli transducer at low frequency ranging from 5 kHz to 1 MHz for a predetermined period of time (10-20 seconds). Between the stimuli pulse periods, the control electronics apply variable frequency signals to pumping transducer segments, the frequency of the ultrasonic pumping pulses lie in the 50 MHz to 300 MHz. And also, there are some short pulses between the stimuli pulse periods produced by the infrared (IR) emitter or laser emitter in order to improve the drug delivery effectiveness. The IR or laser emitter can improve the operation of the system by heating the skin to increase the blood flow. This causes the drug being delivered to dissipate faster through the body.

In essence, ultrasound is used by this new transdermal system to open the channels in the skin surface and then pushes the drug through the channels into the skin via stimulating the nervous system of the skin. According to its basic operation concept, the ultrasound application area should be large enough, which includes more nerve ends, sweat glands and hair follicles. However, the more nerves ends there are, the higher the sensitivity of the skin, and the system cannot apply higher ultrasonic energy to the skin, otherwise, there will be pain. Another limitation of this system is the manner in which the structure is constructed. The ultrasonic assembly has one stimuli transducer and many pumping transducer segments. All these segments work together with extra IR or laser pulses, the skin local temperature will rise fast. According to Lipkovker's investigation [16], 20 seconds ultrasonic pulse application will keep skin opening its dermal-epidermal junction membrane and capillary endothelial cell joints and pores for approximately 20 minutes. During this period of time, drug will continue to diffuse passively into the skin via the opened pores although the skin temperature sensor or the analysis sensor stops ultrasound application to the skin surface. The system cannot control the drug release

dose precisely. Furthermore, after the first use, the air or vacuum gap appears between the top stimuli transducer and drug liquid because the device does not have refilled channels, almost all the ultrasonic wave is reflected by this gap. There is not enough ultrasound energy applied to stimulate the skin nervous system, skin may not open its capillary channels for drug delivery. And also, with further use, the effective contact area between drug liquid and transducer segments becomes smaller and smaller, only part of the ultrasound energy produced by transducer segments is utilized for transdermal transport of the drug. The effectiveness of the system will decrease gradually.

2.6.3 *Transdermal Drug Delivery Device with Circulating System*

Transdermal drug delivery device with circulating system was invented by Shunro Tachibana in 1989 [99]. It is an endermic application device for external medicine that comprises a liquid retaining section, a pump for supplying drug from additional drug container to drug delivery container, a drug permeable layer attached to the drug delivery container to cover the bottom opening, and an ultrasonic oscillator located inside the drug delivery container (Figure 2.16).

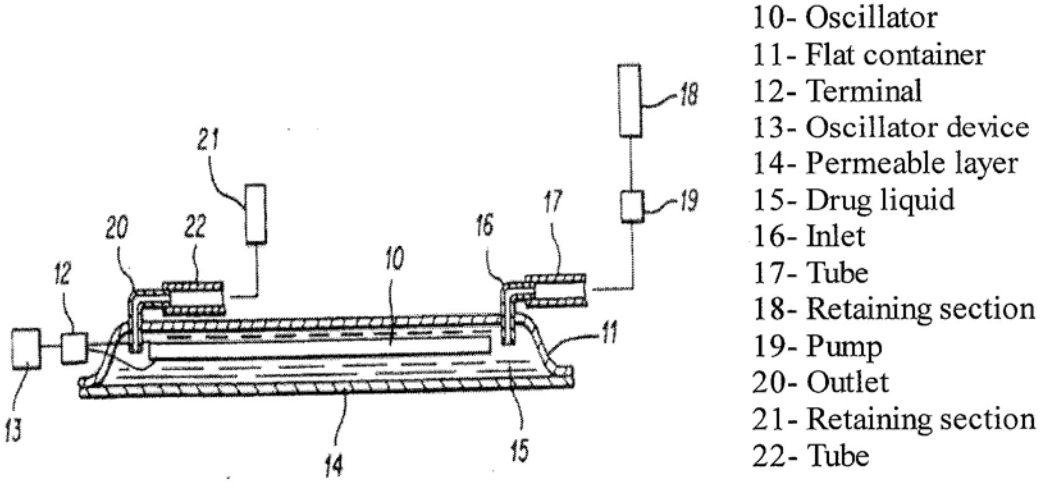

Figure 2.16. An explanatory cross-sectional view of a portable type endermic application kit [99].

Normally, the drug to be applied onto the skin is encompassed in a closed cavity, in which a pump and an additional drug container are utilized to apply the drug continuously to the drug delivery container and keep it full during the time the device is used. Also, it is possible to easily change concentration of the drug or applied to the patient, or change one drug to another drug without interruption of the operation. In addition to these two advantages, since the drug liquid flow through the drug delivery container, the ultrasonic oscillator is always cooled. As a result, a powerful ultrasonic oscillator can be used.

2.6.4 Transdermal Drug Delivery Device with Transfer Promoting System

It is well known art to employ ultrasound energy for affecting and enhancing the delivery of the drugs. And also, it has been found that certain foregoing and related objects can be combined to make a novel and even unexpected device.

Figure 2.19 shows a novel apparatus invented by Flanagan in 1991 [100]. The apparatus transfers the substances through the skin at a treatment site, which is promoted by the combined effects of ultrasonic energy and positive and negative pressure. The apparatus comprises two major chambers: interior chamber and surrounding annular chamber. The treating substance is supplied into interior chamber that is subjected to the positive pressure and ultrasonic energy. A piezoelectric bimorph is mounted on the wall of the interior chamber, which is adapted to vibrate at ultrasonic frequency when supplied with electric power and leads a flexible diaphragm to vibrate.

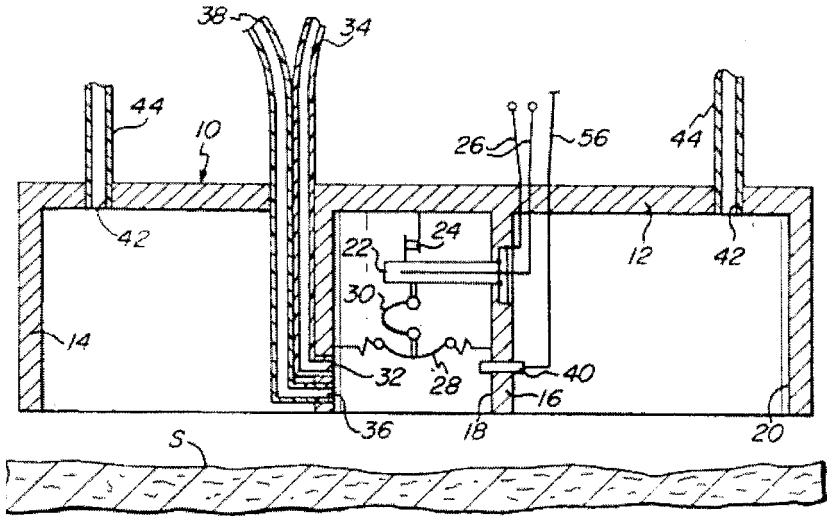

10- Device body
12- End wall
14- Cylindrical sidewall
16- Interior wall
18- Interior chamber
20- Annular chamber
22- Piezoelectric elements
24- Connecting elements
26- Leads
28- Diaphragm
30- Spring
32- Inlet port for nitrogen gas
34- Tube
36- Inlet port for drug liquid
38- Tube
40- Thermocouple
42- Apertures
44- Tubes
56- Transmission line

Figure 2.17. A diagrammatic view of a novel apparatus invented by Flanagan in 1991 [100].

The surround annular chamber whose four tubes connect to a vacuum source applies the vacuum negative pressure on the skin surface, which serves to stretch the skin and to increase the exposure surface and to open the pores, glands and follicles. Vacuumization is believed to generate a sub-epithelial force that draws the applied substance into the skin.

Actuation of the drug and nitrogen gas supply will cause the treating substance to be delivered under pressure to a zone of the interior chamber; actuation of the electric signal causes the piezoelectric bimorph and diaphragm to vibrate, which will subject the

central area to the ultrasonic energy. The combined effects of the applied gas pressure, the ultrasonic energy, and the maintained vacuum negative pressure may cause the delivered substance to permeate to the skin in a highly effective manner. However, the supplied pressure nitrogen gas will stay between the diaphragm and drug liquid resulting an acoustic impedance mismatched layer, which causes the ultrasonic energy to reflect back, and almost no ultrasonic energy is combined with other transfer promoting elements. This condition will cause the delivered substance to permeate the skin in a low efficient manner.

2.6.5 Transdermal Drug Delivery Device Using Multiple Frequency

In transdermal delivery, one frequency is preferably chosen to enhance the permeation of the substance through the stratum corneum layer of the skin. In general, tissue penetration is inversely proportional to the ultrasonic frequency [101]. Ultrasonic energy at a frequency chosen to maximize diffusion across the straturn corneum may not provide sufficient penetration to significantly enhance diffusion to the target underlying tissue [102]. It is limited in its ability to deliver a wider variety of drugs to the deeper layers of the skin. This limitation was identified by Shimada who provided a new concept to use multiple frequencies in one transdermal delivery device.

The method of Shimada's invention uses two or more distinct frequencies of ultrasonic energy simultaneously to enhance permeation of substance through the tissue below the outmost layer of the skin. By using multiple frequencies to control and enhance the diffusion allows the delivery of a large number of substances to the site to be treated.

This method can also decrease the time required to administer substances using diffusion and reduce the cost of administration.

As described above, ultrasonic energy is the key point for enhancing diffusion through the skin. Figure 2.18 shows the relative energy of two different frequencies, f_1 at 1 MHz and f_2 at 3 MHz, has a different axial energy that varies over the distance. The energy typically does not coincide and, as a result, the use of a multiple frequency system can provide a more uniform axial energy over a greater distance than a single frequency ultrasound system can. For example, at the distance 4, the energy of f_1 is 0% while the energy of f_2 still remains at about 80%. This graph shows the major advantage of this multiple frequency device in that deep penetration maybe possible due to the differences in axial energy as a function of axial distance.

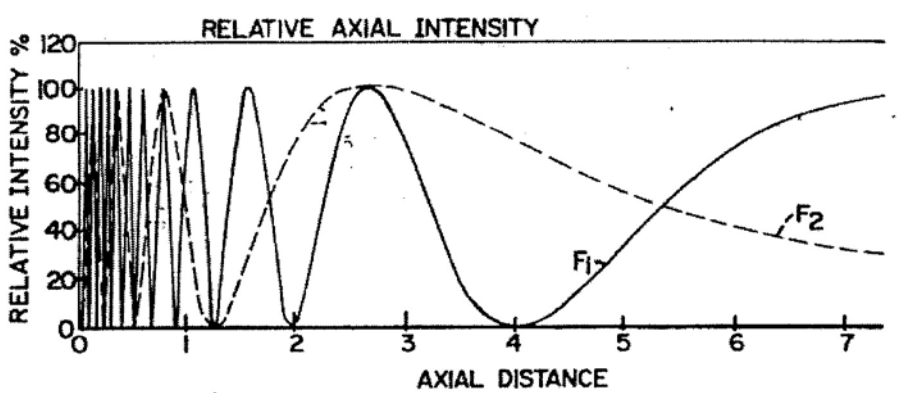

Figure 2.18. The relative axial intensity of the ultrasonic energy produced by a dual frequency ultrasound system as a function of axial distance [102].

Figure 2.19 shows the transdermal delivery device with an ultrasonic transducer that is mounted in a slide-type housing attached to a pouch. The transducer is backed by an insulating, acoustically reflective material that focuses the ultrasonic energy toward the treated area. The multiple frequency device in which the transducer is on the top of the

cavity, has a similar structure with reference [99]. However, when a single piezoelectric transducer is used to generate multiple frequencies, only one operating frequency is fundamental resonance frequency and the others are sub-harmonic frequencies resulting in potentially low energy transformation efficiency. The whole device requires a large amount of power to achieve suitable penetration enhancement and most of the electric energy is converted into heat that makes the temperature rise rapidly.

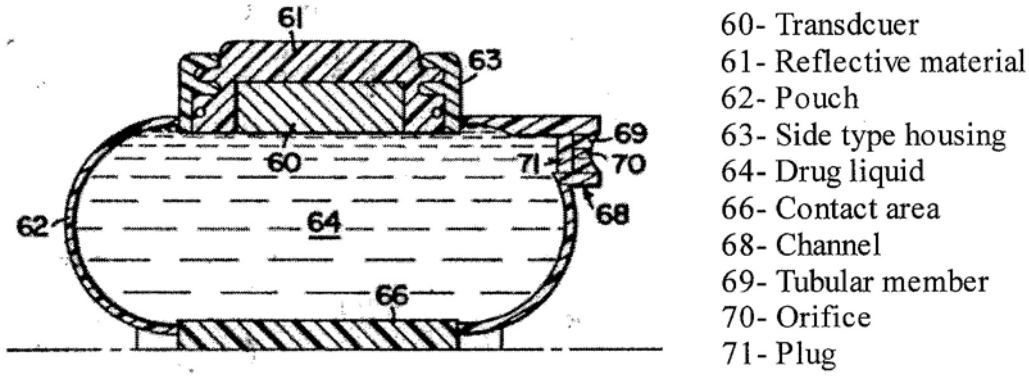

Figure 2.19. A schematic illustration of the apparatus [102].

2.6.6 *Sonophoresis Device with Controlled-release and Recover Function*

The basic structure of the sononphoresis device with controlled-release and recover function is given in Figure 2.20 [17]. It consists of three parts: an ultrasonic skin-conditioning device, a constant volume flexible sleeve and a power supply.

The ultrasonic skin-conditioning device comprises a piezoelectric transducer in a plastic housing and connecting wire. The piezoelectric transducer is designed to operate at two frequencies. In the range of 15 kHz to 25 kHz, the transducer operates at one of sub-harmonic frequencies of its natural resonance frequency. The low-frequency

ultrasonic pressure waves are applied to the skin of sufficiently high intensity to cause cavitation in the skin that disorders the skin lipid bilayers and enhances the transdermal transport of the medicaments. At the megahertz frequency range, the transducer operates at its natural resonance frequency. Ultrasonic waves generate very short wavelength vibration in the keratin fibers and surrounding lipid bilayer to augment the body's natural function to reestablish the order of the lipid bilayers in the stratum corenum, and seal the body against further permeation [17].

Another feature of this sonophoresis device is to control the penetration depth of the therapeutic agents using a particular ultrasonic burst width. Bock [17] found that the depth of penetration of therapeutic agents for a certain frequency is proportional to the burst width of this frequency. So his suggestion was "when a burst is terminated and the ultrasonic pressure waves are stopped, the molecules passing through the passageways will also stop" [17]. Previous study [11] indicated that ultrasound-induced cavitation disorders the structure of lipid bilayer and causes the skin electrical resistance to decrease, which forces the skin to lose its barrier function temporarily. Moreover, the temporal losing barrier function cannot be recovered as long as the ultrasonic waves are stopped.

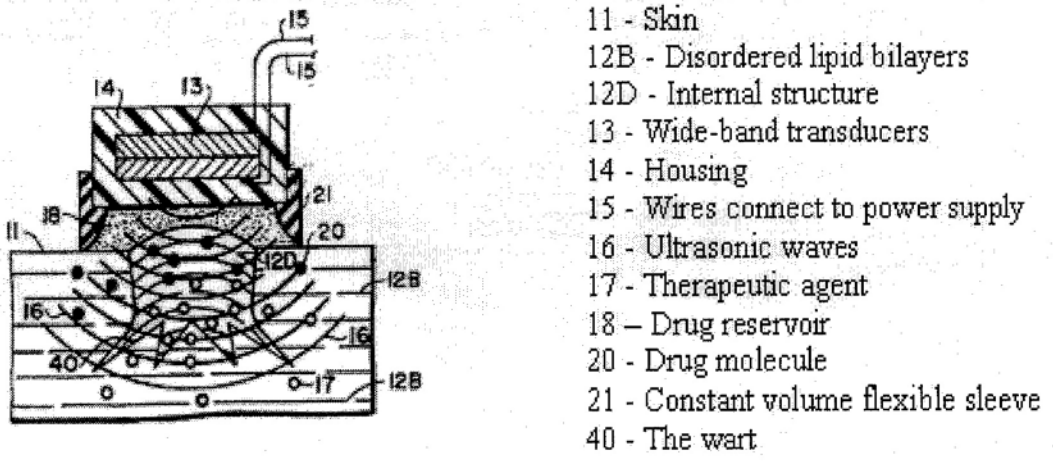

Figure 2.20. A diagrammatic view of the sonophoresis device with controlled-release and recover function [17].

2.6.7 *Sonophoresis Device with Focused Ultrasound Beam*

Application of low-frequency ultrasound appears to induce cavitation inside as well as outside the skin and disorganize the stratum corneum lipid bilayers thus enhancing transdermal transport. Transdermal transport enhancement induced by ultrasound increases with increasing ultrasound pressure amplitude. However, application of high ultrasound intensity is prohibited by the discomfort associated with it. The device described in Figure 2.21 [20] [103] provides a new method to utilize low-frequency ultrasound for enhancing transdermal transport.

The ultrasound transducer is made hemispherical shaped and defines the drug cavity, as shown in Figure 2.21 (A). The radius of curvature of the transducer is designed to focus the ultrasound beam to an area around 10 mm in diameter on the surface of the skin. Focused ultrasound beam can also be achieved by using array of transducers as shown in Figure 2.21 (B). The transducer array consists of multiple individual transducers arranged to form a hemispherical wall. Each transducer of the phased array is individually activated and the whole device is operated in the range of 20 kHz to 200 kHz. Thus, the number of pain receptors within the ultrasound application site decreases as the application area decreases. The application of ultrasound to a small area will produce less sensation and will allow higher ultrasound intensity to be administrated on the skin surface with a little pain or discomfort.

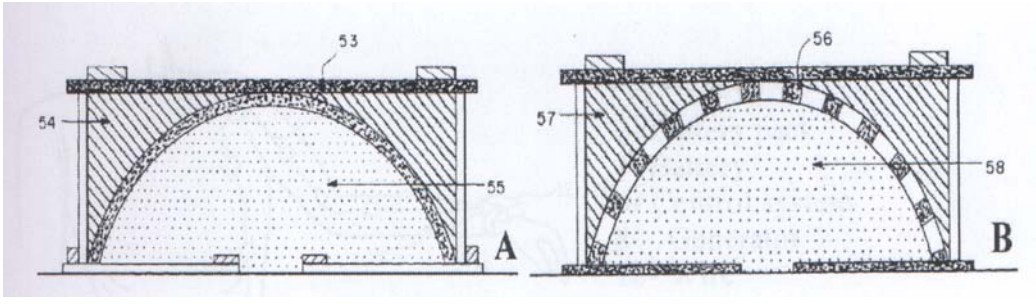

53- Hemi-spherical transducer
54/ 57- Backing material
55/ 58- Coupling medium
56- Array consists of multiple individual transducers

Figure 2.21. (A). A schematic view of an ultrasound chamber with a hemi-spherical transducer, (B). A schematic view of an ultrasound chamber with an array of transducers arranged hemi-spherically [20] [103].

2.6.8 Sonophoresis system with feedback phase-tracking loop

As shown in Figure 2.22 [104], the sonophoretic drug delivery system comprises a power source, a control system, at least one high frequency generator, an acoustic transmission line, and a wide-band ultrasound transducer.

The feedback-phase loop is designed to ensure that the frequency of the wide-band transducer matches the frequency of the amplified input signal [104]. The feedback-phase loop senses the response of the transducer to the frequency of the amplified signal and locks in a frequency to give the maximum match. This feedback-phase loop may avoid the under-utilization of the amplified electrical signal and also avoid the additional electrical power converting into heat.

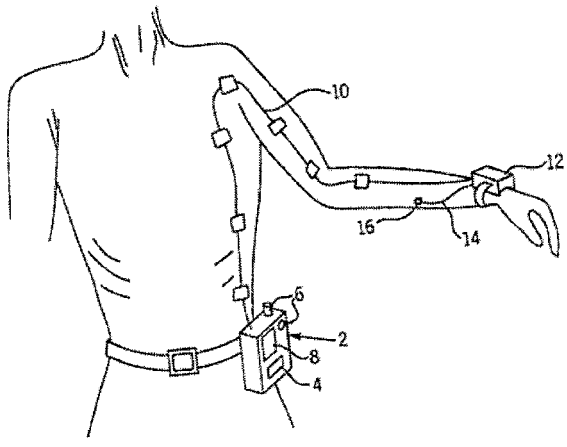

2- Battery pack
4- Battery
6- Control system
8- Generator
10- Wire
12- One transducer
14- Acoustic transmission line
16- Drug reservoir

Figure 2.22. A patient wearing the sonophoretic drug delivery system [104].

The acoustic transmission line relative to the transducer contacts the skin directly. When a drug reservoir is used, the end of the transmission line may contact the drug reservoir that in turn contacts the patient's skin. The major application of the acoustic transmission line is for sanitary purposes. It is necessary to discard and replace the transmission line and drug reservoir after transferring the drug. The acoustic transmission line can lead the ultrasound energy to any place on the surface of the body. The drug reservoir can be made into different shapes and sizes to adapt to the different sites, which the ultrasound transducer is placed at a fixed place, such as on the wrist.

2.6.9 Standing wave type sonophoresis device

All previous work using ultrasound to enhance permeation and mass transport through the skin are based on ultrasonic traveling wave technology. However, "traveling waves do not enhance mass transport of the interstitial fluids. High velocity gradients exhibited by a standing wave sound field can provide enhanced mass transport specifically at the boundary layer and at air-fluid interface within the structure of skin" [18].

According to Elstrom, standing waves differ from traveling waves in radiation force and the radiation force generated by a standing wave is larger than that produced by a traveling wave [18]. So there are several advantages of using standing waves in enhancing skin permeability and mass transport. First, the energy required for enhancing skin permeability is less than that required for traveling waves. Second, a standing wave uses significantly less intensity but effectively to produce the necessary permeability and mass transport effects [18]. Finally, the acoustic effect of standing waves can be localized within the stratum corenum whereas the low frequency waves tend to penetrate deeply into skin significantly beyond the stratum corenum.

In short, the sonophoresis device uses a surface acoustic wave device to generate the standing waves with the stratum corenum region as a means for enhancing permeability and mass transport across the skin. However, the mechanism still remains unclear.

2.6.10 Sonophoresis Device with Floating Mass Transducer

For transdermal drug delivery, sonophoresis is usually achieved using piezoelectric ultrasound transducer that is mechanically coupled to the drug or drug reservoir device. Piezoelectric ultrasound transducers generally operate only on a single primary frequency, thus limiting the ability to change the frequency for different applications or change the frequency during the course of a single procedure with a particular patient. According to their option, it would be desirable to provide sonophoresis drug delivery systems which allow the frequency to be changed for different purposes in a single procedure. If a piezoelectric transducer does not work at its first resonance frequency, it is relatively inefficient, which can result in excessive power consumption

from electric power. Additionally, piezoelectric transducer requires relatively high voltage for excitation.

Ball et al. designed a new sonophoresis device with a floating mass transducer as shown in Figure 2.23 [19]. The floating mass transducer includes a magnet disposed inside a housing. The magnet generates a magnetic field and is capable of movement within the housing. A coil is mounted in the housing, unlike the magnet, the coil cannot move within the housing. When an alternating current is provided to the coil, the coil will generate an alternative magnetic field that interacts with the magnetic field of the permanent magnet, causing the magnet and housing to vibrate relative to each other. This vibration of the housing is transferred to the drug or drug reservoir device to enhance the permeation of the skin.

The advantages of this sonophoresis device with a floating mass transducer are as follows. First, the driver may be oscillated at a wide of range of frequencies depending on the frequency of the electrical driving signal which is applied to the coil. Additionally, the coil magnet oscillatory driver of this device may be programmed to operate at different frequencies at different periods during the treatment. Last, the oscillatory assembly of this sonophoresis device can be fabricated at relatively low cost, provide for efficient conversion of electrical energy into mechanical energy, provide a relatively large amplitude compared to piezoelectric transducer, and furthermore operated at a lower voltage.

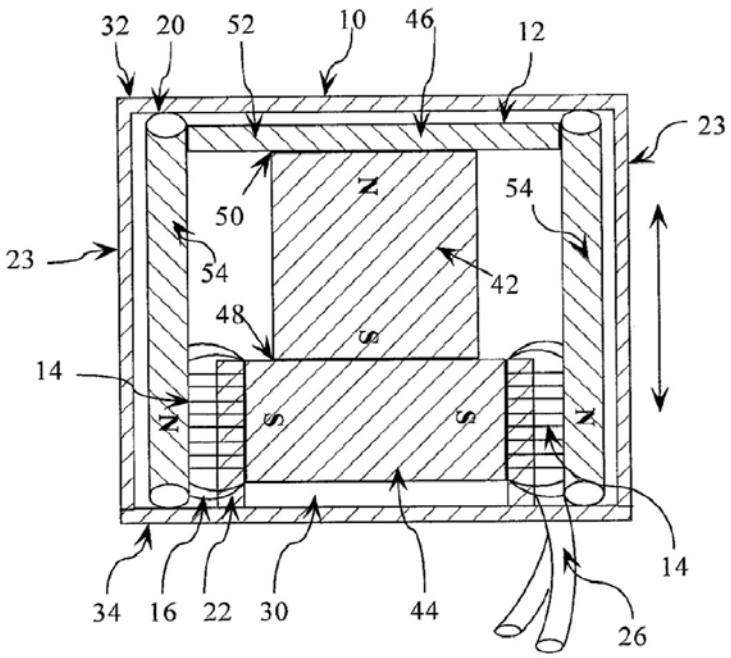

10- Housing
12- Magnetic assembly
14- Coil
16- Air gap
20- Silicone button
22-Interior wall
23- Outer wall
26- Wires
30- Air space

32- First face
34- Second face
42- Permanent magnet
44- First cylindrical pole piece
46- Second pole piece
48/ 50- End
52- Bottom of second pole piece
54- Parallel wall of second pole piece

Figure 2.23. A pictorial view of the sonophoresis device with floating mass transducer [19].

The applications of this sonophoresis device are based on the structure and material. The device can be made into cylindrical capsule shape having a diameter in the range from 0.5mm to 4 mm and a thickness in the range from 2mm to 4mm, and is made from biocompatible material such as titanium. Thus, the device can be implanted, semi-implanted or stick on the skin surface with pump/micropump, drug reservoir, flowing tubes, and electrical power, as shown in Figure 2.24 (a), (b) and (c).

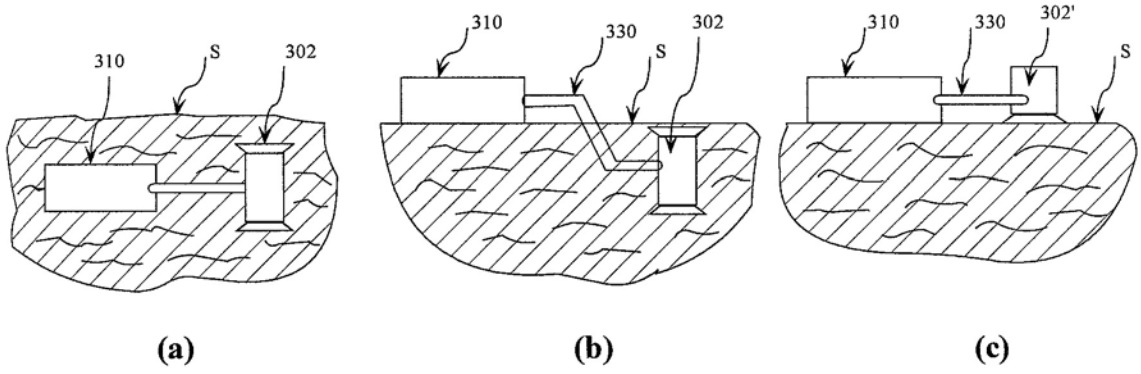

302 / 302' - First enclosure; 310 - Second enclosure; 330 - Connector; S – Skin.

Figure 2.24 (a) (b) (c). Applications of the sonophoresis device with floating mass transducer [19].

2.6.11 Horn Type Sonophoresis Device

The SonoPrep® device shown in Figure 2.25 consists of a battery operated power and control unit, a hand piece containing the ultrasonic horn and the disposable coupling medium cartridge, and a return electrode [105]. It is a hand-held device that allows a user to enhance the skin permeability through a brief application of low frequency ultrasound. The ultrasound frequency of 55 kHz is applied to the skin using a liquid coupling medium that mediates the disorganization of the lipid-bilayer of the stratum corneum via cavitation. The device contains a unique feedback technology that monitors changes in the permeability of the stratum corneum in a painless manner without causing skin irritation.

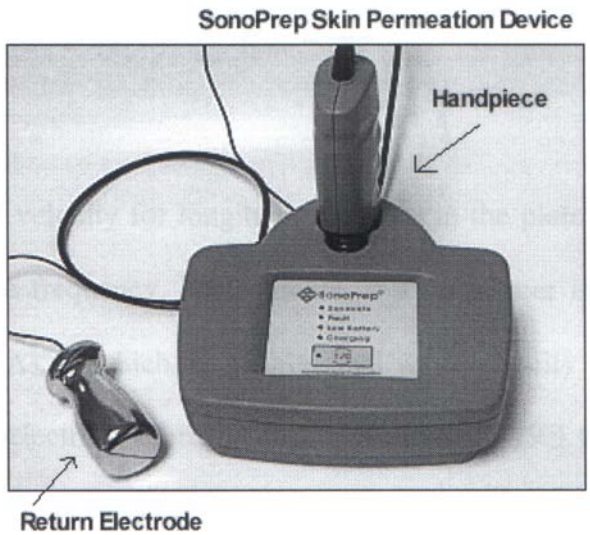

Figure 2.25. SonoPrepB Skin Permeation Device [105].

2.7 Limitations of Existing Sonophoresis Devices

Based on this literature review, it is found that most of the sonophoresis devices consist of four major parts: ultrasound transducer assembly, drug reservoir, electric power signal, and control system. Almost all the devices are based on two basic concepts: stimulating the skin nervous system to open the pores or using ultrasonic energy to disrupt the skin structure temporarily to make the aqueous channels. Despite the difference in design, fabrication technology and device components used, the existing sonophoresis devices have the following common shortcomings.

2.7. 1 Large physical size and heavy weight

Current sonophoresis technology uses low frequency ultrasound ranging from 20 to 100 kHz and the piezoelectric material is operated in the axial direction. The thickness, t_{piezo} of the piezoelectric material is simply defined as:

$$t_{piezo} = \frac{v}{2f_1} \tag{2.1}$$

Where, v is the sound velocity for longitudinal waves in the plate material, and f_1 is the fundamental resonance frequency. For example, if a transducer is made from zirconate piezoceramics (PZT-5A), in which the longitudinal wave velocity is about 3880 m/s, the thickness of the piezoelectric material is in the range from 19.4 to 97.0 mm. Thus, the transducer becomes large in physical size and the corresponding weight of the device also increases.

On the other hand, the conventional sonophoresis device is constructed of a converter and a horn section. The converter is made up of a stack of piezoelectric disks designed to vibrate in an axial direction. This so-called horn type device, although it is quite efficient at producing permeation enhancement, is typically about 150 to 200 mm long and weighs as high as one kilogram. These large and heavy devices are cumbersome and obviously would not be desirable for wearable applications.

2.7.2 *Power consumption*

There is another type of conventional sonophoresis transducer device which does not have converter and horn section. It only relies on one or a small number of piezoelectric disks that vibrate in a simple axial mode. This is the second type of sonophoresis device called disk type device. Although the sonophoresis transducer can be relatively small and lightweight, it is generally not operated at its fundamental resonance frequency and thus it is very inefficient. It requires a large amount of power to achieve suitable permeation enhancement. Moreover, even if a suitable high power source is available to use with a disk type device, there may be a serious problem with heat

generation. Much of the energy used by a sonophoresis transducer operating in an axial vibration and non-resonant mode is converted into heat. When the amount of power required is too high relative to the size of the device, it becomes so hot that can cause scald.

2.7.3 Low efficiency

The drug reservoir, such as hemi-spherical shaped [20] [103] or truncated-cone shaped drug reservoir [16], is large enough to contain drug liquid for prolonged use. The ultrasound transducers are mounted on the top and around the reservoir as shown in Figure 2.26.

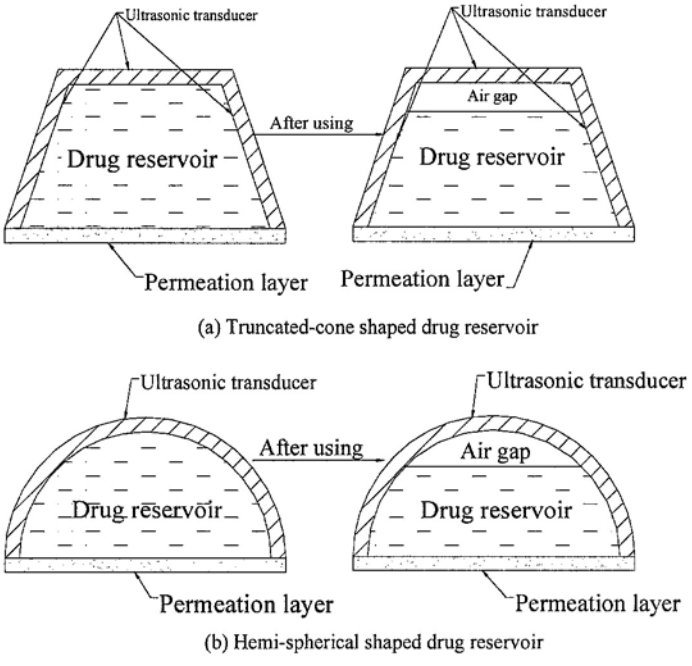

Figure 2.26. Structures of conventional large drug reservoir and ultrasound transducer.

Air gap will exist in the drug reservoir when the drug is discharged. The ultrasound reflection coefficient, R_{coeff} is expressed as:

$$R_{coeff} = \frac{(Z_1 - Z_2)^2}{(Z_1 + Z_2)^2} \tag{2.2}$$

Where, Z_1 and Z_2 are the characteristic impedance of ultrasound transducer and air, respectively. If the air gap exists, Eq. (2.2) gives rise to 99.99% reflection coefficient. Most of ultrasound energy is reflected back by the air gap and thus very limited ultrasound energy will be applied on the skin surface. The insufficient ultrasound energy could not change the skin structure effectively to enhance the skin permeability. For the energy produced by ultrasound transducers surrounding the drug reservoir, only the energy emitted from the effective contact area can produce transdermal transport effect. Moreover, the effective contact area reduces with respect to the duration in use. The ultrasound energy is not adequate to enhance the transdermal delivery if the effective contact area is reduced significantly. This will result in remnant of drug liquid left in the reservoir (i.e. “dead” drug solution).

2.8 Summary

The background knowledge and advantages of FEA have been briefly reviewed in this chapter. Several commercial FEA softwares such as PZFLEX™, ATILA™ and ANSYS™ are available to provide the analyses of the electromechanical modeling. Many types of ultrasound transducers with different boundary conditions and assumptions have been modeled and analyzed using FEA methods. In this study, it was decided to use ANSYS™ for the structural analyses of the flat flextensional ultrasound transducer.

Techniques in drug delivery, ultrasound, and its application in transdermal drug delivery have also been reviewed in this chapter. It was found that the enhancement of transdermal transport induced by ultrasound varies from a few percent to several orders of

magnitude [8-9, 12]. Low frequency ultrasound of less than 100 kHz has been found to be the most effective in enhancing the transdermal transport. As compared to the other enhancing methods such as iontophoresis or electroporation, sonophoresis has the following advantages:

1. Not immunologically sensitizing
2. Not ionizing the drugs
3. Ideal for the delivery of both low and high molecular weight drugs

On the other hand, the efficacy of low frequency ultrasound in enhancing the transdermal transport of drugs can be increased synergistically with the addition of the chemicals. Synergistic effects were also observed when ultrasound is combined with iontophoresis or electroporation. However, combination increases the complexity of the drug delivery devices. In this study, only ultrasound effects were considered to be used for drug delivery application.

In considering the types of ways to generate the ultrasound, some substantial selections have to be undertaken since there are many types of ultrasound transducers available. The emphasis on ultrasound enhanced drug delivery allows the research project to be restricted but some consideration such as future developments must be made. For this reason the types of transducers have been narrowed down to:

1. Piezoelectric transducers
2. Magnetostrictive transducers

In comparison with magnetostrictive transducers, piezoelectric transducers are more efficient and structurally simple than their counterparts. Thus, in this study, piezoelectric transducer was selected to generate ultrasound for drug delivery application.

The literature which concerned sonophoresis devices has also been reviewed in order to determine the current state of the art of the techniques used in sonophoresis devices and to provide a reference point for the original work which is undertaken in this study. The investigation of the conventional sonophoresis devices found to be limited by:

1. Large physical size and heavy weight
2. High power consumption
3. Low efficiency

In order to overcome or minimize the shortcomings of the conventional sonophoreis devices, the objective of this study is to develop a new ultrasonic transducer device for drug delivery application, which is not only aimed in achieving simple structure and light weight but also to generate high ultrasonic energy with low power requirement to enhance the drug delivery rate with high efficiency.

In the next chapter, the characteristics of the flat flextensional ultrasonic transducer are discussed in light of the potential use in ultrasound enhanced drug delivery. The acoustic field induced by dual flat flextensional transducers is analyzed in order to find a solution to increase the output acoustic intensity and reduce the power requirement simultaneously.

CHAPTER THREE
FLAT FLEXTENSIONAL ULTRASOUND TRANSDUCER

In the preceding chapter, the limitations of conventional sonophoresis devices have been illustrated. In order to overcome the shortcomings, in this chapter, two new methods of using flat flextensional transducer for ultrasound enhanced drug delivery are presented. The feasibility of the flat flextensional transducer for ultrasound enhanced drug delivery is discussed. The theoretical analysis of the acoustic field produced by dual flat flextensional transducers is studied in this chapter.

3.1 New Method 1: Using Flat Flextensional Transducer for Ultrasound Enhanced Drug Delivery

Flextensional transducers were first developed in the 1920s and have been used as underwater transducers since 1950s [106]. They consist of an active piezoelectric or magnetostrictive drive element and a mechanical shell structure. The shapes of the shell of the flextensional transducers are categorized into seven types as shown in Figure 3.1 [107]. However, all these flextensional transducers have quite complex structures and fabrication processes, which are difficult to be used as portable or wearable sonopohoresis devices.

An ideal ultrasonic transducer should be simple enough to be integrated with a control system and a drug reservoir to form the sonophoresis device that can be

positioned on the arm or waist. The flat flextensional ultrasound transducer, which is often used as ultrasonic distance or obstacle sensors and transducers for telephonic application [108], produces a vibrating flexible action in response to an electrical voltage signal rather than a simple expansion and contraction action. As compared to the traditional seven classes of flextensional transducers, the structure and fabrication process of the flat flextensional transducer are very simple, easy and inexpensive for mass-production.

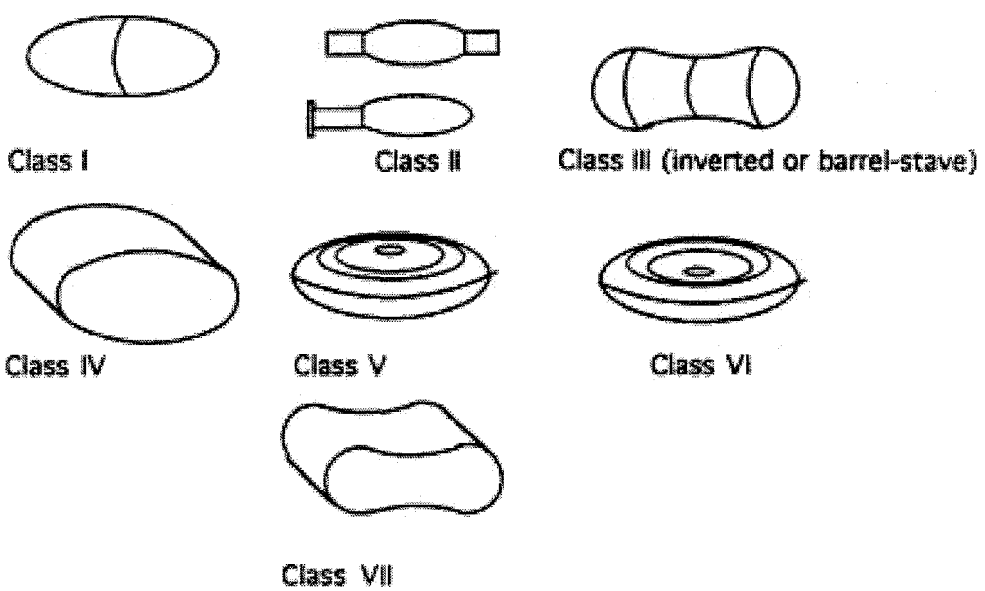

Figure 3.1. Seven classes of flextensional transducers for underwater application [107].

Flat flextensional transducers have various designs. A typical flat flextensional transducer, in its simplest form, comprises at least one circular vibrating plate bonded to at least one piezoelectric material disk layer, which is sometimes referred to as a unimorph as shown in Figure 3.2 (a). Multiple layers of vibrating plates or piezoelectric layers may also be used. The construction of one vibrating plate sandwiched between two piezoelectric layers is referred to as a bimorph as shown in Figure 3.2 (b). When a flat flextensional transducer is driven electrically with the field parallel to the poling

direction, the piezoelectric material expands axially in proportion to the material's piezoelectric longitudinal coefficient (d_{33}). In addition, the lateral dimension contracts as a function of the piezoelectric transverse coefficient (d_{31}). The lateral contraction is amplified and transferred to the axial direction through the flexible vibrating plate. This results in an addition of d_{33} and d_{31} effects. In general, the flat flextensional transducer is usually supported at the periphery and vibrates at its flexure vibration mode as shown in Figure 3.2 (c).

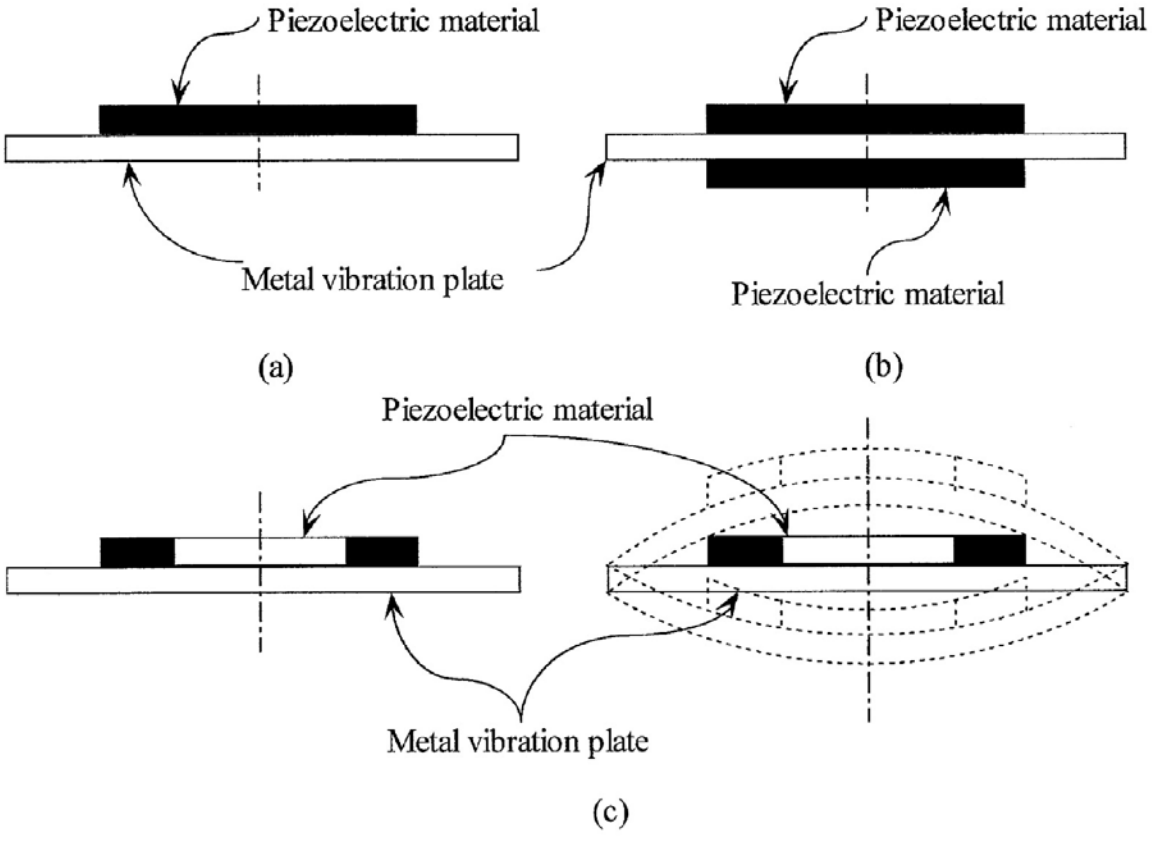

Figure 3.2. Simplest form of flat flextensional transducers. (a). Unimorph (b). Bimorph (c). Schematic drawing and vibration mode of a flat flextensional transducer.

Thus, the flexible vibrating plate converts and amplifies the small radial displacement of the disk into a much larger axial displacement normal to the surface of the vibrating plate. When operated underwater this contributes to a much larger acoustic pressure output than that produced only by piezoelectric materials [109]. Arising from the literature review in section 2.5.1.1, more acoustic cavitation, which is the main role to enhance the drug transportation rate, would be induced when higher acoustic pressure is generated underwater at the fixed ultrasonic frequency. For these reasons, the flat flextensional transducer was decided to be used for ultrasound enhanced drug delivery application in this study.

3.2 New Method 2: Using Dual Flat Flextensional Transducers for Ultrasound Enhanced Drug Delivery

3.2.1 Introduction

Arising from the literature review, in most of drug delivery applications the device has to operate at around its fundamental resonance frequency to provide sufficient acoustic power. Since the dimensions of an ultrasound transducer inside a sonophoresis device is smaller than the acoustic wavelength in water at the resonance, it has low radiation resistance and relative high reactance, which means that the transfer of radiated acoustic power from surface of the transducer to the water is inefficient. Generally, the radiation resistance is proportional to the radiating surface area of the ultrasound transducer. Enlarging the radiating surface increases its physical size resulting in enhanced radiated acoustic power. But these poor radiation characteristics often call for high electric power for the device to work. The downside to this is it may result in mechanical fracture and fatigue, heat generation and depolarization [110]. Furthermore,

this will pose a safety concern to patients when the device is applied in such a manner. Thus, it is necessary to develop a new ultrasonic device that could generate higher acoustic power with lower required electric power.

3.2.2 Acoustic intensity induced by dual flat flextensional transducers

Many acoustic sources can be treated as a combination of point monopoles that radiate the acoustic waves that are only a function of the radial distance from the acoustic source. The analytical method presented here can be extended to more complicated acoustic sources.

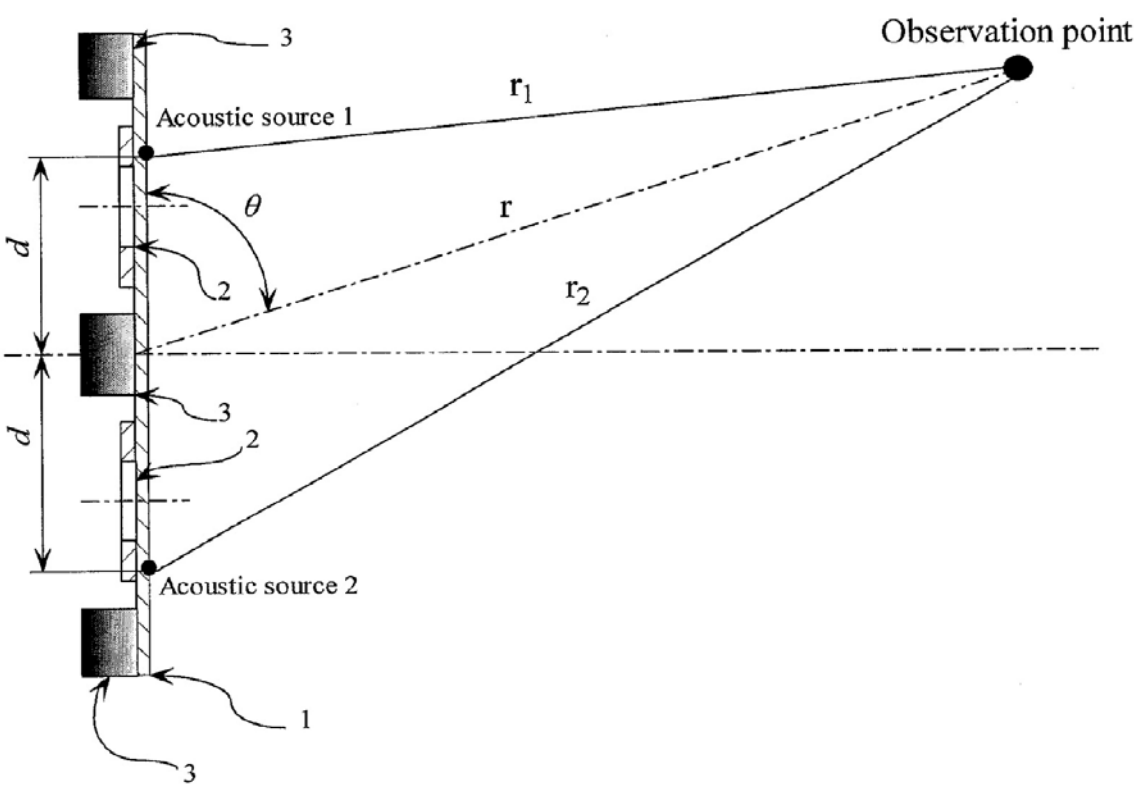

1- Stainless steel vibrating plate, 2- Piezoelectric ring, 3- Stainless steel body.

Figure 3.3. Two point monopoles on the surface of the two flat flextensional transducers.

Consider two point monopoles separated by a distance of $2d$ on the surfaces of two flat flextensional transducers as shown in Figure 3.3. The total of velocity potential $\phi(r,t)_{sum}$ for two point monopoles is the sum of the individual velocity potentials. Thus,

$$\phi(r,t)_{sum} = \phi(r_1,t)_1 + \phi(r_2,t)_2 \tag{3.1}$$

Where $\boldsymbol{r}$ is the distance from the center point of two acoustic sources to the observation point, $\boldsymbol{t}$ is time and r_1 and r_2 are the distances from acoustic source 1 and 2 to the observation point respectively. According to the law of cosine, r_1 and r_2 could be expressed as:

$$r_1 = \sqrt{r^2 + d^2 - 2rd\cos\theta} \tag{3.2a}$$

$$r_2 = \sqrt{r^2 + d^2 + 2rd\cos\theta} \tag{3.2b}$$

If the observation point is in the far field $(r>>d)$, then Eq. (3.2a) and (3.2b) can be approximately redefined as:

$$r_1 = r - d\cos\theta \tag{3.3a}$$

$$r_2 = r + d\cos\theta \tag{3.3b}$$

In general, the velocity potential, $\boldsymbol{\phi(r,t)}$, of the point monopole is the function of source strength and it is expressed as:

$$\phi(r,t) = -\frac{Q(t)}{4\pi r} e^{-jkr} \tag{3.4}$$

Where ***k*** is the wave number and defined as $k = \frac{\omega}{c_0}$. *Q(t)* is the source strength of the point monopole that defined as the surface area times the surface velocity of the point monopole. Substituting Eq. (3.4) and (3.3) into Eq. (3.1) yields:

$$\phi(r,t)_{sum} = -\frac{Q(t)_1}{4\pi r_1} e^{-jkr_1} - \frac{Q(t)_2}{4\pi r_2} e^{-jkr_2} \tag{3.5}$$

If r, r_1 and r_2 are very large, then $r_1 \approx r_2 \approx r$. Therefore, in the expression $\phi(r_1,t)_1$ and $\phi(r_2,t)_2$, $r_1 = r_2 = r$. However, it is necessary to maintain the expressions for r_1 and r_2 in the complex exponential expressions for each acoustic source in order to account for the time difference when two acoustic waves travel from two acoustic sources to reach the observation point. Thus Eq. (3.5) is rewritten as:

$$\phi(r,t)_{sum} = -\frac{Q(t)_1}{4\pi r} e^{-jk(r-d\cos\theta)} - \frac{Q(t)_2}{4\pi r} e^{-jk(r+d\cos\theta)} \tag{3.6}$$

If the acoustic sources are two harmonic point monopoles, in Eq. (3.6), $Q(t)_1$ and $Q(t)_2$ can be expressed as:

$$Q(t)_1 = Q_1 e^{j\left(\omega t + \frac{\varphi}{2}\right)}$$
$$Q(t)_2 = Q_2 e^{j\left(\omega t - \frac{\varphi}{2}\right)} \tag{3.7}$$

Where φ is the total phase angle between two point monopoles. Substituting expressions of $Q(t)_1$ and $Q(t)_2$ in Eq. (3.7) into Eq. (3.6) and yields:

$$\phi(r,t)_{sum} = -\frac{Q_1 e^{j(\omega t - kr)}}{4\pi r} e^{j\left(kd\cos\theta + \frac{\varphi}{2}\right)} - \frac{Q_2 e^{j(\omega t - kr)}}{4\pi r} e^{-j\left(kd\cos\theta + \frac{\varphi}{2}\right)} \tag{3.8}$$

Noting that

$$e^{\pm j\left(kd\cos\theta + \frac{\varphi}{2}\right)} = \cos\left(kd\cos\theta + \frac{\varphi}{2}\right) \pm j\sin\left(kd\cos\theta + \frac{\varphi}{2}\right)$$ and let then **Eq. (3.8)**

becomes

$$\phi(r,t)_{sum} = \frac{Q_1 e^{j(\omega t - kr)}}{4\pi r}\left[(1+Q)\cos\left(kd\cos\theta + \frac{\varphi}{2}\right) + j(1-Q)\sin\left(kd\cos\theta + \frac{\varphi}{2}\right)\right] \tag{3.9}$$

The velocity potential can be related to the acoustic pressure, p, and the particle velocity, u, using the following expression

$$p = -\rho_0 \frac{\partial \phi}{\partial t} = z_0 u \tag{3.10}$$

Where, z_0 is called characteristic acoustic impedance. ρ_0 is equilibrium density. Substituting Eq. (3.9) into (3.10) yields the acoustic pressure and the particle velocity in the acoustic and geometric far field.

$$p(r,t)_{sum} = \frac{Q_1 jkz_0 e^{j(\omega t-kr)}}{4\pi r}\left[-(1-Q)\sin\left(kd\cos\theta+\frac{\varphi}{2}\right)+j(1+Q)\cos\left(kd\cos\theta+\frac{\varphi}{2}\right)\right] \tag{3.11}$$

$$u(r,t)_{sum} = \frac{Q_1 jke^{j(\omega t-kr)}}{4\pi r}\left[-(1-Q)\sin\left(kd\cos\theta+\frac{\varphi}{2}\right)+j(1+Q)\cos\left(kd\cos\theta+\frac{\varphi}{2}\right)\right] \tag{3.12}$$

Acoustic intensity is defined as the time-averaged rate of energy transmission through a unit area normal to the direction of propagation [111]. Since the signals associate with the present discussion are harmonic and $p(r, t)_{\text{sum}}$ and $u(r, t)_{\text{sum}}$ are complex quantities, the intensity can be expressed as:

$$I(r)_{sum} = \frac{1}{2}\text{Re}\left[\left(\tilde{p}(r,t)_{sum}\,\tilde{u}(r,t)^{*}_{sum}\right)\right] \tag{3.13}$$

Where, $\tilde{p}(r,t)_{sum}$ and $\tilde{u}(r,t)_{sum}$ represent the complex numbers of $p(r, t)_{\text{sum}}$ and $u(r, t)_{\text{sum}}$ respectively and $\tilde{u}(r,t)^{*}_{sum}$ is the complex conjugate of $u(r, t)_{\text{sum}}$. Thus, acoustic intensity in the acoustic far field is written as:

$$I(r)_{sum} = \frac{Q_{1(rms)}{}^2 k^2 z_0}{16\pi^2 r^2}\left[(1+Q)^2\cos^2\left(kd\cos\theta+\frac{\varphi}{2}\right)+(1-Q)^2\sin^2\left(kd\cos\theta+\frac{\varphi}{2}\right)\right]$$

$$= \frac{Q_{1(rms)}{}^2 k^2 z_0}{16\pi^2 r^2}\left\{1+Q^2+2Q\left[\cos^2\left(kd\cos\theta+\frac{\varphi}{2}\right)-\sin^2\left(kd\cos\theta+\frac{\varphi}{2}\right)\right]\right\} \quad (3.14)$$

$$= \frac{Q_{1(rms)}{}^2 k^2 z_0}{16\pi^2 r^2}\left[1+Q^2+2Q\cos\left(2kd\cos\theta+\varphi\right)\right]$$

And the acoustic intensity for each point monopole is expressed as:

$$I(r)_1 = \frac{Q_{1(rms)}{}^2 k^2 z_0}{16\pi^2 r^2}$$

$$I(r)_2 = \frac{Q_{2(rms)}{}^2 k^2 z_0}{16\pi^2 r^2} \quad (3.15)$$

So if two point monopoles have the same source strength ($Q_{1(rms)} = Q_{2(rms)}$), the ratio of acoustic intensity radiated from two point monopoles divided by the acoustic intensity from a single point monopole is

$$\frac{I_{sum}}{I} = 2+2\cos\left(2kd\cos\theta+\varphi\right) \quad (3.16)$$

According to above equation, if two acoustic sources are in phase ($\varphi = 0$) and kd is very small (i.e. $kd \to 0$), then the total radiated acoustic intensity is four times the intensity of a single point monopole of equal source strength. For this case ($kd \to 0$), it is indicated that the two point monopoles already combine together resulting in a point monopole with double source strength. On the other hand, at $\theta = 90^o$ (along the center

line in Figure 3.3), the radiated acoustic intensity of the two point monopoles is always four times the intensity of a single point monopole of equal source strength.

For another case, when the observation point is very near to the two point monopoles ($r \ll d$), this observation point is considered to be placed in the geometric near field. For ultrasound enhanced drug delivery application, generally the ultrasound transducer is placed 1 to 5 mm above the diffusion membrane, so it is necessary to determine the interference effects of point monopoles in the geometric near field.

As shown in Figure 3.3, in the geometric near field, Eq. (3.3) is not suitable for simplifying Eq. (3.2). The sum of the acoustic pressure of two point monopoles now is written as

$$p(r,t)_{sum} = jkz_0 \frac{Q_1 e^{j\left(\omega t - kr_1 + \frac{\varphi}{2}\right)}}{4\pi r_1} + jkz_0 \frac{Q_2 e^{j\left(\omega t - kr_2 - \frac{\varphi}{2}\right)}}{4\pi r_2} \tag{3.17}$$

And according to Eq. (3.13), the total acoustic intensity is given as

$$I(r)_{sum} = \frac{k^2 z_0}{32\pi^2}\left\{\frac{Q_1^2}{r_1^2} + \frac{Q_2^2}{r_2^2} + \frac{Q_1 Q_2}{r_1 r_2}\left\{e^{j\left[k(r_1-r_2)-\varphi\right]} + e^{-j\left[(r_1-r_2)-\varphi\right]}\right\}\right\}$$

$$= \frac{Q_{1(rms)}{}^2 k^2 z_0}{16\pi^2}\left\{\frac{1}{r_1^2} + \frac{Q^2}{r_2^2} + \frac{2Q}{r_1 r_2}\left[\cos k(r_1-r_2)\cos\varphi + \sin k(r_1-r_2)\sin\varphi\right]\right\}$$

$$= \frac{Q_{1(rms)}{}^2 k^2 z_0}{16\pi^2}\left\{\frac{1}{r_1^2} + \frac{Q^2}{r_2^2} + \frac{2Q}{r_1 r_2}\cos\left[k(r_1-r_2)-\varphi\right]\right\} \tag{3.18}$$

Therefore, Eq. (3.15) and (3.16) are changed to

$$I(r)_1 = \frac{Q_{1(rms)}{}^2 k^2 z_0}{16\pi^2 r_1^2}$$

$$I(r)_2 = \frac{Q_{2(rms)}{}^2 k^2 z_0}{16\pi^2 r_2^2} \tag{3.19}$$

$$\frac{I_{sum}}{I_1} = r_1^2\left\{\frac{1}{r_1^2} + \frac{Q^2}{r_2^2} + \frac{2Q}{r_1 r_2}\cos\left[k(r_1-r_2)-\varphi\right]\right\}$$

When $r_1 = r_2$, Eqs. (3.20a) and (3.20b) are written as:

$$\frac{I_{sum}}{I_1} = \frac{I_{sum}}{I_2} = 1 + Q^2 + 2Q\cos\varphi \tag{3.21}$$

From Eq. (3.21), if the two point monopoles are in phase ($\varphi = 0$) and have the same source strength ($Q = 1$), it is clearly shown that the sum of the radiated acoustic intensity along the center line as shown in Figure 3.3 is always four times of the acoustic intensity generated by single point monopole.

Therefore, in the geometric near or far field, as long as the point of interest is placed on the center line of the acoustic structure as shown in Figure 3.3, the total radiated acoustic intensity is always four times higher than that produced by single point monopole. Extending this analysis to two flat flextensional transducers, it is concluded that the output acoustic intensity along the centerline normal to the surface of the transducer is increased four times, which provide more acoustic intensity to enhance the permeability than that of a single ultrasound transducer. Hence, if the effect of enhanced permeability and ultrasound application area remains unchanged, the required electrical power to operate the individual ultrasound transducer will reduce because of the dual ultrasound transducers induced constructive interference.

3.3 Summary

In this chapter, the characteristics of the flat flextensional ultrasonic transducer have been discussed. It was found that the flat flextensional transducer is more efficient to generate a larger axial displacement and higher acoustic pressure underwater than that of the piezoelectric disk transducer.

Two typical structures of the flat flextensional transducers namely unimorph and bimorph were described. In comparison with unimorph transducer, bimorph transducer

has more complex structure and may not be much suitable for drug delivery application due to the following reasons:

1. It is necessary to electrically insulate the piezoelectric material in the drug solution.
2. It is necessary to prevent the plumbum leakage into the drug solution.

In this study, the unimorph type of the flat flextensional transducer was selected for the development of sonophoresis device. It is the first effort to use the flat flextensional transducer for ultrasound enhanced drug delivery application.

Due to the poor radiation characteristic of a single transducer, another new device was first proposed based on the acoustic interference principle. It consists of dual flat flextensional transducers in one sonophoresis device. The detailed theoretical analysis of the acoustic field produced by the dual flat flextensional transducers has been investigated. Theoretically, it was found that the dual flat flextensional transducers have the capability to increase the output acoustic intensity and simultaneously reduce the required electric power.

The next chapter deals with the development of the finite element models, which is aimed to study the effects of materials' properties and dimensional changes on the performance of two newly proposed ultrasonic devices with flat flextensional transducers.

CHAPTER FOUR
FINITE ELEMENT ANALYSIS OF THE FLAT FLEXTENSIONAL TRANSDUCER

The development of new ultrasonic devices with a single and dual flat flextensional transducers for drug delivery application is presented in this chapter. The results of the finite element analysis of the flat flextensional transducers are described and compared with experimental results where possible. The effects of material properties and dimensional changes on the performance of the flat flextensional transducer are studied. In the last section of this chapter, the fabrication process of the new ultrasonic devices is briefly described.

4. 1 Introduction

The simplest structure of a flat flextensional transducer consists of a piezoelectric material bonded to a metal vibration layer. The preferred piezoelectric material comprises a piezoceramic or other piezoelectric materials such as piezoelectric polymers. The metal vibration layer serves as a mechanical transformer that transforms the high impedance and small extensional motion of the piezoelectric material into low impedance and larger flexural motion of the metal vibration layer. The selection of materials will depend on the particular intended applications. For the ultrasound enhanced drug delivery application, the bottom surface of the metal vibration layer in contact with medical solution or other chemicals is preferably made of a material that does not react with the liquid and resist the erosive effects that can be caused by

cavitation. Furthermore, the flexible metal vibration layer could be joined to the piezoelectric material in several ways such as riveting, encasement and adhesive bonding. Viewed from these points, if the flat flextensional transducers have the same physical size with different constructive materials or bonding conditions, the performances of the transducers will be different. On the other hand, various types of possible structures of the transducers could be developed to achieve the same intended applications. Thus, it is quite difficult to choose a better structure for the transducer.

Finite element analysis allows the designer to manipulate and test the effects of all the possible design variables using computer analysis rather than by the more tedious alternative of building and testing prototype designs.

4.2 Finite Element Analysis

4.2.1Principle

The finite element analysis of the flat flextensional transducer was performed using ANSYS® software package version 7.0. Due to the underwater application of the sonophoresis device, the vibration of the structure in contact with water is transferred to the water motion and results in a discernible increase in the kinetic energy of the total system. It is generally known that the natural frequencies of a structure that are in contact with water decrease significantly compared to the natural frequencies in air [112]. This problem is referred to as the fluid-structure interaction problem. In addition to the standard structural analysis, the ANSYS® analysis code also has the capability of simulating coupled-field phenomena (such as piezoelectricity) as well as acoustic fluid and fluid-structure interaction effects.

For piezoelectric coupling analysis, the electromechanically constitutive equations usually given by manufacturers or available in published data are rewritten in the form of a matrix:

$$\{S\} = \left[s^E\right]\{T\} + [d]\{E\} \tag{4.1}$$

$$\{D\} = [d]^t\{T\} + \left[\varepsilon^T\right]\{E\} \tag{4.2}$$

Where,

$\{D\}$: Electric displacement vector (three components **x,** y, z)

$\{S\}$: Strain vector (six components x, y, z, yz, xz, xy)

$\{E\}$: Electric field vector (three components x, y, z)

$\{T\}$: Stress vector (six components x, y, z, yz, xz, xy)

$[d]$: Piezoelectric matrix relating strain and electric field

$[d]^t$: Transposed piezoelectric matrix relating strain and electric field

$\left[\varepsilon^T\right]$: Dielectric matrix evaluated at constant stress

$\left[s^E\right]$: Compliance matrix evaluated at constant electric field

However, ANSYS® requires data in the following forms [37]:

$$\{T\} = \left[c^E\right]\{S\} - [e]\{E\} \tag{4.3}$$

$$\{D\} = [e]^t\{S\} + \left[\varepsilon^s\right]\{E\} \tag{4.4}$$

Where,

$\left[c^E\right]$: Stiffness matrix evaluated at constant electric field

[e] : Piezoelectric matrix relating stress and electric field

$[e]^t$: Transposed piezoelectric matrix relating stress and electric field

$[\varepsilon^S]$: Dielectric matrix evaluated at constant strain

In order to convert the data presented in the forms of Eqs. (4.1) and (4.2) to the forms that are suitable for Eqs. (4.3) and (4.4), the following manipulations are performed:

$$\{S\} = [s^E]\{T\} + [d]\{E\}$$

$$[s^E]\{T\} = \{S\} - [d]\{E\} \tag{4.5}$$

$$\{T\} = [s^E]^{-1}\{S\} - [s^E]^{-1}[d]\{E\}$$

Substituting {T} into Eq. (4.2) and yields

$$\{D\} = [d]^t\{T\} + [\varepsilon^T]\{E\}$$

$$\{D\} = [d]^t\left([s^E]^{-1}\{S\} - [s^E]^{-1}[d]\{E\}\right) + [\varepsilon^T]\{E\} \tag{4.6}$$

$$\{D\} = [d]^t[s^E]^{-1}\{S\} + \left([\varepsilon^T] - [d]^t[s^E]^{-1}[d]\right)\{E\}$$

Upon comparison of Eqs. (4.6) and (4.5) with Eqs. (4.3) and (4.4), the relationships between manufacturer-supplied data and ANSYS® required data are given as follows:

$$\left[c^E\right]=\left[s^E\right]^{-1}$$

$$\left[\varepsilon^S\right]=\left[\varepsilon^T\right]-\left[d\right]^t\left[s^E\right]^{-1}\left[d\right] \tag{4.7}$$

$$\left[e\right]=\left[s^E\right]^{-1}\left[d\right]=\left[d\right]^t\left[s^E\right]^{-1}$$

These equations will form the basis of the conversion routes to transform published data to the forms accepted by ANSYS®. Note that the published data has mechanical vector in the form {x, y, z, yz, xz, xy} where ANSYS's mechanical vector is in the form {x, y, z, xy, yz, xz}.

In acoustic fluid-structure interaction problems, the structural dynamics equation needs to be considered along with the Navier-Stokes equations of fluid momentum and the flow continuity equation [113]. It usually involves modeling the fluid medium and the surrounding structure. Typical quantities of interest are the pressure distribution in the fluid at different frequencies, pressure gradient, particle velocity, the sound pressure level, as well as, scattering, diffraction, transmission, radiation, attenuation, and dispersion of acoustic waves. Basically, it assumes that the fluid is compressible, but allows only relatively small pressure changes with respect to the mean pressure. Also, the fluid is assumed to be non-flowing and inviscid (that is, viscosity causing no dissipative effects). Uniform mean density and mean pressure are assumed, with the pressure solution being the deviation from the mean pressure, not the absolute pressure.

ANSYS® also has the capability of performing different types of structural analysis such as static, modal, harmonic, transient dynamic, spectrum and bulking. The

harmonic response analysis determines the steady-state response of a linear structure to loads that vary sinusoidally with time. The objective is to calculate the structure's response at several frequencies and to obtain a graph of some response quantity (usually displacements) versus frequency. The modal analysis is used to determine the natural frequenciesand mode shapes of a structure. The results discussed in section 4.3 are all obtained from these two analytical methods.

4.2.2 Modeling

4.2.2.1 Structures of portable sonophoresis devices

Two types of ultrasonic devices for drug delivery application were proposed in this research project. They were named device 'A' and 'B'. Device 'A' consists of a single flat flextensional transducer that comprises a piezoelectric ring and a vibration metal plate bonded together. The whole flat flextensional ultrasonic transducer was assembled onto a rigid stainless steel body (Figure 4.1). The height of the body was decided by the drug delivery experimental setup.

As mentioned in Chapter 3, in order to increase the output acoustic intensity and at the same time reduce the required electric power for the transducer, the sonophoresis device 'B' with dual flat flextensional transducers was proposed based on the acoustic interference principle. The detailed structure is given in Figure 4.2.

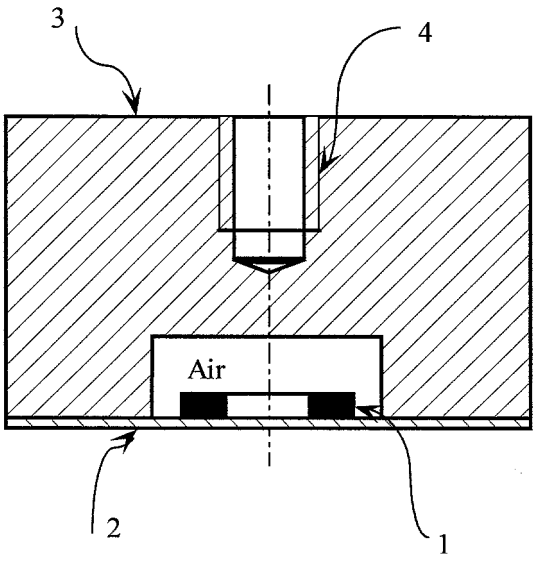

1- Ring-shaped PZT; 2- Metal vibration plate; 3- Stainless steel body; 4- Threaded hole (M6).

Figure 4.1. Schematic structure of the sonophoresis device 'A'.

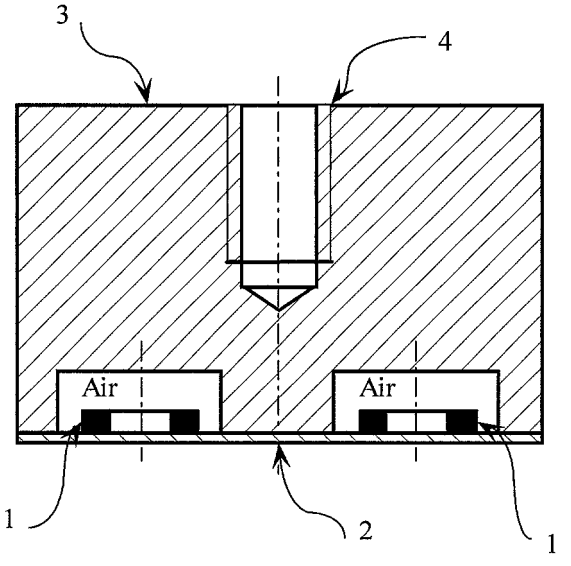

1- Ring-shaped PZT; 2- Metal vibration plate; 3- Stainless steel body; 4- Threaded hole (M6).

Figure 4.2. Schematic drawing of the proposed sonophoresis device 'B' with double flat flextensional ultrasonic transducers.

As shown in Figure 4.2, device 'B' consists of double piezoelectric rings and a metal vibration plate bonded together. The whole structure will be assembled onto a rigid stainless steel body that has two blind holes with the same diameter and depth, separated at a fixed center-to-center distance. The separated blind holes accommodate two structurally independent flextensional ultrasound transducers and each piezoelectric ring is concentric with respect to the blind hole. This assembly theoretically, if each transducer is suitably controlled, can provide acoustic intensity four times higher than that of single transducer due to the above mentioned acoustic interference theory.

4.2.2.2 Simplified structures of the flat flextensional transducers for the finite element analysis

Ultrasound frequency at a range of 20 to 100 kHz has been shown to enhance transdermal transport of a variety of drug molecules. The enhancement is determined by various parameters, including frequency, ultrasound intensity, duty cycle, and application time. The most important parameters are ultrasound frequency and intensity applied on the skin surface [33]. Previous research work showed that significant transdermal transport of model drug such as insulin (MW=6000 Da) has been achieved using 20 kHz commercial sonicator operating at intensities from 12.5-225 mW/cm^2 **[9].** Thus the sonophoresis device should be operated at its first vibration mode at a frequency similar to that of the commercial sonicator with intensities that have been shown to transdermally deliver drugs such as insulin. From this point of view, in order to design the proposed structure as shown in Figure 4.1 and 4.2, the following dimensions as shown in Figures 4.3 and 4.4 must be determined:

1. The thickness t_p of the piezoelectric ring
2. Inner diameters d_i of the piezoelectric ring
3. Outer diameters d_p of the piezoelectric ring

4. The distance S between two piezoelectric rings
5. The thickness t_m of the metal vibration plate
6. The diameter d_m of the vibrating zone of the metal vibration plate

The following conditions are assumed:

1. The diameter of the sonophoresis device is 29.6 mm. This dimension is limited by the inner diameter of the donor compartment of the Franz diffusion cell (31.0 mm).
2. The frequency range is about 20 to 40 kHz, which is frequently used in ultrasound enhanced drug delivery experiments [8] [11] [93-94] [114].
3. Only the first vibration mode of the metal vibration plate is considered, and the first resonance frequency should be in the above-mentioned frequency range.

Unless otherwise noted, the simulation results reported in this chapter are for single flat flextensional transducer with various materials properties and dimensions. The detailed finite element analysis model, selected element types, boundary conditions will be presented in the next section.

4.2.2.3 Finite element analysis model of the flat flextensional transducer

As shown in Figure 4.3, the device 'A' with a single flat flxtensional ultrasonic transducer exhibits axisymmetry about its central axis, it was modeled as a two dimensional axis-symmetric body, which offers the advantages over the corresponding three-dimensional model with lesser numbers of the elements and processing time. The corresponding two-dimensional axis-symmetric FEA model is given in Figure 4.5 (a). The FEA model for simplified structure of the proposed ultrasonic device 'B' is shown in Figure 4.5 (b). Both FEA models consist of the following components:

1. Ring-shaped PZT

2. Metal vibration plate
3. Stainless steel body
4. Interface elements between fluid elements and structural elements
5. Interface elements between fluid elements and skin
6. Interface elements between fluid elements and glass wall Fluid domain without structural elements

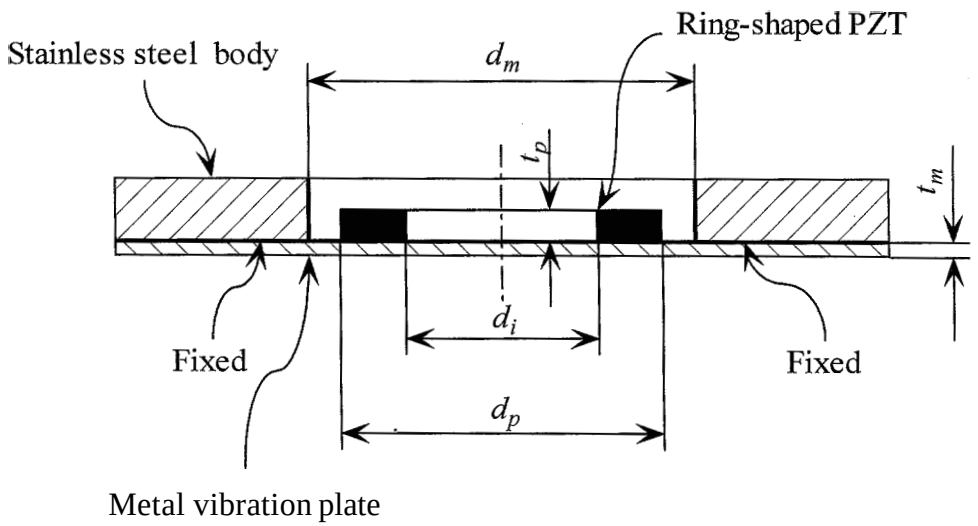

Figure 4.3. Simplified simulation structure of the sonophoresis device 'A' with a flat flextensional ultrasound transducer and the key parameters should be calculated.

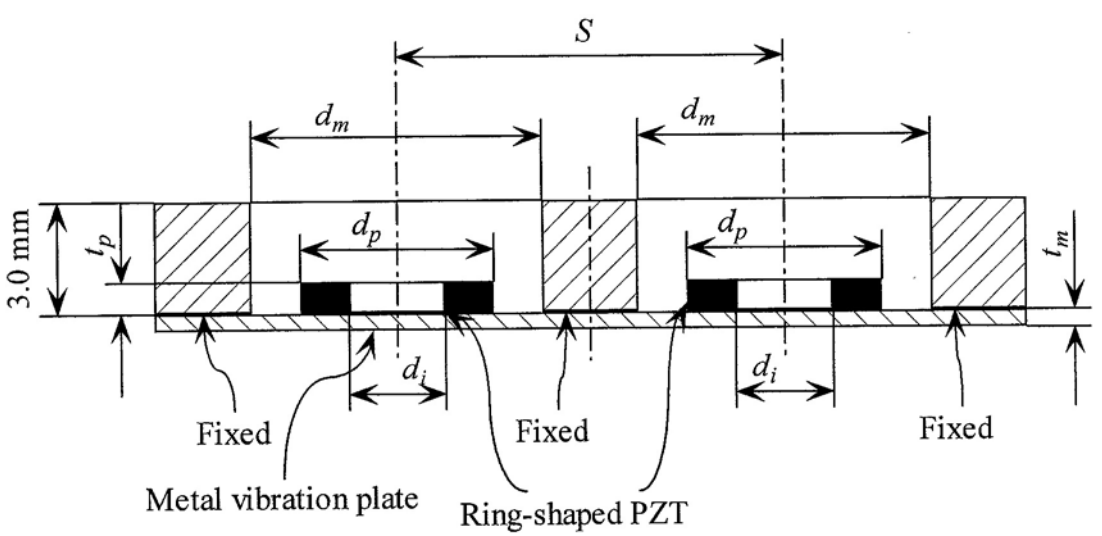

Figure 4.4. Simplified structure of the proposed sonophoresis device 'B' with dual flat flextensional transducers.

The fluid medium was modeled by 2D element FLUID29 that has the capability of modeling the interface in fluid/structure interaction problems. Typical applications include sound wave propagation and submerged structure dynamics. The governing equation for acoustics, namely the 2-D wave equation, has been discretized, taking into account the coupling of acoustic pressure and structural motion at the interface [115].

For the metal vibration plate and the stainless steel body, it was assumed that their properties are linear and isotropic. In this study, the aim of FEA is to study the effects of the properties and dimensional changes of the piezoelectric material and vibration plate on the performance of the proposed ultrasonic device. Thus, the metal vibration plate is one of the key structures of the device. The analytical results would determine the structural dimensions of the ultrasonic device. Therefore, PLANE 82**,** which is a 2D-8-node element that was selected to model the metal vibration plate in order to obtain more accurate results. In contrast, the stainless steel body is not a key structure of the ultrasonic device, which was considered as a rigid and non-deformed structure compared with the metal vibration plate. It is not necessary to get accurate results of the stainless steel body. Thus, 2D-4-node element PLANE 42 was used to model the structure of the stainless steel body. The element is well suited to modeling a simple structure with a minimum of processing time.

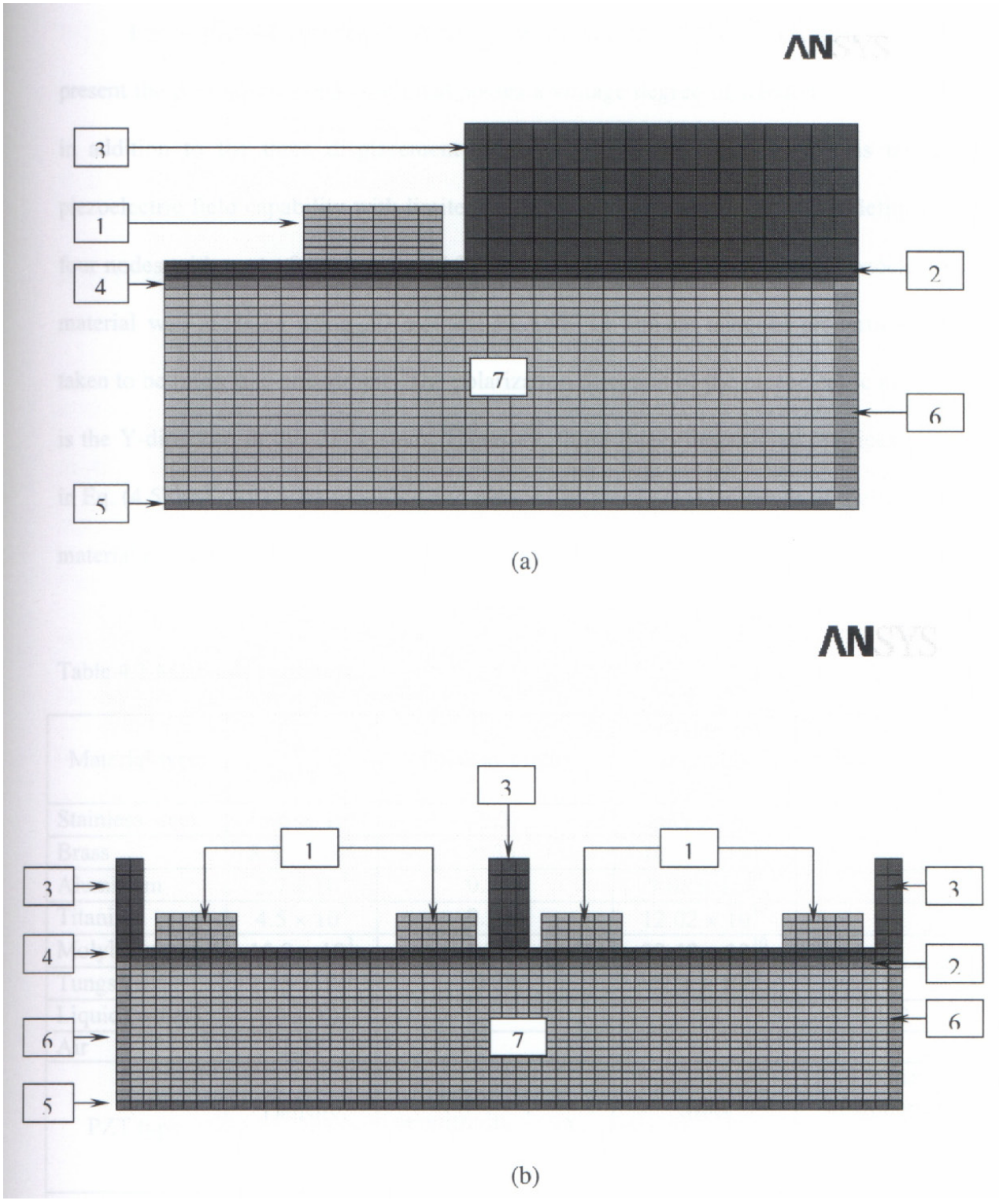

Figure 4.5. (a). Two-dimensional axisymmetric FEA model of the proposed device 'A' with considering the fluid elements. (b). Two-dimensional FEA model of the proposed device 'B' with considering the fluid elements.

For a piezoelectric analysis to be performed in ANSYS®, elements used to present the piezoelectric material must posses a voltage degree of freedom at each node in addition to the three displacement degrees of freedom. PLANE 13 has the 2D piezoelectric field capability with limited coupling between the fields, and is defined by four nodes with up to four degrees of freedom per node [115]. Hence, the piezoelectric material was modeled using 2D element PLANE 13 and its material properties were taken to be linear and anisotropic. The polarization direction of the piezoelectric material is the Y-direction in this 2D system. Therefore, those three-dimensional matrices given in Eq. (4.5) and (4.6) were modified and reduced further [37]. The values of the required material properties necessary for the analysis are listed in Table 4.1.

Table 4.1 Materials constants.

Material type	Density (kg/m^3)	Poisson's ratio		Yong's modulus (N/m^2)	Velocity (m/s)
Stainless steel	7.86×10^3	0.3		20.7×10^{10}	
Brass	8.55×10^3	0.35		10.06×10^{10}	
Aluminum	2.7×10^3	0.345		7.06×10^{10}	
Titanium	4.5×10^3	0.361		12.02×10^{10}	
Molybdenum	10.2×10^3	0.293		32.48×10^{10}	
Tungsten	19.3×10^3	0.28		41.1×10^{10}	
Liquid (water)	1.0×10^3				1480
Air	1.21				344
PZT type	Density (kg/m^3)	Relative permittivity $\varepsilon_{11}^s / \varepsilon_0$	Q_m	Piezoelectric stress coefficient e_{31} (C/m^2)	Elastic compliance s_{11}^E (m^2/N) $\times 10^{-12}$
C-203	7.7×10^3	755	2000	-4.1	13.9
C-91	7.8×10^3	2557	30	-17.3	17.1

The boundary condition was such that any translational motion of the model was prohibited. In addition, absorption coefficient of sound at the interface of liquid and skin (indicated by number 5), which was obtained empirically [116], was included. In this

analysis, the glass wall was considered as a rigid material, thus the velocity of the fluid particles is zero at the interface of the fluid-glass wall (indicated by number 6).

4.3 Results and discussion

4.3.7 Vibration modes

Figure 4.6 shows the calculated mode shapes of the flat flextensional transducer in contact with water corresponding to the (0, 1),(0, 2) and (0, 3) modes. In general, the modes are designated by the pair of integers *(m, n)*, where *m* determines the number of radial nodal lines and the second integer *n* determines the number of nodal circles [111]. Since the two dimensional axisymmetric structure was modeled in this analysis, the vibration of the flat flextensional transducer is symmetric, so m is always zero. Generally, in most of ultrasound enhanced drug delivery application, the transducer has to be operated around its fundamental resonance frequency to generate more energy. Hence, in this analysis, all calculated results were obtained at the first resonance frequency corresponding to the (0, 1) vibration mode of the flat flextensional transducer.

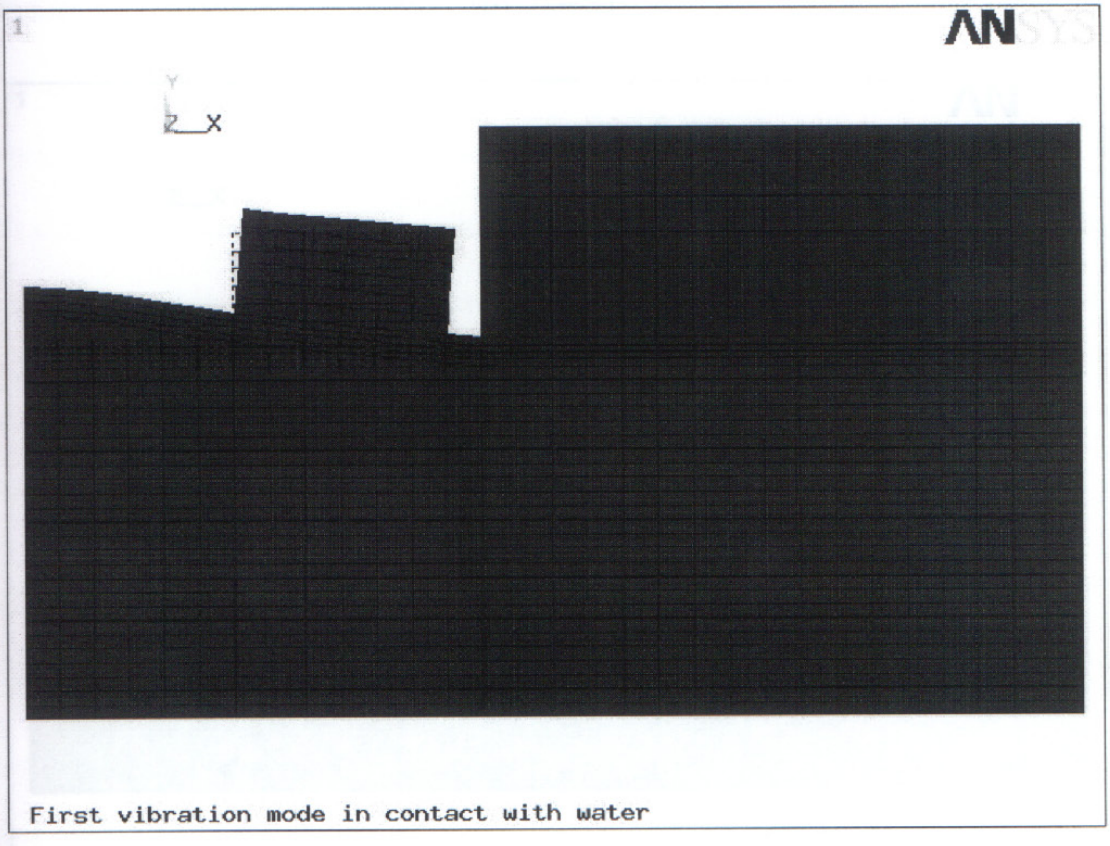

(0,1) mode

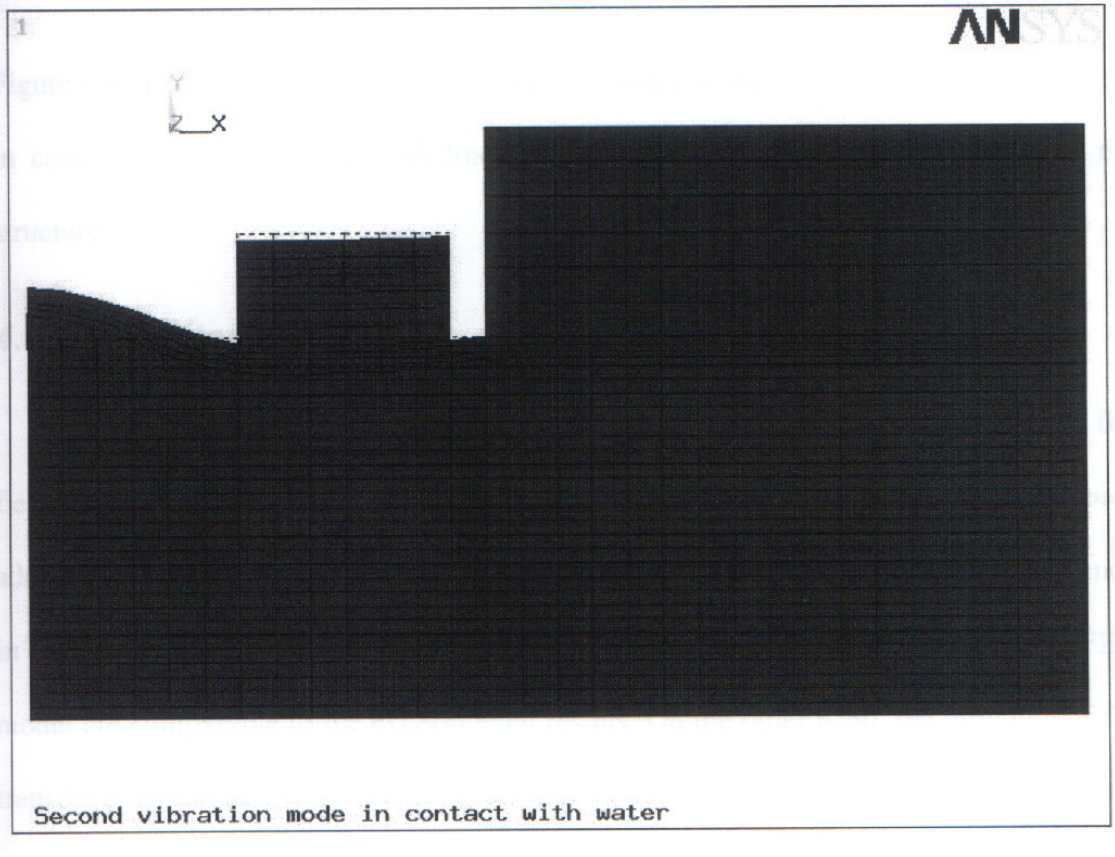

(0, 2) mode

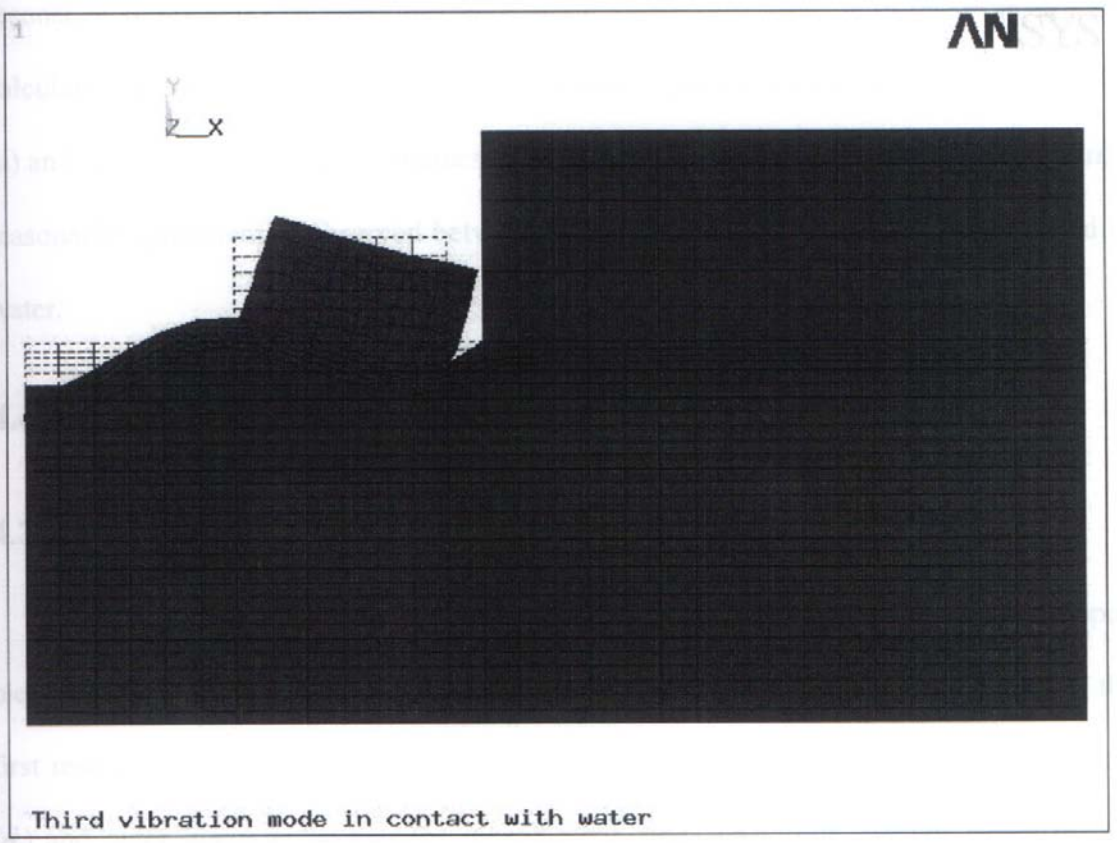

(0, 3) mode

Figure 4.6. The calculated first three vibration modes of the flat flextensional transducer in contact with water. The dash lines in all diagrams are undeformed shape of the structure.

4.3.2 Admittance

The comparisons of the calculated and measured admittance of a flat flextensional transducer are given in Figures 4.7 (a) and (b). It is clearly shown that both admittance spectra have similar trend and the difference in the first resonance frequency in air is less than 3 kHz. It is indicated that the calculated results obtained from the FEA model are comparable to the experimental results. On the other hand, the vibration of the transducer in contact with water is transferred to the water motion and results in the mass

loading and a discernible increase in the kinetic energy of the total system. Thus the first resonance frequencies in water decrease significantly compared with those in air. The calculated and experimentally obtained admittance spectra are displayed in Figures 4.8 (a) and (b). The first resonance frequency in water shifts to the lower frequency. Again, a reasonable agreement is observed between calculated and measured results in air and in water.

4.3.3 First resonance frequency

4.3.3.1 PZT d_i / d_p ratio

In a typical flat flextensional transducer, a disk-shaped or a ring-shaped piezoelectric material could be used as an active element. As indicated in Figure 4.9, the first resonance frequency of the transducer is influenced by the ratio of inner diameter (d_i) and outer diameter (d_p) of the piezoelectric ring. The finite element analysis (see Figure 4.9) confirmed:

(1) The flat flextensional transducer with disk-shaped PZT ($d_i / d_p = 0$) has higher first resonance frequency compared to that of the transducer with ring-shaped PZT. This is because the structure with the disk-shaped PZT has higher stiffness than that of the structure with ring-shaped PZT.

(2) When $d_i / d_p < 0.5$, in air, the first resonance frequency drops slowly. In contrast, the first resonance frequency in water falls fast and is almost linearly proportional to the ratio value. However, when $d_i / d_p > 0.5$, for both cases, the first resonance frequency declines sharply which may be caused by the decrease of the effective contact area between the piezoelectric ring and the metal vibration plate.

The results show that for a fixed size flat flextensional transducer, the first resonance frequency in water could be easily adjusted simply by changing the d_i / d_p ratio of the piezoelectric ring.

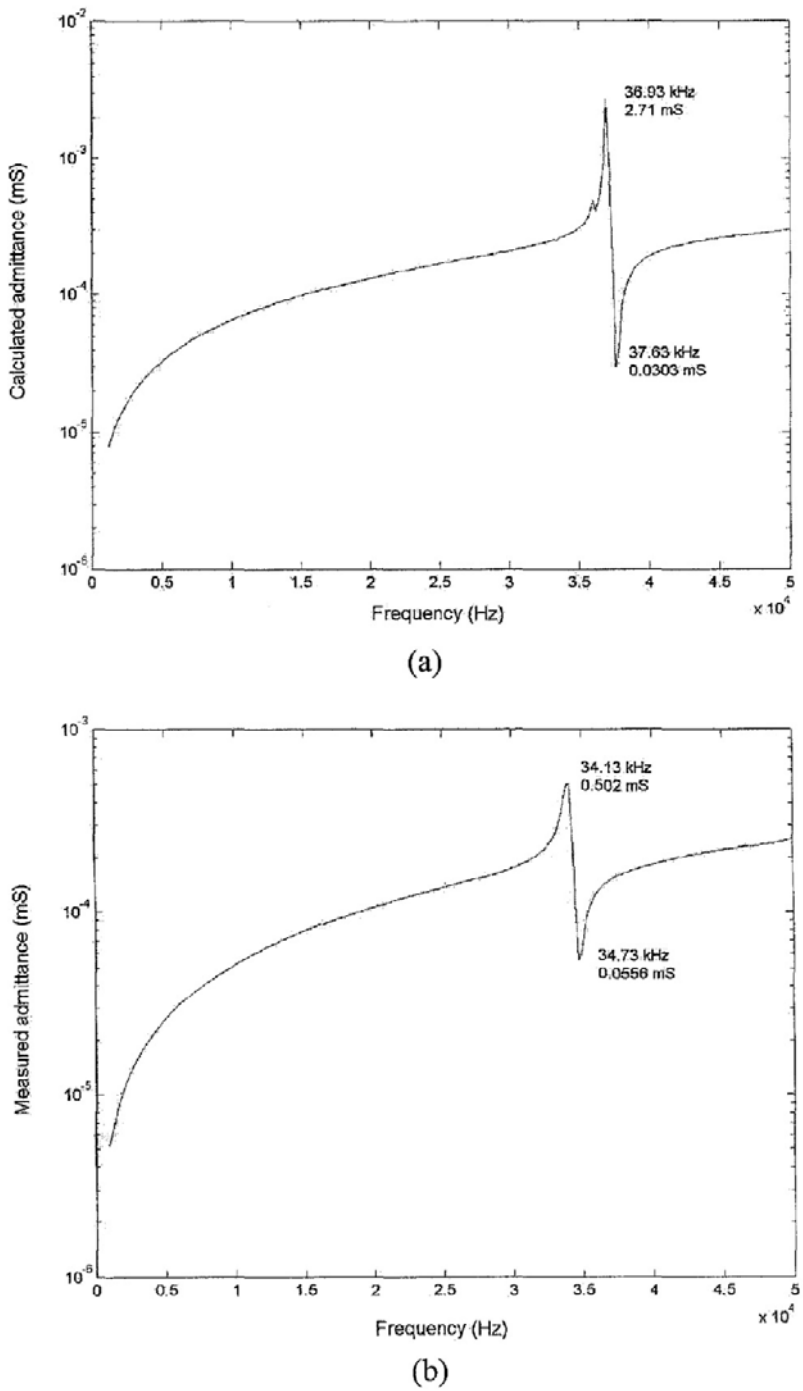

Figure 4.7. Calculated and measured admittance of a flat flextensional transducer in air (piezoelectric material: C-203, $t_p = 1.2$ mm, $d_i = 6.0$ mm, $d_p = 12.0$ mm, $d_m = 13.0$ mm, $t_m = 0.4$ mm, stainless steel vibration plate).

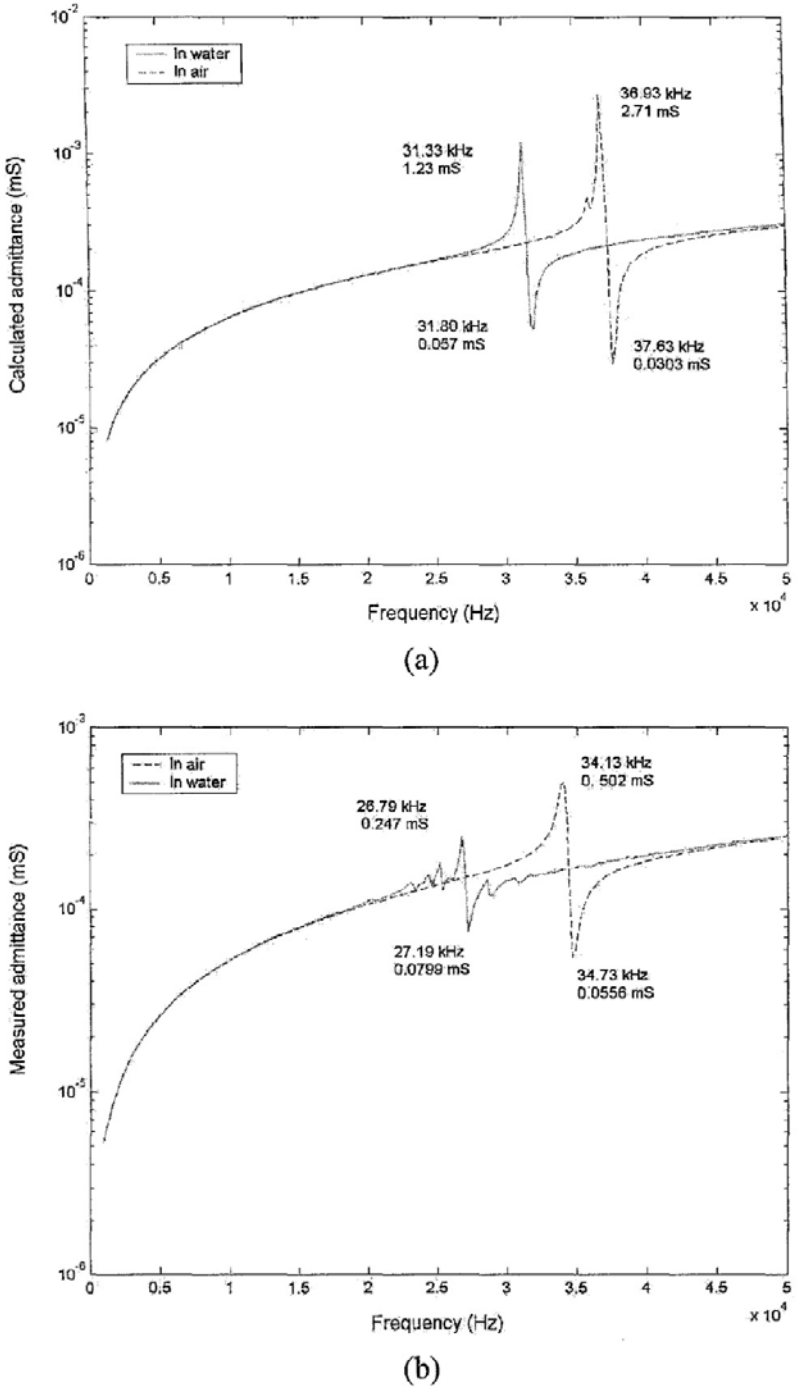

Figure 4.8. Calculated and measured admittance of a flat flextensional transducer in air and in water (piezoelectric material: C-203, $t_p = 1.2$ mm, $d_i = 6.0$ mm, $d_p = 12.0$ mm, $d_m = 13.0$ mm, $t_m = 0.4$ mm, stainless steel vibration plate).

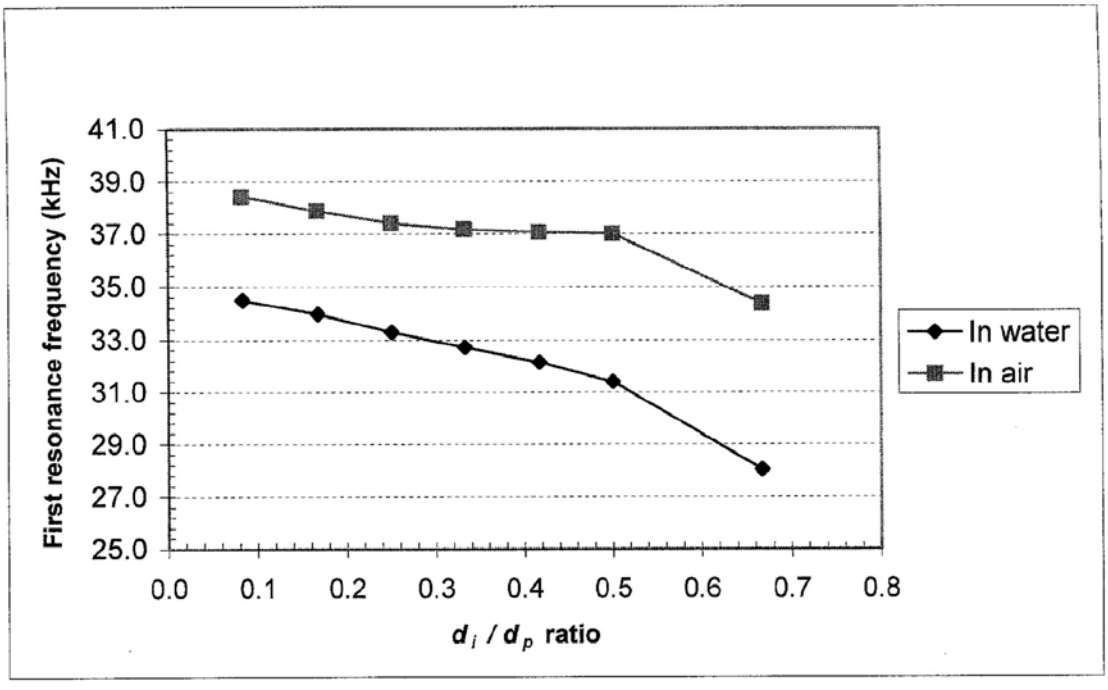

Figure 4.9. The first resonance frequency in water and in air as a function of the d_i / d_p ratio of the piezoelectric ring (piezoelectric ring C-203, $d_p = 12.0$ mm, $t_p = 1.2$ mm, $t_m = 0.4$ mm, $d_m = 13.0$ mm, stainless steel vibration plate).

4.3.3.2 PZT material type and thickness

The plots in Figure 4.10 show the first resonance frequency changes with different piezoelectric material types and thickness. It is illustrated that the first resonance frequencies are affected little by the types of the piezoelectric materials. The first resonance frequency differences between soft and hard PZT are less than 2 to 3 kHz in water and in air respectively (see Figure 4.10). As to the effect of PZT thickness, though the trend of each curve is similar, it is divided into two stages. When the PZT thickness is less than 0.5 mm ($t_p < 0.5$ mm), which is also less than the thickness of the metal vibration plate ($t_m = 0.4$ mm), viewed from Figure 4.10, any change of the PZT thickness in the range from 0.25 to 0.5 mm does not significantly affect the change of the first resonance frequency. Under this condition ($t_p < 0.5$ mm), the increase of the PZT thickness from 0.25 to 0.5 mm will not make significant changes in the stiffness of the

structure, which is determined by the thickness of the metal vibration plate. When the PZT thickness is larger than 0.5 mm ($t_p > 0.5$ mm), it is also larger than the vibration plate thickness ($t_m = 0.4$ mm). As seen in Figure 4.10, it is clearly shown that the increase of the first resonance frequency is almost a linear function of the PZT thickness. Therefore, if a flat flextensional transducer has the fixed thickness of the vibration plate, the first resonance frequency could be changed easily when $t_p > t_m$.

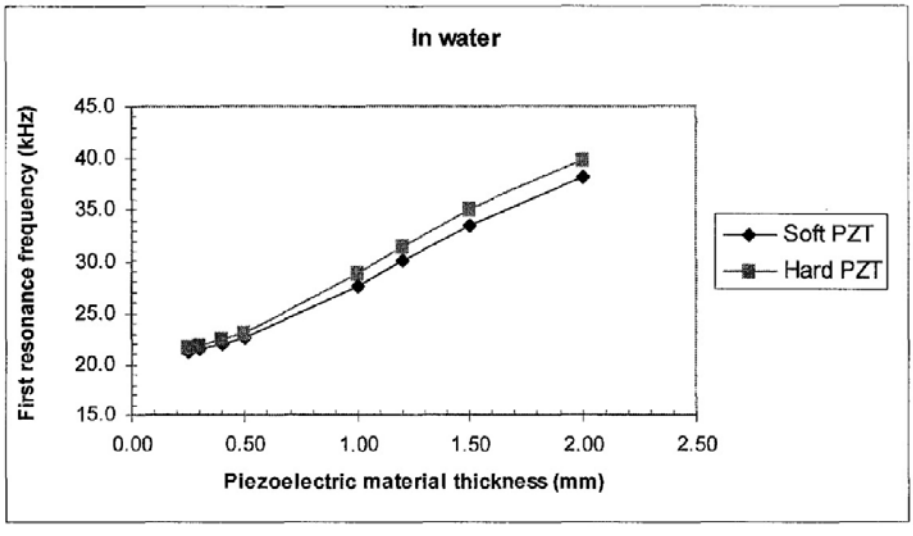

(a)

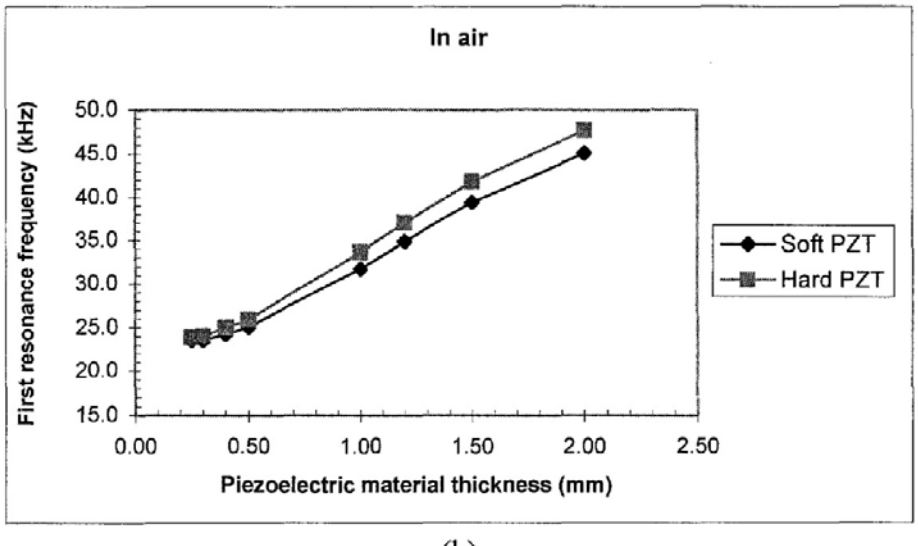

(b)

Figure 4.10. The first resonance frequency in water and in air as a function of the PZT thickness and piezoelectric material types (piezoelectric ring C-203 and C-91, $d_p = 12.0$ **mm**, $d_i = 6.0$ mm, stainless steel vibration plate, $t_m = 0.4$ mm, $d_m = 13.0$ mm).

4.3.3.3 Thickness and property of the vibration plate

For the flat flextensional transducers with fixed dimensions of the piezoelectric material, and with different thickness and types of materials of the vibration plates, the fundamental resonance frequency is found to increase proportionally with the vibration plate thickness. The first resonance frequencies in water and in air are plotted as a function of the thickness of the vibration plate in Figure 4.1 1. In this analysis, a total of six types of material were selected due to their non-corrosive properties to the atmosphere and the chemicals (alkali and weak acid). Both figures (a) and (b) reveal that the first resonance frequency has the similar trends both in water and in air. It clearly illustrates that a flat flextensional transducer with fixed dimensions of the piezoelectric material the first resonance frequency is adjusted easily by changing the vibration plate thickness or material types. Furthermore, it is known that the vibration of structure in contact with water is transferred to the water motion and results in a discernible increase in the kinetic energy of the total system. Practically, the nondimensionalized added virtual mass incremental (NAVMI) factor is used to make the relationship of the resonance frequency in water and in air [112]

$$\frac{f_w}{f_a} = \frac{1}{\sqrt{1+\Gamma\left(\frac{\rho_w}{\rho_p}\right)\left(\frac{a}{t}\right)}} \tag{4.8}$$

Where,

f_w: The resonance frequency in water

f_a: The resonance frequency in air

a: The radius of the vibration plate

t: The thickness of the vibration plate

ρ_w : The density of water

ρ_p : The density of vibration plate

Γ : The nondimensionalized added virtual mass incremental factor which is decided by the boundary conditions of the vibration plate (i.e. simply support, free vibration and clamp).

Based on the simulation results as shown in Figures 4.11 (a) and (b), the percentage change in the first resonance frequency from in-air to in-water is given in Figure 4.12 as a function of the ratio of the water density to the vibration plate density. It reveals a clear trend of the change in the first resonance frequency as a square root function. Therefore, the flat flextensional transducer with a low density vibration plate (i.e. aluminum) which is closer to the density of water will have more changes in the first resonance frequency than the same transducer with a high density vibration plate when it vibrates in contact with water (i.e. tungsten).

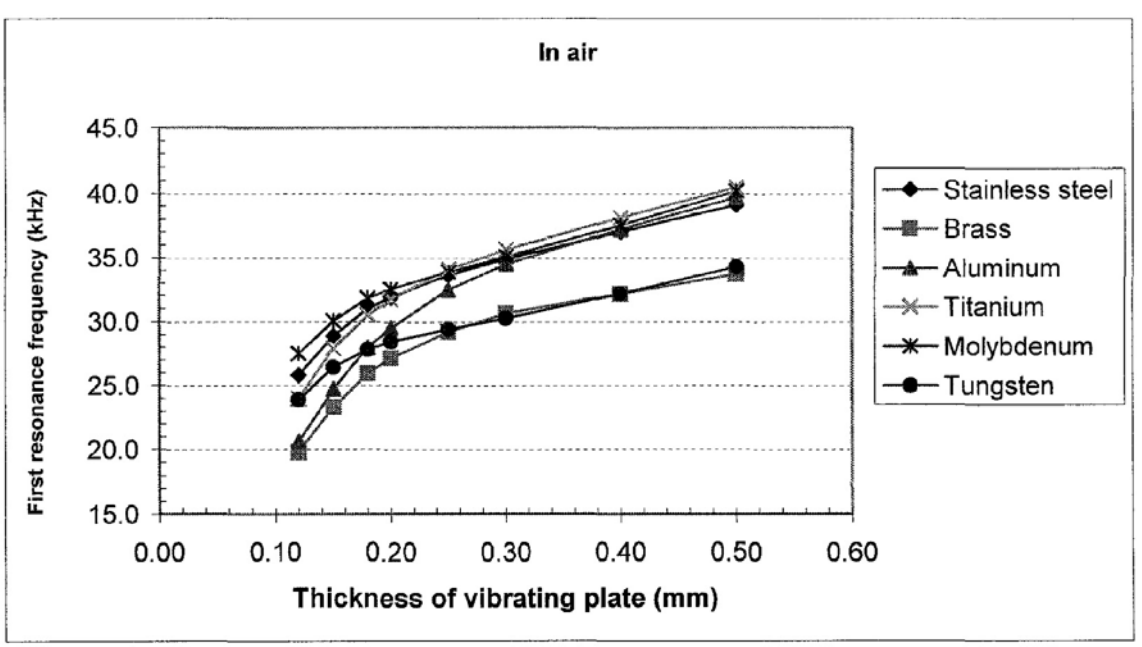

(a)

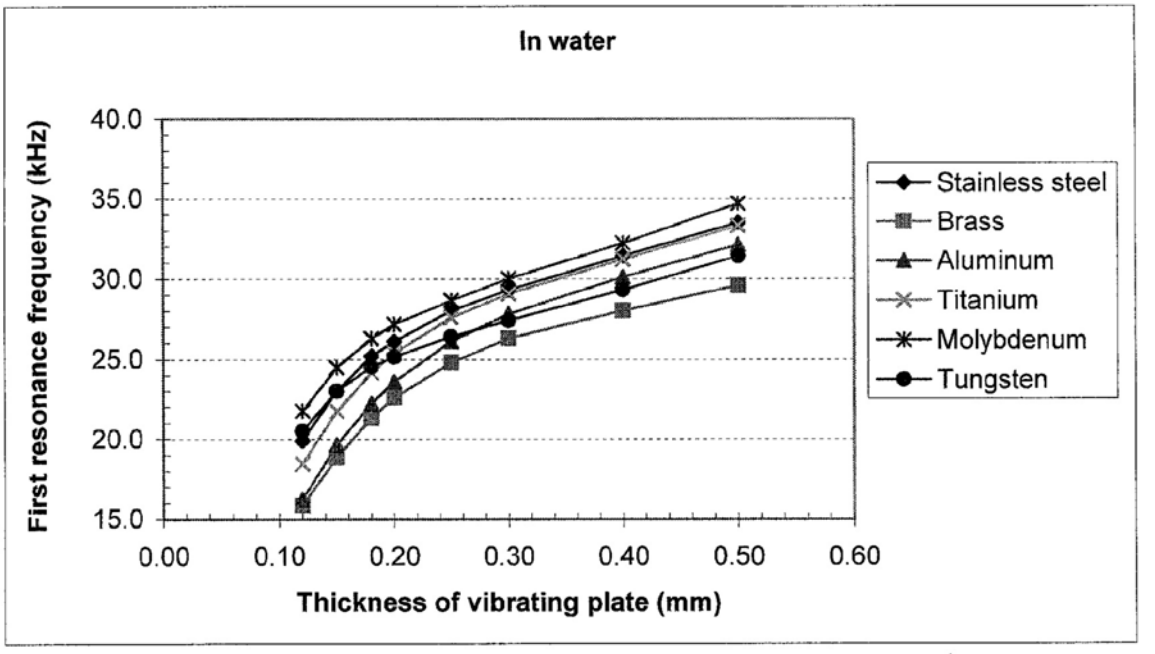

(b)

Figure 4.11. Vibration plate thickness versus the first resonance frequency of the flat flextensional transducer in waiter and in air (ring-shaped PZT C-203, $d_p = 12.0$ mm, $d_i =$ 6.0 mm, $t_p = 1.2$ mm, $d_m = 13.0$ mm).

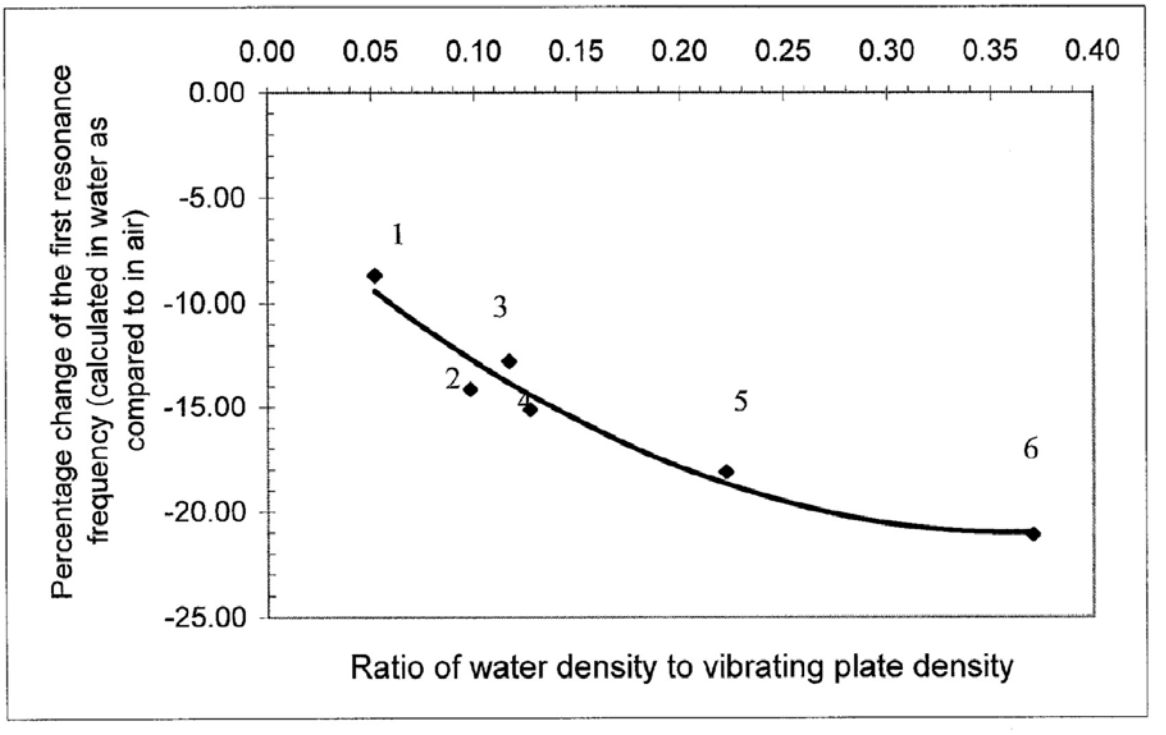

1-Tungsten; 2-Molybdenum; 3-Brass; 4-Stainless steel; 5-Titanium; 6-Aluminum

Figure 4.12. The percent change in the first resonance frequency as a function of the ratio of the water density to the vibration plate density.

4.3.3.4 Vibrating zone diameter d_m

As discussed in sections 4.3.3.1, 4.3.3.2 and 4.3.3.3, changes of the dimensions or the properties of the piezoelectric materials and the vibration plates thickness have large effects on the first resonance frequency of the flat flextensional transducer. Further study shows that changes of the vibrating zone diameter (d_m) also caused significant effect on the first resonance frequency when the dimensions of the piezoelectric material and the vibration plate thickness are constant. (see Figure 4.13). For a typical flat flextensional transducer which consists of a standard sized piezoelectric ring ($di = 6.0$ mm, $dp = 12.0$ mm *and* $tp = 1.2$ mm) and a vibration plate with fixed thickness ($t_m = 0.4$ mm), the first resonance frequency can be adjusted from 15 to 33 kHz by changing the vibrating zone diameter from 13.0 to 18.0 mm.

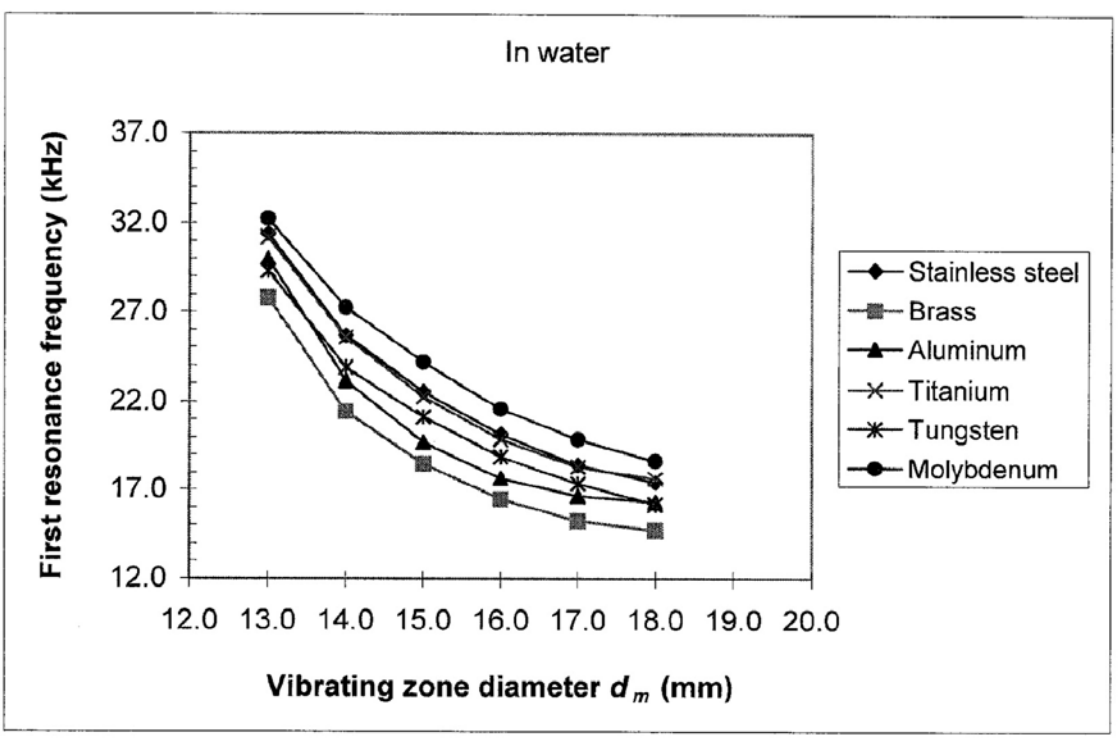

Figure 4.13. The effect of change in the diameter of the vibrating zone on the first resonance frequency in water (Piezoelectric material (C-203, $d_i = 6.0$ mm, $d_p = 12.0$ mm, $t_p = 1.2$ mm, $t_m = 0.4$ mm).

4.3.4 Center displacement of the vibration plate

In the flat flextensional transducer, the function of the vibration plate is to enlarge the small displacement of the piezoelectric material into a much larger axial displacement normal to the surface of the vibration plate. When the transducer vibrates in contact with water this could attribute a much larger acoustic pressure output. Parametric analyses were conducted to determine the influence of the ratio d_i / d_p on the center displacement of the vibration plate. As seen from Figure 4.14, when d_i / d_p ratio is less than 0.33 the normalized center displacement of the vibration plate is less than 0.53, which is larger than that of the disk type flat flextensional transducer ($d, 1d, = 0$). The possible reason is that the stiffness of the vibrating structure will increase following the decrease of the inner diameter of the piezoelectric ring, thus the flexible displacement will reduce. On the other hand, when d_i / d_p ratio is larger than 0.4 the displacement also decreases. The plausible explanation is that the effective contact area between the piezoelectric ring and metal vibration plate reduces with increase of the inner diameter hence the flexible displacement reduces gradually. When $d_i / dp = 1$ the displacement becomes zero. Moreover, as Figure 4.14 indicates when $d_i / d_p = 0.42$, the maximum center displacement of the vibration plate was achieved.

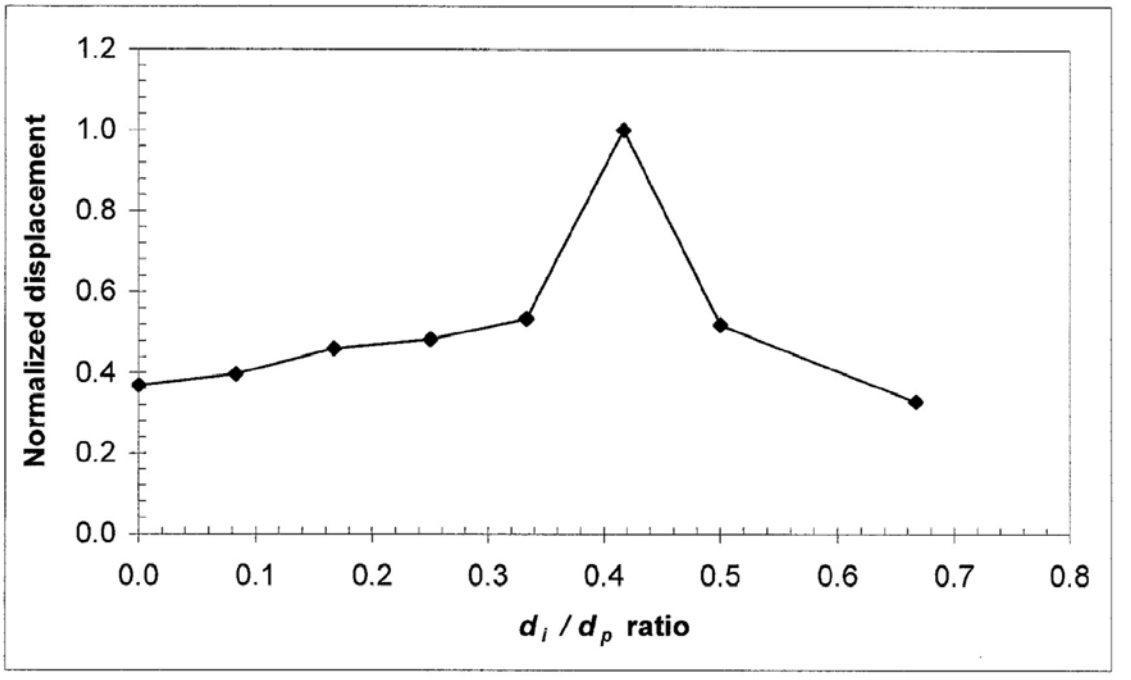

Figure 4.14. Normalized displacement (ratio of displacement to its maximum value) at the center of the vibration plate as a functionof d_i / d_p, where d_i and d_p are the inner and outer diameter of the piezoelectric ring ($t_p = 1.2$ mm, $d_p = 12.0$ mm, $d_m = 13.0$ mm, $t_m =$ 0.4 mm, stainless steel vibration plate).

4.3.5 Output acoustic pressure

Previous research has demonstrated that the first resonance frequency and acoustic intensity are the two major parameters for ultrasound enhanced transdermal drug delivery [33].In general, the acoustic intensity is proportional to the acoustic pressure square and is written as:

$$I = \frac{p^2}{2\rho c} \tag{4.9}$$

Where,

I: Acoustic intensity

P: Acoustic pressure

ρc: The acoustic impedance of an infinite medium

In this section, the output acoustic pressure in water was calculated and compared with the experimental results. The calculated output acoustic pressure is based on the single transducer FEA model (Figure 4.5 (a)). The comparison with the measured results is shown in Figure 4.15. It is clearly shown that the calculated and measured output acoustic pressures have a similar trend and are linearly proportional to the applied voltages. From the diagram it is found that in order to increase the output acoustic pressure, a simple method is to increase the applied voltage to the piezoelectric material.

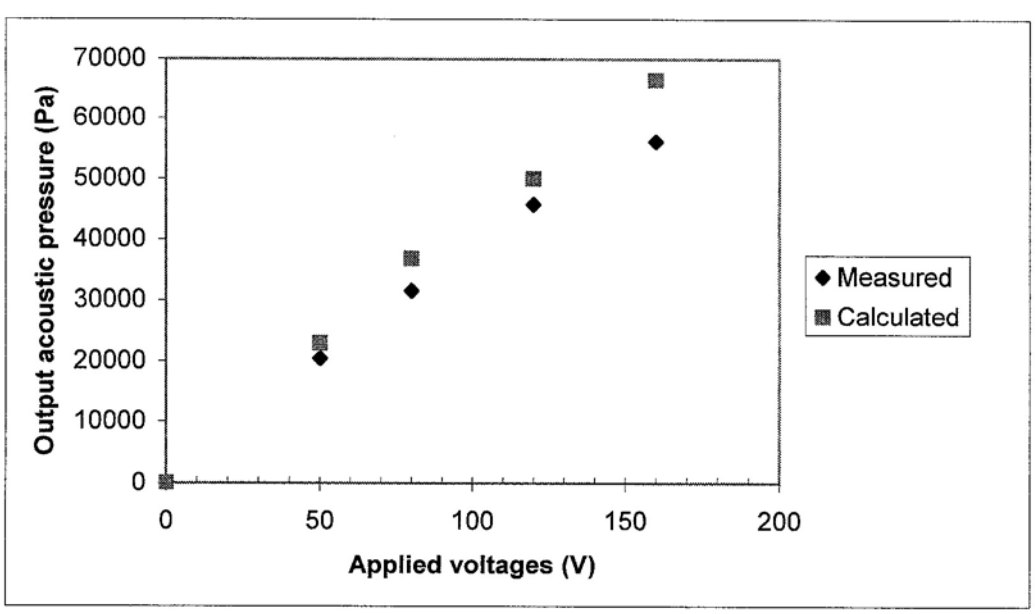

Figure 4.15. Calculated output acoustic pressure in water as a function of applied voltages (t_p = *1.2* mm, d_p = *12.0* mm, d_i = 6.0 mm, d_m = *16.0* mm, t_m = *0.4* mm, stainless steel vibration plate).

Since the fatigue strength of the piezoelectric material is only 1/10 to 1/5 that of the vibration plate, and the stress is applied to both the piezoelectric material and the vibration plate, piezoelectric material is broken as the vibration amplitude increases with

the increase of the applied electric power [117]. In addition, high electric power also has higher probability to cause the depolarization of the piezoelectric material. Hence, dual flat flextensional transducers were employed for the prototype device 'B' in order to obtain higher output acoustic power with lower input electric power. Its output acoustic pressure was calculated by using dual transducers FEA model (Figure 4.5 (b)). The calculated results are plotted in Figure 4.16 (a). The output acoustic pressure is almost two times higher than that generated by Transducer '1' or Transducer '2 in device 'B' when both transducers vibrate simultaneously. According to Eq. (4.9), thus the corresponding output acoustic intensity becomes four times higher. In Figure 4.16 (b), each data point on curve 1 has the same output acoustic pressure as that of the corresponding data point on curve 2. However, the applied voltage of each data point on curve 1 is only half value of that of the corresponding data point on curve 2.

In Figure 4.16 (c), the calculated results were compared with part of the experimental results. For a single transducer (Transducer '1' and Transducer '2') with the low applied voltage (80 V), both the calculated and experimental results have nearly same output acoustic pressures. Since the applied voltage increases from 80 to 160 V, the increase of the vibration amplitude creates the issues of the fatigue strength of the piezoelectric material and heat generation. The former could generate the cracks within the piezoelectric and bonding material, and the latter may soften the bonding layer during the vibration [117]. These issues generated the different effects on the performance of Transducer '1' and Transducer '2'. Thus, the measured output acoustic pressures of Transducer '1' are different from the calculated and measured acoustic pressures of Transducer '2'. As shown in Figure 4.16 (c), the output acoustic pressures are higher than those generated by single transducer when Transducer '1' and Transducer '2'

vibrated simultaneously. Two specific data points are displayed in Figure 4.16 (c). Data point 1 and 2 represent the output acoustic pressures at the low and high-applied voltage (80 V and 160 V), for the dual transducers and single transducer respectively. Both data points are close to the dashed line that indicates they have nearly same values. Therefore, as the simulation results conclude that the device with dual flat flextensional transducers has the capability to increase the output acoustic pressure and at the same time reduce the required electrical power.

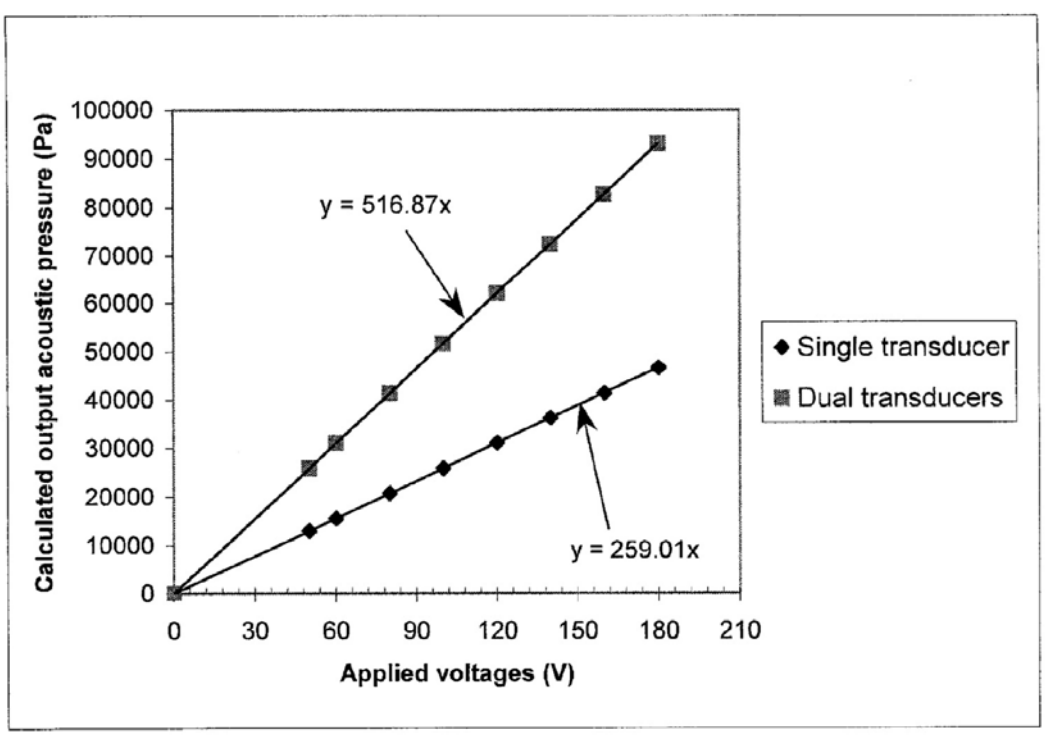

(a)

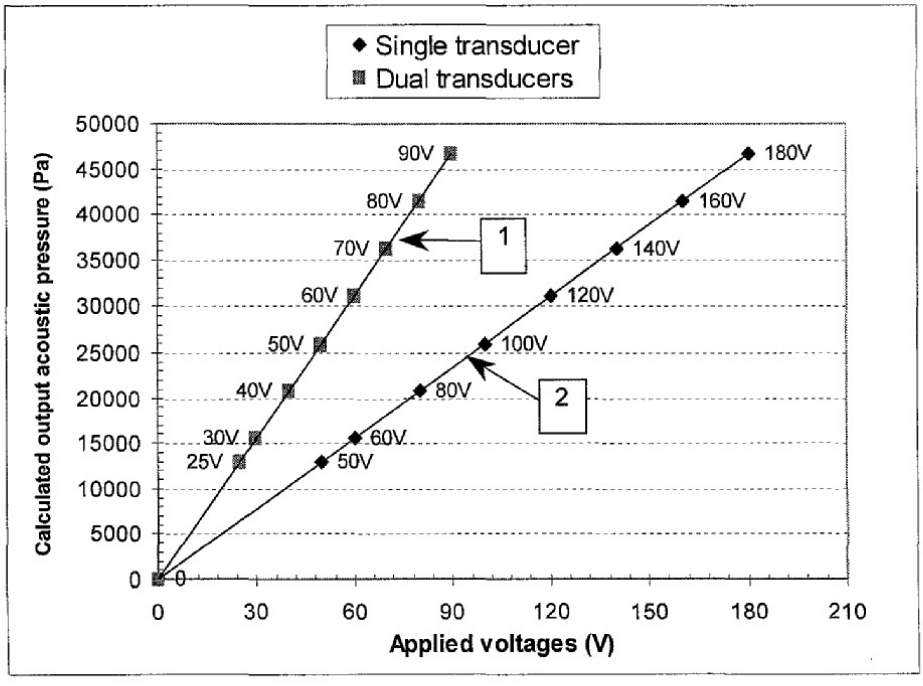

(b)

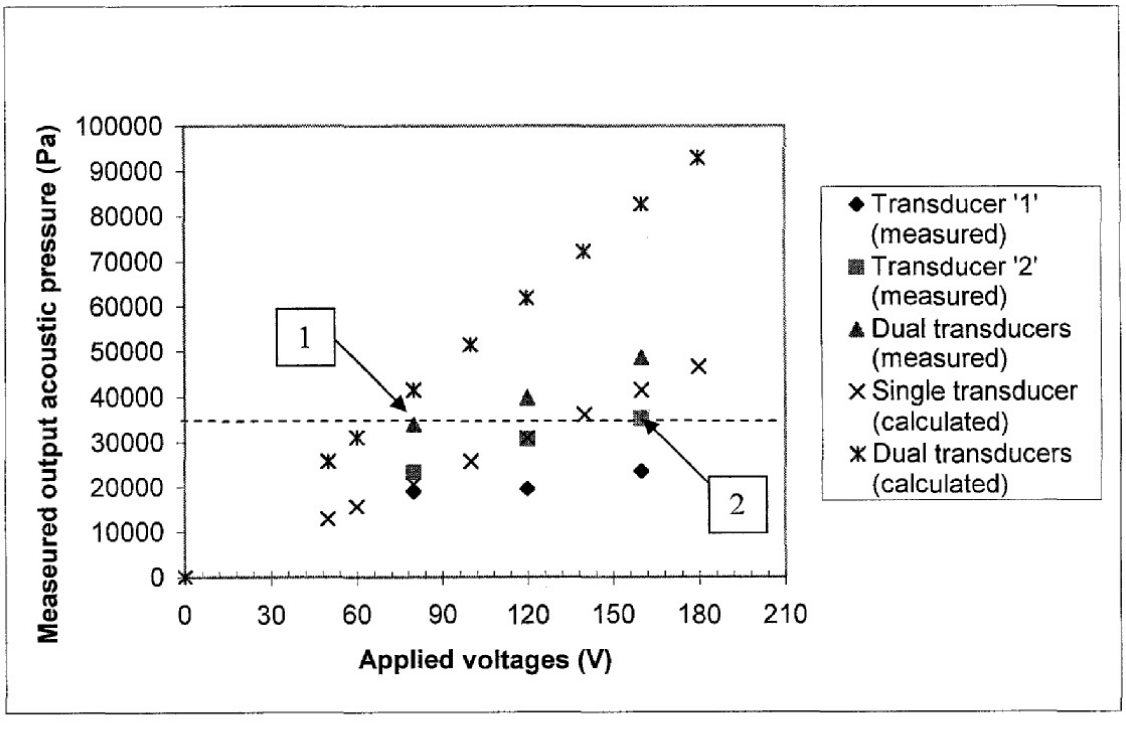

(c)

Figure 4.16. Comparison of calculated output acoustic pressure generated by both transducers and each of them in water as a function of applied voltages ($t_p = 1.2$ mm, $d_p = 12.0$ mm, $d_i = 6.0$ mm, $d_m = 13.0$ mm, $t_m = 0.4$ mm, stainless steel vibration plate) Transducer '1' and Transducer '2' have the same output acoustic pressure.

4.3.6 Final dimensions of the flat flextensional transducers in devices 'A' and 'B'

In this section, the final dimensions of the flat flextensional transducers in devices 'A' and 'B' were determined based on the first and second assumptions in section 4.2.2.2. According to the FEA results, the first resonance frequency of the flat flextensional transducer is determined by the properties, shapes, types and dimensions of the piezoelectric material and the vibration plate. To simplify the calculation procedure, the standard-sized piezoelectric material was selected for the flat flextensional transducers in the prototype devices 'A' and 'B'. Accordingly, the calculation procedure was simplified to determine the parameters of t_m and d_m. In addition, as discussed in section 4.2.2.2, 20 kHz is highly preferred frequency for the ultrasound enhanced drug delivery. So more detailed simulation work has been conducted to choose the suitable material for the metal vibration plate and determine the dimensions of transducer with the first resonance frequency about 20 kHz. The detailed values of the first resonance frequency of the transducers with six different types of metal vibration plates were calculated and listed in Table 4.2. As shown in Table 4.2, the first resonance frequency of the flat flexitensional transducer with stainless steel or titanium vibration plate is mostly close to 20 kHz. Both of them are highly resistant to corrosion attack by organic acids, weak mineral acids and atmospheric oxidation. In this study, stainless steel sheet was selected as a vibration plate for the flat flextensional transducer.

However, for the transducers in device 'B', due to the restriction of the overall size of the stainless steel body (see Figure 4.2 and first assumption in section 4.2.2.2), dual flat flextensional transducers with dimension $d_m = 16.0$ mm could not be assembled onto the stainless steel body. It is necessary to re-calculate the parameter of d_m and the

corresponding first resonance frequency of the transducer. Therefore, simulation work was performed only to calculate the first resonance frequency and determine d_m. Standard-size piezoelectric ring was selected and only the various thickness of stainless steel plate were changed for the calculation. The results are listed in Table 4.3. As shown in Table 4.3, when d_m is 13.0 mm, all the first resonance frequencies are found to be in the range of 20 to 40 kHz. Therefore, the final configuration of the flat flextensional transducers in device 'B' is given in Table 4.4. Plate thickness t_m of 0.4 mm is obtained from device 'A'.

Table 4.2. Simulation results of key parameters and first resonance frequency.

Material type	d_i (mm)	d_p (mm)	t_p (mm)	d_m (mm)	t_m (mm)	f_1 (kHz)
Stainless steel	6.0	12.0	1.2	16.0	0.4	20.14
Brass	6.0	12.0	1.2	16.0	0.4	16.44
Aluminum	6.0	12.0	1.2	16.0	0.4	17.66
Titanium	6.0	12.0	1.2	16.0	0.4	19.87
Tungsten	6.0	12.0	1.2	16.0	0.4	18.89
Molybdenum	6.0	12.0	1.2	16.0	0.4	21.58

Table 4.3, First resonance frequencies versus various thickness of stainless steel vibration plate.

	Material: Stainless steel, $E = 207$ GPa, $\rho = 7.86 \times 10^3$ kg/m^3, $\sigma = 0.3$, $d_m = 13.0$ mm.									
Thickness t_m (mm)	0.15	0.18	0.20	0.25	0.30	0.40	0.50	0.60	0.80	1.0
First resonance frequency (kHz)	20.06	23.37	25.56	26.68	27.56	28.81	30.71	31.91	33.84	36.85

Table 4.4. Configuration of the flat flextensional transducers in device 'B'.

d_p (mm)	d_i (mm)	t_p (mm)	t_m (mm)	d_m (mm)	S (mm)
12.0	6.0	1.2	0.4	13.0	14.5

4.4 Fabrication

The piezoelectric ring-shaped material (C-203, Fuji Ceramic) has a thickness 1.2 mm with inner diameter and outer diameter of 6.0 mm and 12.0 mm, respectively. The piezoelectric ring is poled in the thickness direction. The silver electrode on the piezoelectric ring is ground with abrasive paper to remove the oxide layer and then cleaned with acetone. Stainless steel sheet was selected as a vibration plate which is cut by using a wire cut machine (a single station stamping tool can be used to obtain the vibration metal plate in the future) and ground with sandpaper. The piezoelectric ring is then bonded to the stainless steel vibration plate. The bonding material is electrically conductive silver epoxy (Acoustic Technologies, Singapore). The whole assembly is cured in the oven for 75 minutes at 130 °C and then it is kept at room temperature for 24 hours. The stainless steel vibration plate with ring-shaped PZT of devices 'A' and 'B' as shown in Figure 4.17 (a) and (c) is bonded to the stainless steel body using the same procedure. The entire structure of the sonophoresis device 'A' and 'B' after fabrication is shown in Figure 4.17. Both devices 'A' and 'B' have the same diameter of 29.6 mm and cross-sectional area of 6.88 cm^2. As compared to the ultrasonic probe or converter from a commercial sonicator (weighs almost a kilogram), the weight of each device is only 71.5 and 73.3 gm, respectively.

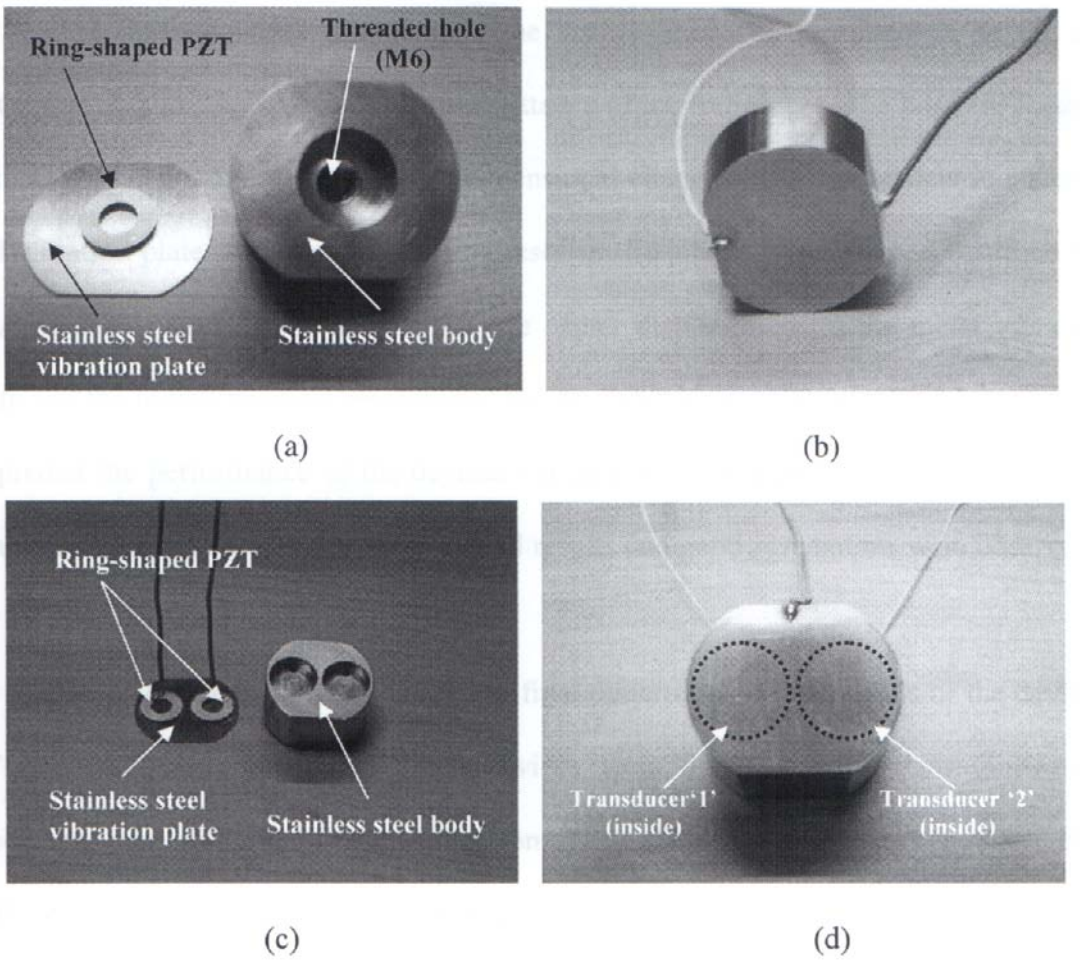

Figure 4.17. (a) Components of device **'A'** before assembly. (b) Front view of whole structure of device 'A'. (c). Components of device 'B' before assembly. (d) Front view of whole structure of device 'B'. The proposed ultrasonic device consists of three parts: ring-shaped PZT, stainless steel vibration plate and stainless steel body with threaded hole (M6).

4.5 Summary

In this chapter, the designed structures of devices 'A' and 'B' and their simplified structures for finite element analysis have been given. The FEA models of devices 'A' and 'B' were developed by giving consideration to the fluid-structure interactions.

The first resonance frequency of the flat flextensional transducer in-air and in-water was obtained by calculating the admittance of the transducer. The possible factors, such as material properties, types and dimensional changes of the piezoelectric material and vibration plate, which affect the first resonant frequency, were studied based on the FEA model of device 'A'. In addition, the center displacement of the metal vibration plate and the output acoustic pressures of the devices 'A' and 'B' were also investigated to predict the performance of the devices via their FEA models. Part of the simulation results was compared with the experimental results and good agreements were observed.

Based on the analytical results, the final dimensions and materials of the devices 'A' and 'B' were determined. Both devices were fabricated and their fabrication procedures were described in the last section of this chapter. The physical characteristics of the devices 'A' and 'B' will be experimentally studied in the next chapter.

CHAPTER FIVE
PHYSICAL CHARACTERISTICS OF THE NEWLY DEVELOPED PROTOTYPE DEVICES 'A' AND 'B'

5.1 Introduction

Although the commercia1 sonicator is an excellent device to demonstrate the ultrasound enhanced transdermal drug delivery, a compact and lightweight ultrasound transducer device is necessary. It should be simple enough to be integrated with drug reservoir and control system to form the sonophoresis device that is placed on the arm or waist to be used as a wearable device. From this point of view, two prototype devices 'A' and 'B' with the flat flextensional ultrasound transducers were developed and fabricated in Chapter 3 and 4. The physical characteristics of the prototype devices will be studied in this chapter. Generally, ultrasound frequency at a range of 20 to 100 kHz has been shown to enhance transdermal transport of a variety of drug molecules. According to the previous research [33], acoustic frequency and intensity are two major parameters for the ultrasound enhanced transdermal drug delivery as well as the ultrasound triggered responsive drug delivery systems. Therefore, it is necessary to measure the fundamental resonance frequencies and output acoustic intensities of our newly developed prototype devices 'A' and 'B'.

5.2 First Resonance Frequency Measurement

As mentioned in Chapter 4, the flat flextensional ultrasound transducers were made to be operated at their first resonance frequency in which the electrical and

mechanical energy transformation rate is the highest. In order to measure the first resonance frequency in water, two methods were implemented.

5.2.1 First resonance frequency of device 'A'

5.2.1.1 Electric scanning methods

As shown in Figure 5.1, a cap screw (CB 6-15, SANSHO**)** was attached to the threaded hole of the ultrasound transducer through a hole on the wall of an acrylic water tank (190 mm x 100 mm x 70 mm) with 1 liter of degassed deionized water, where the ultrasonic device was mounted (Figure 5.1 (c)). In the first method, the electric impedance was measured with Solartron impedance/gain-phase analyzer (SI 1260, Solartron analytical) that is powerful, accurate and flexible frequency response analyzer. Virtually, every liquid and solid is able to pass current when a voltage is applied to it. If a variable (ac) voltage is applied to the material, the ratio of voltage to current (V/I) is known as the impedance. In many materials, especially those which are not generally regarded as conductors of electricity, the impedance varies with the frequency of the applied voltage changes, in a way that is related to the properties of the liquid or solid. Thus, if the frequency of the applied voltage equals the resonance frequency of the structure, the output impedance at that frequency is the minimum value. Using this method the fundamental resonance frequency of the transducer could be found out. In this experiment, the transducer was operated with applied AC voltage of 0.4 V_{rms} and the sweeping frequency range was set from 1 kHz to 50 kHz and sweeping step was 500. The driving frequency versus electric impedance diagram (Figure 5.2) shows that the first resonance frequency of the flat flextensional transducer measured in water was 17.466 kHz.

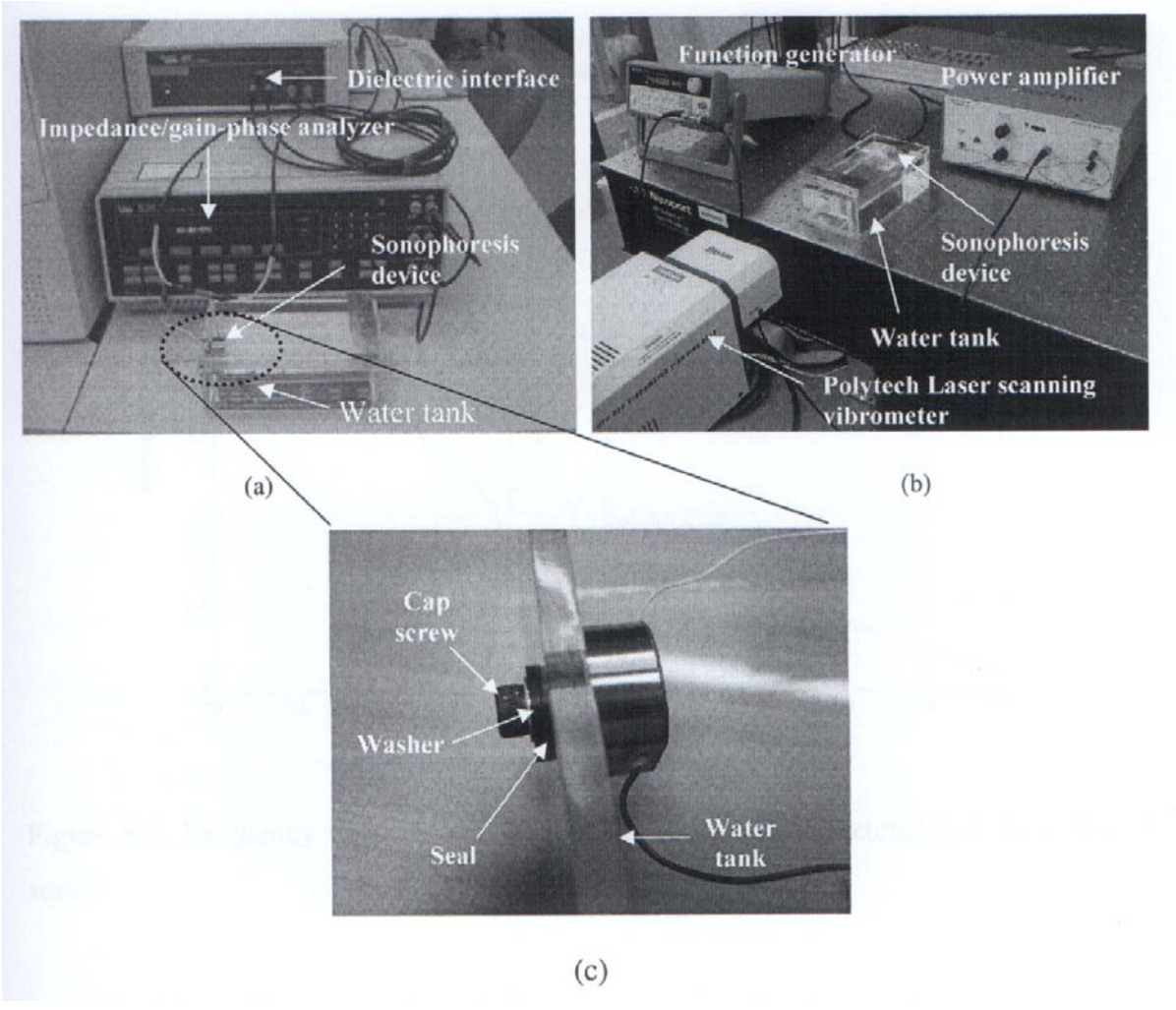

Figure 5.1. Two experimental setups for the first resonance frequency measurement in water. (a) Solartron SI1260 impedance/gain-phase analyzer measurement. (b) Polytec laser scanning vibrometer measurement. (c) A close-up photograph of device mounting method.

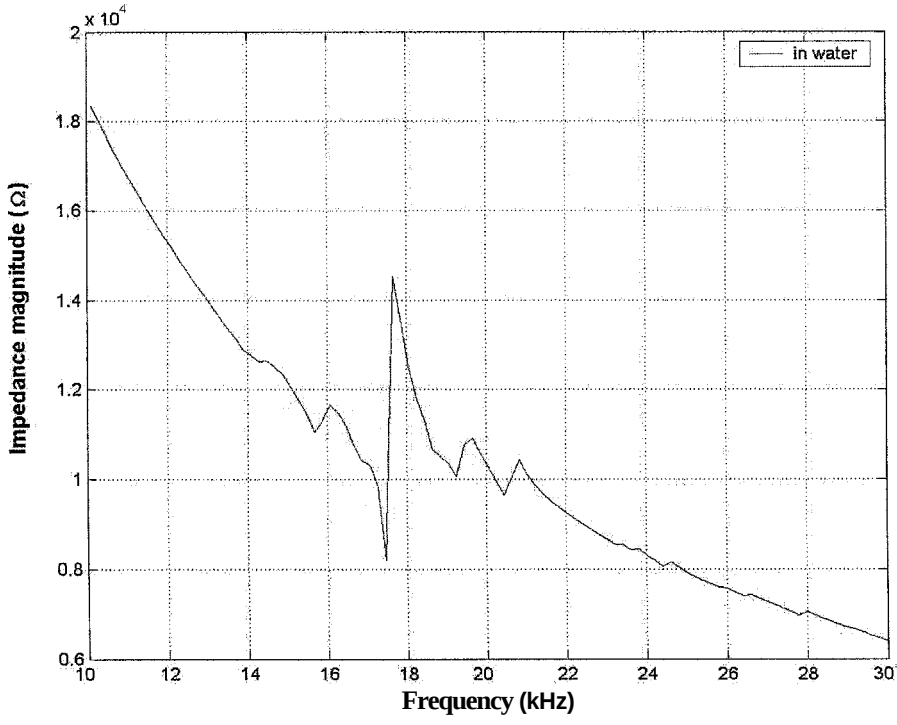

Figure 5.2. Frequency impedance characteristic for the flat flextensional transducer in water.

5.2.1.2 Laser scanning method

The second method analyzed the vibrating velocity of the stainless steel plate as a function of various driving frequencies in water. A laser scanning vibrometer (Polytec PSV-300, GmbH) was utilized in the experiment (Figure 5.1 (b)). The heart of the PSV-300 system is the laser Doppler vibrometer which is a very precise optical transducer for measuring vibration velocity at a point by sensing changes in frequency of light backscattered from a moving surface. The live video image together with advanced point selection (APS) software is used to define the scan point locations. The scanning process is controlled by the data manage system (DMS) operating under WindowsNT™. Analogue velocity signals together with up to three reference signals are digitized and displayed as time signals or spectra. In this experiment, a square-shaped scanning area

was selected in which there were 323 scanning points. The bandwidth of the sweep frequency was set to start fromzero and end at 50 kHz. The data of each scanning point is transferred to the analysis software Polytec PSV 7.11 and the result is shown in Figure 5.3. The first resonance frequency is 17.406 kHz. Both the experimental results indicate the first resonance frequency of the proposed flat flextensional transducer at approximately 17.4 kHz which is marginally smaller than that of the simulation result (20.14 kHz) as shown in Table 4.2. The frequency difference is probably due to the presence of conductive epoxy layer between PZT material and metal vibration plate which was not considered in the simulation model. The geometrical error during the fabrication and assembly of the device may also be responsible for the difference.

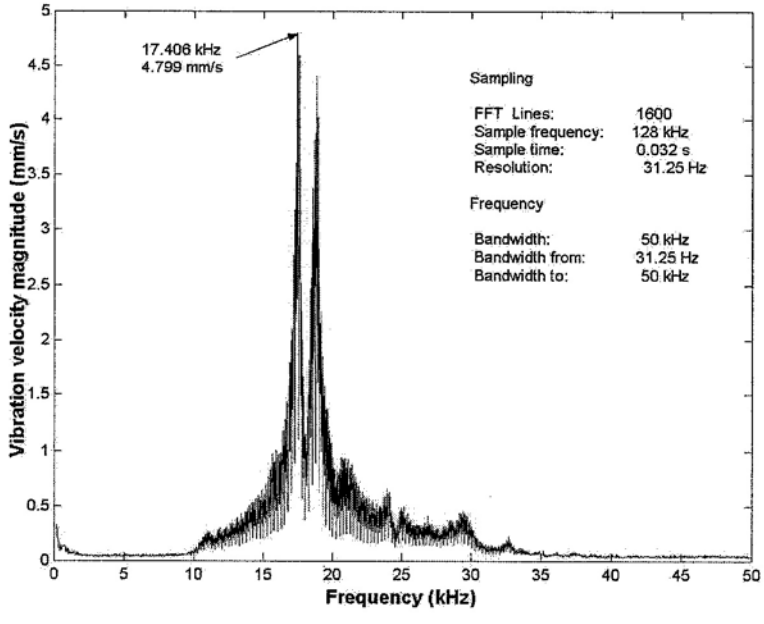

Figure 5.3. Resonant frequencies scanning results of device 'A' in water.

5.2.2 First resonance frequency of device 'B'

Compared with these two different measurement methods, although laser scanning vibrometer PSV-300 system is much more powerful, it will take long time to align the vibration surface of the transducer vertical to the laser beam in order to obtain

the maximum reflect back signals. It is also required to select a suitable scanning area and the quantities of the scanning points to achieve accurate results. Furthermore, auxiliary instruments such as the function generator and the power amplifier are required to drive the ultrasound transducer so that the experimental setup is a little bit complex. On the other hand, using impedance analyzer to determine the resonance frequencies of the dynamic structure (i.e. ultrasound transducer) is relatively simple. It only needs to connect the positive and negative electrodes of the analyzer to the device and select the sweeping frequency range and output parameters. Thus, in order to obtain the fundamental resonance frequency of device B, the same Solartron impedance/gain-phase analyzer (SI1260, Solartron analytical) was used to measure the electrical impedance of each flat flextensional ultrasound transducer in device 'B' in air and in water. The experimental set-up is shown in Figure 5.1 (a). In air, the device was mounted on the wall of an acrylic water tank (190 mm x 100 mm x 70 mm) and one transducer was operated with applied AC voltage of 0.4 V_{rms} while the other was short circuited. The sweeping frequency range was set from 1 kHz to 100 kHz and sweeping step was 500. The result of output impedance of each ultrasound transducer in device 'B' is shown in Figure 5.4 (a). From Figure 5.4 (a), the first resonance frequency in air of both transducers is at proximately 34 kHz. The difference is not greater than 0.2 kHz.

In water, the first resonance frequency was measured with the same experimental setup (Figure 5.1 (a)) and configuration but with the device totally immersed in 1 liter of degassed and distilled water. The experimental results are shown in Figure 5.4 (b), which illustrate that both transducers have the same first resonance frequency (26.83 kHz) with small difference in impedance. The first resonance frequency is slightly less than that of

the simulated results (Table 4.3) and the difference is less than 2 kHz**.** The simulated results agree well with the experimental results.

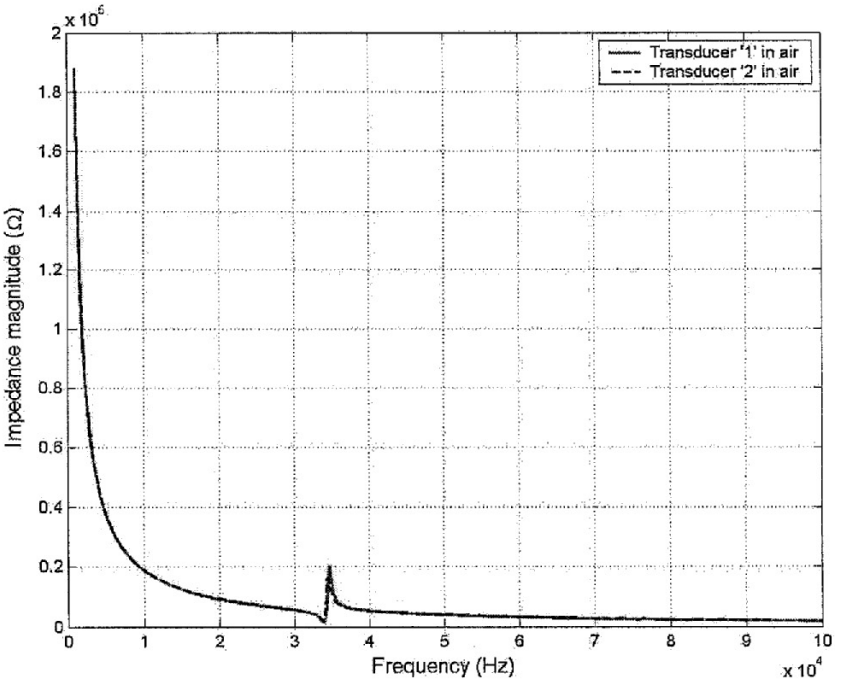

(a) In air

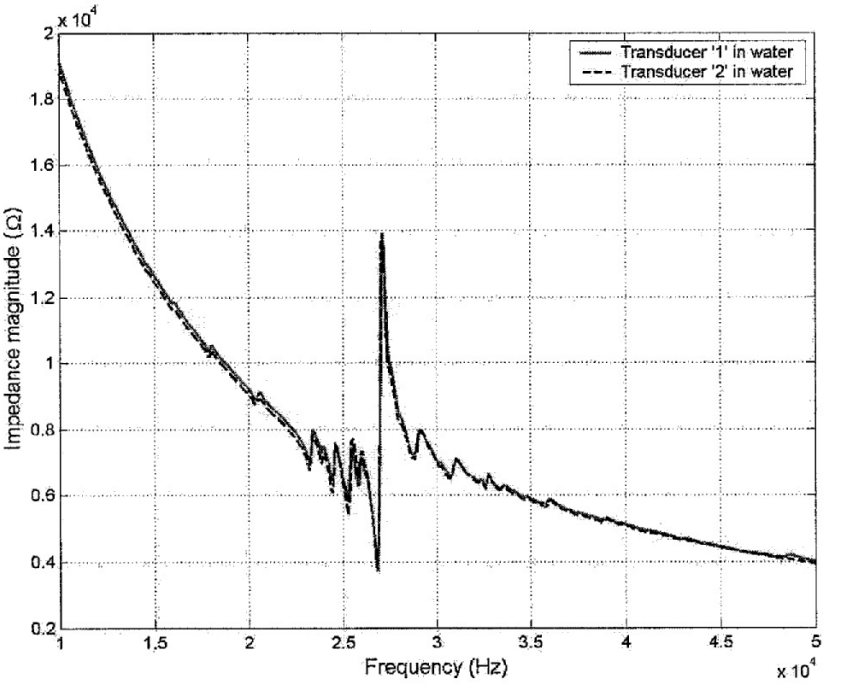

(b) In water

Figure 5.4. Experimental results of fundamental resonance frequency of each ultrasound transducer in the proposed device 'B'.

5.3 Acoustic Bubble Observation

Generally, depending on the application, the acoustic intensity required for sonophoresis at low frequency (20-100 kHz) will be between about 0 to 2.6 W/cm^2. In this intensity range, the proposed dominant mechanism of sonophoresis, although not completely understood, has been suggested to be the result of cavitation that refers to the formation and the subsequent dynamic life of bubbles in liquids [12]. Cavitation phenomena may cause biological changes to surrounding materials due to transient cavitation induced high temperatures, high pressures and stable cavitation generated microstreaming [74]. Thus the drug molecules can diffuse through the skin. However, the problems associated with predicting the cavitation threshold or the effects of cavitation are many. The location, type and size of the cavitation nuclei in vivo are all largely unknown. Mechanism of cavtation phenomena is a complex study. Nevertheless, if the acoustic bubbles are observed, it indirectly demonstrates that the acoustic intensity induced by the proposed flextensional transducer will be beyond the cavitation threshold. The cavitation phenomena may be considered to be a strong indicator of the relationship between the skin permeability and the performance of the sonophoresis device.

5.3.1 Experimental setup

The schematic drawing of experimental setup for acoustic bubble observation is given in Figure 5.5. The proposed transducer device was mounted on the wall of an acrylic water tank, which was filled with 1 liter of water. The transducer was driven by a pulsed signal with a pulse duty cycle of 20% generated by an arbitrary function generator (AFG320, Sony Tektronix) and amplified by a power amplifier (Model EPA-102, Piezo sytems). The function generator was operated at 17.466 kHz with 4 V, 6 V and 8 V (amplitude) output and was amplified 20-fold by the amplifier. A 20x magnifications

SONY CCD (charge coupled device) camera was used and connected to a PC to record the activity of the bubbles.

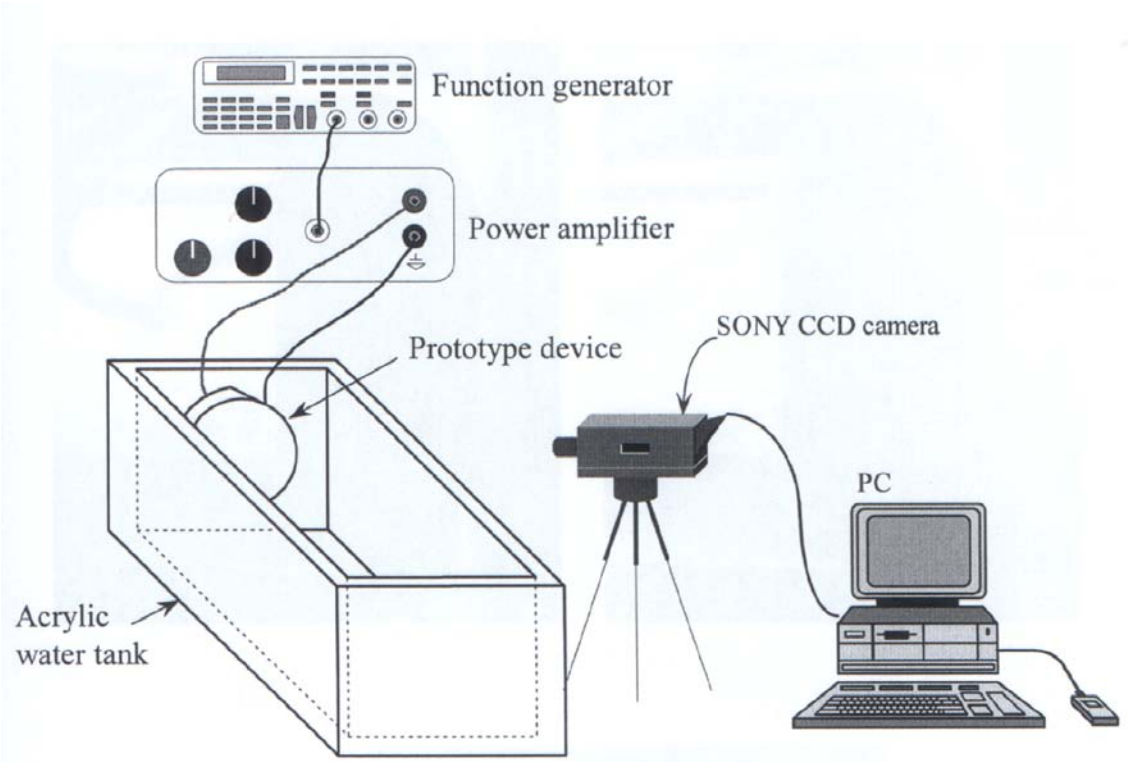

Figure 5.5. Schematic drawing of experimental setup for acoustic bubble observation.

5.3.2 *Acoustic bubble observation of device 'A'*

Figure 5.6 shows the acoustic bubble activities depending on various applied voltages. From these three images, it is clearly shown that the acoustic bubble vibrated on the surface of the metal vibrating plate and the bubble quantities increased with the increase of the applied voltages. Although the acoustic intensity generated by the vibration metal plate is beyond the cavitation threshold, no large sized bubbles were observed at the vicinity of the vibration plate. Most of the acoustic intensity exists at the interface of the metal vibration plate and water. Because of the mismatch of the acoustic impedance between the stainless steel vibrating plate and the water, there is inadequate

acoustic intensity radiated into the water and enable the sub-micron or micro-sized bubbles to grow in a manner visible by naked eyes.

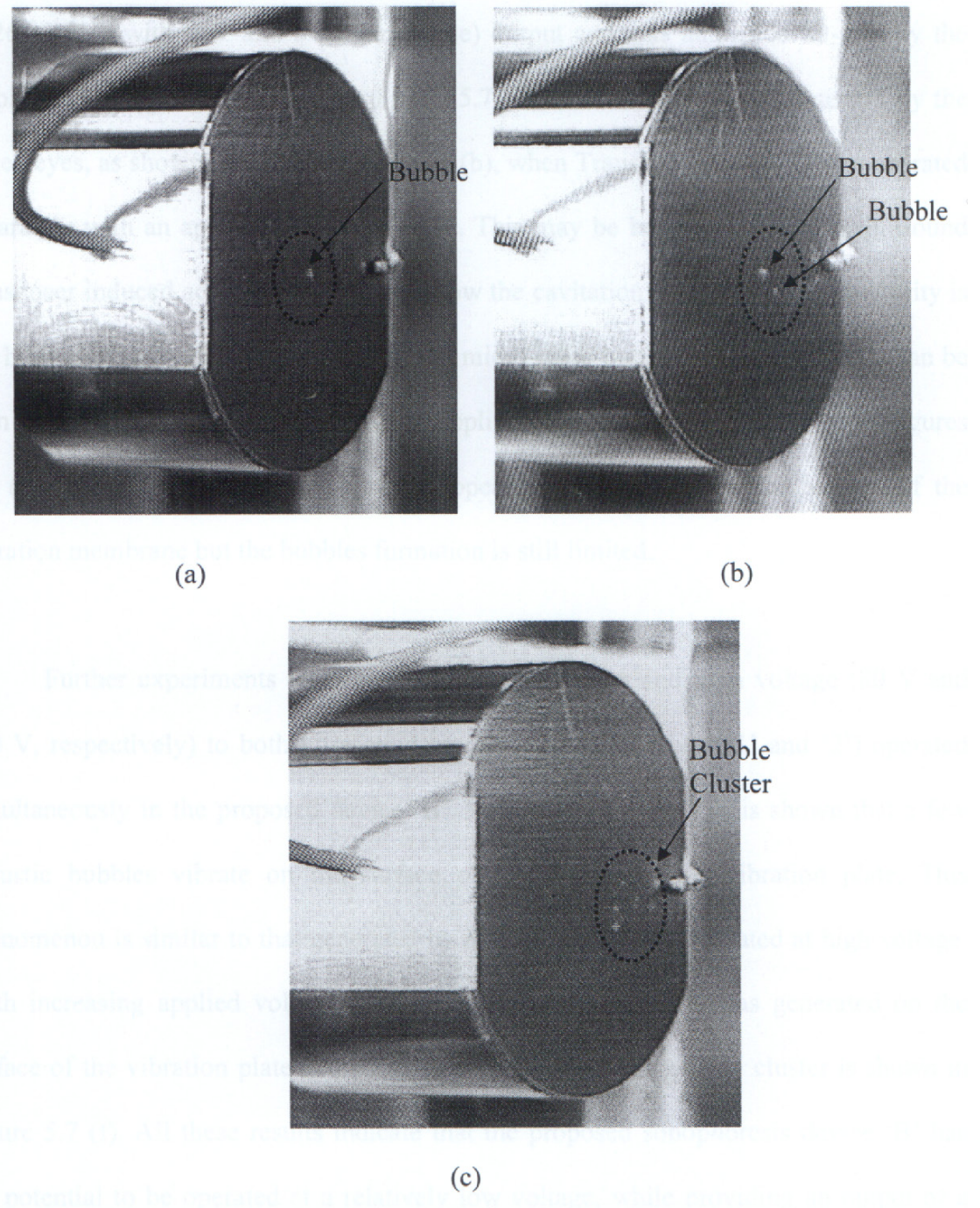

Figure 5.6. Acoustic bubble phenomena as a function of applied AC voltages. (a) 80 V. (b) 120 V. (c) 160 V.

5.3.3 *Acoustic bubble observation of device 'B'*

In order to observe the cavitation phenomena produced by the device 'B', the same experimental setup (Figure *5.5)* was utilized. The function generator was operated at 26.83 kHz with 4 V and 8 V (amplitude) output and was amplified 20-fold by the amplifier. The results are shown in Figure 5.7. There were no bubbles observed by the naked eyes, as shown in Figures *5.7* (a) and (b), when Transducer '1' or '2' was operated separately with an applied voltage of 80 V. This may be because the single ultrasound transducer induced acoustic intensity is below the cavitation threshold, or the intensity is not high enough to allow the sub-micron or micro-sized bubbles to grow to a size can be seen by naked eyes. Upon increasing the applied voltage to 160 V, as shown in Figures 5.7 (c) and (d), more acoustic bubbles appeared and vibrated on the surface of the vibration membrane but the bubbles formation is still limited.

Further experiments were performed to apply low and high voltage (80 V and 160 V, respectively) to both ultrasound transducers (Transducers '1' and '2') operated simultaneously in the proposed device 'B'. From Figure 5.7 (e), it is shown that a few acoustic bubbles vibrate on the surface of the stainless steel vibration plate. This phenomenon is similar to that generated by a single transducer operated at high voltage. With increasing applied voltage, significant acoustic cavitation was generated on the surface of the vibration plate and water domain. An acoustic bubble cluster is shown in Figure *5.7 (f)*. All these results indicate that the proposed sonophoresis device 'B' has the potential to be operated at a relatively low voltage, while providing an output of a high acoustic power in a portable or wearable device for ultrasound enhanced drug delivery.

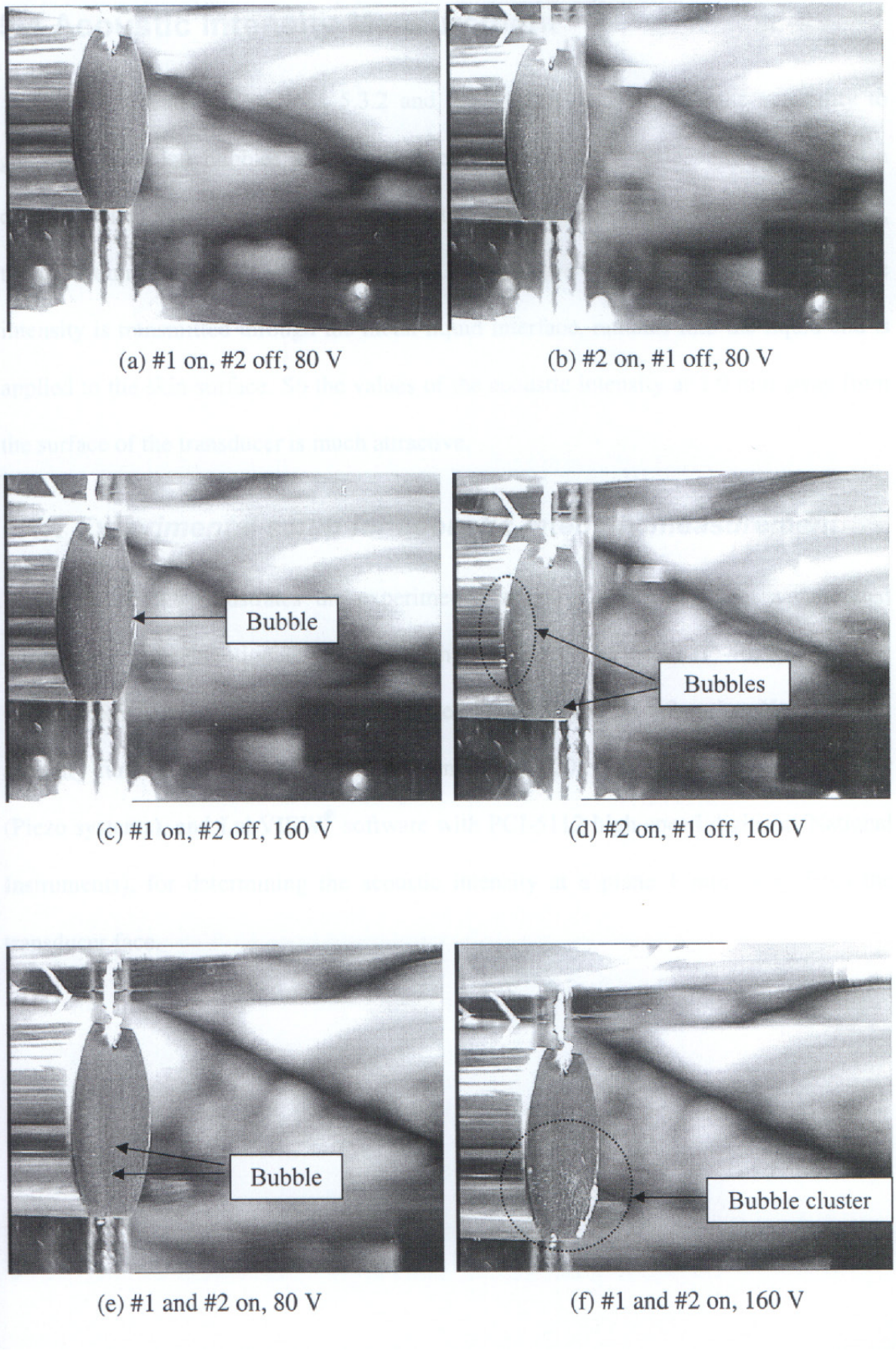

Figure 5.7. The activities of acoustic bubbles under different conditions (# 1 represents Transducer '1'. #2 represents Transducer '2').

5.4 Acoustic Intensity Measurement

As indicated in sections 5.3.2 and 5.3.3, both devices have the capability to generate cavitation bubbles at the interface of the vibration plate and the water at a certain applied voltage. However, for the ultrasound enhanced drug delivery, in general, the ultrasound transducer is placed about 1.0 mm above the skin surface. The acoustic intensity is transmitted through the metal-liquid interface, radiates into the liquid and is applied to the skin surface. So the values of the acoustic intensity at 1.0 mm away from the surface of the transducer is much attractive.

5.4.1 Experimental setup for acoustic intensity measurement

Figure 5.8 illiustrates the experimental setup, which consists of a calibrated miniature omni-directional reference hydrophone (Model TC-4013, RESON OFFSHORE Ltd.), three computer controlled linear stages (M462 series, Newport), an arbitrary function generator (SONY Tektronix, AFG320) along with a power amplifier (Piezo systems), and LabVIEW® software with PCI-5112 high speed digitizer (National Instruments), for determining the acoustic intensity at a plane 1 mm away from the transducer face.

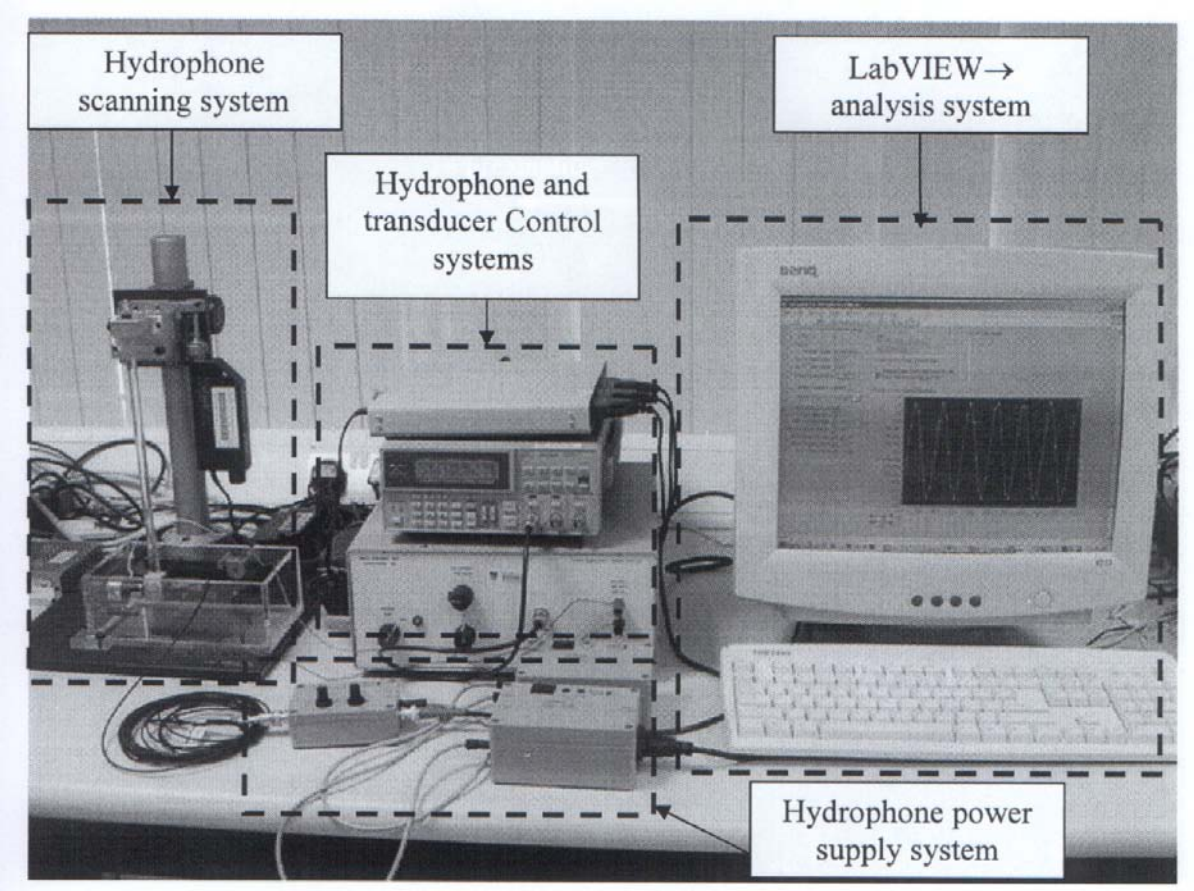

Figure 5.8. The whole experimental setup for the acoustic intensity measurement.

In this experimental setup, the TC-4013 hydrophone offers a useable frequency range from 1 Hz to 170 kHz with high receiving sensitivity (-211 dB±3dB re 1V/μ Pa). It also provides uniform omnidirectional sensitivities in both horizontal and vertical planes up to high frequencies. During the experiment, the TC-4013 hydrophone captures the acoustic pressure signal in the water and converts it to an electrical signal via an acoustic sensor inside of the chloroprene rubber. The TC-4013 hydrophone does not have a built-in preamplifier. In order to supply the sufficiently high level signal to the PCI-5112 high-speed digitizer, a preamplifier (VP-1000) along with a DC supplier and a charger were utilized. The detailed hydrophone connection method is given in Figure 5.9.

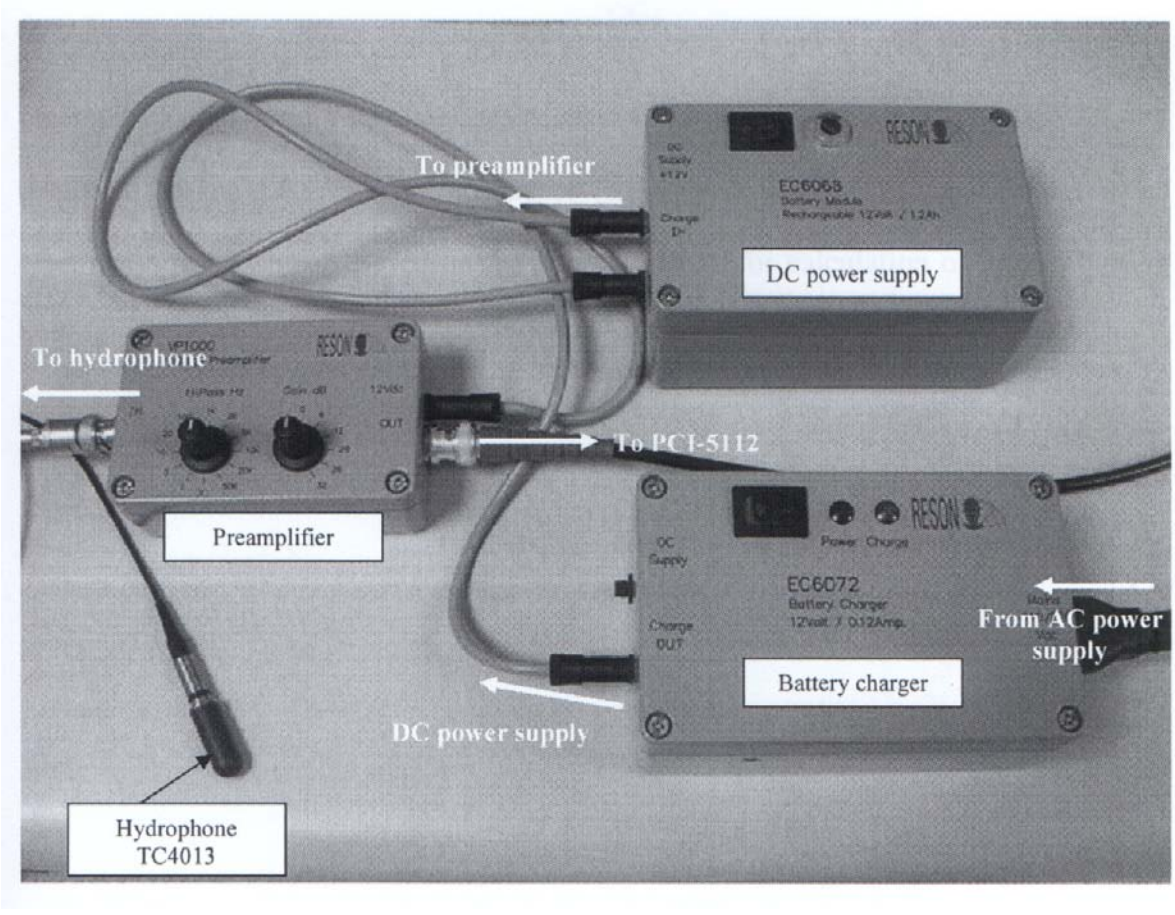

Figure 5.9. Hydrophone connection method.

A PCI-5112 high-speed digitizer has two analog input channels for data logging of range from ±25 mV to ±25 V variable in 10 percent steps. The analog input stage has functions of a selectable input impedance of 1 MΩ or 50 MΩ, selectable AC or DC coupling and onboard self-calibration. Each analog input channel has its own 100 MS/s, 8-bit analog-to-digital converter so it can simultaneously acquire data on each channel sampled at rates from 100 MS/s to 1 S/s. In this experimental setup, the PCI-5112 high-speed digitizer is integrated fully with LabVIEW® software which is a graphical programming language using icons instead of lines of text to create applications. It contains comprehensive libraries for data collection, analysis, presentation and storage. The working flow chart of the data acquisition in this acoustic intensity measurement is given in Figure 5.10. As shown in the figure, a small acoustic signal is collected by the

TC-4013 hydrophone and converted to an electrical signal. It will be enlarged by a preamplifier to a certain level and transferred to the PCI-5112 high speed digitizer and displayed in the LabVIEW® front panel (see Figure 5.11). The final output is an electrical voltage signal. Based on the IEEE standard for calculation of intensity using hydrophone voltage waveform [118], the output spatial peak-temporal-peak intensity is expressed as

$$I_{sptp} = \frac{V_{TP}^{\ 2}}{K_f^{\ 2}} \ \mathrm{W/cm^2} \tag{5.1}$$

And,

$$K_f^{\ 2} = \left(10^6 \rho c\right)\left(10^{M/10}\right) \ \mathrm{V^2W^{-1}cm^2} \tag{5.2}$$

Where, ρ is the density of water in $\mathrm{kg/m^3}$ and c is the speed of sound in water in m/s. M is the sensitivity of the hydrophone in dB re $1\ \mathrm{V/\mu Pa}$. V_{TP} is determined by measuring compressional peak (v_-) and rarefactional peak (v_+) voltage amplitude in volts and choosing the larger value of v_+ and $|v_-|$

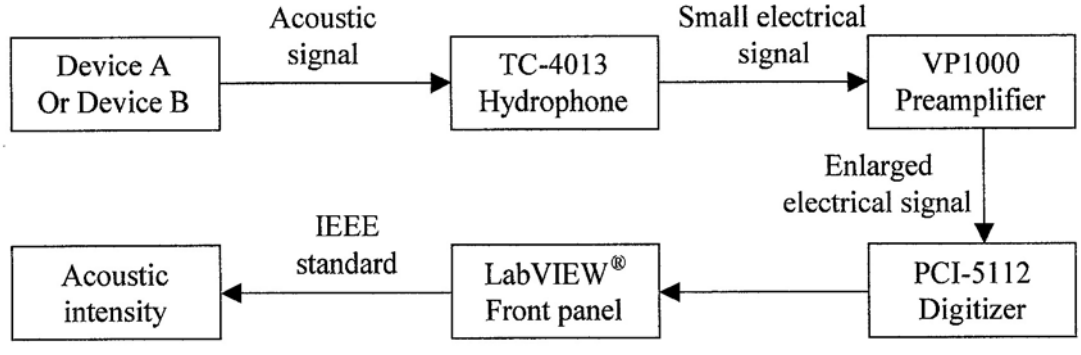

Figure 5.10. The working flow chart of the data acquisition and output acoustic intensity calculation.

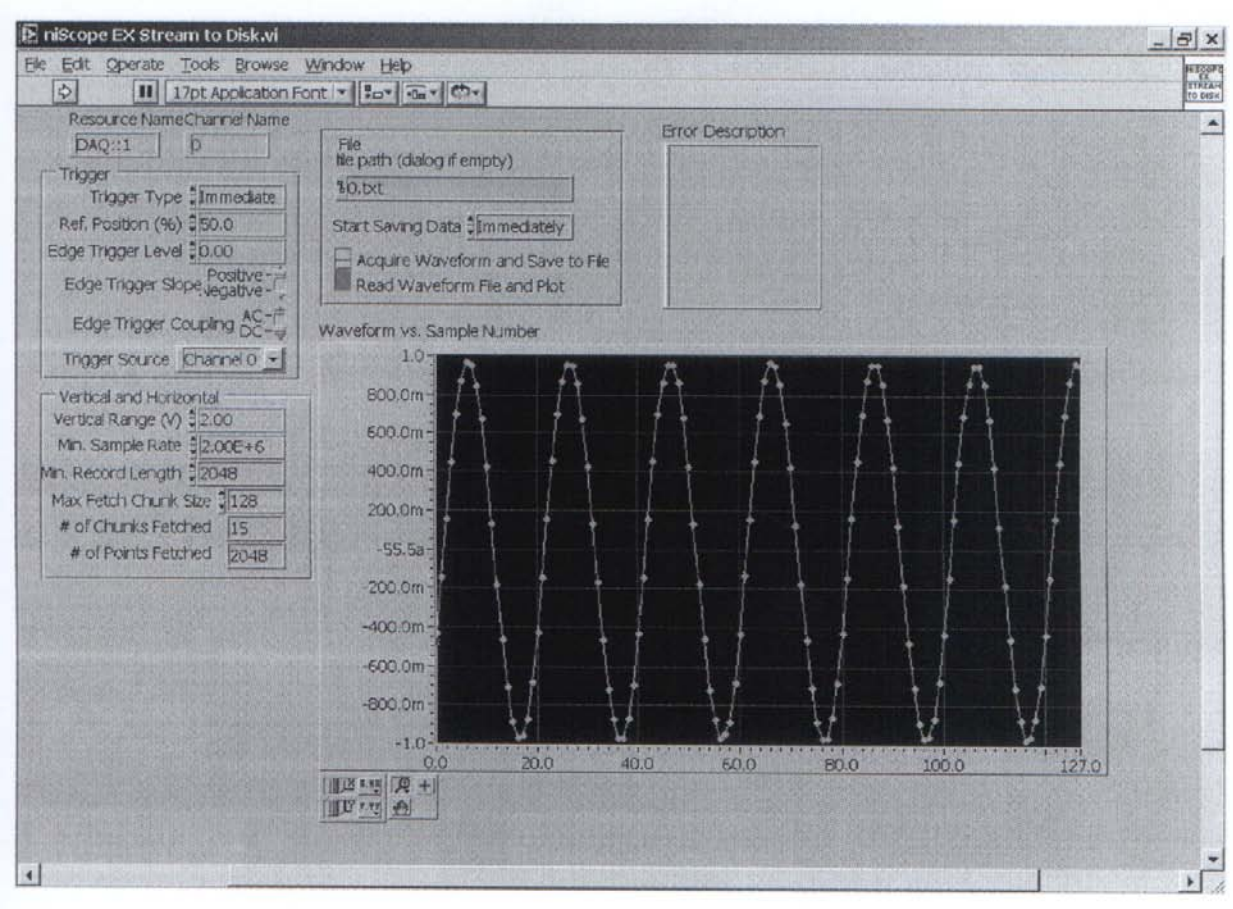

Figure 5.11. A typical LabVIEW® front panel used in the acoustic intensity measurement. The waveform in the figure was obtained directly from the output signal of function generator.

Figure 5.12 indicates the hydrophone holding method. The TC-4013 hydrophone is fixed in an aluminum holder and connected to a self-designed locating block, which is mounted on the Z-direction linear stage, through an acrylic shaft. The movement of hydrophone is realized by three computer controlled linear stages whose maximum x, y and z travel is 25.0, 30.0 and 25.0 mm, respectively. All these linear stages are driven by Newport 850G linear actuators. The scanning area for the acoustic intensity measurement was 27 mm x 24 mm and the scanning step was set to 1.0 mm. The prototype sonophoresis device was driven by a pulsed signal with 20% duty cycle generated by an arbitrary function generator (AFG320, Sony Tektronix) and amplified by a power amplifier (Model EPA-102, Piezo Systems).

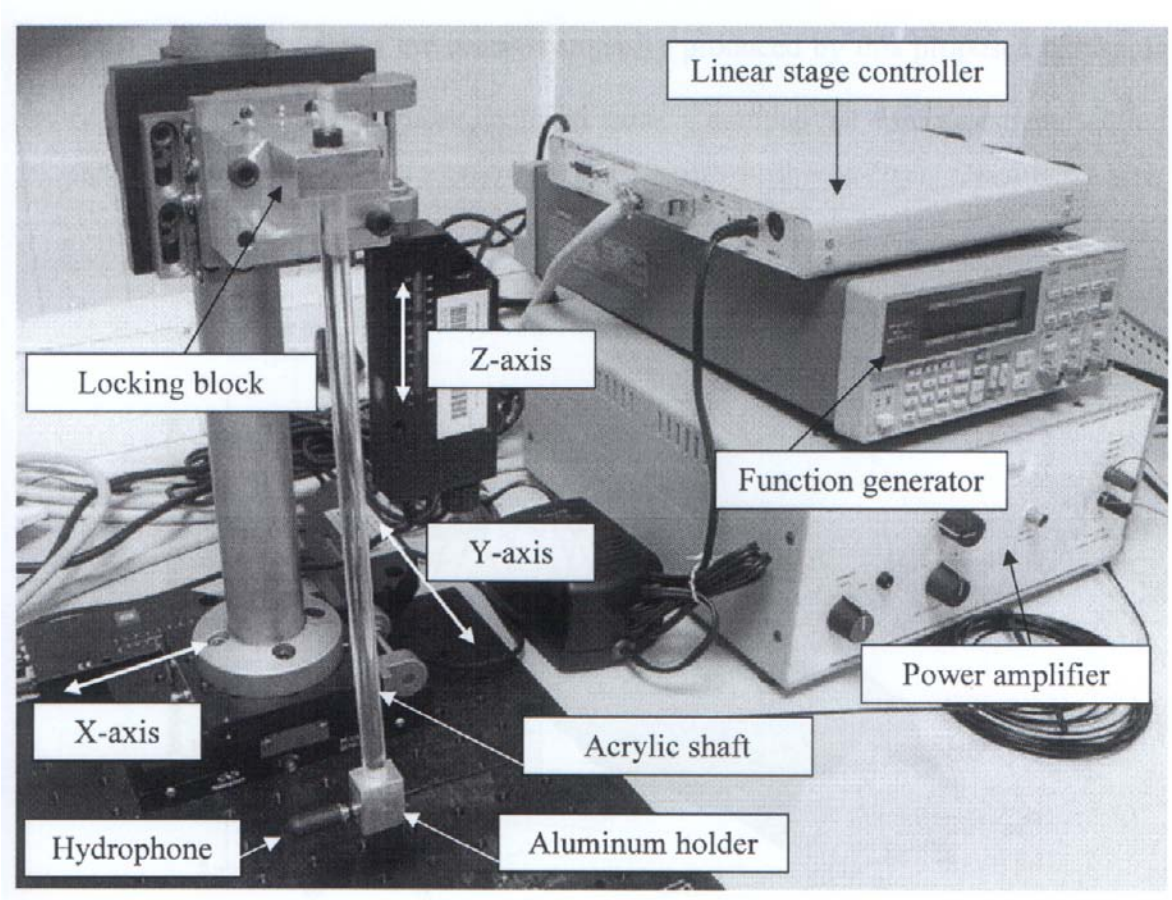

Figure 5.12. Hydrophone holding method.

5.4.2 Output acoustic intensity of device 'A'

Figures 5.13 (a), (b) and (c) show the three-dimensional scanning diagram of the acoustic intensity produced by transducer device 'A'. It indicates that for a certain acoustic intensity applied on the skin surface or diffusion membrane, the corresponding effective area increases with the increase of applied voltages. Figure 5.14 plots the detailed results of the maximum spatial peak-temporal-peak intensity versus the applied voltages. When the acoustic transmission coefficient is determined, the maximum spatial peak-temporal-peak intensity increased with the increment of driven voltages. The maximum spatial peak-temporal-peak intensity under three different driven voltages (80 V, 120 V and 160 V) was approximately 41.13 mW/cm^2, 69.66 mW/cm^2 and 105.09

mW/cm^2, respectively. Thus the acoustic intensity produced by this proposed ultrasonic device 'A' is comparable to those achieved using a commercial sonicators (see section 5.3).

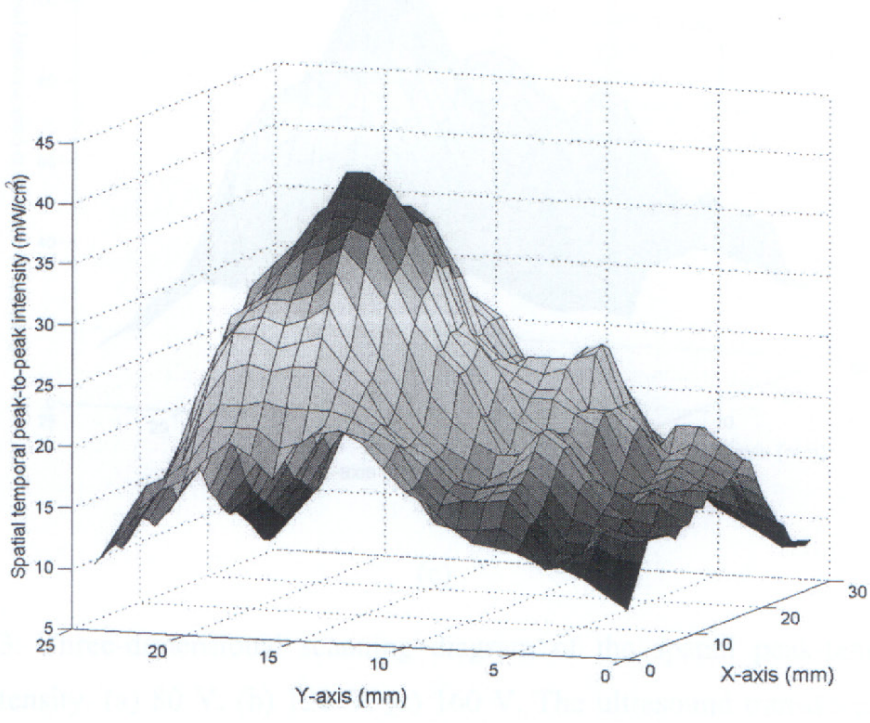

(a)

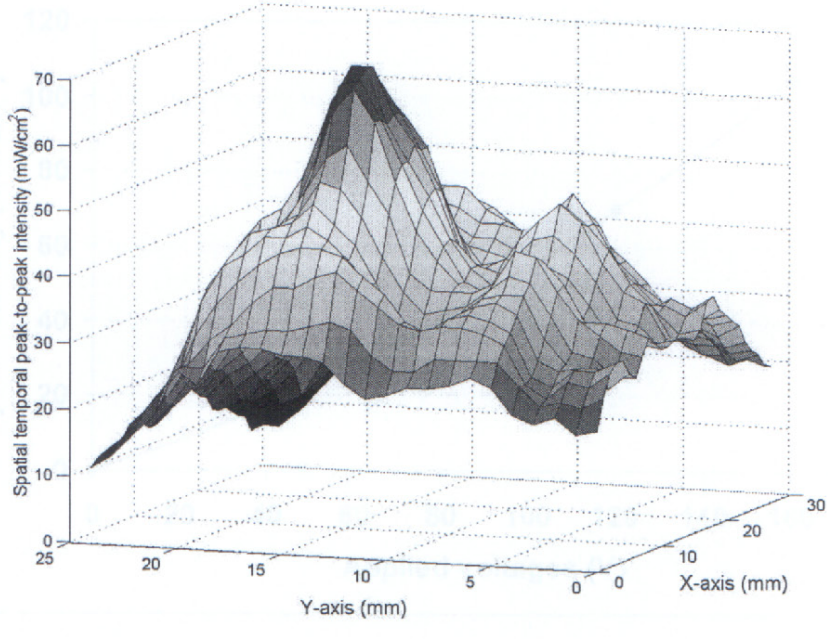

(b)

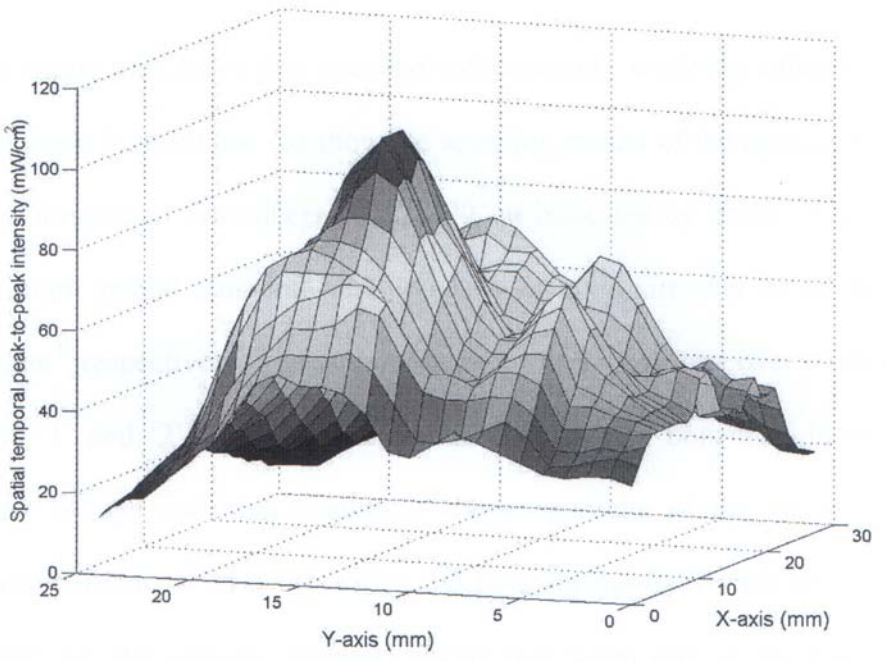

(c)

Figure 5.13. Three-dimensional scanning diagram of the spatial peak-temporal-peak acoustic intensity. (a) 80 V. (b) 120 V. (c) 160 V. The ultrasound transducer of device 'A' was operated with pulsed electric signal with 20% duty cycle.

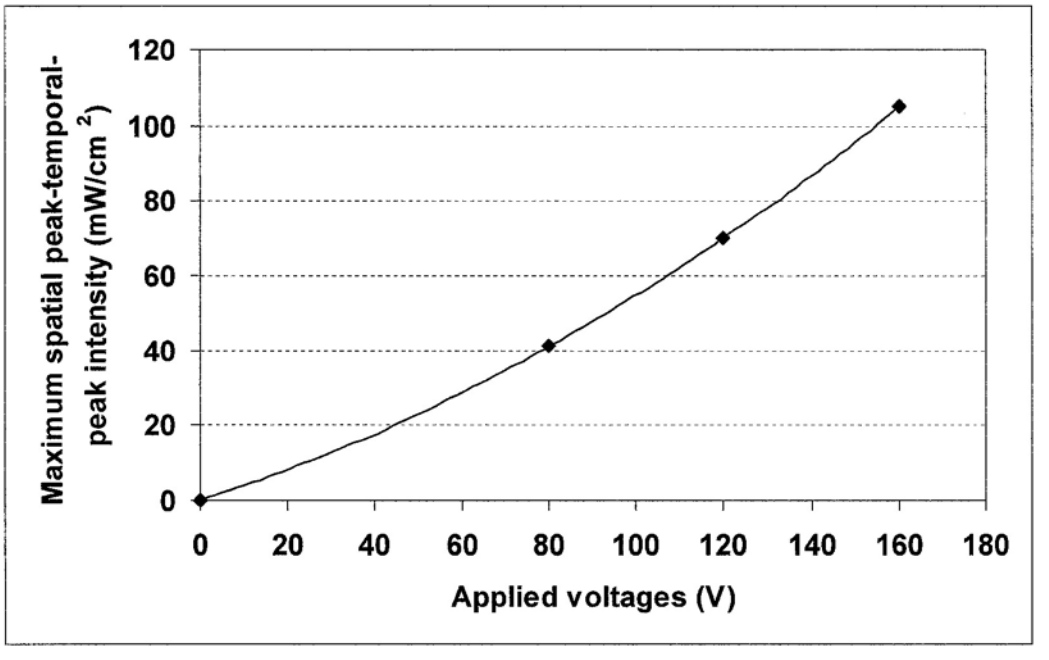

Figure 5.14. The maximum spatial peak-temporal-peak intensity with different applied voltages.

5.4.3 Output acoustic intensity of device 'B'

The single transducer was operated independently while the other one was short circuited. Figures 5.15 (a) and (b) show the scanning results of the spatial temporal peak intensity for ultrasound Transducers '1' and '2' as indicated by arrows. Each transducer has a maximum spatial temporal peak intensity of approximately 18.62 mW/cm^2 and 41.95 mW/cm^2, respectively. The output acoustic intensity differs over twofold between Transducers '1' and '2'. One possible reason is that when both transducers vibrate at high driving voltage and high amplitude, the temperature of the vibration plate and piezoelectric material increases to soften the bonding non-uniformly [117]. In Figures 5.15 (a) and (b), the acoustic intensity shows that when one of the transducers was active, the ultrasound energy was radiated from the active as well as the inactive transducer. The results of this work may be affected by the physical structure of the device. The basic structure of this sonophoresis device is a solid steel plate with water on one side. At the interface between a fluid and an elastic solid, two kinds of surface waves can propagate. One is the leaky Rayleigh wave; the other is the Stoneley wave [119]. The Stoneley wave is a non-leaking wave with most of the energy residing in the liquid, while the leaky Rayleigh wave has most of energy in the plate. The undamped and nearly nondispersive Stoneley wave can cause significant cross coupling because it will carry the energy directly from an active ultrasound transducer to its inactive neighboring transducer [120]. Therefore, in Figures 5.15 (a) and (b), it is clearly shown that most of the acoustic power was radiated from the active transducer (in Figure 5.15 (a), active transducer is #l; in Figure 5.15 (b), active transducer is #2) and only a small part of acoustic power (approximately 8.49 mW/cm^2 and 6.48 mW/cm^2 in Figures 5.15 (a) and (b), respectively) was transferred to the inactive transducer and radiated.

For the operation of double ultrasound transducers, two positive electrodes were connected together and operated under the same driving conditions. Figure 5.15 (c) shows a scanning plot of the temporal peak intensity for double ultrasound transducers simultaneously operated at 26.83 kHz. The proposed sonophoresis device has a maximum spatial peak intensity of approximately 78.64 mW/cm^2 within the whole measurement area (24.0 mm x 27.0 mm). From Figure 5.15 (c), the spatial temporal peak intensity is found to be approximately 2 to 4 times larger than that produced by a single active ultrasound transducer.

Further experiments were conducted to investigate the potential capability to reduce the required electrical power. The same experimental setup and conditions were used for the experiments. In Figures 5.16 (a) and (b), the applied voltage decreased from 120 V to 80 V and the corresponding maximum spatial peak intensities were 53.05 mW/cm^2 and 38.47 mW/cm^2, respectively. In Figures 5.15 (c), 5.16 (a) and 5.16 (b), it is shown that when the driving voltage becomes low, the shape and peak of the acoustic intensity profile changes and shifts. This may also be due to the temperature induced change of the non-uniform interior properties of both transducers. However, the shape and position of the acoustic intensity peak will not effect the ultrasound enhanced drug penetration through the skin, according to the results of the previous research work [8]. Furthermore, compared with the results as shown in Figures 5.15 (a) and (b), if only one ultrasound transducer (Transducer '1' or '2') in the proposed sonpohresis device is operated, high applied voltage (160 V) is required and the maximum acoustic intensity can approximately reach the result as shown in Figure 5.16 (b) (low applied voltage of 80 V). From this viewpoint, the voltage of the applied signal is generally reduced at least twofold.

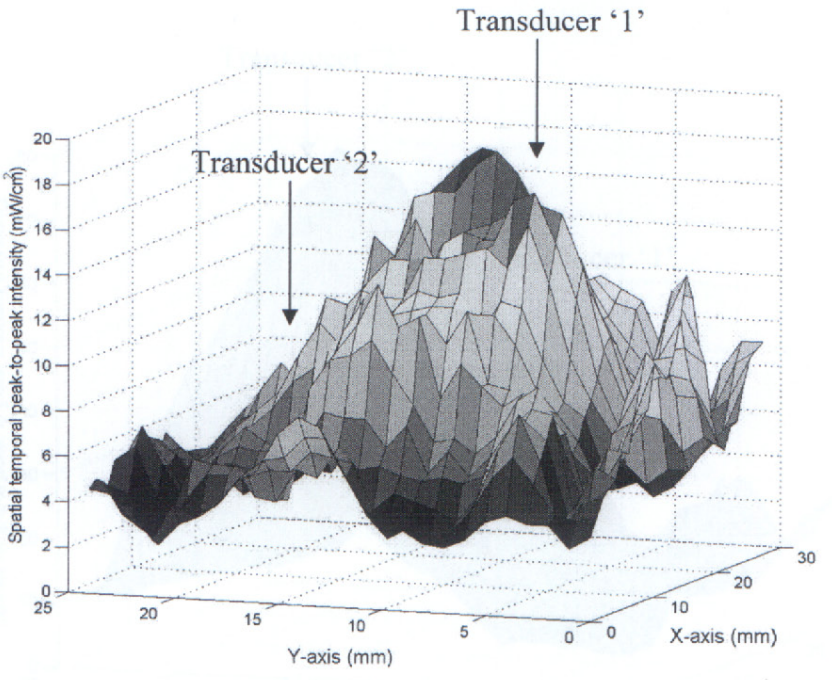

(a) 160 V (#1 on, #2 off)

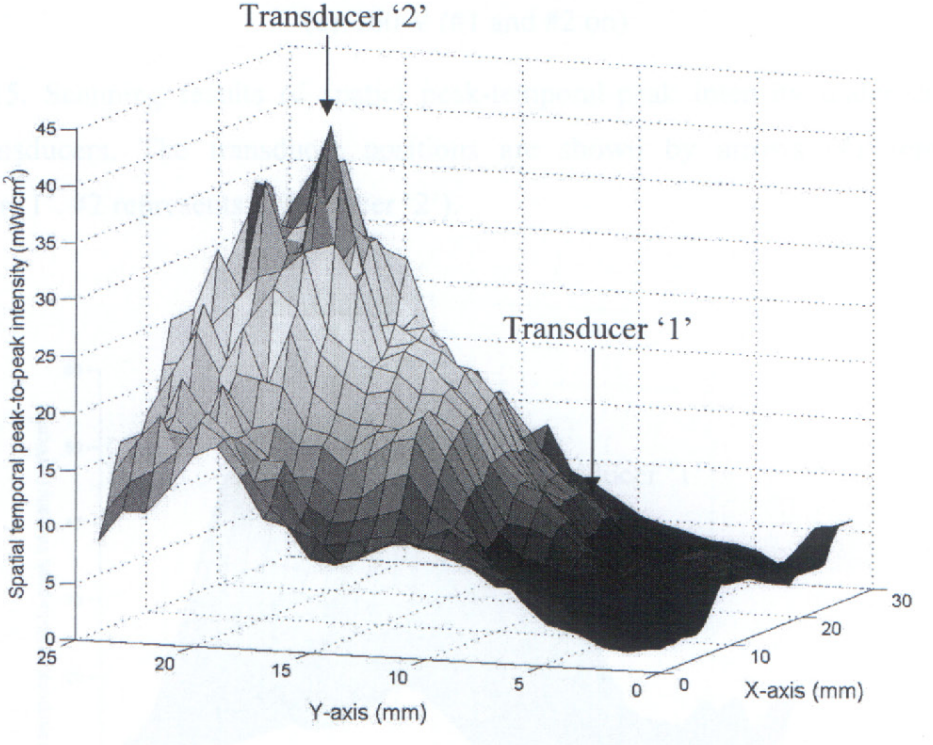

(b) 160 V (#1 off, #2 on)

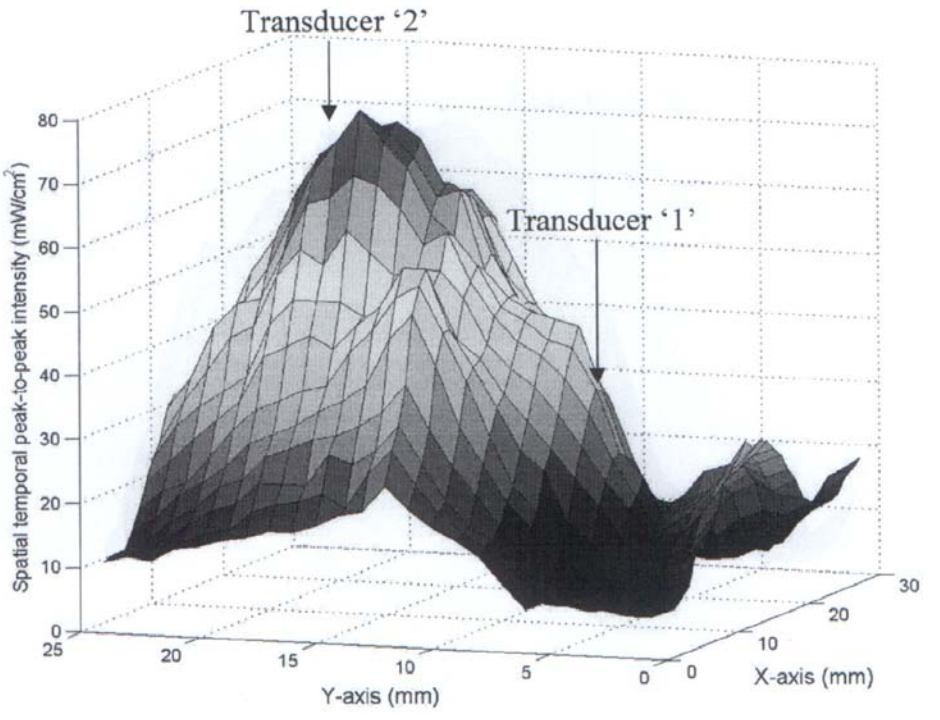

(c) 160 V (#1 and #2 on)

Figure 5.15. Scanning results of spatial peak-temporal-peak intensity under different active transducers. The transducer positions are shown by arrows (# 1 represents Transducer ' 1 '. #2 represents Transducer '2').

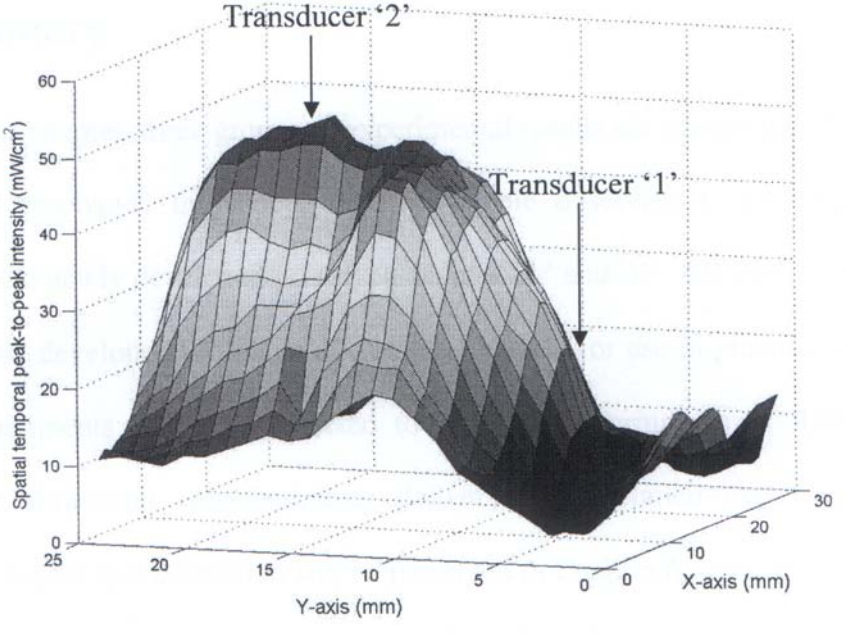

(a) 120 V (#1 and #2 on)

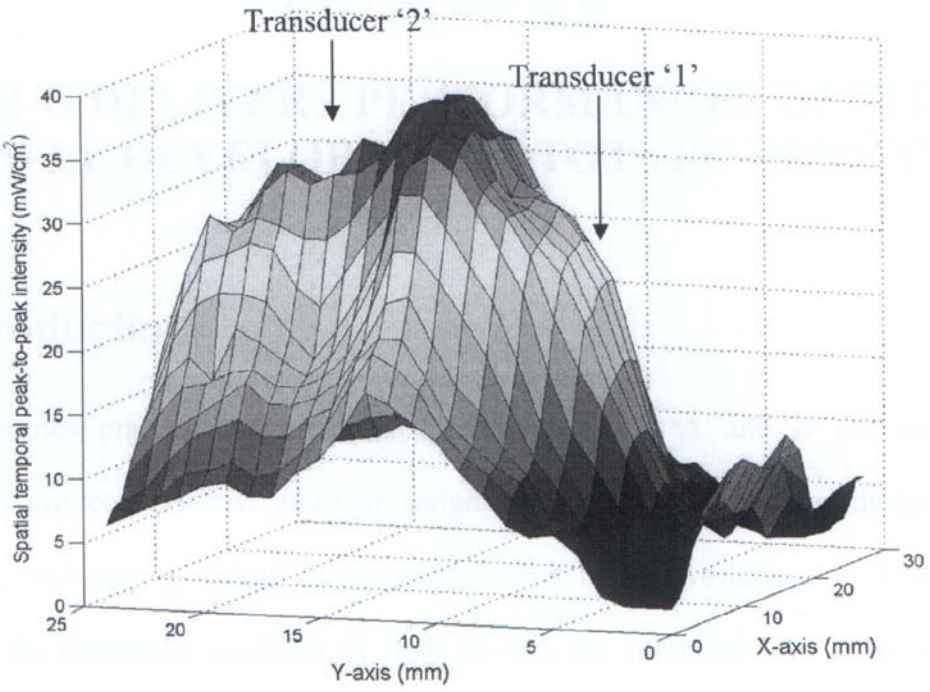

(b) 80 V (#1 and #2 on)

Figure 5.16. Scanning results of spatial peak-temporal-peak intensity under different applied voltages (#1 represents Transducer ' 1 '. #2 represents Transducer '2').

5.5 Summary

In this chapter, three groups of experimental results are presented, which includes fundamental resonance frequency, acoustic bubble observation and output acoustic intensity of the newly developed prototype devices 'A' and 'B'. All these results indicate that the newly developed prototype devices are feasible for use in practical applications. Further experiments will be conducted to test the performances of these prototype devices for ultrasound enhanced drug delivery. The detailed experimental setups, procedures, results and discussion will be presented in Chapter 6.

CHAPTER SIX

DRUG DELIVERY PERFORMANCES OF THE NEWLY DEVELOPED PROTOTYPE DEVICES

6.1 Introduction

Two new practicable sonophoresis prototype devices 'A' and 'B' (i.e. simplicity in the structure, cost effective and light weight for portability) have been designed and fabricated, and their physical characteristics have been investigated in Chapter 5. Although the intensities produced by both devices are comparable to those achieved using a commercial sonicator, the performances of the prototype devices for drug delivery are not well understood. The objective of this chapter is to explore the feasibility of using ultrasound produced by newly developed prototype devices for drug delivery application.

In the next section, the detailed experimental setups, materials and experimental procedures will be described. All the ultrasound enhanced drug delivery experiments are divided into two groups. The first group is to study the feasibility of device 'A' for drug delivery. At the same time, the effects of ultrasound irradiation on the permeability of the silicone rubber are also investigated using the same device. The experimental results and discussion of device 'A' is presented in section 6.3 and 6.4, respectively. The second group is to study the drug delivery performances of device 'B'. The aim of this study is to verify the capability of device 'B' that could efficiently enhanced permeability of the silicone rubber with low power requirement. The experimental results and discussion is

presented in section 6.5 and 6.6. The overall summary of this chapter is given in section 6.7.

6.2 Materials and methods

6.2.1 Ultrasonic prototype devices and mounting method

Two low frequency ultrasonic prototype devices based on the flat flextensional transducer were used for drug delivery experiments. The design, fabrication and electrical characteristics of both prototype devices have been discussed in detail in Chapter 4 and Chapter 5. Both devices have the same cross-sectional area and height for the stainless steel body and an M6 threaded hole is introduced for fixing. A shoulder screw (MMSB 8-20, SANSHO) is attached to the threaded hole through an elliptical hole in an acrylic plate of thickness 13.3 mm. The acrylic plate is placed on the top of the donor compartment of the vertical Franz diffusion cell, so the sonophoresis ultrasound device is submerged in the donor compartment and is placed about 1.0 mm away from the membrane as shown in Figure 6.1. A flexible insulated wire thermocouple probe (Cole-Parmer) was introduced into donor compartment to monitor the temperature during the ultrasound application.

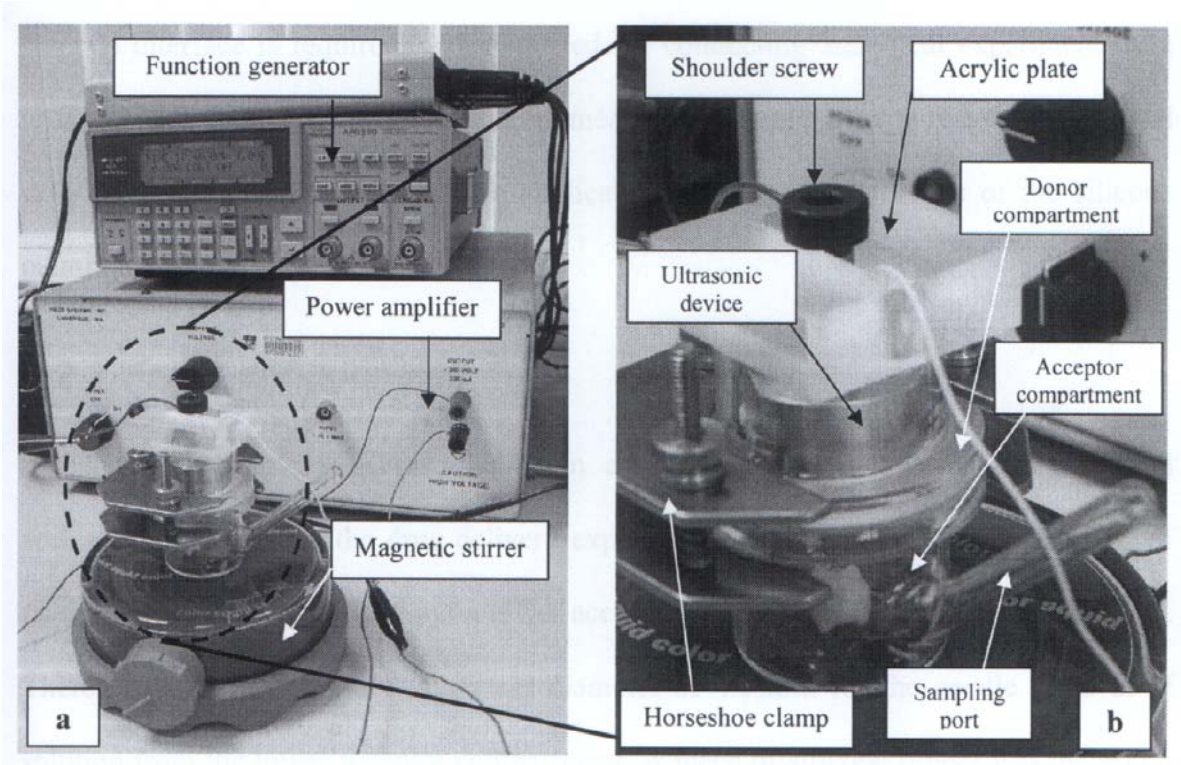

Figure 6.1. Experimental setup for ultrasound enhanced drug delivery. (a) Overall photo of the setup. (b) Enlarged photo to show the mounting method of the ultrasonic device.

6.2.2 Silicone rubber

Although in principle almost all polymers can be used to prepare rate-limiting membranes for controlled release devices, the bulk of the published work has been limited to relatively few materials. The silicone rubber group of polymers has been widely used to construct controlled release drug delivery devices. Silicone polymers have outstanding combination of biocompatibility, ease of fabrication, and high permeability to many important classes of drugs. In addition, silicone polymers can withstand heat sterilization, an important consideration in the construction of implant devices. In these drug delivery experiments, the biomedical grade silicone rubber (DOW CORNING® 7-4107) was obtained from DOW CORNING, which is a thin film of 100% of cured silicone rubber. It is supplied on a rigid polycarbonate carrier film. The silicone membrane has been used in the construction of various medical devices in which a

silicone interface is required, and also used for conducting analytical experiments and tests as biocompatible supportive film, permeation membrane in drug release testing, and skin simulating surface in skin care applications [121]. The thickness of the silicone membrane is about 70-90 μm.

6.2.3 Franz diffusion cell

A customer-made Franz diffusion cell (Permegear, Inc.) was designed and specially fabricated for the drug delivery experiments (Figure 6.2). The cell consists of an upper donor compartment and a lower acceptor compartment with a 26.8 ml volume. There is one sampling port with inner diameter of 4.0 mm for the needle removal of solution from the lower acceptor compartment. A piece of silicone rubber was placed on top of the acceptor compartment. A horseshoe clamp was used to secure the silicone rubber and the two compartments. The opening of the silicone rubber is about 31 .0 mm. A uniform mixture was maintained using a magnetic stirrer bar placed at the bottom of the acceptor compartment above a stirrer (Model 84001-00, Cole-Parmer). A photograph of the actual cell is shown in Figure 6.3.

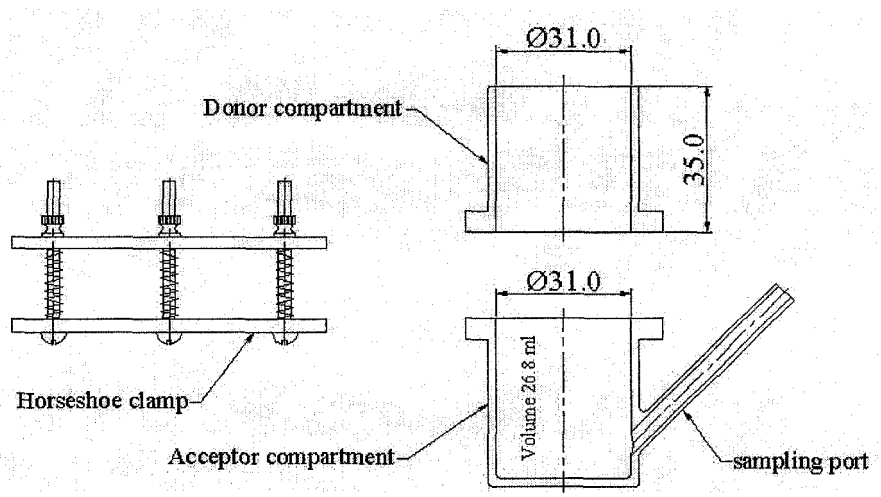

Figure 6.2. The self-designed Franz diffusion cell especially for this project that consists of a donor compartment, an acceptor compartment and a horseshoe clamp.

Figure 6.3. Photograph of the Franz diffusion cell.

6.2.4 UV-Visible spectrometer measurement

Absorbance measurements were used for determining the enhancement of the lidocaine delivery across the silicone membrane using an UV-Visible spectrometer (HP 8453). At the beginning of the ultrasound enhanced drug delivery experiments, lidocaine and the phosphate buffer (pH=7.0, Merck) concentrations of 0.01709, 0.03599, 0.0972, 0.0484, 0.1192, and 0.1616 mg/ml were prepared for the absorbance measurement at 263 nm to determine the relationship between the absorbance and the concentration as plotted in Figure 6.4. Regression analysis of the absorbance based on the lidocaine concentrations generates a linear regression equation along with the R^2 value of the equation.

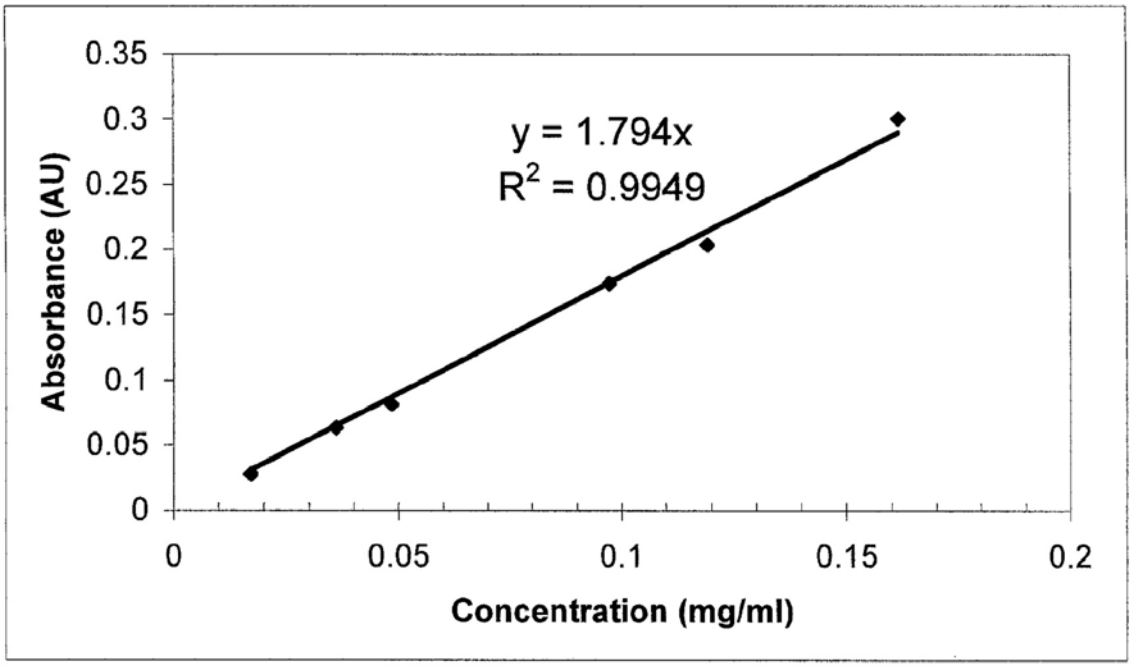

Figure 6.4. The calibration curve of the absorbance as a function of the lidocaine concentration with a linear regression equation and R^2 value.

6.2.5 Scanning electron microscope

A possible reason for the enhancement is ultrasound induced cavitation that may have the capability to damage the polymer structure [27-28]. Therefore, the effect of ultrasound irradiation on the surface morphology of the sonicated membrane was examined using a Leica Cambridge S360 scanning electron microscope (SEM) with an acceleration voltage of 20000 volts. Dry silicone membrane samples were gold-coated prior to scanning.

6.2.6 Experimental procedure

All the drug delivery experiments were conducted at room temperature (about 24.5°C). At the beginning of an experiment, the silicone rubber was cut into small pieces (40.0 mm x 40.0 mm) and checked for surface morphology using a optical microscope in order to confirm the integrity of the silicone rubber. The thickness of the silicone

rubber was measured by an ultrasonic thickness gauge. After the acceptor compartment was filled with the phosphate buffer, the silicone rubber was peeled off carefully from the polycarbonate film and mounted on top of the acceptor compartment. Both compartments were clamped together. Care was taken to remove all bubbles from the acceptor compartment and make sure complete contact between the silicone rubber and the phosphate buffer. The solution in the acceptor compartment was stirred with a magnetic stirrer.

The ultrasonic prototype device was placed inside of the donor compartment (see Figure 6.1). 6 ml of over saturated lidocaine solution was filled in the donor compartment. A flexible insulated wire thermocouple probe (Cole-Parmer) was introduced into donor compartment to monitor the temperature during ultrasound application. 1.0 ml of solution in the acceptor compartment was taken out and put into a capped transfer bottle that was filled with 4.0 ml of phosphate buffer solution for dilution. Another 1.0 ml of phosphate buffer solution was replaced back in the acceptor compartment. Absorbance measurement of lidocaine in the acceptor compartment was measured using the UV-visible spectrometer. Using the calibration curve given in Figure 6.3 and knowing the volume of the acceptor compartment, the penetrated and accumulative amounts of lidocaine through the silicone rubber are obtained.

6.3 Study the feasibility of device ‘A’ for drug delivery

Although the intensity produced by the flat flextensional transducer is comparable to that achieved using a commercial sonicator, the performance of the flat flextensional transducer for drug delivery is not well understood. The objective of this section is to explore the feasibility of using ultrasound produced by newly developed

practical sonophoresis prototype device 'A' with a single flat flextensional transducer (i.e. simplicity in the structure, cost effective and light weight for portability) for drug delivery application.

Passive diffusion testing without ultrasound application was performed followed by enhancement testing with ultrasound irradiation and the results are shown in Figure 6.5. For diffusion testing without ultrasound application (indicated by the symbol A), the cumulative amount of lidocaine in the acceptor compartment increases slowly and reaches a relatively constant level (average value is about 20.62 mg) after the 4^{th} hour. On the other hand, for enhancement testing with ultrasound application (pulsed ultrasound signal, 17.47 kHz, 20% duty cycle, and 41.13 mW/cm^2), the cumulative amount of lidocaine (indicated by the symbol ◆) is 1.55 to 1.82 times higher than that without ultrasound application at the 4^{th} hour and increases continuously in the next 20 hours.

The temperature increase of the silicone membrane while exposed to ultrasound was recorded by placing a thermocouple probe on the surface of the membrane and it is found to be less than 3.0 ^{o}C (Figure 6.7). As compared with storage and working temperatures of below 50 ^{o}C, the temperature increase of 3.0 ^{o}C could not change the properties of the silicone rubber. So a rise of 3.0 °C cannot account for this 2.9-fold increase in diffusibility observed in Figure 6.5.

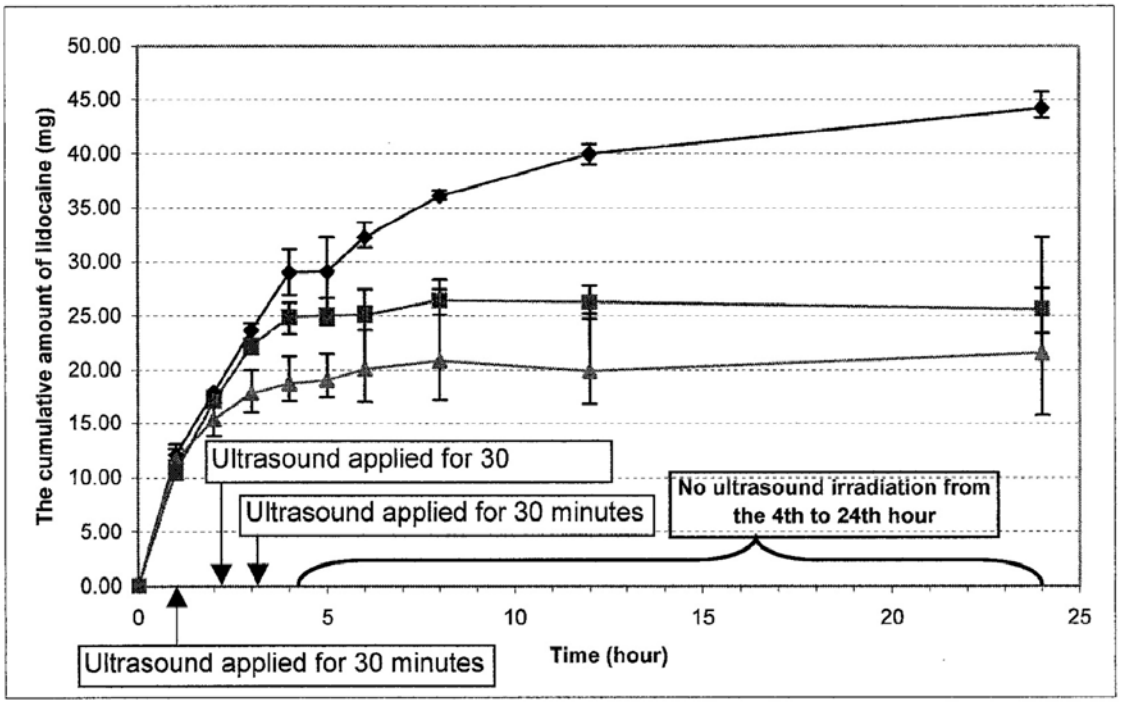

Figure 6.5. The cumulative amount of lidocaine in the acceptor compartment (with/ without ultrasound application). Ultrasound was applied for 1-1.5 hours, 2-2.5 hours and 3-3.5 hours (no ultrasound irradiation at 0-1st hour and 4th-24th hour). Pulsed ultrasound signal, 17.47 kHz, 20% duty cycle, and applied voltage AC 80 V. (◆) With ultrasound irradiation; (▲) Without ultrasound irradiation; (■) Reversible permeability after 20 hours post-irradiation.

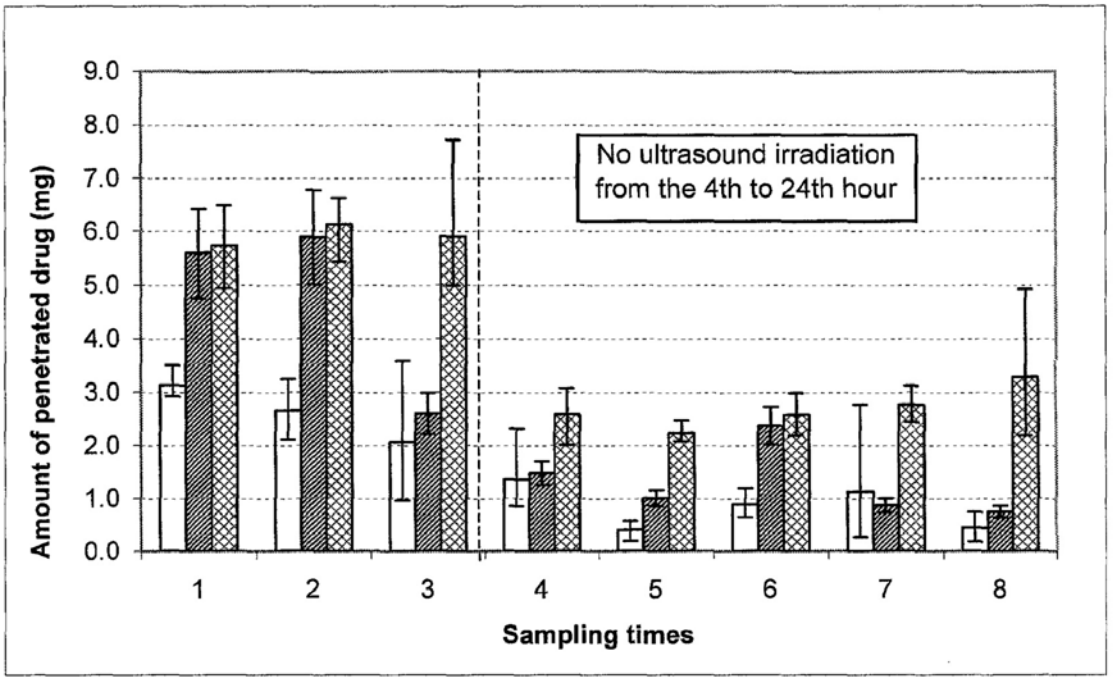

Figure 6.6. The amount of the penetrated drug through the silicone membrane by different methods. (▩) With ultrasound irradiation; (□) Without ultrasound irradiation; (▨) Reversible permeability.

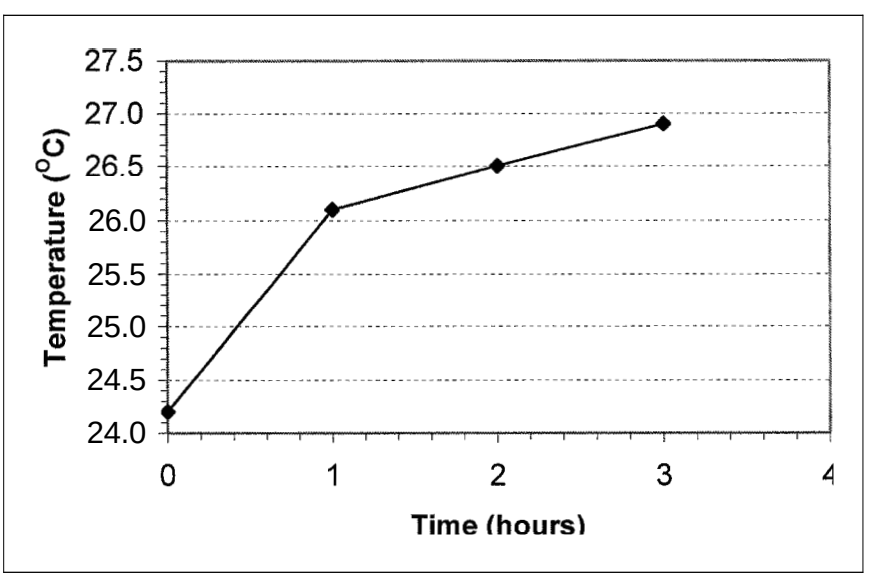

Figure 6.7. Temperature increment during ultrasound irradiation.

Furthermore, during the ultrasound irradiation time, acoustic bubbles were observed at the bottom surface of the silicone membrane, stainless steel vibrating plate of the ultrasound transducer and in the liquid of the acceptor compartment. It is confirmed that cavitation was generated inside both of the donor and the acceptor compartments. The experimental work indicated that ultrasound induced cavitation maybe one of the reasons for the enhanced polymer permeability and drug release [122]. Ultrasound-induced cavitation leads to an increase in the pore radius, an overall increase in pore density and to the formation of cracks on the polymer membrane, which could enhance the permeability of the polymer membrane [123]. However, the recovery of the permeability of the silicone membrane is crucial for its membrane-controlled release application. Experiments were therefore conducted to investigate the diffusion performance of the silicone membrane after exposure to ultrasound. The previous sonicated silicone membrane was then subjected to a 24-hour passive diffusion experiment after 20 hours post-exposure to ultrasound and results are plotted in Figure 6.5 (indicated by the symbol ■). Up to the 4^{th} hour, there is no difference in the release rate between the sonicated membrane and the "released" membrane. After the 4^{th} hour, the cumulative amount of drug in the acceptor compartment achieves a constant value (average value is 25.83 mg), which compared to the value without ultrasound irradiation (average value is 20.62 mg) is 25.3% higher. It appears that the permeability recovered partially. This may be caused by some of the enlarged pores on the silicone membrane that could not return to their original size after 20 hours post-exposure to ultrasound. So, if membrane-controlled drug delivery systems (for example, certain reservoir systems, where diffusional resistance across the polymeric membrane controls the overall drug release rate) are regulated using external ultrasound irradiation for emergency drug release, the irreversible formation of pores in the membrane could cause drug dumping

or irreversibility in membrane permeability when the external trigger is removed. The relevance of these results to the recovery of the sonicated silicone membrane needs to be further investigated.

The calculated amount of penetrated drug of reversible experiments was also shown in Figure 6.6 (indicated by the hatched area), which drops sharply from the third sampling point (corresponding time period is 3^{rd} to 4^{th} hour). The calculated enhanced and reversible permeation rate of the silicone elastomer membrane is given in Table 6.1, It is demonstrated that the low intensity and low frequency (< 20 kHz) ultrasound enhances the permeability of the silicone elastomer membrane effectively.

Table 6.1. Calculated enhanced and reversible permeation rate of silicone membrane.

	Time period	Enhanced rate [%]	Recovered rate [%]
Ultrasound on	1st-2nd	182.98	
	2nd-3rd	231.09	
	3rd-4th	286.69	
Ultrasound off	4th-5th		75.89
	5th-6th		83.68
	6th-8th		61.43
	8th-12th		85.91
	12th-24th		87.80

6.4 Study of the effects of ultrasonic irradiation on the permeability of the silicone rubber

In the last section, the experimental results confirm that the prototype device 'A' has the capability to enhance the permeability of the silicone rubber. Moreover, in order to better understand the performance of device 'A', the parameters, namely ultrasound

irradiation time and acoustic intensity have been investigated in this section. The surface shapes of the silicone rubber before and after ultrasonic irradiation were checked by a scanning electron microscope (SEM).

6.4.1 Effect of ultrasound irradiation time

The effect of the ultrasound irradiation time on the permeability of the silicone rubber was examined. The flexible ultrasound transducer was activated by pulsed signal with 20% duty cycle under three different applied voltages (50 V, 80 V and 160 V). The relationship between the cumulative amount of the drug and the ultrasound irradiation time under different applied voltages is given in Figure 6.8. It is found that the cumulative amount of drug increases in proportion to the ultrasonic irradiation time for each applied voltage. It is confirmed that in order to obtain the higher cumulative amount of the drug, longer ultrasonic irradiation time is required.

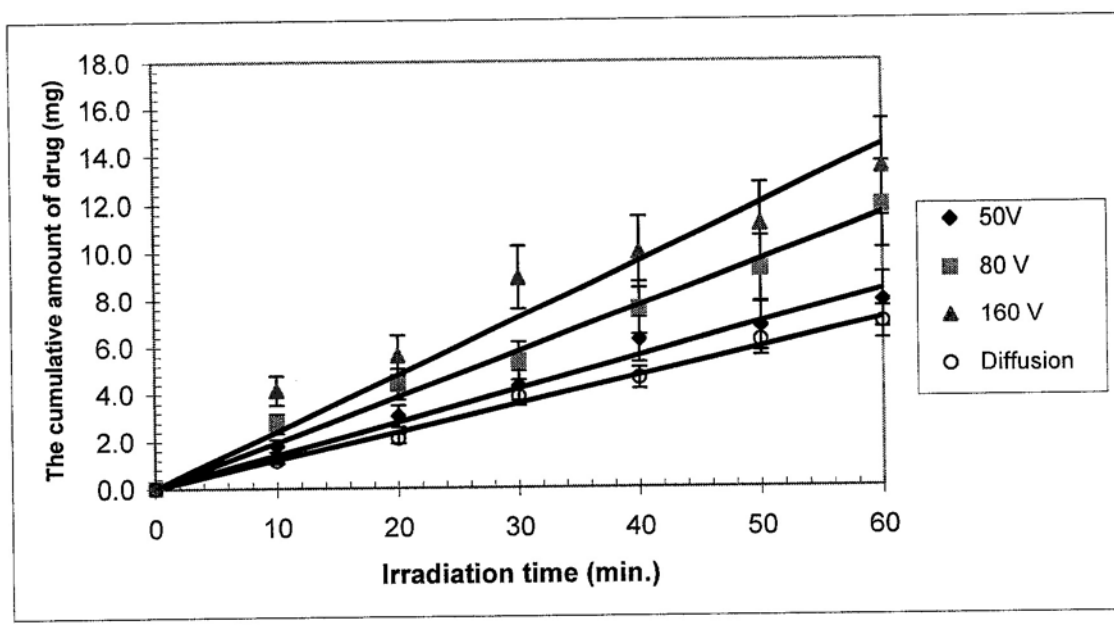

Figure 6.8. The cumulative amount of drug as a function of ultrasonic irradiation time under different applied voltages.

6.4.2 Effect of acoustic intensity

As shown in Table 6.2, when the applied voltages are 50, 80 and 160 V, the corresponding maximum output acoustic intensities at the membrane surface are 26.76, 41.13, and 105.09 mW/cm^2 respectively. Cavitation occurred when the acoustic intensity was in the range from 26.76 mW/cm^2 to 105.09 mW/cm^2. Figure 6.9 shows the dependence of cumulative amount of drug during sonophoresis experiments on the acoustic intensity for six different irradiation times. The cumulative amount of drug increases with increasing intensity for all exposure times. The permeability of the silicone membrane was enhanced 2.81±0.73-fold when exposed to ultrasound compared with unexposed membrane.

Table 6.2. Maximum output acoustic intensities with various applied voltages.

Applied voltage (V)	50	80	160
Maximum acoustic intensity (mW/cm^2)	26.76	41.13	105.09

The temperature change was also recorded during the ultrasound irradiation by placing a thermocouple probe on the surface of the membrane. The initial temperature for all the experiments was at 24.5°C. As shown in Figure 6.10, the temperature increases fast within the first 10 minutes and reaches the relative stable state in the next 50 minutes. Although the temperature varies with different applied voltages, the increase of the temperature during the ultrasound irradiation time is 1.9 to 2.6°C, which could not change the properties of the silicone rubber and obtain the 2.81±0.73-fold increases in the permeability observed in Figure 6.9.

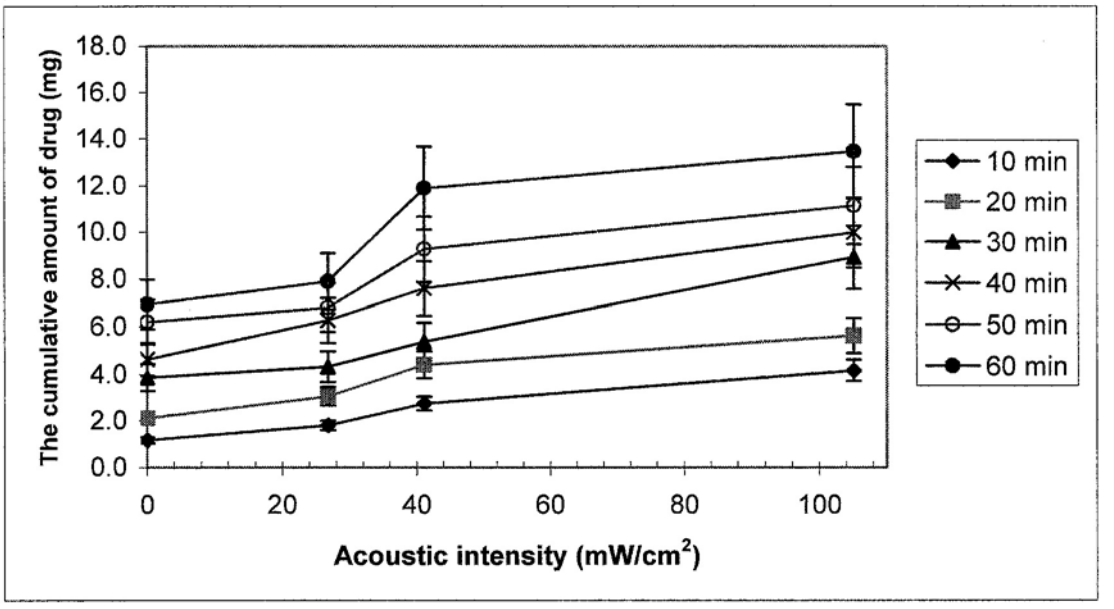

Figure 6.9. The dependence of cumulative amount of drug during sonophoresis experiments on the acoustic intensity for six different irradiation times.

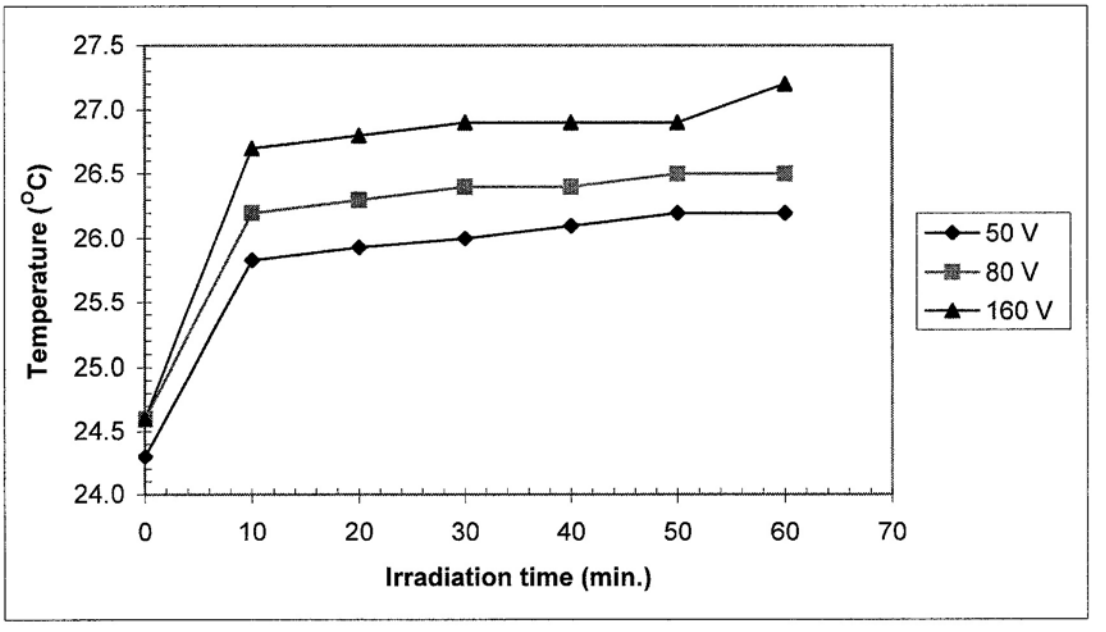

Figure 6.10. The relationship between the ultrasound irradiation time and the temperature.

6.4.3 Scanning of the surface morphology of the silicone rubber

The proposed mechanism of the enhanced permeability of the silicone rubber maybe because of the ultrasound induced-cavitation. In general, cavitation phenomenon is proportional to the ultrasound intensity, which may cause damage to biological materials in several ways [74]. Plesset [124] speculated that the shock waves radiating from collapsing bubbles could be the cause of mechanical damage of surrounding material. But it has noted that the collapse would have to occur very close to the substrate. During the sonophoresis experiments, the acoustic bubbles appeared and vibrated on the top and bottom surface of the silicone membrane. Therefore, the surface morphology of the silicone membrane before and after ultrasound irradiation was observed using a Leica Cambridge S360 scanning electron microscope. Figures 6.11 (a), (b) and (c) illustrate the surface morphology of the silicone rubber. Due to the limited resolution of the SEM used in this study, no holes and cracks in the micro-sized range were found in the silicone membranes as shown in Figures 6.11(a), (b) and (c). However, the experimental results (Figures 6.8 and 6.9) indicate that the permeability of the silicone membrane increases with acoustic intensity and ultrasonic irradiation time. One possible reason for the enhancement is caused by cavitation that may cause enhanced polymerization or depolymerization reactions by temporarily dispersing aggregates or permanently breaking chemical bonds in the polymer chains [27-28]. These modifications are in the molecular scale that cannot be identified using the limited resolution SEM in this study.

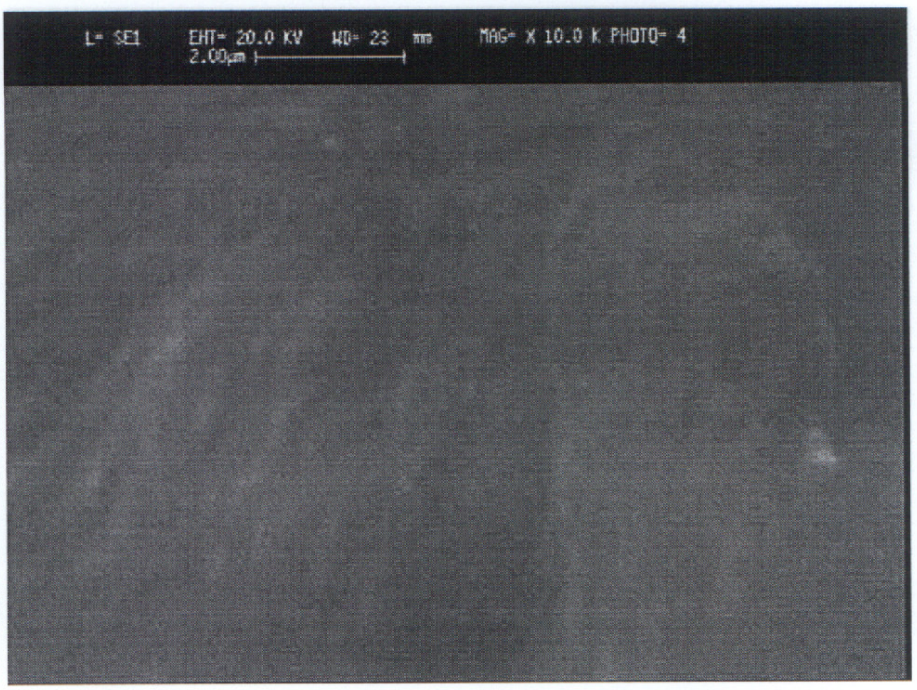

(a) Without ultrasound irradiation.

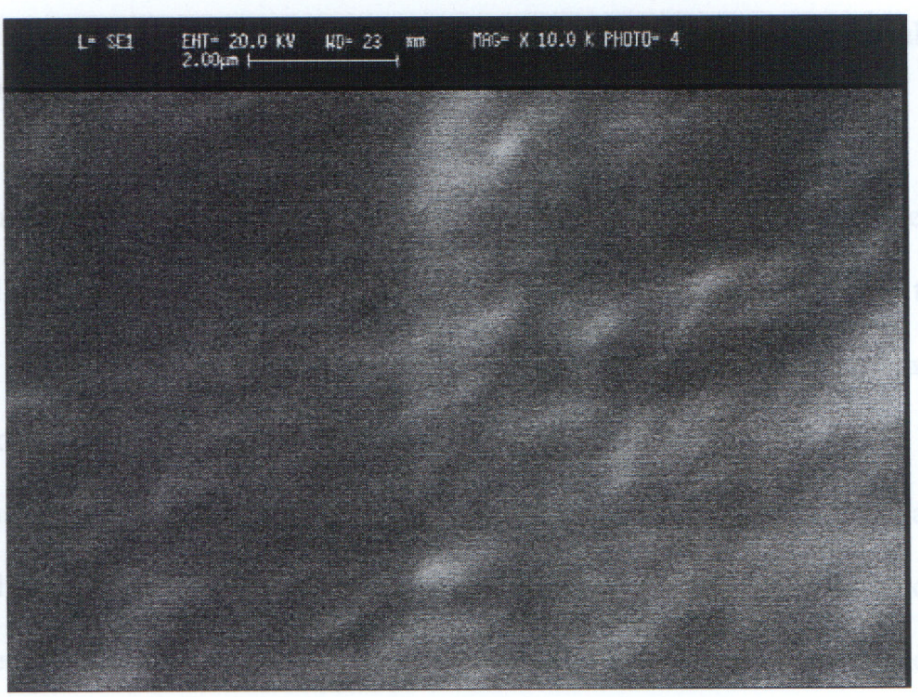

(b) With ultrasound irradiation for 30 minutes (80 V, 20% duty cycle).

(c) With ultrasound irradiation for 30 minutes (160 V, 20% duty cycle).

Figure 6.11. Surface morphology of the silicone membranes before and after ultrasound irradiation. Magnification of each photo is 10,000.

Another possible reason for the enhancement in diffusion can be mainly attributed to the phenomenon of acoustic streaming which could enhance the mass transfer [125]. In a general diffusive experiment without ultrasound application, the velocity of liquid particles at the liquid-membrane interface is little or zero. Thus the mass transfer resistance at the liquid-membrane interface is high. When the ultrasound is generated in the liquid, the acoustic pressure will cause the liquid particles to flow in the same direction as the ultrasound waves propagate [126]. This has been explained by the radiation pressure gradient due to the attenuation of the sound and the bubbles generated by the high amplitude ultrasound waves. This phenomenon is called acoustic streaming that is well known for its transport properties [125] [127]. The flow of the liquid particles is increased by the reduction of the resistance of the mass transfer at the liquid-

membrane interface and therefore the permeability of the silicone membrane is enhanced.

6.4.4 Reversibility of the silicone membrane

The recovery of the permeability of the silicone membrane is crucial for its membrane-controlled release application. Two sets of experiments were conducted to compare the permeability of the sonicated silicone membrane with that of the non-irradiated silicone membrane under different experimental conditions.

Firstly, silicone membranes were sonicated using the same acoustic intensity ($41.13\ \mathrm{mW/cm^2}$) and duty cycle of 20% with three different irradiation times: 15, 30 and 60 minutes. After 24 hours, these sonicated silicone membranes were used to conduct the diffusive experiments without ultrasound application to investigate the recovered permeability of the silicone membrane. Figure 6.12 shows the results of the cumulative amount of drug permeated through the sonicated membranes are about 10.7% to 34.1% higher than that through the non-irradiated silicone membrane. It is indicated that the permeability of the sonicated silicone membrane recovered partially.

Before the commencement of the second set of similar diffusive experiments, silicone membranes were irradiated by three different acoustic intensities (26.76, 41.13, and $105.09\ \mathrm{mW/cm^2}$) with the same duty cycle of 20% and the irradiation time of 15 minutes. The permeabilities of the sonicated and the non-irradiated silicone membrane are plotted in Figure 6.13. It is illustrated that the permeabilities of the sonicated silicone membranes are about 3.9% to 30.3% higher than those of the non-irradiated membrane.

From the experimental results as shown in Figures 6.12 and 6.13, the permeability of the sonicated silicone membrane could not recover back to its original value. The silicone membrane sonicated with longer irradiation time or higher acoustic intensity has higher permeability than that of the membrane non-irradiated or sonicated with shorter time or lower acoustic intensity. The possible explanation is attributed to the ultrasound generated cavitation phenomena. In general, the implosion or cavitation processes of the bubbles could produce pressure change of up to 10^8 Pa and temperature of several thousand degrees Kelvin [128]. Thus the cavitation of the bubbles provides a primary source of energy required for the degradation of the sample. Although the cavitation phenomena are not substantial in this study, it is believed that cavitation causes local degradation of the silicone membrane resulting in partial recovered permeability, which may also be another possible reason for the enhanced permeability of the silicone membrane with ultrasonic irradiation.

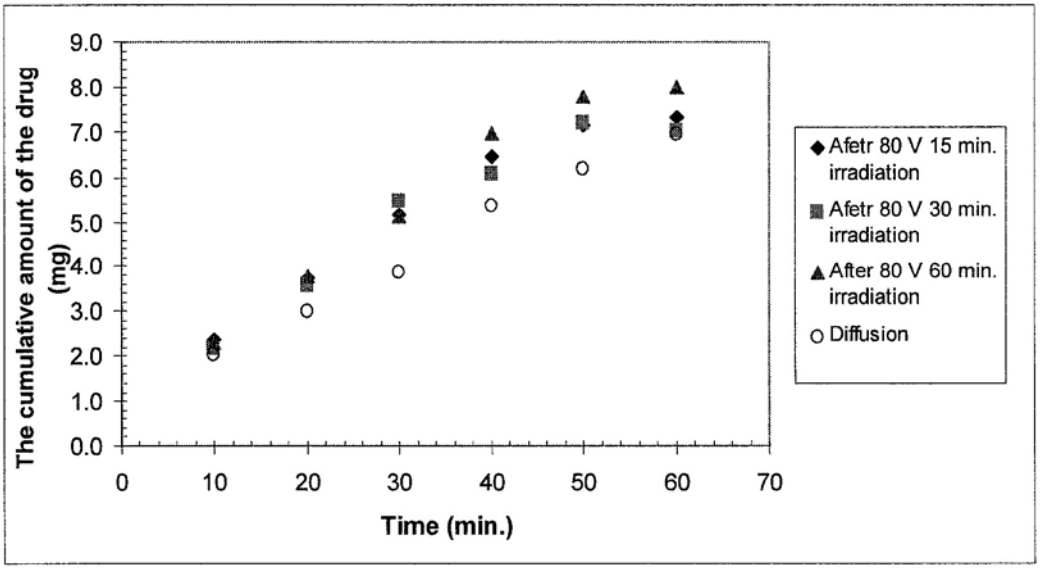

Figure 6.12. The cumulative amount of the penetrated drug through the sonicated and the non-irradiated silicone membrane. The silicone membranes were sonicated with the same acoustic intensity (41.13 mW/cm^2) and pulsed signals (20% duty cycle). The irradiation periods are 15, 30 and 60 minutes, respectively.

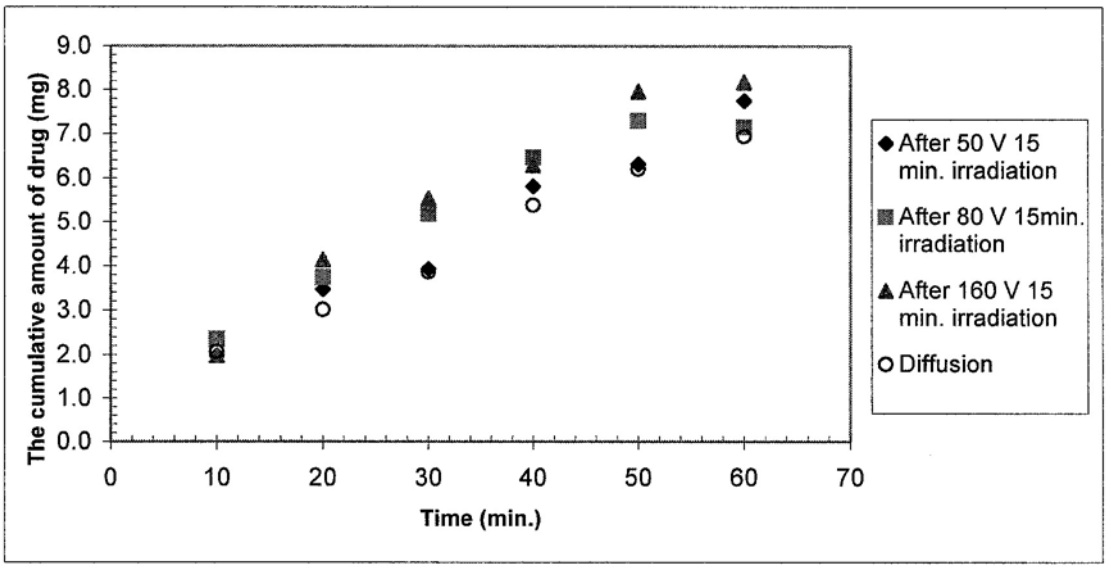

Figure 6.13. The cumulative amount of the penetrated drug through the sonicated and non-irradiated silicone membrane. The silicone membranes were sonicated with same irradiation time (15 minute) and pulsed signals (20% duty cycle). The applied voltages are 50, 80 and 160 V respectively.

6.5 Enhanced Permeability of the Silicone Rubber by Device 'B'

The physical characteristics and the performances of the prototype device 'A' in the drug delivery experiments have been studied. All the experimental results have indicated that the flat flextensional transducer is a good candidate for ultrasound enhanced drug delivery application. However, the poor radiation characteristic of a single transducer implies high electrical power is required to activate the device. Therefore, prototype device 'B' with dual flat flextensional transducers has been designed and fabricated with the objectives of increasing the output acoustic intensity in water and at the same time reducing the required electrical power. Although the physical characteristics of prototype device 'B' showed that it has the ability to increase the output acoustic intensity 2 to 4-fold and to reduce the required electrical power at least 2-

fold, the performance of device 'B' in the drug delivery experiments is not clearly understood. So, the focus of this section is to study the feasibility of device B to enhance the permeability of the silicone rubber.

The drug delivery experiments for device 'B' which has two transducers were conducted in the following order:

1. Single transducer (Transducer '1' or '2') was operated independently with low input electrical power (80 V).
2. Single transducer (Transducer '1' or '2') was operated independently with high input electrical power (160 V).
3. Dual transducers (Transducer '1' and '2') were activated simultaneously with low input electrical power (80 V).

Again, at the beginning of the experiments, the output acoustic intensities of each transducer in the device 'B' were measured under the different applied voltages. The results are listed in Table 6.3. The experimental setup, materials and methods are same as those described in Section 6.2.

Table 6.3. The output acoustic intensities for each transducer inside of device 'B' under different applied voltages.

Transducers	Output acoustic intensities (mW/cm^2)	
	80 V	160 V
Transducer '1'	13.99	18.62
Transducer '2'	16.30	41.95
Transducers '1' and '2'	38.47	78.64

6.6 Results and Discussion

6.6.7 Transducers '1' and '2' operated independently at 80 V and 760 V

A comparison of the cumulative amount of lidocaine transported through the silicone rubber in the presence and the absence of ultrasound (control) is shown in Figure 6.14. The passive transportation of the lidocaine (indicated by the symbol ▲) attained relative steady value after four hours. Two groups of experiments in the presence of ultrasound were conducted with different applied voltages (80 and 160 V). The ultrasound energy was only generated from Transducer '1'. It is clearly shown that the transportation in the presence of ultrasound exhibits a large variation. Firstly, when Transducer '1' was operated by applied AC voltage of 80 V, the cumulative amount of lidocaine in the acceptor compartment increases from 1.13-fold at the first period of the ultrasound irradiation time (1^{st} to 2^{nd} hour) up to 1.35-fold compared with that of the control at the 4^{th} hour. In order to enhance the permeability further, high electrical power (160 V) was used to drive Transducer '1' and the experimental results indicated by the symbol ◆. As seen from Figure 6.14, the plots for both experimental results in the presence of ultrasound (80 V and 160 V) have similar trends. The output of the cumulative amount of lidocaine increases only 1.23-1.43-fold at high electrical power (160 V) compared with that of the control during the ultrasound irradiation time period (1^{st} to 4^{th} hour). In addition, the transport rates are proportional to the slopes of the corresponding curves, which are 1.91 and 2.11 times higher than those of the control for low input electrical power (80 V) and high input electrical power (160 V), respectively.

Figure 6.15 shows the experimental results in the presence and absence of ultrasound using the same experimental procedures, Transducer '2' was activated initially by low input electrical power (80 V) and then followed by high input electrical power (160 V). The cumulative amount of lidocaine in the acceptor compartment increases 1.06 to 1.39-fold for low input electrical power (80 V) and 1.36 to 1.58-fold for high input electrical power (160 V) during the ultrasound exposure time period (1st to 4th hour). The transport fluxes of both cases in the presence of ultrasound are 2.01-fold and 2.52-fold higher than those of the passive diffusion experiments without ultrasound application.

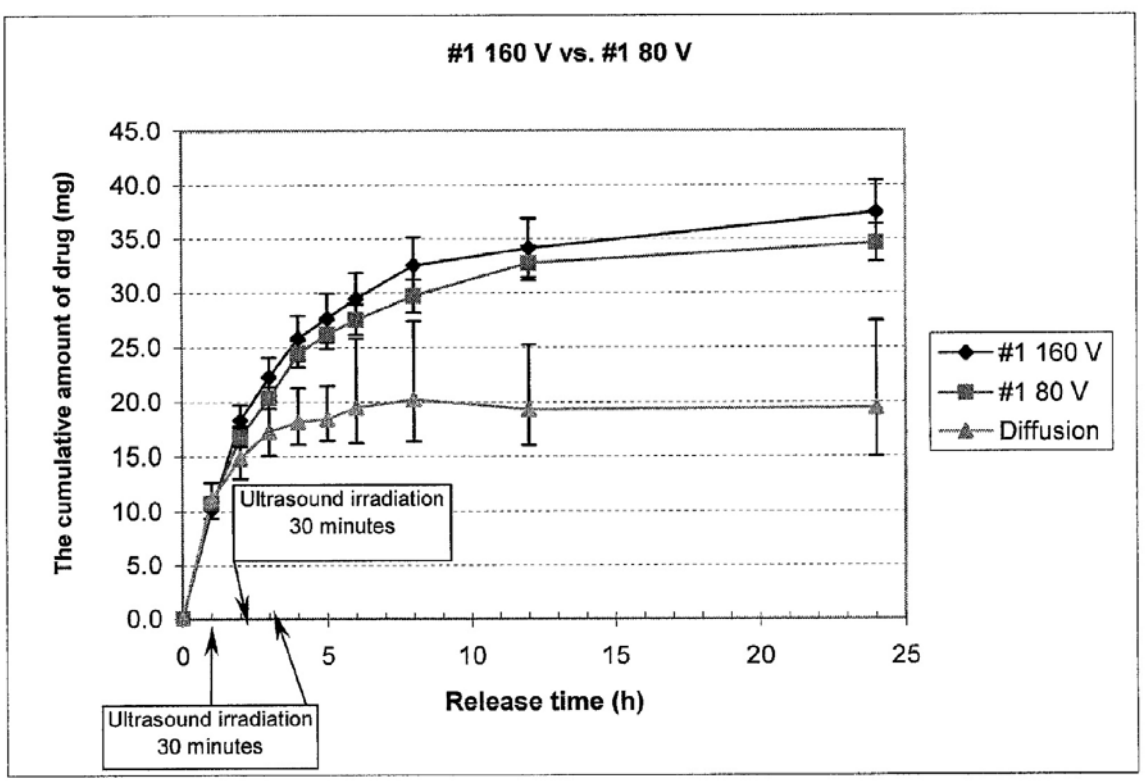

Figure 6.14. The cumulative amount of lidocaine in the acceptor compartment (with/ without ultrasound application). Ultrasound was generated by Transducer '1' and applied for 1-1.5 hours, 2-2.5 hours and 3-3.5 hours (no ultrasound irradiation at 0-1st hour and 4th-24th hour). Pulsed ultrasound signal, 26.83 kHz, 20% duty cycle, and applied voltage

AC 80 V and 160 V. (◆) With ultrasound irradiation (160 V); (■) With ultrasound irradiation (80 V); (▲) Without ultrasound irradiation.

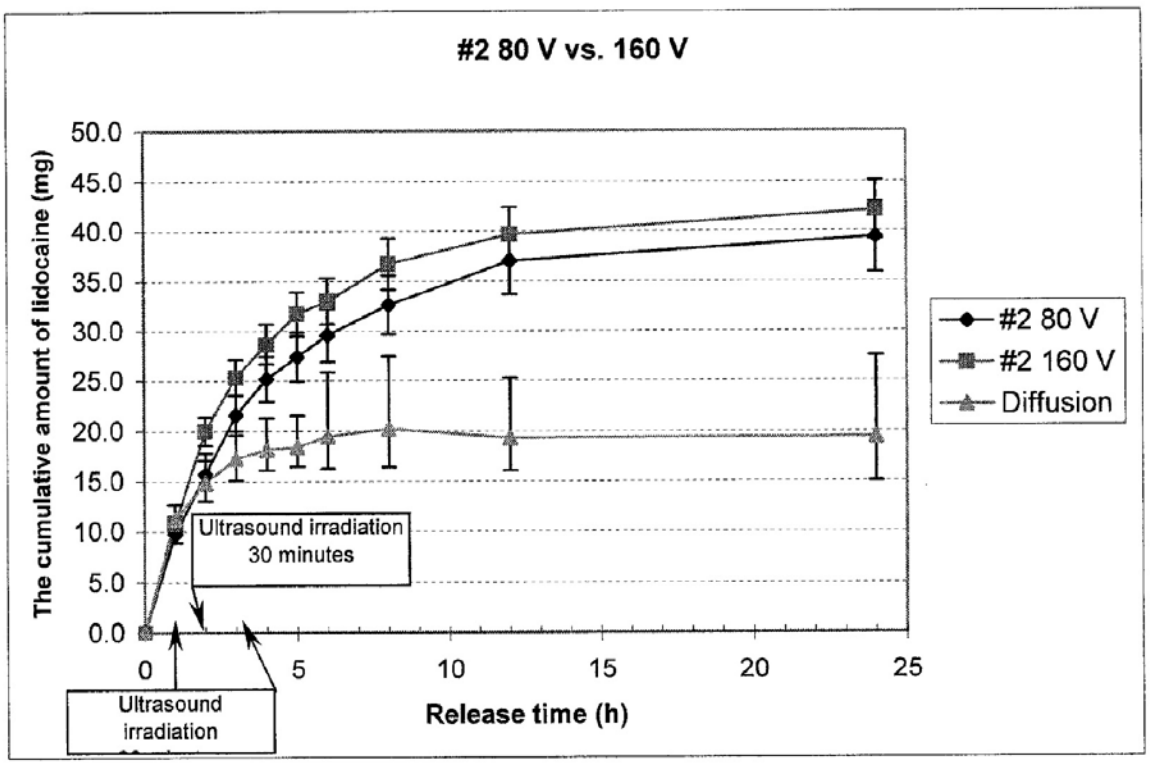

Figure 6.15. The cumulative amount of drug in the acceptor compartment (with/ without ultrasound application). Ultrasound was generated by Transducer '2' and applied for 1-1.5 hours, 2-2.5 hours and 3-3.5 hours (no ultrasound irradiation at 0-1st hour and 4th-24th hour). Pulsed ultrasound signal, 26.83 kHz, 20% duty cycle, and applied voltage AC 80 V and 160 V. (◆) With ultrasound irradiation (80 V); (■) With ultrasound irradiation (160 V); (▲) Without ultrasound irradiation.

In order to analyze the performance of each transducer in the experiments with ultrasound irradiation, the experimental results are summarized in Table 6.4. It is found that the enhancement of each transducer in the device 'B' are almost identical when they were operated independently with a low input electrical power (80 V), at which both transducers have similar output acoustic intensities (see Table 6.3). Previous research work [8] [12] demonstrated that cavitation effect is the major mechanism of the

ultrasound enhanced transdermal/trans-membrane drug delivery. However, physical experimental results have shown that no acoustic cavitation was generated when Transducer '1' or Transducer '2' was operated at 80 V. The possible reason for the enhancements at 80 V obtained in Figures 6.14 and 6.15 may be due to vibration induced liquid flow between vibration plate and silicone membrane. In a general diffusion experiment, the liquid in the boundary layer has little or no flow, thus the mass transfer resistance in it is high. By using Fick's law, the diffusional flux across the membrane is written as:

$$N_A = -D_A \frac{dC_A}{dZ} \tag{6.1}$$

Where, N_A, D_A and C_A are molar flux, molecular diffusivity and molar concentration of component A, respectively. Z is the coordination number of the membrane. The overall flux of the molecules through the membrane is directly proportional to the mean molecular velocity and the mean free path [129]. When the irradiation is carried out with ultrasound, irradiation pressure will cause the liquid to flow in the direction of propagation of the acoustic waves, which is known as acoustic streaming and defined as [75]:

$$f = -\nabla p + \left[\mu' + (4/3)\mu\right]\nabla\nabla \bullet u - \mu\nabla \times \nabla \times u$$

Where, f is the net force per unit volume due to stress, p is the pressure in the liquid, μ and μ' are the shear viscosity coefficient and bulk viscosity coefficient of the liquid respectively, u is the liquid velocity that can be written as:

$$u = u_1 + u_2 + \ldots \tag{6.3}$$

$$u_1 = Ae^{-\alpha x}\cos(\omega t - kx) \tag{6.4}$$

Where u_1 is the first-order approximation to steady-state solution, A is the amplitude of the acoustic wave, and u_2 is the streaming velocity that is proportional to the square of the amplitude A [75]. In the presence of ultrasound irradiation, the flow of the liquid particles reduces the resistance of mass transfer at the liquid-membrane interface. In addition, when the liquid flows, eddy diffusivity (E_D) will also contribute to the overall flux. The mass transfer Eq. (8) is written to include both molecular and eddy diffusivities as:

$$N_A = -(D_A + E_D)\frac{dC_A}{dZ} \tag{6.5}$$

Thus the permeability of the silicone rubber is increased. Furthermore, the eddy diffusivity is not a molecular property of the liquid but depends on the level of turbulence of the system [129]. When the applied voltage of each transducer was increased from 80 to 160 V, the increment of the vibration velocity resulted in the acoustic streaming velocity increase, which enhances the level of turbulence of the system. Thus, as shown in Table 6.4, the increased magnitudes of the transport rate have higher values at 160 V. At the same time, cavitation was generated when Transducers '1' and '2' were operated independently at 160 V, which may cause enhanced polymerization or depolymerization reactions by temporarily dispersing aggregates or

permanently breaking chemical bonds in polymer chain resulting in enhanced permeability of the silicone rubber [27-28].

However, the high electrical power induced mechanical fatigue, fracture and heat generation making the physical performances of Transducers '1' and '2' have large differences (see Table 6.3). One plausible explanation for this difference is that the above-mentioned shortcomings of the high electrical power cause the non-uniform changes in the properties of the piezoelectric materials or the bonding material. Thus, as seen from Table 6.4, when the applied voltage was increased from 80 to 160 V, the performances of Transducer '1' have small difference compared with those of Transducer '2' during the drug delivery experiments in the presence of ultrasound. Nevertheless, all these results reveal that each transducer in the device could enhance the permeability of the silicone rubber when it is activated either by low electrical power or by high electrical power.

An attempt to further evaluate the temperature effects of high input electrical power on the performance of each transducer during drug delivery experiments with ultrasound exposure (see Figure 6.16). It is found the temperature change was less than 3°C when each transducer was operated using low input electrical power (80 V). In contrast, when the applied voltage was increased to 160 V, Transducer '1' and '2' induced temperature changes of the silicone rubber were up to 8.4°C and 5.2°C, respectively. As illustrated in Figures 6.14, 6.15, and 6.16, it is indicated that using high electrical power to drive the transducer could achieve a higher cumulative amount of the lidocaine in the acceptor compartment and higher transport rate, at the same time, the temperature of the silicone rubber increases quickly.

Table 6.4 Summary of the experimental results.

	Increased magnitudes in cumulative amount of lidocaine compared with the control		Increased magnitudes in transport rate compared with the control	
	80 V	160V	80 V	160 V
Transducer '1'	1.13-1.35	1.23-1.43	1.91	2.11
Transducer '2'	1.06-1.39	1.36-1.58	2.01	2.52
Transducers '1' and '2'	1.26-1.68	---	2.77	---

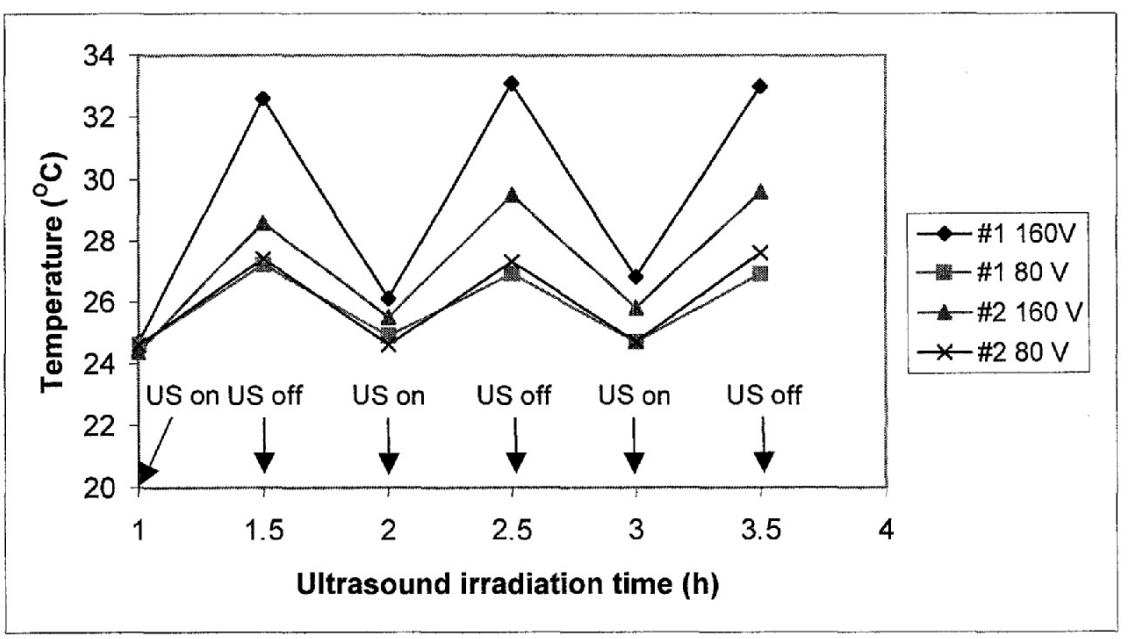

Figure 6.16. The temperature increase for Transducers '1' and '2' under different applied voltages.

6.6.2 Transducer '1' and '2' operated simultaneously at 80 V

More experiments were conducted to investigate the drug delivery performance of the device 'B' when Transducers '1' and '2' were operated simultaneously. All the experiments were performed only at low input electrical power (80 V). Under this condition, the output acoustic intensity is more than 2 times higher than that generated by

a single transducer (Table 6.1) and more acoustic cavitation was generated (Figure 5.7). Figure 6.17 compares the experimental results obtained from two different conditions. One is that Transducers '1' and '2' were operated simultaneously. The results are indicated by symbol ▲, for simplicity in this report, which is called dual transducer results. The other is that Transducer '1' and '2' were activated independently. The corresponding result for each transducer is displayed by symbol ■ and ◆, and named #1 mono-result and #2 mono-result respectively in this report. It is clearly seen that the large differences between the dual transducer results and the two mono-results in the cumulative amount of the lidocaine throughout the release time. For dual transducer results, the cumulative amount of lidocaine in the acceptor compartment is about 1.26 to 1.68 times higher than that of the control during the ultrasound application time period (1_{st} to 4^{th} hour) and the transport rate also increases 2.77-fold. According to the results in Figure 6.17, the amount of the penetrated lidocaine through the silicone rubber was calculated and plotted in Figure 6.18. From these two diagrams it is concluded that better performance of device 'B' could be achieved using both transducers to enhance the permeability of the silicone rubber rather than using a single transducer.

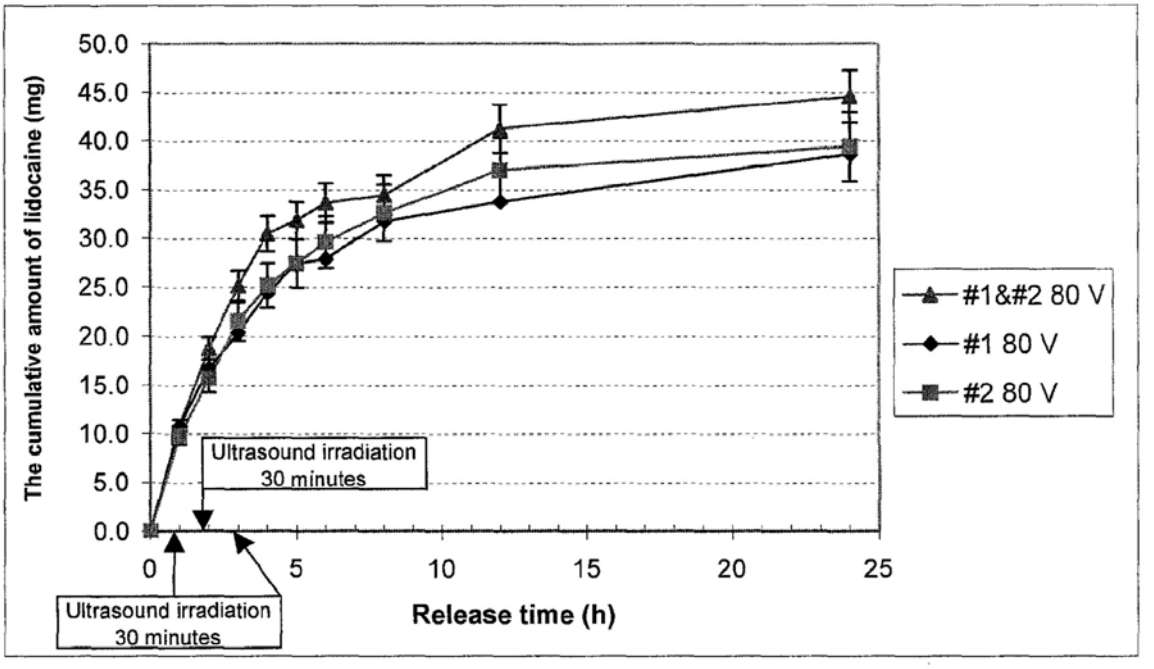

Figure 6.17. The cumulative amount of lidocaine in the acceptor compartment (with/ without ultrasound application). Ultrasound was generated by Transducers '1' and '2' and applied for 1-1.5 hours, 2-2.5 hours and 3-3.5 hours (no ultrasound irradiation at 0-1st hour and 4th-24th hour). Pulsed ultrasound signal, 26.83 kHz, 20% duty cycle, and applied voltage of AC 80 V. (◆) #1 mono-result (80 V); (■) #2 mono-result (80 V); (▲) Dual transducer results (80 V).

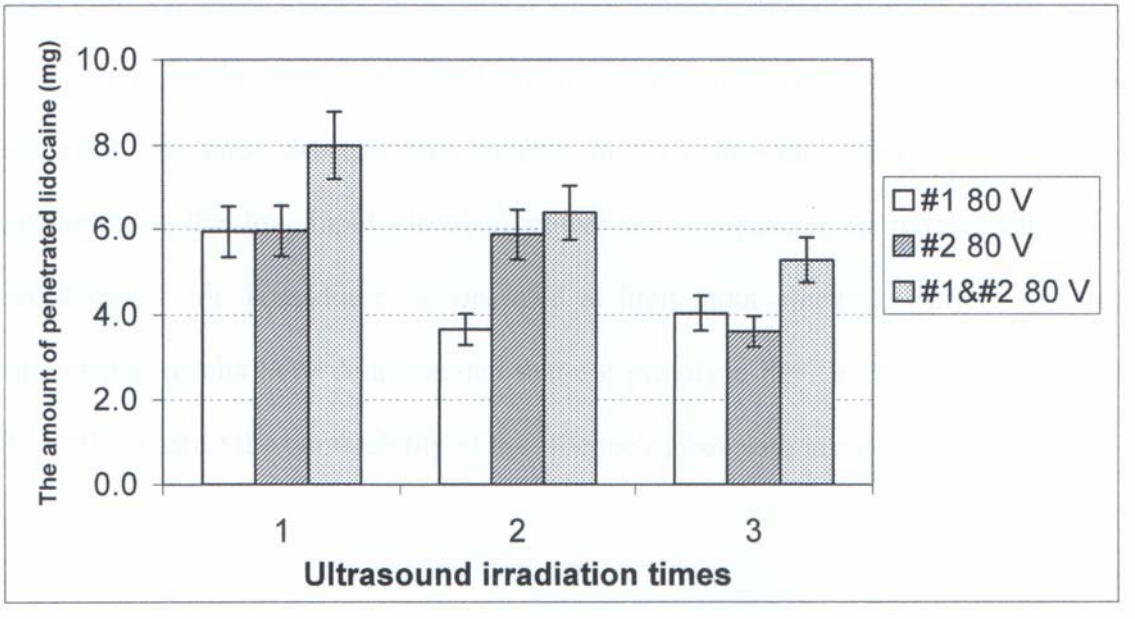

Figure 6.18. Comparison of the penetrated amount of lidocaine through the silicone rubber when Transducers '1' and '2' were operated at low input electrical power (80 V).

The potential application of the device 'B' to be used as a low power consumption device for ultrasound enhanced drug delivery was verified. The comparison of the dual transducer results obtained at low input electrical power (80 V) and #1 and #2 mono-results obtained at high input electrical power is given in Figure 6.19. A similar pattern is seen in the dual transducer results and the #2 mono-result. As indicated in Table 6.3, the output acoustic intensity value from both transducers at low input electrical power (80 V) is approximately the same as that generated by Transducer '2' at high input electrical power (160 V). It is known that, for ultrasound enhanced drug delivery, ultrasound frequency and intensity are two of important parameters that affect the drug delivery results significantly [12]. Thus, when the transducers vibrate at the same frequency with similar output acoustic intensity, they will have similar performances in the drug delivery experiments. However, there is a large difference between dual transducer results and #1 mono-result. It is clearly illustrated in Table 6.3, the output acoustic intensity for dual transducers at low input electrical power (80 V) is more than 2 times higher than that generated by Transducer '1' at high input electrical power (160 V), which causes the large variations between dual transducer results and #1 mono-result. Similarly, the penetrated amount of lidocaine was calculated and given in Figure 6.20. As these two diagrams indicate, the experimental results obtained by dual transducers at the low input electrical power are comparable to those achieved by Transducer '1' or Transducer '2' operated at high input electrical power. All these experimental results have demonstrated that the prototype device 'B' has the ability to efficiently enhance the permeability of the silicone rubber with low power requirement.

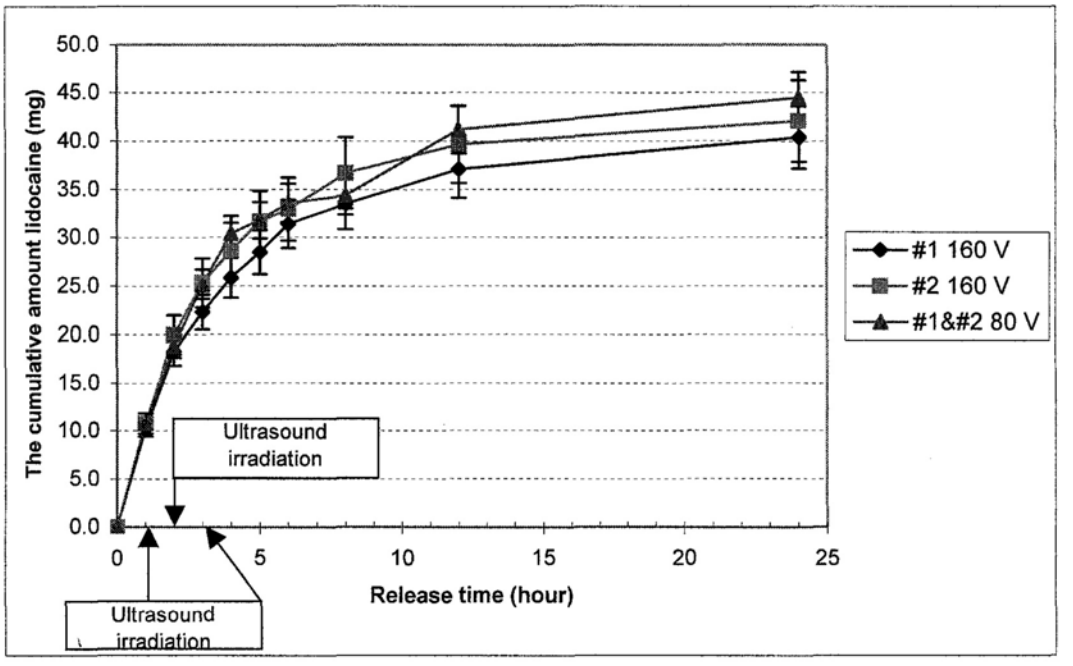

Figure 6.19. The cumulative amount of the drug in the acceptor compartment (with/ without ultrasound application). Ultrasound was generated by Transducers '1' and '2', and applied for 1-1.5 hours, 2-2.5 hours and 3-3.5 hours (no ultrasound irradiation at 0-1st hour and 4th-24th hour). Pulsed ultrasound signal, 26.83 kHz, 20% duty cycle, and applied voltage AC 80 V. (◆) #1 mono-result(160 V); (■) #2 mono-result (160 V); (▲) Dual transducer results (80 V).

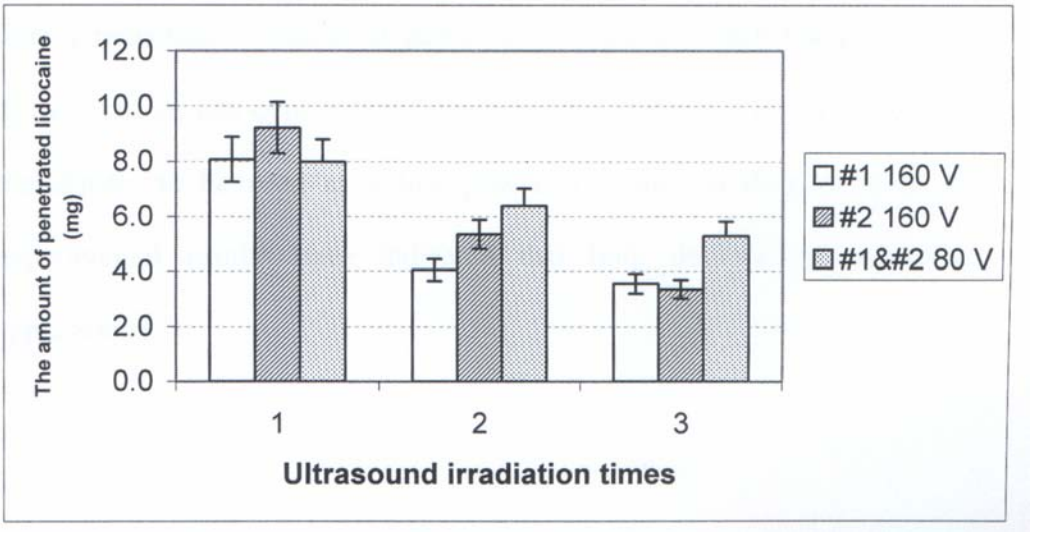

Figure 6.20. Comparison of the penetrated amount of the lidocaine through the silicone rubber with two different conditions: 1) dual transducers were operated at low input electrical power (80 V) and 2) single transducer was activated at high input electrical power (160 V).

6.7 Summary

Drug delivery performances of the prototype devices 'A' and 'B' have been studied in this chapter. Two sets of drug delivery experiments were conducted with the silicone rubber. In the first set, device 'A' was utilized to generate the relatively low acoustic power to explore the potential of the device to be used as an external ultrasonic source to trigger the responsive polymeric devices. The key parameters such as acoustic intensity, ultrasound irradiation time and reversibility of the silicone rubber have been studied. The newly developed device 'A' performed well during ultrasound irradiation. It is found that the sonicated silicone rubber recovered its permeability partially. The reversibility of the sonicated silicone rubber is related to the acoustic intensity and ultrasound irradiation time. In the second set, dual transducers in the device 'B' were used to study the relationship between the power supply and the drug delivery characteristics. The comparative analysis has shown that dual transducers generated more acoustic intensity to enhance the permeability of the silicone rubber and at the same time a reduction of electrical power by twofold for each transducer in the prototype device. The results demonstrated the potential of device 'B' with dual flat flextensional transducers to be used as a low power consumption drug delivery device. All the experimental results have indicated that both devices are feasible for practical applications,

CHAPTER SEVEN

CONCLUSIONS AND RECOMMENDATIONS FOR FUTURE WORK

7.1 Conclusions

The aim of this research project was to develop a new ultrasonic transducer for ultrasound enhanced drug delivery applications. As discussed in the previous chapters, for practical applications of ultrasound enhanced drug delivery, a smaller and lighter device is necessary. A practical device should have a flat and low profile. It should be simple enough to be integrated with drug reservoirs and a control system to form the sonophoresis device that is situated against the arm or the waist to be used as a wearable device. The device also should be operated at a similar frequency and a comparable output acoustic intensity with a sonicator. With these goals, prototype devices 'A' and 'B' were designed, fabricated and their physical characteristics and drug delivery performances were investigated in this research. The overall design and technique used were realized in this research work. In the following sections, overall conclusions concerning the development and evaluation of the devices will be summarized.

7.1.1 Finite element analysis

Considering the coupling of acoustics and the fluid-structure interaction, and boundary conditions of the drug delivery experiment, the FEA models of a single and dual flat flextensional transducers were developed.

In order to determine the detailed dimensions of the structure of the prototype devices, the admittance, first resonance frequency, center displacement of the vibration plate and output acoustic pressure were calculated based on the FEA modes. According to the calculated and measured results, the first resonance frequency has a significant change in air and in water. The difference between calculated result and measured result is up to 5 kHz and 7 kHz, respectively. The calculated results of the first resonance frequency obtained from finite element method are comparable and consistent with the experimental results. According to the calculated results, the factors such as the PZT d_i/d_p ratio, PZT material types and thickness, vibration plate thickness and properties, and vibration zone diameter d_m, which affect the first resonance frequency in-water and in-air are summarized as follows:

1. The PZT d_i/d_p ratio did not have large effect on the first resonance frequency of the flat flextensional transducers. The frequency changes are 6.5 kHz in-water and 4.1 kHz in-air when the d_i/d_p ratio is in the range from 0.083 to 0.667.
2. The first resonance frequency of the flat flextensional transducer changed 18 kHz in-water and 24 kHz in-air respectively when the piezoelectric material thickness is in the range from 0.25 mm to 2.0 mm. Significant change in the first resonance frequency could be obtained when $t_p > t_m$. Different types of the piezoelectric material (soft PZT and hard PZT) do not have significant effect on the first resonance frequency. The maximum differences are 1.9 kHz in-water and 2.7 kHz in-air when the piezoelectric material thickness is in the range from 0.25 mm to 2.0 mm.
3. The first resonance frequency of the flat flextensional transducer could be easily changed by adjusting the vibration plate thickness. The frequency

changes are 16 ltHz in-water and 19 kHz in-air when the vibration plate is in the range from 0.12 mm to 0.5 mm. Moreover, the frequency changes are influenced by the ratio of the water density to the vibration plate density. The flat flextensional transducer with a low-density vibration plate which is closer to the density of water will introduce more changes in the first resonance frequency than the same transducer with a higher density vibration plate.

4. When the dimensions and properties of the piezoelectric materials and vibration plates are constant value, the dimensional change of the vibration zone contributed to a significant effect on the first resonance frequency of the flat flextensional transducer. The frequency changes from 18 kHz to 33 kHz in-water when the diameter of the vibration zone was adjusted from 13.0 mm to 18.0 mm.

The relationship between d_i / d_p ratio of the piezoelectric ring and the center displacement of the vibration plate was examined. The flat flextensional transducer with ring-shaped piezoelectric material has a larger center displacement than that of the transducer with disc-type piezoelectric material $(d_i / d_p = 0)$. The maximum displacement was achieved when $d_i / d_p = 0.42$ in this study.

Using the single transducer FEA model and the dual transducers FEA model, the output acoustic pressure of the flat flextensional transducer was calculated, which is proportional to the applied voltages for both FEA models. Results from the dual transducers FEA model show that when dual transducers are operated simultaneously the output acoustic pressure is 2 times higher than that generated by a single

transducer in the same model. The acoustic intensity is proportional to the square of the acoustic pressure, thus the output acoustic intensity is 4 times higher than that generated by a single transducer in the same model. It has the same results as that predicted theoretically. Further, the output acoustic pressure generated by dual transducers at 80 V has the same values as those produced by a single transducer at 160 V in the same dual transducers FEA model. Thus, the device with two transducers has the capability to reduce the required input electrical power twofold theoretically.

7.1.2 *Device fabrication*

The prototype devices 'A' and 'B' were fabricated. In comparison with the other flextensional ultrasound transducers, the key features of the newly developed devices are their simplicity in structure, cost effectiveness and lightweight for portability. The cross-sectional area of both devices is 6.88 cm^2 and height is 1.5 cm. Compared with an ultrasonic probe or a converter from the commercial sonicator which can weigh about one kilogram, the prototype devices 'A' and 'B' with flat flextensional ultrasound transducer weigh only 71.5 and 73.3 gm, respectively.

7.7.3 *Measured first resonance frequency*

The first resonance frequency was measured using two different methods: the laser scanning vibrometer and the impedance analyzer. The values of the first resonance frequency of devices 'A' and 'B' are 17.41 kHz and 26.83 kHz, respectively. The experimental results indicate the first resonance frequencies of prototype devices are slightly less than those of the calculated results (20.14 kHz for device 'A' and 28.81 kHz for device 'B') and the difference is within 3 kHz. The simulated results agree well with the experimental results.

7.1.4 Measured acoustic intensity

The output acoustic intensity was obtained by placing a mini hydrophone at 1.0 mm away from the vibration plate and the spatial peak-temporal-peak intensity was calculated according to the IEEE standard. The maximum spatial peak-temporal-peak intensity of device 'A' under three different applied voltages (80 V, 120 V and 160 V) was approximately 41.13 mW/cm^2, 69.66 mW/cm^2 and 105.09 mW/cm^2, respectively. It is clearly shown that the output acoustic intensity is proportional to the applied voltages which has the same trend predicted using the single transducer FEA model. In addition, the experimental results of device 'A' are comparable to those obtained using a commercial sonicator. It is concluded that the prototype device 'A' could be used for ultrasound enhanced drug delivery.

For device 'B' with dual transducers, due to the physical structure of device 'B', cross-coupling between the active and its inactive neighboring transducer affects the performance of a single transducer. Under the same driving conditions, the maximum spatial peak to peak intensity produced by two ultrasound transducers is about 2 to 4 times higher than that generated by a single ultrasound transducer in device 'B'. Additionally, device 'B' is able to reduce the required voltage at least twofold. It is demonstrated that the prototype device 'B' has the capability to be used as an ultrasonic source to generate higher acoustic power with low required electrical power.

7.1.5 Feasibility study of device 'A' for drug delivery

The effects of low ultrasound frequency and intensity on the permeability of the silicone elastomer membrane were studied. Device 'A' with a single flat

flextensional ultrasound transducer performed well during ultrasound irradiation. It was found that the permeability of the silicone membrane was up to 2.9 times higher when exposed to low intensity (41.13 mW/cm^2) and low frequency (17.47 kHz) ultrasound compared to that of the unexposed membrane. The reversible permeation rate of the silicone membrane is within 25% of the non-irradiated membrane and the cumulative amount of drug in the acceptor compartment at the constant release level is 25.3% higher than that without ultrasound application. It is indicated that the permeability of the silicone membrane is partially reversible after low frequency and low intensity ultrasonic irradiation. It is demonstrated that the prototype device 'A' could be used as an external ultrasonic source to trigger the regulated polymeric device to release the drug on demand.

7.1.6 Effects of the ultrasonic irradiation on the permeability of fhe silicone rubber

The ultrasonic irradiation time and acoustic intensity on the ultrasound-enhanced permeability of the silicone membrane have been studied. It is found that the cumulative amount of drug penetrated through the silicone membrane with ultrasonic irradiation is 2.87 ± 0.73 times higher than that without ultrasound application. The increase in the cumulative amount of drug increases with the ultrasonic irradiation time and acoustic intensity. During the different sonophoresis experiments, the temperature increase of the silicone membrane was less than 3°C which does not attribute to the substantial enhancement to the permeability of the siliconemembrane.

In the passive diffusion experiments, the cumulative amount of the drug diffused through the sonicated silicone membrane is about 3.9% to 34.1% higher than that through the non-irradiated membrane. It is clearly shown that the permeability of the sonicated silicone membrane recovered partially. And also, the silicone membrane sonicated with longer irradiation time or higher acoustic intensity has higher permeability than that of the membrane sonicated with shorter time or lower acoustic intensity.

On the other hand, the surface morphology of the silicone membrane before and after ultrasound irradiation was examined by scanning electron microscope. Although cavitation was generated during the ultrasound irradiation, no micro holes and cracks were found in the sonicated silicone membrane. However, the modified permeability demonstrated that the structure of the sonicated silicone membrane was changed permanently. The modifications of the silicone membranes may be in the molecular scale, which could not be identified by the limited resolution SEM used in this study.

Finally, these results indicate that the prototype device 'A' is able to enhance the permeability of the silicone rubber at low frequency with relatively lower acoustic intensity. Again, the prototype device 'A' has the potential to be used as an external ultrasonic source to trigger the responsive polymeric device.

7.17 Ultrasound enhanced drug delivery by device '5'

Prototype device 'B' has been used as a tool to enhance the permeability of the silicone rubber. The drug delivery performance of each transducer in the device 'B' has been studied. It is found that the permeability of the silicone rubber was enhanced

by each transducer in the device 'B' at low input electrical power (80 V). The enhanced transport rate is up to 1.91-fold and 2.11-fold obtained by Transducer '1' and Transducer '2', respectively. The performance of each transducer is almost the same due to their similar physical characteristics at the low input electrical power. Temperature increase of the silicone rubber is less than 38C that does not have effect on the permeability enhancement of the silicon rubber.

At the high input electrical power (160 V), the transport rate increased up to 2.01-fold and 2.52-fold for Transducer '1' and Transducer '2', respectively. It is confirmed that the single transducer in the device 'B' generated high efficiency for ultrasound enhanced drug delivery when it was activated at high electrical power. But the performances of two transducers in drug delivery experiments have large difference which is caused by high input electrical power induced physical property changes to the transducers. Moreover, at high input electrical power both transducers generated more heat that causes temperature increase of the silicone rubbers to $8.4^{O}C$ and $5.2^{O}C$. However, high input electrical power and the temperature might pose the safety problems if it is applied to wearable medical devices. Thus ultrasound transducers in device 'B' should be operated at a low input electrical power.

The drug delivery performances of the dual transducers in device 'B' have been studied when they were operated simultaneously at low input electrical power. The transport rate increases up to 2.77-fold. It is found that better performance of device 'B' was achieved using dual transducers to enhance the permeability of the silicone rubber rather than using a single transducer in the same device. Moreover, the experimental results obtained by dual transducers at low electrical input power are

comparable to those achieved by a single transducer operated at high input electrical power. In addition, it is also demonstrated that dual transducers could generate more acoustic intensity to efficiently enhance the permeability of the silicone rubber, at the same time, reduce the required electrical power by two-fold for each transducer in device 'B'.

7.2 Recommendations for future work

Finite element analysis models for single and dual flat flextensional transducers were developed to determine the structure of the prototype devices 'A' and 'B'. Both devices have been used to enhance the permeability of the silicone rubber. Recommendations of future work for the devices are listed in the following subsections.

7.2.1 Structure optimization and transducer array in device 'B'

Device 'B' with dual flat flextensional transducers has been developed to increase the output acoustic power and at the same time to reduce the required electrical power. This is an important feature for a wearable medical device. Due to the physical structure of the device 'B', the undamped and nearly nondispersive Stoneley wave at the fluid-structure interface causes significant cross coupling that affects the performance of the device. According to the features of Stoneley wave, the cross coupling may be reduced by separating the transducers in device 'B'. However, device 'B' has only two transducers that could not continue to increase the output acoustic power. In order to increase the output acoustic power further, based on the acoustic interference principle, a transducer array is needed. It is well known that in closely packaged arrays, the acoustic interactions occur that lead to different acoustic loading on each transducer element, depending on its position in the array. This then

results in significant variations in the volume velocity of each array element. These acoustic interactions reduce the acoustic power output of the transducer array. So it is necessary to optimize the structure and performance of the transducer array in device 'B'.

7.2.2 Microdevice approach of device 'B'

The ultrasound application area of conventional sonophoresis devices is large in physical size and higher ultrasonic energy is required to disrupt the skin structure for transdermal enhancement. However, many nerve endings are in a large application area, so the skin is sensitive to the external stimulation when the higher ultrasonic energy is applied. The heat-induced pain and discomfort on the therapeutic site will take place. Therefore, high ultrasonic energy applied on the skin should be avoided. On the other hand, use of low ultrasonic energy may lead to low efficiency of transdermal drug delivery. Moreover, low efficiency also can be caused by the structure of drug reservoir. Microfabrication technology is a possible way to overcome above-mentioned shortcomings. Device 'B' will comprise of multiple micro-sized drug reservoirs in which ultrasound transducer array will be placed to increase the output acoustic power. Because of the micro-sized reservoir, the ultrasound application area for each reservoir is reduced to the range of micrometer square which contains very small number of cells and nerve endings, thus much higher ultrasound energy can be applied without pain and discomfort. In fact, when the opening of drug reservoir is reduced to micro-size, the requirement of ultrasound energy to disrupt the skin structure is not significantly higher as compared with that of a large skin area. Finally, the micro-device has multiple micro-sized drug reservoirs with nano-liter volume in order to control the drug release dosages precisely. The

micro-device with multiple micro-sized reservoirs can store the same or different drug types and be adhered to the skin surface for a long duration.

7.2.3 Future applications of the microdevice

In the future, the microdevice will be integrated with microcomputer control system, biosensor analysis system, data transmitter and receptor system, and power system (battery belt). It is not only a wearable medical device for self-monitoring and self-treatment but also a tool to establish the relationship between patients and remote medical centers (see Figure 7.1).

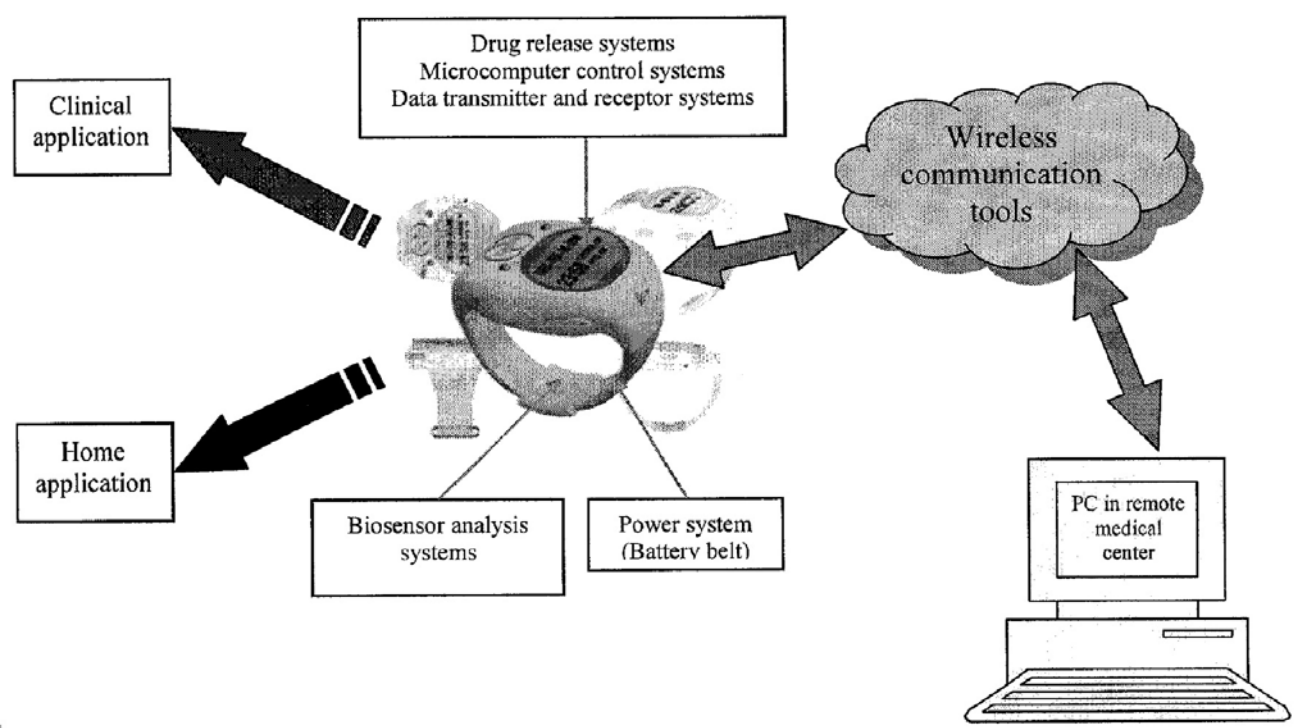

Figure 7.1. Flow chart of the potential applications of the proposed future commercial wearable sonophoresis device.

RELATED PUBLICATIONS

Journal papers:

1. Yeo, S. H., & Zhang, H. Y. (2003). Development of a novel sonophoresis microdevice. *Biomedical Microdevices, 5* (3), 201-206.

2. Zhang, H. Y., & Yeo, S. H. (2004). Design and fabrication of a sonophoresis device with a flat flextensional transducer for transdermal drug delivery. *Sensors and Actuators A: Physics, 115* (1), 133-139.

3. Zhang, H. Y., & Yeo, S. H. (2004). Dual flat flextensional ultrasound transducers for enhancement of transdermal drug delivery. *Japanese Journal of Applied Physics, **43*** (9A), 6488-6493.

4. Zhang, H. Y., & Yeo, S. H. (2005). Single flexible ultrasound transducer for enhancement of permeability of silicone membrane. *Sensors and Actuators A: Physics, 120* (1), 37-43.

Conference papers:

5. Yeo, S. H., & Zhang, H. Y. (2004). Sonophoresis device with single flat flextensional transducer developed for ultrasound enhanced transdermal drug delivery. *Proceedings of the Second Internal Conference of Biomedical Engineering*, pp. 572-577. February 16-18, 2004, Innsbruck, Austria.

6. Zhang, H. Y., & Yeo, S. H. (2005). Enhancement of permeability of silicone elastomer rubber with dual flexible ultrasound transducers. *International Conference on Materials for Advanced Technologies (ICMAT2005) & International Union of Materials Research Societies' International Conference on Advanced Materials (IUMRS-ICAM2005)*, 3 - 8 July, 2005, Singapore.

Invited book chapter:

7. Yeo, **S.** H., & Zhang, H. Y. (2004). Techniques in sonophoresis biomedical devices and their applications. In C. T. Leondes (Ed.) MEMS/ NEMS Handbook: Techniques and Applications (Tentative title). Netherlands: Kluwer Academic Publisher.

REFERENCES

1. *HealthyHormones.com -- Aarisse Health Care Products Homepage.* (2000). Retrieved March 11, 2004, from http://www.healthyhormones.com/trans.htm.

2. Franz, T. J., Tojo, K., Shah, K. R., & Kydonieus, A. (1992). Transdermal delivery. In A. Kydonieus (Ed.), *Treatise on controlled drug delivery* (pp. 341-421). New York: Marcel Dekker.

3. *University of Florida, College of Pharmacy Homepage.* (2001). Retrieved May 6, 2002, from http://www.cop.ufl.edu/safezone/prokai/pha5 110/tdds.htm.

4. Potts, R. O., & R. H. Guy (1997). *Mechanics of transdermal drug delivery.* New York: Marcel Dekker.

5. Johnson, M. E., Mitragotri, S., Patel, **A.** Blankschtein, D., & Langer, R. (1996). Synergistic effect of chemical enhancers therapeutic ultrasound on transdermal drug delivery. *Journal of Pharmaceutical Science, 85* (7), 670-679.

6. Green, P. G., Flalagan, M., Shroot, B., & Guy, R. H. (1993). Iontophoretic drug delivery. In K. A. Walters, & J. Hadgraft (Ed.) *Pharmaceutical skin penetration enhancement* (pp. *300-320).* New York: Marcel Dekker.

7. Prausniz, M. R., Bose, V., Langer, R., & Weaver, J. C. **(1993).** Electroporation of mammalian skin: a mechanism to enhance transdermal drug delivery. *Proceedings of the National Academy of Sciences, 90* (22), 10504-10508.

8. Tezel, A., Sens, A., Tuchscherer, J., & Mitragotri, S. (2001). Frequency dependence of sonophoresis. *Pharmaceutical Research,* 18(12), 1694-1700.

9. Mitragotri, S., Blankschtein, D. & Langer, R. (1995, August 11). Ultrasound mediated transdermal protein delivery. *Science,* 269, 850-852.

10. Mitragotri, S., & Kost, J. (2001). Transdermal delivery of heparin and low molecular weight heparin using low frequency ultrasound. *Pharmaceutical Research, 18* (8), 1151-1156.

11. Mitragotri, S., Blankschtein, D., & Langer, R. (1996). Transdermal drug delivery using low frequency sonophoresis. *Pharmaceutical Research, 13* (3), 411-420.

12. Mitragotri, S., Edwards, D. A., Blankschtein, D., & Langer, R. (1995). A mechanical study of ultrasonically enhanced transdermal drug delivery. *Journal of Pharmaceutical Sciences, 84* (6), 697-706.

13. Mitragotri, S., Blankschtein, D., & Langer, R. (1997). An explanation for variation of the sonophoretic transdermal transport enhancement from drug to drug. *Journal of Pharmaceutical Sciences, 86* (10), 1190-1192.

14. Fox, M. D. (1988). Disposable piezoelectric polymer bandage for percutaneous delivery of drugs and method for such percutaneous delivery (A). *Us Patent 4,787,888.*

15. Klopotek, P. J. (1993). Method and apparatus for generating localized hyperthermia. *US Patent 5,230,334.*

16. Lipkovker, L. M. (1995). Ultrasonic transdermal drug delivery system. *US Patent 5,421,816.*

17. Bock, R. T. (1997). Ultrasonic method and apparatus for cosmetic and dermatological applications. *US Patent 5,618,275.*

18. Elstrom, T. A., Shain, E. B., & Henning, T. P. (1999). Transdermal transport using ultrasonic standing waves. *US Patent 5,895,362.*

19. Ball, G. R., & Katz, B. H. (2000). Apparatus and method for sonically enhancemed drug delivery. *US Patent 6,024,717.*

20. Rowe, S., Kost, J., Mitragotri, S., Pishko, M., & Davis, M. (2001). Ultrasound enhancement of transdermal transport. *US Patent 6,234,990 B1*.

21. *Encapsulation Systems Inc. Homegape.* (2003). Retrieved June 13, 2004, from http://www.encsys.com/default.html .

22. Sontra Medical, Inc. Homepage. (2004). Retrieved June 13, 2004, from http://www.sontra.com/technology/nooninvasivedevice/.

23. Decarpigny, J. N., Harmonic, B., & Wilson, Jr, **O.** B. (1991). The design of low frequency underwater acoustic projectors present status and future trends. *IEEE Journal of Ocean Engineering, 16* (1), 107-122.

24. Kost, J., & Langer, R. (1990). Magnetically and ultrasonically modulated drug delivery systems. In J. Kost (Ed.) *Pulsed and self-regulated drug* ***delivery*** (pp. 3-16). Boca Raton: CRC Press.

25. Portenlanger, G., & Heusinger, H. (1997). The influence of frequency on the mechanical ad radial effects for the ultrasonic degradation of detranes. *Ultrasonics Sonochemistry, **4*** (2), 127-130.

26. Kanwal, F., Liggat, J. J., & Pethrick, R. **A.** (2000). Ultrasonics degradation of polystyrene solutions. *Polymer Degradation and Stability, 68* (3), 445-449.

27. Xu, X. (1997). Structure development and change in properties of polymers during mechanical degradation. *Macromolecular Symposia, 118* (1), 189-194.

28. Peters, D. (1996). Ultrasound in materials chemistry, *Journal of Materials Chemistry, 6* (10), 189-194.

29. Miller, M. W., Battaglia, L. F., & Mazza, S. (2003). Biological and environmental factors affecting ultrasound induced hemolysis in vitro: medium tonicity. *Ultrasound in Medicine and Biology, 29* (5), 713-724.

30. Dalecki, D., Raeman, C. H., Child, S. Z., Cox, C., Francis, C. W., Meltzer, R. S., & Carstensen, E. L. (1997). Hemolysis in vivo from exposure to pulsed ultrasound. *Ultrasound in Medicine and Biology, 23* (2), 307-313.

31. Miller, D. L., & Thomas, R. M. (1996). Contrast agent gas bodies enhance hemolysis induced by lithotripter shock waves and high intensity focused ultrasound in whole blood. *Ultrasound in Medicine and Biology, 22* (8), 1089-1095.

32. Dalecki, D., Child, S. Z., Raeman, C. H., Xing, C., Gracewski, S., & Carstensen, E. L. (2000). Bioeffects of positive and negative acoustic pressures in mice infused with microbubbles. *Ultrasound in Medicine and Biology, 26* (8), 1327-1332.

33. Mitragotri, S., Farrell, J., Tang, H., Takaaki, T., Kost, J., & Langer, R. (2000). Determination of threshold energy dose for ultrasound induced drug transport. *Journal of Controlled Release, 63* (1-2), 41-52.

34. Baran, N. (1988). *Finite Element Analysis on Microcomputers.* New York: McGraw-Hill.

35. Chandrupatla, T. R., & Belegundu, A. D. (1991). *Introduction to Finite Elements in Engineering.* New York: Prentice-Hall.

36. Burnett, D. S. (1987). Finite Element Analysis From Concept to Applications. Boston: Addison-Wesley.

37. ANSYS coupled-field analysis guide: ANSYS release 6.0. (2001). Canonsburg: ANSYS Inc.

38. Hossack, J. A., Zhou, S. W., & Powell, D. J. (2001). Finite element analysis of phased plano-concave multi-layer transducers. *IEEE Ultrasonics Symposium,* 1003-1006.

39. Chin, L. C., Varadan, V. V., & Varadan, V. K. (1991). Finite element analysis of flextensional electroacoustic transducers. *IEEE Ultrasonics Symposium,* 481-484.

40. Kang, K., & Roh, Y. (2003). Optimization of structural variables of a flextensional transducer by the statistical multiple regression analysis method. *The Journal of the Acoustical Society of America, 114* (3), 1454-1461.

41. Schmitt, D. P., Pelinescu, K. I., & Park, S. E. (2002). Optimized flextensional transducers and implant hearing aid. *IEEE Ultrasonics Symposium,* 1273-1276.

42. Zhang, J. D., Haldky-Hennion, A. C., Hughes, W. J., & Newnham, R. E. (2001). Modeling and undertwaer characterization of cymbal transducers and arrays. *IEEE Transactions on Ultrasonics, Ferroelectrics, and Frequency Control, 48* (2), 560-568.

43. Tressler, F., Cao, W. W., Uchino, K., and Newnham, R. E. (1998). Finite element analysis of the cymbal type flextensional transducer. *IEEE Transactions on Ferroelectrics, and Frequency Control, 45* (5), 1363-1369.

44. Dogan, A., Uchino, K., & Newnham, R. E. (1997). Composite piezoelectric transducer with truncated conical endcaps cymbal. *IEEE Transactions on Ultrasonics, Ferroelectrics, and Frequency Control, 44* (3), 597-605.

45. Tressler, J. F., Cao, W. W., Uchino, K., & Newnham, R. E. (1996). Ceramic metal composite transducers for ultrasound acoustic applications. *IEEE Ultrsonics Symposium,* 561-564.

46. Chin, L. C., Vardan, V. V., & Vardan, V. K. (1991). Finite element analysis of flextensional electroacoustic transducers. *IEEE Ultrasonics Symposium,* 481-484.

47. David, J., & Cheeke, N. (2002). *Fundamentals and Applications of Ultrasonic Waves.* Boca Raton: CRC Press.

48. Ensminger, D. (1988). Ultrasonic: Fundamentals, Technology, Applications. New York: Marcel Dekker.

49. Berlincourt, D. A., Curran, D. R., & Jaffe, H. (1964). Piezoelectric and piezomagnetic materials and their function in transducers. In W. P. Mason (Ed.) *Physical Acoustics: Principles and Methods* (Vol. 1A, pp. 169-270). New York: Academic Press.

50. *The piezoelectric effect in a cylinder of PZT material.* (2000). Retrieved March 21, 2004, from http://www.apc.thomasregister.com/olc/03482007/notes1.htm.

51. Ikeda, F. (1990). *Fundamentals of Piezoelectricity.* New York: Oxford University Press.

52. Zdenko, F. (1996). *Ultrasonic measurements and technologies.* New York: Chapman & Hall.

53. Santini, J. T., Jr., Richards, A. C., Scheidt, R. M., Cima, J., & Langer, R. (2000). Microchips as controlled drug-delivery devices. *Angewandte Chemie International Edition, 39* (14), 2396-2407.

54. Berner, B., & Dinh, S. (1992). Fundamental concept in controlled release (pp. 1-35). In A. Kydonieus (Ed.) *Treatise on controlled drug delivery.* New York: Marcel Dekker.

55. Gliadel® (2004) Retrieved March 18, 2004, from Musella Foundation Homepage: http://virtualtrials.com/Gliadel/.

56. ReGel® (2004) Retrieved March 18, 2004, from MacroMed Inc. Homepage: http://www.macromed.com/technology.htm.

57. Langer, R. (1998, April 30). Drug delivery and targeting. *Nature*, 392, SUPP. 5-10.

58. Uhrich, K.E., Cannizzaro, S. M., Langer, R., & Shakesheff, K. M. (1999). Polymeric systems for controlled release. *Chemical Reviews, 99* (11), 3181-3198.

59. Franz, T. J., Tojo, K. K., Shah, R., & Kydonieus, **A.** (1992). Transdermal delivery. In **A.** Kydonieus (Ed.) *Treatise on controlled drug delivery* (pp. 341-421). New York: Marcel Dekker.

60. Tissues. Retrieved March 18, 2004, from Pennsylvania State University, Department of Biochemistry & Molecular Biology Website: http://www.bmb.psu.edu/courses/bisci004a/tissues/skin.jpg.

61. Willams, **A.** C., & Barry, B. W. (1992). Skin absorption enhancers. *Critical Reviews in Therapeutic Drug Carrier Systems, 9* (3-4), 305-353.

62. Foldvari, M. (2000). Non-invasive administration of drugs through the skin: challenges in delivery system design. *Pharmaceutical Science & Technology Today*, 3 (12), 417-425.

63. Chien, T. W. (1993). Systemic delivery of peptide-based pharmaceuticals by transdermal periodic iontherapeutic system. In R. Gurny, & **A.** Teubner (Eds.) *Dermal and Transdermal Drug Delivery-New Insights and Perspectives* (pp. 129-152). Stuttgart: Wissenschaftliche Verlagsfesellschaft mbH.

64. Gazelius, B. (1999, January). Innovation in microvascular diagnosis. Iontophoresis theory. Retrieved March 19, 2004, from http://www.perimed.se/p_Applications/IontophoresisTheory.pdf.

65. Nagendu, D. R., Dev, B., Fewell, J., Smith, L. C., Widera, G., & Zhang, L. (2003). Enhancement of therapeutic drug and DNA delivery into cells by electroporation. *Journal of Physics D: Applied Physics, 36* (4), 348-363.

66. Mir, L. M., & Orlowski, S. (1999). Mechanisms of electrochemotherapy. *Advanced Drug Delivery Reviews, 35* (1), 107-118.

67. Heller, R., Gilbert, R., & Jaroszeski, M. J. (1999). Clinical applications of electrochemotherapy. *Advanced Drug Delivery Reviews, 35* (1), 119-129.

68. Prausnitz, M. R. (1996). The effects of electric current applied to skin: A review for transdermal drug delivery. *Advanced Drug Delivery Reviews, 18* (3), 395-425.

69. Vanbever, R., & Préat, V. (1999). In vivo efficacy and safety of skin electroporation. *Advanced Drug Delivery Reviews, 35* (1), 77-88.

70. Tachibana, K., & Tachibana, S. (1991). Transdermal delivery of insulin by ultrasonic vibration. *Journal of Pharmacy and Pharmarcology,* ***43*** (4), 270-271.

71. Tachibana, K. (1992). Transdermal delivery of insulin to alloxan-diabetic rabbits by ultrasound exposure. *Pharmaceutical Research, 9* (7), 952-954.

72. Merino, G., Kalia, Y. N., Delgado-Charro, M. B., Potts, R. O., & Guy, R. H. (2003). Frequency and thermal effects on the enhancement of transdermal transport by sonophoresis. *Journal of Controlled Release, 88* (1), 85-94.

73. Flynn, H. G. (1964). Physics of acoustic cavitation in liquid. In W. P. Mason (Ed.) *Physical Acoustics: Principles and Methods* (Vol. 1B, pp. 58-172). New York: Academic Press.

74. Frizzell, L. A. (1988). Biological effects of acoustic cavitation. In K. S. Suslick (Ed.) *Ultrasound Its Chemical, Physical, and Biological Effects* (pp. 287-303), Germany: VCH Verlagsgesellschaft mbH.

75. Nyborg, W. Le M. (1965). Acoustic streaming. In W. P. Mason (Ed.) *Physical Acoustics: Principles and Methods* (Vol. 2B pp. 265-331). New York: Academic Press.

76. Tang, H., Blankschtein, D., & Langer, R. (2002). An investigation of the role of cavitation in low frequency ultrasound mediated transdermal drug transport. *Pharmaceutical Research, 19* (8), 1160-1169.

77. Tezel, **A.,** Sens, **A.,** & Mitragotri, S. (2002). Investigation of the role of cavitation in low frequency sonophpresis using acoustic spectroscopy. *Journal* of *Pharmaceutical Sciences, 91* (2), 444-453.

78. Mitragotri, **S.,** & Kost, J. (2004). Low frequency sonophoresis. *Advanced Drug Delivery Reviews, 56* (5), 589-601.

79. Miller, M. W., Battaglia, L. F., & Mazza, S. (2003). Biological and environmental factors affecting ultrasound induced hemolysis in vitro: medium tonicity. *Ultrasound in Medicine and Biology, 29* (5), 713-724.

80. Dalecki, D., Raeman, C. H., Child, **S.** Z., Cox, C., Francis, C. W., Meltzer, R. **S.,** & Carstensen, E. L. (1997). Hemolysis in vivo from exposure to pulsed ultrasound. *Ultrasound in Medicine and Biology, 23* (2), 307-313.

81. Miller, D. L., & Thomas, R. M. (1996). Contrast agent gas bodies enhance hemolysis induced by lithotripter shock waves and high intensity focused ultrasound in whole blood. *Ultrasound in Medicine and Biology, 22* (8), 1089-1095.

82. Dalecki, D., Child, **S.** Z., Raeman, C. H., Xing, C., Gracewski, S., & Carstensen E. L. (2000). Bioeffects of positive and negative acoustic pressures in mice infused with microbubbles. *Ultrasound in Medicine and Biology, 26* (8), 1327-1332.

83. Coleman, **A.** J., & Saunders, J. E. (1993). **A** review of the physical properties and biological effects of the high amplitude acoustic fields used in extracorporeal lithotripsy. *Ultrasonics, 31* (2), 75-89.

84. Fry, F. *Y.*, Sanghvi, N. T., Foster, R. **S.,** Bihrle, R., & Hennige, C. (1995). Ultrasound and microbubbles: their degeneration, detection and potential ultilization in tissue and organ therapy - Experimental. *Ultrasound in Medicine and Biology, 21* (8), 1227-1237.

85. Shi, W. T., Forsberg, F., Tornes, **A.,** Ostensen, J., & Goldberg, B. B. (2000). Destruction of contrast microbubbles and the association with inertial cavitation. *Ultrasound in Medicine and Biology, 26* (8), 1009-1019.

86. Mornstein, V. (1997). Cavitation-induced risks associated with contrast agents used in ultrasonography. *European Journal of Ultrasound, 5* (2), 101-111.

87. Everbach, E. C., Makin, I. R. S., Azadniv, M., & Meltzer, R. S. (1997). Correlation of ultrasound-induced hemolysis with cavitation detector output in vitro. *Ultrasound in Medicine and Biology, 23* (4), 619-624.

88. Miller, M. W., & Battaglia, L. F. (2003). The relevance of cell size on ultrasound-induced hemolysis in mouse and human blood in vitro. *Ultrasound in Medicine and Biology, 29* (10), 1479-1485.

89. Mitragotri, S. (2000). Synergistic effect of enhancers for transdermal drug delivery. *Pharmaceutical Research, 17* (11), 1354-1359.

90. Kalia, Y. N., & Guy, R. H. (1997). Interaction between penetration enhancer and iontophoresis: effect on human skin impedence in vivo. *Journal of Controlled Release, 44* (1), 33-42.

91. Grewal, B. S., Naik, A. W., Irwin, J., Gooris, G., Grauw, De C. J., H. G., & Gerritsen, J. A. B. (2000). Transdermal macromolecular delivery: real-time visulization of iontophoresis and chemically enhanced transport using tow photon excitation microscopy. *Pharmaceutical Research, 17* (7), 788-795.

92. Ilic, L., Gowrishankar, T. R., Vaughan, T. E., Herndon, T. O., & Weaver, J. (1999). Spatially constrained skin electroporation with sodium thiosulfate and urea creates transdermal microconduits. *Journal of Controlled Release, 61* (1-2), 185-202.

93. Mitragotri, S., Ray, D., Farrell, J., Tang, H., Yu, B., Kost, J., Blankschtein, D., & Langer, R. (2000). Synergistic effect of low-frequency ultrasound and sodium lauyl

sulfate on transdermal transport. *Journal of Pharmaceutical Sciences, 89* (7), 892-900.

94. Tezel, A., Sens, A., Tuchscherer, J., & Mitragotri, S. (2002). Synergistic effect of low-frequency ultrasound and surfactants on skin permeability. *Journal of Pharmaceutical Sciences, 91* (1), 91-100.

95. Le, L., Kost, J., & Mitragotri, S. (2000). Combined effect of low-frequency ultrasound and iontophoresis: applications for transdermal heparin delivery. *Pharmaceutical Research, 17* (9), 1151-1154.

96. Kost, J., Pliquett, U., Mitragotri, S., Yamamoto, A., Langer, R., & Weaver, J. (1996). Synergistic effect of electric field and ultrasound on transdermal transport. *Pharmaceutical Research, 13* (5), 633-638.

97. Bommanon, D., Tamada, J., Leung, L., & Potts, R. (1994). Effects of electroporation on transdermal iontophoretic delivery of leutinizing hormone releasing hormone. *Pharmaceutical Research, 11* (12), 1809-1814.

98. Chang, S., Hofman, G., Zhang, L., Deftos, L., & Banaga, A. (2000). The effect of electroporation on iontophoretic transdermal delivery of calcium regulating hormone. *Journal of Controlled Release, 66* (2-3), 127-133.

99. Tachibana, S., & Shibata, U. (1990). Endermic application **kits** for external medicines. *US Patent 4,953,565.*

100. Flanagan, D. F. (1992). Endermic method and apparatus. *US Patent 5,171,215*.

101. Tyle, & Agrawala (1989). Drug delivery by phonophoresis. *Pharmaceutical Research, 6* (5), 355-361.

102. Shimada, J., & Shapland, J. E. (1993). Drug delivery by multiple frequency phonophoresis. *US Patent 5,267,985.*

103. Rowe, S., Kost, J., Mitragotri, S., Pishko, M., & Davis, M. (2002). Ultrasound enhancement of transdermal transport. *US Patent 0045850A1*.

104. Ogden, J. E. (1997). Sonophoresis drug delivery system. *US Patent 5,656,016.*

105. SonoPrepB Skin Permeation Device. Retrieved May 4, 2004, from Sontra Medical Corporation Homepage, Technology Platform http://www.sontra.com/technolonv/nooninvasivedevice/.

106. Rolt, K. D. (1990). History of the flextensional electroacoustic transducers. *Journal of the Acoustical Society of America, 87* (3), 1340-1346.

107. Hughes, W. J. (1998). Testing of underwater transducers. In *Encyclopedia of Applied Physics* (Online, Vol. 22). New York: Wiley VCH.

108. Denkmann, W. J., Nickell, R. E., & Stickler, D. C. (1973). Analysis of structure-acoustic interactions in metal-ceramic transducers. *IEEE transaction on audio and electroacoustics, AU-21* (4), 317-323.

109. Butler, S. C., Butler, J. L., Butler, A. L., & Cavanagh, G. H. (1997). A low frequency directional flextensional transducer and line array. *Journal of the Acoustical Society of America, 102* (1), 308-314.

110. Decarpigny, J. N., Harmonic, B., & Wilson, O. B., Jr (1991). The design of low frequency underwater acoustic projectors present status and future trends. *IEEE Journal of Ocean Engineering, 16* (1), 107-122.

111. Kinsler, L. E., Frey, A. R., Coppens, A. B., & Sanders, J. V. (2000). *Fundamentals of acoustics (4th ed.).* New York: John Wiley & Sons.

112. Kwak, M. K., & Kim, K. C. (1991). Axisymmetric vibration of circulat plates in contact with fluid. *Journal of Sound and Vibration, 146* (2), 381-389.

113. *ANSYS theory reference release 6.0* (2001, Vol. 1). Canonsburg: ANSYS Inc.

114. Keyhani, K., Guzman, H. R., Parsons, **A.,** Lewis, T. N., & Prausnitz, M. R. (2001). Intracellular drug delivery using low frequency ultrasound: quantification of molecular uptake and cell viability. *Pharmaceutical Research, 18* (12), 1514-1520.

115. ANSYS Elements Reference: **ANSYS** release 5.7 (2000, Vol. 1). Canonsburg: ANSYS Inc.

116. Katz, B. F. G. (2000). Acoustic absorption measurement of human hair and skin within the audible frequency range. *The Journal of the Acoustic Society of America, 108* (5), 2238-2242.

117. Okada, H., Kurosawa, M., Ueha, **S.,** & Masuda, M. (1994). New airborne ultrasound transducer with high output sound pressure level. *Japanese Journal of Applied Physics,* 33 (Pt. 1), 3040-3044.

118. IEEE Standard Board (1989). *IEEE guide for medical ultrasoundfield parameter measurements* New York: Institute of Electrical and Electronics Engineers, Inc.

119. Uberall, H. (1973) Surface waves in acoustics. In W. P. Mason & R. N. Thurston (Ed) *Physical Acoustics: Principles and Methods, Academic Press* (Vol. 10, pp. 1-57), New York: Academic Press.

120. Roh, **Y.** & Khuri-Yakub, B. T. (2002). Finite element analysis of underwater capacitor micromechined ultrasonic transducers. *IEEE transactions on Ultrasonics, Ferroelectronics and Frequency Control, 49* (3), 293-298.

121. Product information of DOW CORNING® 7-4107 silicone elastomer membrane.

122. Kost, J., Loeng, K., & Langer, R. (1989). Ultrasound enhanced polymer degradation and release of incorporated substances. *Proceedings of the National Academy of Sciences of the United States of America, 86* (20), 7663-7666.

123. Masselin, I., Chasseray, X., Laurence, D. B., Laine, J. M., Syzaret, P. Y., & Lemordant, D. (2001). Effect of sonication on polymeric membrane. *Journal of Membrane Science, 181* (2), 213-220.

124. Plesset, M. S. (1966). Shockwaves from cavity collapse, *Philosophical Transactions of The Royal Society 260A* (2) 241-246.

125. Kawahara, N., Yarin, **A.** L., Brenn, G., Kastner, O., & Durst, F. (2002). Effect of acoustic streaming on the mass transfer from a sublimating sphere. *Physics of Fluids, 12* (4), 912-923.

126. Wu, J. R., & Du, G. H. (1997). Streaming generated by a bubble in an ultrasound field, *The Journal of the Acoustical Society of America, 101* (4), 1899-1907.

127. Rooney, J. A. (1988). Other Nonlinear Acoustic Phenomena. In K. S. Suslick (Ed.) *Ultrasound Its Chemical, Physical, and Biological Effects* (pp. 65-96) New York: VCH Publishers, Inc.

128. Price, G. J. (1990) The use of ultrasound for the controlled degradation of polymer solutions. In T. J. Mason (Ed.) *Advanced In Sonochemistry* (Vol. 1, pp. 231-287), London: Alden Press.

129. Hines, A. L., & Maddox, R. N. (1985). *Mass Transfer Fundamentals and Applications*. New Jersey: Prentice Hall.